

UNCLASSIFIED

AD 423798

FN
DEFENSE DOCUMENTATION CENTER

FOR

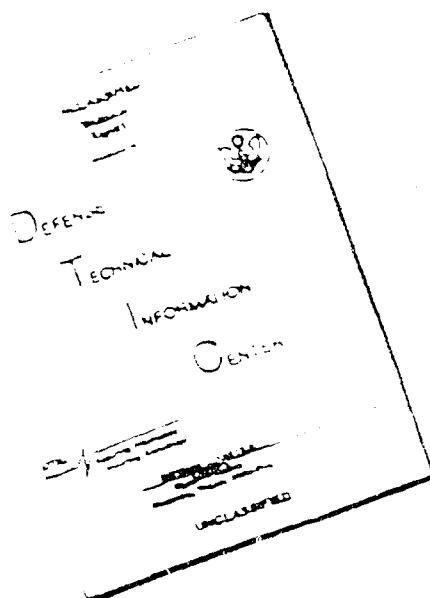
SCIENTIFIC AND TECHNICAL INFORMATION

CAMERON STATION, ALEXANDRIA, VIRGINIA



UNCLASSIFIED

DISCLAIMER NOTICE



THIS DOCUMENT IS BEST
QUALITY AVAILABLE. THE COPY
FURNISHED TO DTIC CONTAINED
A SIGNIFICANT NUMBER OF
PAGES WHICH DO NOT
REPRODUCE LEGIBLY.

REPRODUCED FROM
BEST AVAILABLE COPY

THIS DOCUMENT CONTAINED
BLANK PAGES THAT HAVE
BEEN DELETED

NOTICE: When drawings or other drawings, specifications or other data are used for any purpose other than in connection with a definitely related government procurement operation, the U. S. Government thereupon incurs no responsibility, nor any obligation whatsoever; and the fact that the Government may have formulated, furnished, or in any way supplied the said drawings, specifications, or other data is not to be regarded by implication or otherwise as in any manner licensing the holder or any other person or corporation or conveying any rights or permission to manufacture, use or sell any patented invention that may in any way be related thereto.

AD# 423798

PROCEEDINGS
OF THE
**SIXTH SYMPOSIUM ON
HYPERVELOCITY IMPACT**



Best Available Copy

**PROCEEDINGS
OF THE
SIXTH SYMPOSIUM ON
HYPERVELOCITY IMPACT**

**CLEVELAND, OHIO
APRIL 30, MAY 1, 2, 1963**

Sponsored by:

U.S. Army
U.S. Air Force
U.S. Navy

Tri-Service Committee:

R. J. Eichelberger, Army, BRL, Chairman
W. H. Dittrich, Air Force, Det. 4, ASD
W. W. Atkins, Navy, NRL

Contract No.
DA-31-124-ARO(D)-16

VOLUME I

AUGUST, 1963

The Firestone Tire & Rubber Co. (Conference Host)

Volume II of the Sixth Symposium on Hypervelocity Impact appears in two parts. Part 1 contains pages 1 through 336; Part 2 contains pages 337 through 609.

The views, conclusions and recommendations expressed herein do not necessarily reflect the official views or policies of either the United States Army, United States Navy or the United States Air Force.

TABLE OF CONTENTS

VOLUME I
PROJECTION TECHNIQUES

TABLE OF CONTENTS	iii
UNPUBLISHED PRESENTATIONS	
A CRITIQUE OF ACCELERATOR TECHNIQUES FOR HYPERVELOCITY IMPACT (Introductory Paper) A. C. Charters	1
EXPERIMENTAL AND THEORETICAL STUDIES ON THE INTERIOR BALLISTICS OF LIGHT GAS GUNS Paul G. Baer and Horace C. Smith	41
AN INVESTIGATION OF THE PERFORMANCE OF A COMPRESSION HEATER FOR USE WITH GUN TUNNELS OR HYPERVELOCITY LAUNCHERS Bo Lemcke	107
COMPUTER ANALYSIS OF TWO-STAGE HYPERVELOCITY MODEL LAUNCHERS R. Piacesi, D. F. Gates, and A. E. Seigel	155
NRL HYPERVELOCITY ACCELERATOR DEVELOPMENT H. F. Swift, C. D. Porter, J. J. Condon and J. R. Baker	175
PERFORMANCE OF A THREE STAGE ARC HEATED LIGHT GAS GUN J. Eckerman and W. L. McKay	247
HYPERVELOCITY AUGMENTATION TECHNIQUES William G. Howell, Rodney F. Recht, and Thomas W. Ipson	395

THE MAGNETOHYDRODYNAMIC HYPERVELOCITY GUN R. L. Chapman, D. E. Harms, and G. P. Sorenson	317
INHIBITED JET CHARGE S. Kronman and A. Merendino	331
SPECIAL EXPLOSIVE PROJECTORS: I. SHAPED CHARGE ACCELERATOR; II. TARGET PLATE ACCELERATOR K. N. Kreyenhagen, J. E. Ferguson, R. R. Randall, and J. P. Joyce	349
(Confidential) ARMOUR RESEARCH FOUNDATION TRAVELING CHARGE GUN (U) Louis A. C. Barbarek	Vol. IV, 395
SUMMARY REMARKS H. F. Swift	375
ATTENDANCE ROSTER	379
AUTHOR INDEX	387

VOLUME II - Part I
THICK TARGET CRATERING AND IONIZATION

TABLE OF CONTENTS	iii
REVIEW OF PLASTIC PROCESSES IN HYPERVELOCITY IMPACT AND PENETRATION (Introductory Paper) Robert L. Bjork	1
HYDRODYNAMICS OF HYPERVELOCITY IMPACT G. M. Walsh and J. H. Tillotson	59
VISCO-PLASTIC SOLUTION OF HYPERVELOCITY IMPACT CRATERING PHENOMENON T. E. Riney	105
THE CALCULATION OF STRESS WAVES IN SOLIDS Mark L. Wilkins and Richard Giroux	141
A HYPERVELOCITY IMPACT MODEL FOR COMPLETELY DEFORMING PROJECTILES J. L. Luttrell	157
A BLAST-WAVE THEORY OF CRATER FORMATION IN SEMI-INFINITE TARGETS William J. Rae and Henry P. Kirchner	163
SPHERICAL SHOCK WAVES AND CAVITY FORMATION IN METALS N. Davids, H. H. Galvit, and O. T. Johnson	229
PROPERTIES OF SPHERICAL SHOCK WAVES PRODUCED BY HYPERVELOCITY IMPACT Ray Kinslow	273
SHOCK FRONT VARIATION IN TIME FOR HIGH SPEED IMPACT INTO WATER James F. Heyda	321

VOLUME II - Part 2

HYPERVELOCITY CRATERING DATA AND A CRATER- DEPTH MODEL FOR THE REGIME OF FLUIDITY Olive G. Engel	337
FLUID IMPACT CRATERS AND HYPERVELOCITY - - HIGH-VELOCITY IMPACT EXPERIMENTS IN METALS AND ROCKS H. J. Moore, R. W. MacCormack, and D. E. Gault	367
ENERGY BALANCES IN HYPERVELOCITY PENETRATION R. B. Pond, C. Mobley, and C. M. Glass	401
THE PARTITION OF ENERGY FOR HYPERVELOCITY IMPACT CRATERS FORMED IN ROCK Donald E. Gault and Ezra D. Heitowitz	419
TRANSIENT OBSERVATIONS OF CRATER FORMATION IN SEMI-INFINITE TARGETS J. H. Kincke, Jr., and Richard Vitali	457
INFLUENCE OF TARGET STRENGTH ON HYPERVELOCITY CRATER FORMATION IN ALUMINUM J. H. Kincke, Jr., and L. G. Richards	513
SOME PHENOMENA ASSOCIATED WITH IMPACTS INTO ALUMINUM S. M. Halperson	525
PARTICLE-SOLID IMPACT PHENOMENA E. H. Goodman and C. D. Liles	543
INVESTIGATION OF THE IMPACT OF COPPER FILAMENTS INTO ALUMINUM TARGETS AT VELOCITIES TO 16,000 FEET PER SECOND C. Robert Nysmith, James L. Summers, and B. Pat Denardo	577
IONIZATION ASSOCIATED WITH HYPERVELOCITY IMPACT J. F. Friichtenicht and J. C. Slattery	591

INVESTIGATION OF IMPACT FLASH AT LOW AMBIENT PRESSURES Robert W. MacCormack	613
AN INVESTIGATION OF THE PHENOMENA OF IMPACT FLASH AND ITS POTENTIAL USE AS A HIT DETECTION AND TARGET DISCRIMINATION TECHNIQUE J. W. Gehring and R. L. Warnica	627
SUMMARY: THEORETICAL AND EXPERIMENTAL STUDIES OF CRATER FORMATION R. J. Eichelberger	683
AUTHOR INDEX	707

TABLE OF CONTENTS

VOLUME III

THIN TARGET PERFORATIONS AND PROTECTION

TABLE OF CONTENTS	iii
INTRODUCTORY PAPER - EXPERIMENTATION L. Zernow	1
TWO DIMENSIONAL ANALYSIS OF A HYPERVELOCITY IMPACT UPON A VISCO-PLASTIC PLATE H. Kraus	13
A METEOROID BUMPER DESIGN CRITERION P. E. Sandorff	41
EXPERIMENTAL AND THEORETICAL RESULTS CONCERNING THE PROTECTIVE ABILITY OF A THIN SHIELD AGAINST HYPERVELOCITY PROJECTILES C. J. Maiden	69
EFFECTS OF 3 TO 12 KM/SEC IMPACTS ON FINITE TARGETS R. B. Mortensen, J. E. Ferguson, J. P. Joyce, and K. N. Kreyenhagen	157
THIN PLATE PERFORATION STUDIES WITH PROJECTILES IN THE VELOCITY RANGE FROM 2 TO 5 KM/SEC R. W. Watson, K. R. Becker, and F. C. Gibson	207
A NEW SYSTEM OF PROTECTION FROM HYPERVELOCITY PARTICLES B. W. Reynolds and R. H. Emmons	249
HYPERVELOCITY PUNCTURING OF SELF-SEALING STRUCTURES Philip J. D'Anna	281
AN INVESTIGATION OF THE PENETRATION OF HYPER- VELOCITY PROJECTILES INTO COMPOSITE LAMINATES A. R. McMillan	309

METEOROID EFFECTS ON NUCLEAR ROCKET SPACE VEHICLE MISSION SUCCESS William H. Sterbentz and Loren L. Long	357
SUMMARY: THIN PLATE PERFORATION AND PROTECTION Dale M. Davis	387
AUTHOR INDEX	393

VOLUME IV
APPLICATIONS

TABLE OF CONTENTS	iii
(Secret) APPLICATION ASPECTS OF HYPERVELOCITY IMPACT - 1963 (U) (Introductory Paper) J. M. Brown and P. K. Margolis	1
(Confidential) JET PELLET PROJECTION TECHNIQUE (U) S. Kronman	21
(Confidential) HYPERVELOCITY PROJECTILE INVESTIGATION FOR MULTIPLE THIN PLATE PENETRATION (U) R. L. Chandler, T. Watmough, and F. J. Zimmerman	37
(Secret) LETHALITY OF HOLLOW SHAPES (U) W. H. Dittrich, D. R. Christman, J. W. Gehring, K. N. Kreyenhagen, and R. B. Mortensen	101
(Confidential) A WARHEAD CONCEPT FOR DEFEAT OF HARD TARGETS IN SPACE (U) Dale M. Davis	151
(Secret) AIMED WARHEAD CONCEPTS (U) Samuel D. Stein, George M. Gaydos, and Edmund M. Harrity	167
(Confidential) HYPERVELOCITY IMPACT EXPERIMENTS WITH LAMINATED COMPLEX TARGETS (U) C. M. Cox and E. S. Thorn	193
(Secret-No Foreign) HYPERVELOCITY IMPACTS INTO ABLATIVE MATERIALS (U) Mario A. Persechino	235
(Confidential) DETERMINATION OF PERFORATION ENERGIES FOR COMPOSITE TARGETS (U) Murray Rockowitz and Charles A. Carey	271

(Secret) A SHORT REVIEW OF THE STATUS OF THE AERO-THERMAL PHASE OF THE HYPERVELOCITY KILL MECHANISMS PROGRAM (U) Coleman duP. Donaldson	305
(Secret-No Foreign) LETHALITY OF SMALL FRAGMENTS VERSUS ICBM RE-ENTRY VEHICLES (U) James J. Dailey	329
(Secret-No Foreign) VULNERABILITY OF LARGE MISSILE SYSTEMS DURING THE LAUNCH PHASE (U) H. S. Zimney, R. B. Mortensen, W. A. Rhea, and R. B. Coley	345
(Confidential) FREE, A HYPERVELOCITY ROCKET WEAPON (U) D. C. Lane	373
(Secret) SUMMARY: APPLICATIONS (U) W. W. Atkins	385
(Confidential) ARMOUR RESEARCH FOUNDATION TRAVELING CHARGE GUN (U) Louis A. G. Barbarek	395
AUTHOR INDEX	417
ATTENDANCE ROSTER	421

UNPUBLISHED PRESENTATIONS

NOTE: Not included in the published Proceedings of the Sixth Symposium on Hypervelocity Impact are:

"Opening Remarks" by Dr. R. J. Eichelberger, Ballistic Research Laboratories.

"Welcoming Remarks" by Dr. V. E. Lucas, Firestone T & R Co.

"Chairman's Remarks" from all six sessions.

Session No. 1 - TECHNIQUES

Dr. M. A. Cook, University of Utah

Session No. 2 - THEORY

Dr. Russell Duff, Lawrence Radiation Laboratory

Session No. 3 - THEORY

Dr. C. M. Herzfeld, Advanced Research Projects Agency

Session No. 4 - EXPERIMENTATION

Dr. Emerson Pugh, Carnegie Institute of Technology

Session No. 5 - APPLICATION

Dr. J. J. Green, Canadian Armament Research and Development Establishment (CARDE)

Session No. 6 - APPLICATION

Dr. Ralph Sin, Army Materiel Command

Luncheon Address. "Continuing Horizons", by Mr. J. E. Trainer, Executive Vice-President, Firestone T & R Co.

Dinner Address by Dr. Abe Silverstein, Director, Lewis Research Center, NASA.

"Closing Remarks" by Dr. R. J. Eichelberger.

Discussions taking place during the Symposium were not transcribed.

A CRITIQUE OF ACCELERATOR TECHNIQUES
FOR HYPERVELOCITY IMPACT

by A. C. Charters

GM DEFENSE RESEARCH LABORATORIES
GENERAL MOTORS CORPORATION
Santa Barbara, California

CRITIQUE OF ACCELERATOR TECHNIQUES

ABSTRACT

The requirements for accelerator techniques are reviewed from the standpoint of their supporting role in the field of high velocity impact. The areas of interest to high velocity impact are noted and their various demands on accelerators are discussed. The performance of the accelerators now in use are critically evaluated in terms of their ability to meet these demands. Future expectations are summarized briefly.

CRITIQUE OF ACCELERATOR TECHNIQUES

LIST OF FIGURES

- Figure 1 Requirements of Mass, Velocity, Density and Shape for Projectiles for Military and Space Missions
- Figure 2 Plan of Experiment with Projectiles having Constant Mass and Varying Shape and Density
- Figure 3 Impact Range C
- Figure 4 Cross-sections of Craters from Impact Tests in Semi-infinite Aluminum (1100F) Targets with Projectiles of Constant Mass (0.32 gms) and Varying Shape and Density at Velocity of 6.5 km/sec
- Figure 5 Effect of Projectile Density on Depth of Penetration and Crater Volume: Projectile, mass = 0.32 gms, shape - sphere; Target, semi-infinite Aluminum (1100F)
- Figure 6 Effect of Projectile Shape on Depth of Penetration and Crater Volume: Projectile, Aluminum (2017), mass = 0.32 gms; Target, semi-infinite Aluminum (1100F)
- Figure 7 Accelerator Requirements for Armor Region of Military Missions
- Figure 8 Accelerator Requirements for Missile Region of Military Missions
- Figure 9 Light-Gas Gun Design
- Figure 10 Accelerator Requirements for Space Missions

CRITIQUE OF ACCELERATOR TECHNIQUES
INTRODUCTION

Techniques for the acceleration of projectiles to high velocity play an important part in advancing our knowledge of high velocity impact. Since this field of science is still largely empirical and a fully comprehensive theory has yet to be developed, the limits of the experiments mark out the boundaries of our understanding. These limits are determined in part by the performance of the accelerators.

Despite their importance, accelerators play a supporting role and represent a means for accomplishing the ends of the experiments. It is important to relate closely the requirements of the accelerators to the needs of the experiments.

The purpose of this paper is to review the performance of accelerators from the standpoint of the demands placed upon them to support the experiments and applications in the field of high velocity impact. **The areas of primary interest will be defined; the requirements for accelerator performance will be listed; the performance of existing accelerators will be criticized; the gap between the performance of existing accelerators and that desired to meet the needs of the field will be discussed.**

CRITIQUE OF ACCELERATOR TECHNIQUES

At this point, I wish to acknowledge the substantial assistance of my colleagues, Dr. C. J. Maiden, Mr. J. W. Gehring, and Mr. R. L. Warnica. It is appropriate to note that a critique inevitably involves subjective opinions to a certain extent, and for that I assume full responsibility. It is hoped that differences from the views of others will serve as a grindstone for sharpening our common understanding.

CRITIQUE OF ACCELERATOR TECHNIQUES

AREAS OF PRIMARY INTEREST

The areas of primary interest to this audience are: (1) the physics of impact, (2) the applications of impact to military weapons systems, and (3) the meteoroid hazard to space flight.

Physics of Impact

The physics of impact is concerned with the dynamics of impact such as projectile fragmentation, cratering, spalling, etc. It involves studies of the properties of materials at high stress and strain rates, of energy transformations and changes in state, and of other basic physical processes.

Military Applications

Impact has been used as a "kill mechanism" in warfare from man's earliest beginnings. The advent of high velocity impact in warfare began with the introduction of the shaped charge⁽¹⁾. Recently a new facet to the high velocity application has been added with the attack on missiles and satellites.

CRITIQUE OF ACCELERATOR TECHNIQUES

In discussing the requirements of accelerators for this area, it is convenient to classify the impact situation as active or passive. In the active situation, a high velocity projectile is hurled at a slow moving or stationary target; in the passive situation, a slow moving projectile is placed in the path of a rapidly moving target.

It is important to note that certain military applications extend the role of impact from that of a kill mechanism to that of a reconnaissance device. The consequences of the impact provide information on the nature of the target.

Meteoroid Hazard to Spacecraft

The latest area of interest to the field of high velocity impact is the meteoroid hazard to spacecraft⁽²⁾. The regions of space in the solar system near the plane of the ecliptic are populated with meteoroids - postulated to be the fragmentary debris of comets and planets. They move at very high velocities, and are sufficiently numerous so that the possibility of being struck by one is a serious hazard to spacecraft.

CRITIQUE OF ACCELERATOR TECHNIQUES

Our knowledge of meteoroids is limited but the evidence at hand suggests the following. In general, their composition is believed to range from a porous, pumice-like substance of meteoroids having a cometary origin to stone and iron for those meteoroids of planetary origin. They are probably irregular fragments for the most part. Their velocities range from roughly 10 to 80 km/sec. Their sizes range from elementary particles such as protons on the small side to asteroids with diameters of several kilometers on the large.

Fortunately for space flight, the meteoroid population is very sparse and the largest meteoroids are the rarest. Their numbers are roughly inversely proportional to their masses, the relation being according to Whipple (1957)

$$\phi = \frac{1.3 \times 10^{-12}}{m} \quad (1)$$

where ϕ is the flux per meter²-sec of particles above mass m in grams.

CRITIQUE OF ACCELERATOR TECHNIQUES

The meteoroid hazard is twofold. First, exposed surfaces - windows, thermal control surfaces, etc. - can be eroded by the small meteoroids and even by elementary particles (protons). Second, the hull of the spacecraft can be penetrated and components such as power plant radiators can be destructively damaged by meteoroids of sufficient size. The spacecraft must be protected against the largest meteoroid it is likely to encounter, taking into account the size of the spacecraft, the length of the journey, and the allowable risk. Three representative cases are summarized in the following table.

MISSION	DURATION days	PROBABILITY OF NO DESTRUCTIVE DAMAGE percent	VULNERABLE AREA (meters) ²	CRITICAL METEOROID MASS grams	CRITICAL METEOROID DIAMETER (Stone) mm
MOON	14	0.999	25	0.04	3
VENUS	320	0.999	25	0.9	9
MARS	500	0.999	25	1.4	10

The results of this table show that meteoroids weighing as much as one gram constitute a hazard to space flight.

REQUIREMENTS FOR ACCELERATORS

An accelerator is required to deliver a projectile of given mass at a specified velocity. The projectile may have certain requirements of shape, construction, and material. In addition, the accelerator design may be restricted by the conditions of its use.

Projectile Velocity and Mass

The velocities required by the physics of impact stretch from a few meters per second for impact in liquids to nearly 100 kilometers per second for the "natural" velocities of bodies in the solar system. Actually, the physics of impact is too broad a subject to set well defined limits on accelerator requirements.

A better definition of requirements is given by the application to warfare and the meteoroid hazard to spacecraft. The masses, velocities, densities, and shapes involved in these areas of interest are indicated in Figure 1. There is no attempt in this Figure to delineate the boundaries in precise detail; rather, the purpose here is to set forth the broad limits of masses, velocities, and projectile characteristics.

CRITIQUE OF ACCELERATOR TECHNIQUES

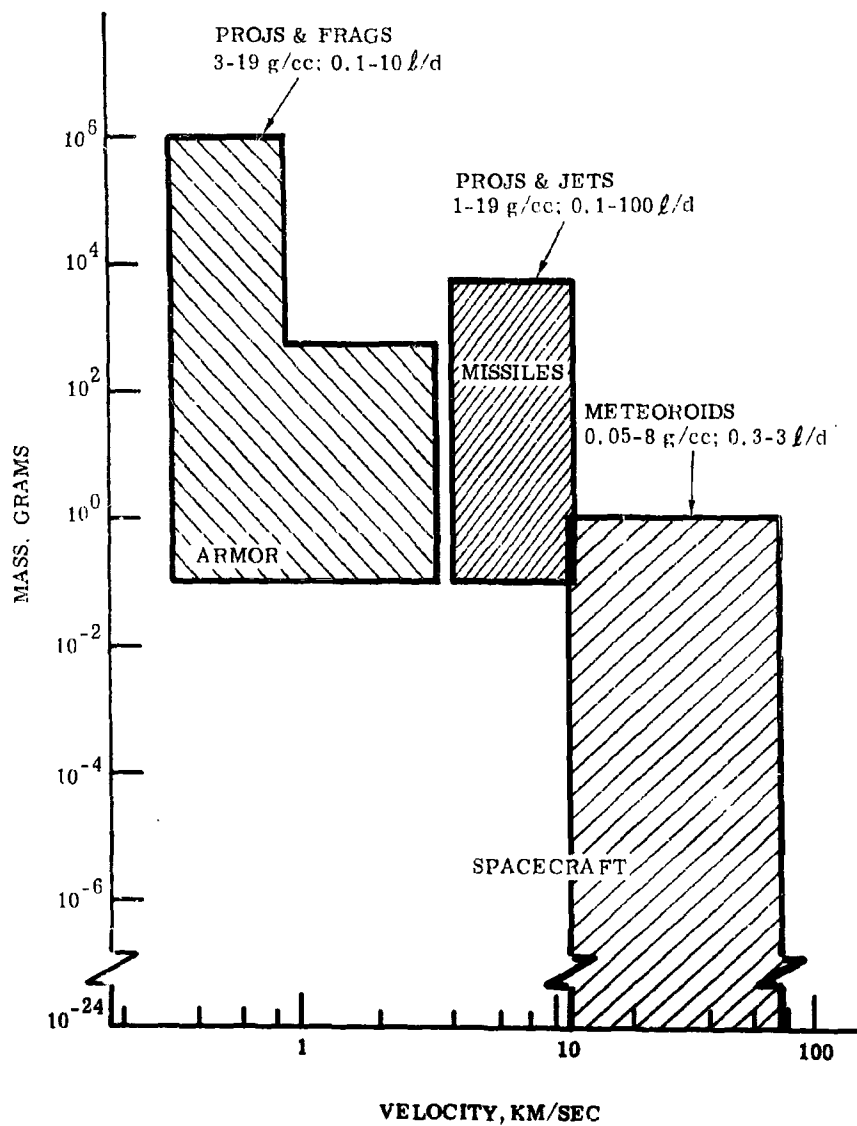


Figure 1 Requirements of Mass, Velocity, Density and Shape for Projectiles for Military and Space Missions

CRITIQUE OF ACCELERATOR TECHNIQUES

The results of this figure show that the masses and velocities divide rather naturally into three regions. The region labeled Armor relates to the attack on a relatively slowly moving target as typified by an armored tank or warship. All impact in this region belongs to the active situation. Both armor-piercing projectiles and HE shell fragments are included. The jets from shaped charges are also included in the Armor category. The masses and velocities of shaped charge jets overlap those in the Missiles region but this sub-region has been left unmarked for the purpose of clarity.

In the Missiles region, the military mission is the use of impact as a countermeasure against IRBMs, ICBMs, and satellites. The requirement for projectiles in this region involves both active and passive attack situations. In the attack situation, the important projectiles are jets and pellets fired by explosive accelerators. In the passive situation, the projectiles are placed in the path of the missile and depend primarily on the velocity of the missile for their impact action. The means of their delivery and distribution can be controlled so that wide variations in projectile design are possible and the projectile can be tailored to a certain extent to produce the effects desired in the particular engagement anticipated.

CRITIQUE OF ACCELERATOR TECHNIQUES

The projectiles of the Spacecraft region are the meteoroids. Their properties have been described earlier. These projectiles are the product of "nature" rather than "man". The requirement insofar as the accelerator is concerned is to launch projectiles similar in composition and velocity to meteoroids.

Projectile Density and Shape

Before giving a critique of accelerators, it is important to define the extent to which the shape of the projectile, its density, and other details of its construction determine the consequences of impact as well as the primary variables of mass and velocity. The projectile's configuration may well be a controlling factor in the selection of an accelerator.

There is common agreement that projectile properties are important in the Armor region. For example, experiments at the Ames Research Center show that at velocities of 2 km/sec both density and shape play a significant role in the impact of semi-infinite, ductile metal targets⁽³⁾. The effects of density can be seen from the Ames formula for spheres,

CRITIQUE OF ACCELERATOR TECHNIQUES

$$P = 2.8 \left(\frac{\rho_p}{\rho_T} \right)^{1/3} \left(\frac{m_p V^2}{\rho_T C^2} \right)^{1/3}$$

$$\text{Vol} = 34 \left(\frac{\rho_p}{\rho_T} \right)^{1/2} \left(\frac{m_p V^2}{\rho_T C^2} \right)$$

- where
- P = Depth of penetration
 - Vol = Crater volume
 - ρ_p = Projectile density
 - ρ_T = Target density
 - m_p = Projectile mass
 - V = Impact velocity
 - C = Bar speed of sound in target material
 - (C = 5.10 km/sec in aluminum)

The Ames data show that penetration varies with the cube root of density and that volume with the square root of density for spheres of constant mass at velocities in the neighborhood of 2 km/sec. In

CRITIQUE OF ACCELERATOR TECHNIQUES

other experiments at Ames, it was shown that varying the shape from a sphere to a rod increased both the depth of penetration and the crater volume.

The question here is whether density and shape are also important for the high velocity regions of missiles and spacecraft. Indirect evidence suggests that the importance of these variables diminishes with velocity, and some investigators have expressed the opinion that projectile density and shape have no influence on cratering at velocities greater than 6 km/sec. However, in my opinion, the evidence at hand was insufficient for a firm conclusion.

Recently, we have carried out an experiment at the GM Defense Research Laboratories⁽⁴⁾ to determine the effect of density and shape on cratering in semi-infinite ductile metal targets at a velocity of 6.5 km/sec. I will digress for a moment to describe the experiment and present the results.

The experiment consisted of firing projectiles of constant mass into semi-infinite targets of soft aluminum at a velocity of 6.5 km/sec.

The plan of the experiment is shown in Figure 2.

CRITIQUE OF ACCELERATOR TECHNIQUES

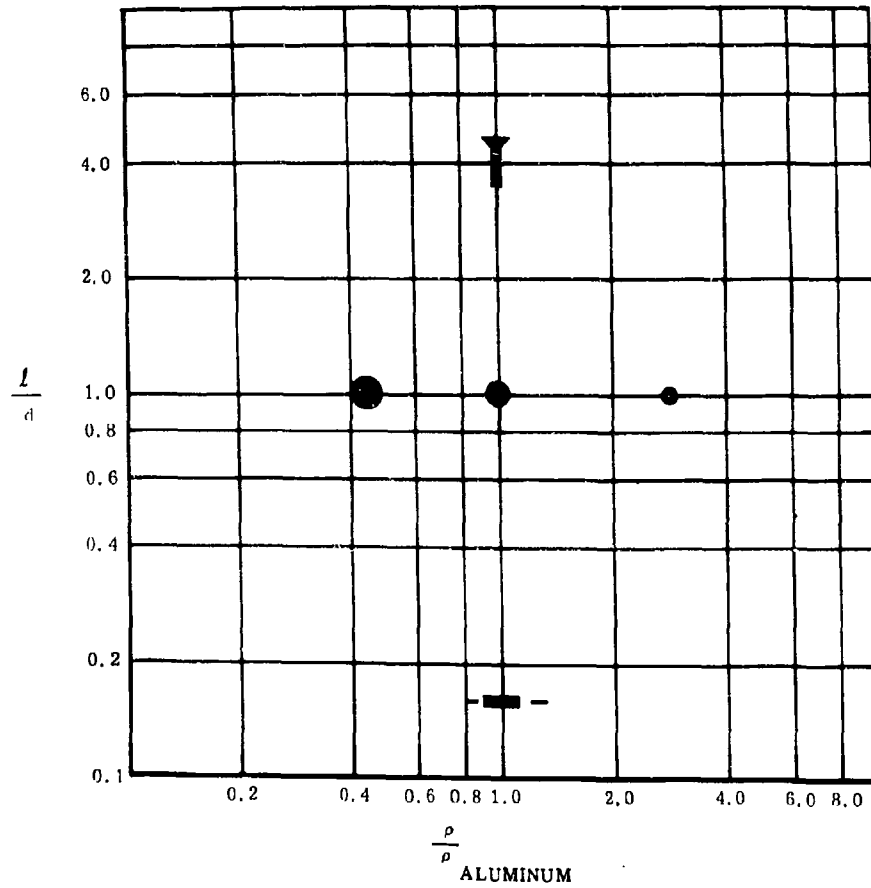


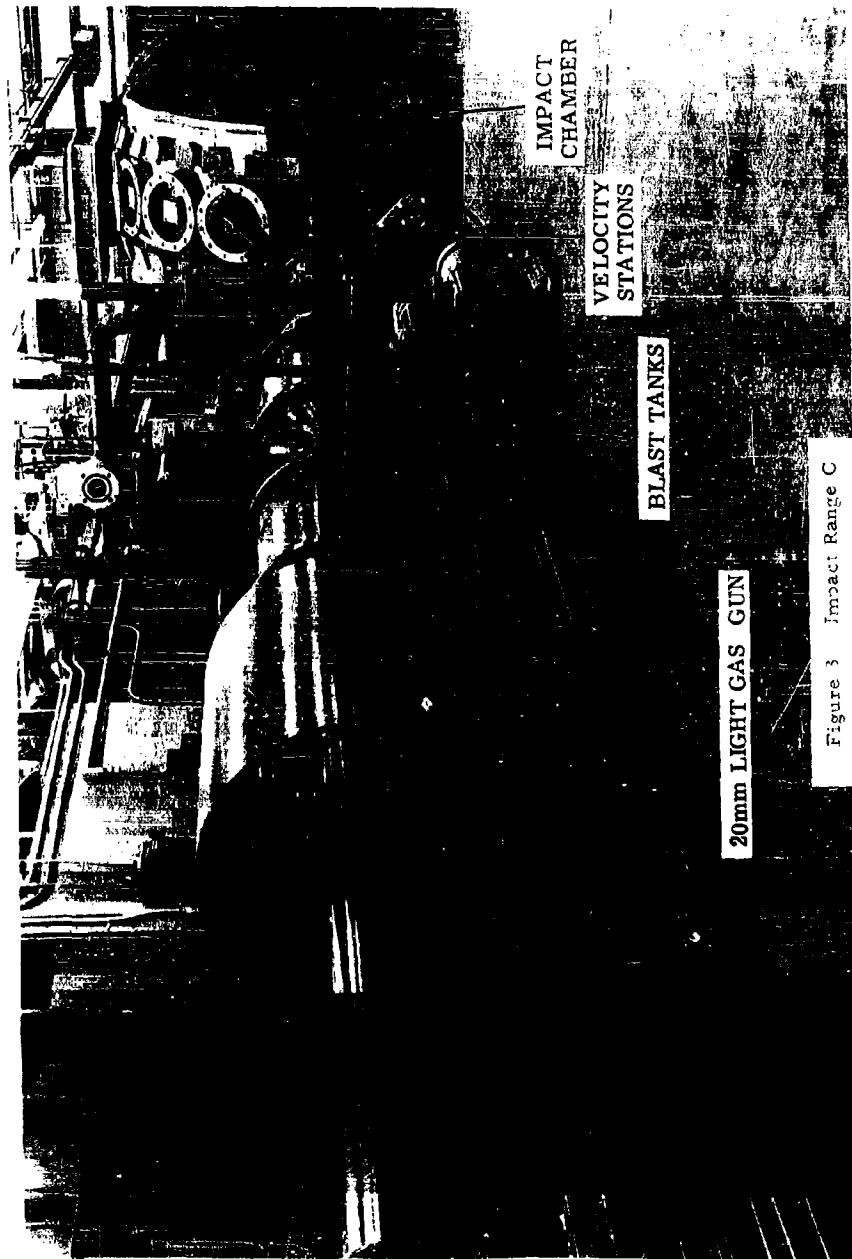
Figure 2 Plan of Experiment with Projectiles having Constant Mass of 0.32 gm and Varying Shape and Density

CRITIQUE OF ACCELERATOR TECHNIQUES

The basic projectile is an 0.32 gm aluminum sphere. In the first experiment, the density of the sphere was varied by changing the material from zelyx M to steel and adjusting the diameter to keep the mass constant. In the second experiment, the shape was varied by changing the projectile from a disc to a rod, making both from aluminum and keeping the mass constant. The targets were massive blocks of soft aluminum (1100F). All their dimensions were large compared to those of the craters so that their size was effectively semi-infinite.

The experiment was carried out in Range "C" of GM's Flight Physics Laboratory (see Figure 3). The apparatus consists of a 20 mm accelerated-reservoir light-gas gun, blast tanks, a flight test chamber, and an impact chamber. All projectiles were fired with segmented sabots, the segments of which separated on leaving the gun and were caught in the blast tank. The flight test chamber is equipped with two spark photography stations and cycle-counter chronographs, and their records gave the velocity and orientation of the projectile. The target was placed in the impact chamber with its face perpendicular to the flight direction. On the disc shot, a B&W framing camera movie was taken of the disc striking the target in order to record its orientation at impact.

CRITIQUE OF ACCELERATOR TECHNIQUES



CRITIQUE OF ACCELERATOR TECHNIQUES

The cross sections of representative targets are shown in Figure 4 (arranged in the format of Figure 2). Silhouettes of the projectiles are superimposed on the photographs and all are reproduced in correct relative scale. It is clear that the crater dimensions vary with both density and shape.

The effect of density on penetration and volume is shown in Figure 5. Both quantities are seen to change significantly with variation in density. The variation in both penetration and volume may be given by a power law with the exponent for penetration being 0.22 and for volume 0.16. These results suggest formulae for penetration and volume at 6.5 km/sec that are similar to the Ames formulae for impact at 2 km/sec, namely

$$P = 3.0 \left(\frac{\rho_p}{\rho_T} \right)^{0.22} \left(\frac{m_p V^2}{\rho_T C^2} \right)^{1/3}$$

$$\text{Vol} = 43 \left(\frac{\rho_p}{\rho_T} \right)^{0.16} \left(\frac{m_p V^2}{\rho_T C^2} \right)$$

CRITIQUE OF ACCELERATOR TECHNIQUES

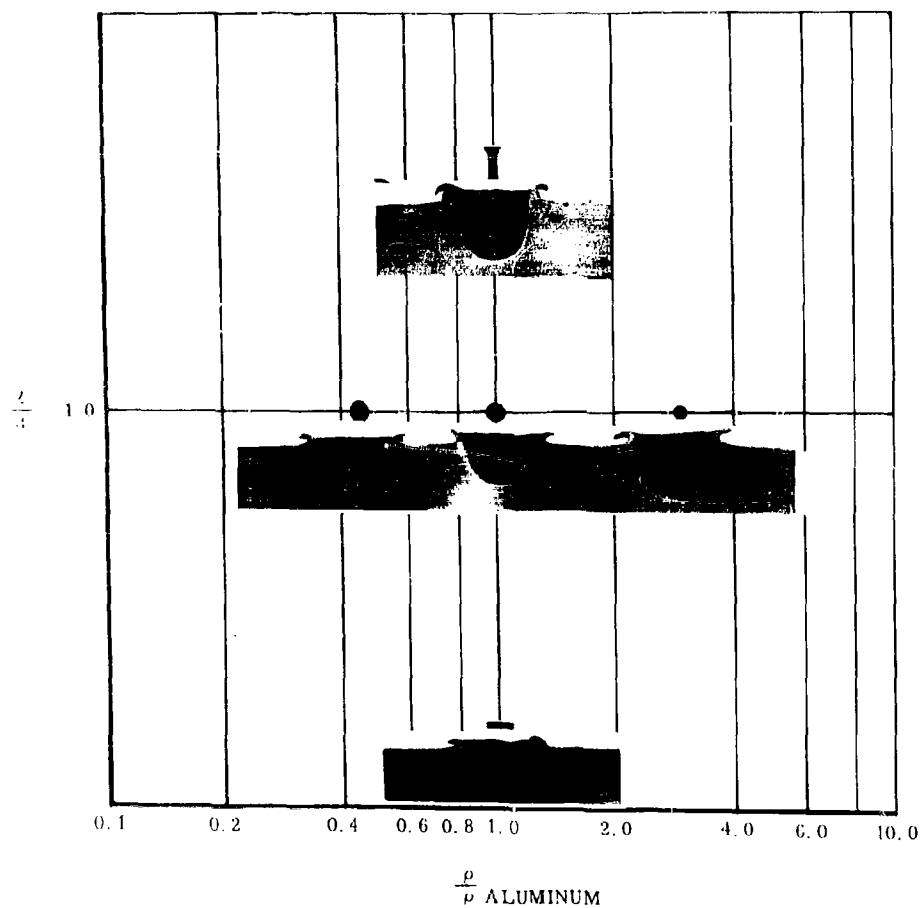


Figure 4 Cross-sections of Craters from Impact Tests in Semi-infinite Aluminum (1100F) Targets with Projectiles of Constant Mass (0.32 gm) and Varying Shape and Density at Velocity of 6.5 km/sec

CRITIQUE OF ACCELERATOR TECHNIQUES

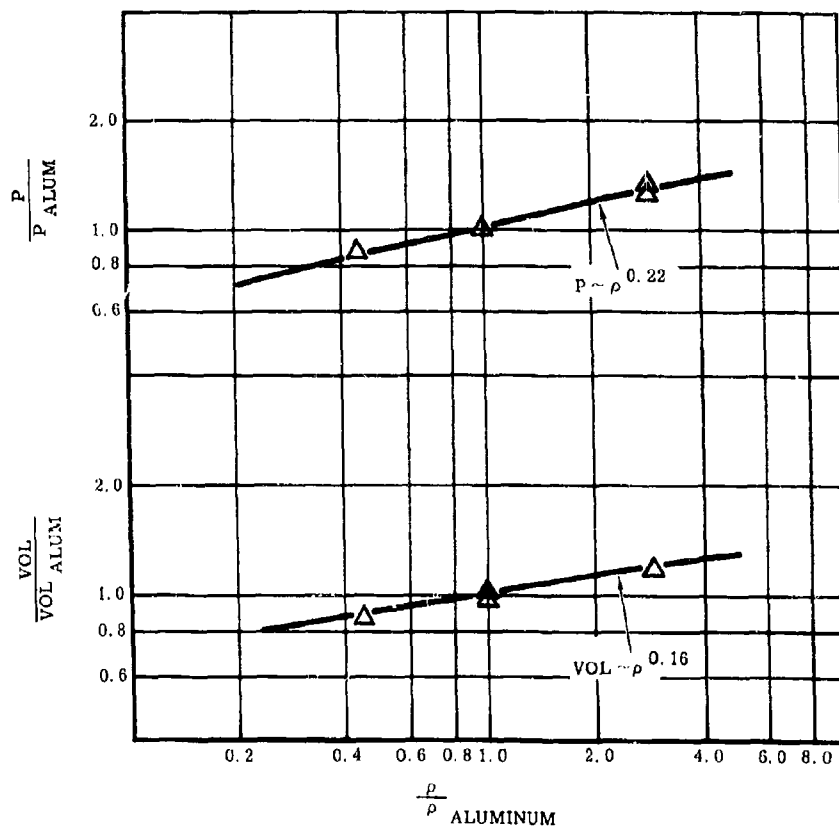


Figure 5 Effect of Projectile Density on Depth of Penetration and Crater Volume. Projectile: mass - 0.32 gm, shape = sphere; Target: semi-infinite Aluminum (1100F); Velocity = 6.5 km/sec

CRITIQUE OF ACCELERATOR TECHNIQUES

These results demonstrate that the depth of penetration and the volume of the crater do vary significantly with the density of the projectile at a velocity of 6.5 km/sec.

It is also correct that the variation at 6.5 km/sec is not as great as that at 2 km/sec. Comparison with the Ames results shows that the exponent of the power law has decreased from 0.33 to 0.24 for penetration and from 0.50 to 0.16 for volume with increases in velocity from 2 to 6.5 km/sec. Nevertheless, density is still a significant variable at 6.5 km/sec. For example, these results predict that the penetration of a tungsten sphere will be nearly twice that of a plastic sphere having the same mass.

The effects of the projectile shape on penetration and volume are shown in Figure 6. Both the penetration and volume are seen to increase significantly with increase in fineness ratio. The penetration of the rod (fineness ratio 4 to 1) is nearly double that of the disc (fineness ratio 1 to 6). These results demonstrate that the shape of the projectile is also an important variable in impact at 6.5 km/sec.

CRITIQUE OF ACCELERATOR TECHNIQUES

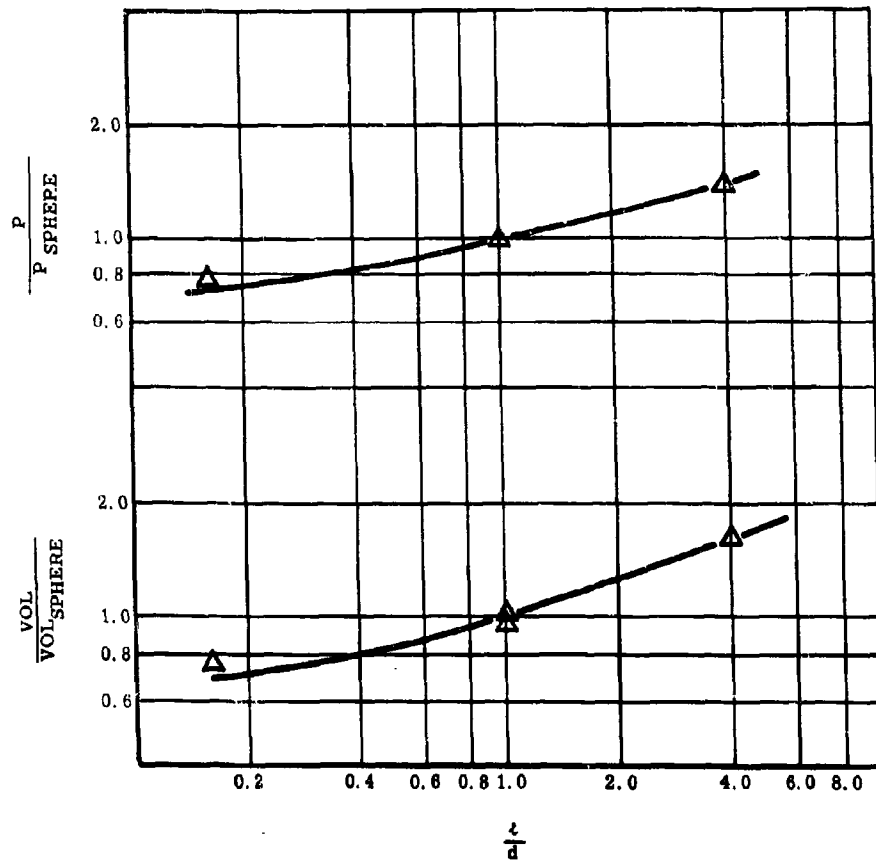


Figure 6 Effect of Projectile Shape on Depth of Penetration and Crater Volume. Projectile: Aluminum (2017), mass = 0.32 gm; Target: semi-infinite Aluminum (1100F); Velocity = 6.5 km/sec

CRITIQUE OF ACCELERATOR TECHNIQUES

In my opinion, the results of these experiments show conclusively that the configuration of the projectile must be taken into account as well as its mass and velocity for all military missions. To illustrate this point, consider the problem facing the designer of an ICBM who must take steps to protect its warhead from an impact kill. He plans to use a massive metallic shield. His reconnaissance tells him that the enemy expects to use tungsten rods; he also knows the mass and fineness ratio of the rods. He has available to him the results of impact tests of aluminum discs on metallic shield structures. Assuming that the effects of density and shape are unimportant, he designs the thickness of his shield to prevent penetration on the basis of these tests by using the penetration of aluminum discs having the same mass as that known for the enemy's tungsten rods. He will be sadly misled. The penetration of tungsten rods will actually be several times that of aluminum discs having the same mass. If the fineness ratio of the rod is 10 to 1 and of the disc is 1 to 6, the shield thickness required to prevent penetration of the tungsten rod must be nearly three times greater than that needed to stop the same weight aluminum disc.

CRITIQUE OF ACCELERATOR TECHNIQUES

The importance of the projectile's shape and density to military missions is based on the impact in semi-infinite targets. On the other hand, the projectile's configuration is equally important for impact in multiple, thin-sheet targets. Evidence to this effect will be given in a subsequent paper at this symposium⁽⁵⁾.

Are density and shape effects still important at the velocities of 10 to 80 km/sec involved in the meteoroid hazard to spacecraft? Comparison of results at 6.5 with those at 2 km/sec certainly suggests that the effect of the projectile's configuration will be less in the Spacecraft region, but how much less is a moot point. In view of our limited knowledge of meteoroids, it is my opinion that engineering estimates of meteoroid impact can be made satisfactorily on the basis of mass and velocity alone. Nevertheless, the real answer to this question depends on precise experimental data obtained at the velocities in question.

Environmental Restrictions on Accelerator Design

The third requirement for accelerators is the restriction that the environment places on their use. For use as a weapon, weight is

CRITIQUE OF ACCELERATOR TECHNIQUES

usually at a premium and accuracy of fire and precision of timing may be critical. On the other hand, if the accelerator is to be used as a laboratory launcher, weight is usually not a large factor, and accuracy of aim and precision of timing, while important, are often not critical. The significance of these will appear in the following section.

CRITIQUE OF ACCELERATOR TECHNIQUES

Military Mission: Armor Region

The requirements of mass and velocity for the Armor Region alone are shown in Figure 7 (including shaped charge jets). The limits marked by the solid lines reflect not only the requirements based on target-kill but also the current performance of guns and HE shells, a consequence of the existing balance between offense and defense. Many improvements are needed for the accelerators of this region, but only two need concern this symposium.

The first is the traveling charge gun: This accelerator combines the advantages of a gun and a rocket. Although it holds forth the

CRITIQUE OF ACCELERATOR TECHNIQUES

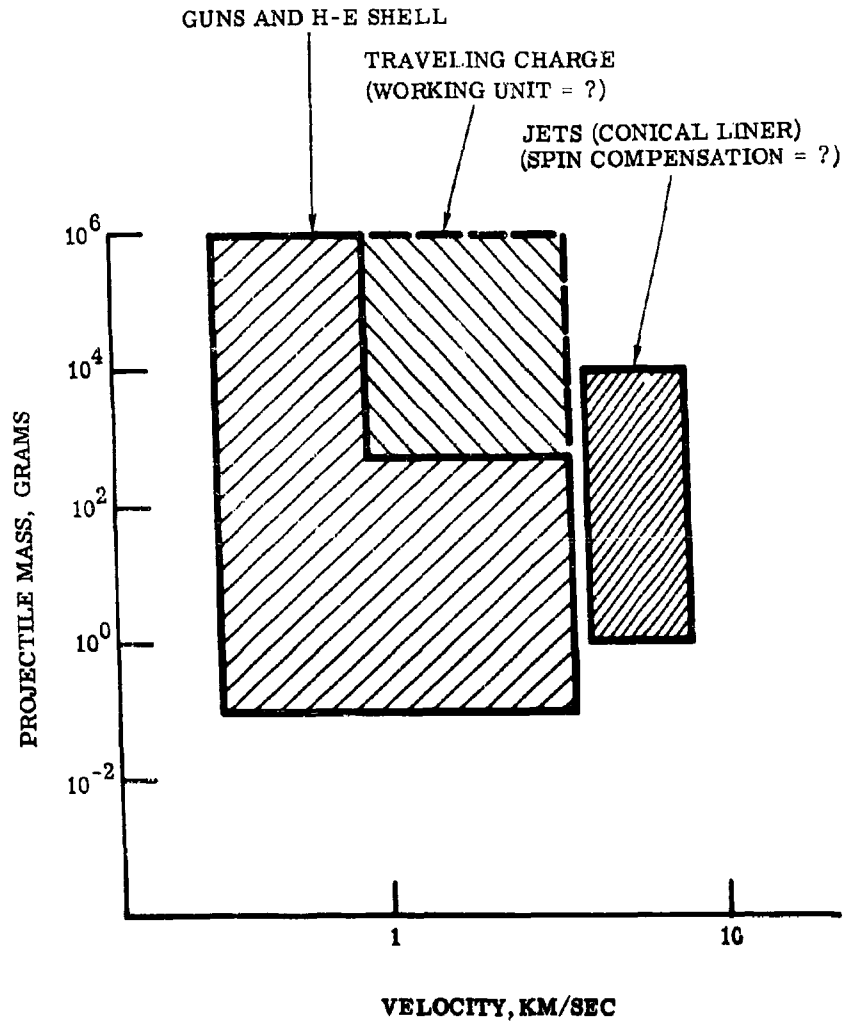


Figure 7 Accelerator Requirements for Armor Region of Military Missions

CRITIQUE OF ACCELERATOR TECHNIQUES

promise of increasing the velocities of guns by improving their ballistic efficiency, proper functioning of the charge requires a burning rate orders of magnitude greater than that of ordinary nitrocellulose propellants⁽⁶⁾. A suitable propellant has not yet been developed.

I refer to the traveling charge gun as the psychotic weapon. It has been analyzed at great length but the technical detail of inventing a fast-burning propellant has remained the stumbling block. If the traveling charge can be gotten out of analysis and into the cannon, something may come of it yet.

The second is spin compensation for shaped charge jets. Good progress has been made in developing methods of spin compensation for low spin rates, but compensation for high spin rates still remains a problem. Spin stabilized shells have advantages in accuracy of fire and simplicity of construction, and a method of spin compensation permitting a marriage of the shaped charge with ordinary artillery shell would represent a significant advance.

CRITIQUE OF ACCELERATOR TECHNIQUES

Military Mission: Missile Region

The use of impact in the Missile and Satellite Region of the military mission is a subject of more immediate concern to this symposium. The approach to the requirements of this Region is diagrammed in Figure 8. I will consider four situations distinguished by, first, the attack being either active or passive and, second, the accelerator being used as a weapon or for experiment and test in the laboratory, and will limit my critique to making a "best choice" of accelerator for each of the four situations.

Consider, first, the active attack with the accelerator used as a weapon. Here, an explosive with a pellet or jet is a "best choice". An explosive gives the maximum ratio of projectile to accelerator weight. It can also fire a projectile on a precise timing signal and with reasonable accuracy.

Consider, second, the active attack with the accelerator used for experiment and test. Here again, the explosive with a pellet or jet is a "best choice". By testing the same explosive-pellet combination used in the AM missile warhead, one duplicates the actual attack

CRITIQUE OF ACCELERATOR TECHNIQUES

ATTACK	USE	OPTIMUM ACCELERATOR	COMMENTS
ACTIVE	WEAPON	EXPLOSIVE WITH PELLETT OR JET	1-MAXIMUM RATIO OF PROJECTILE TO ACCELERATOR WEIGHT 2-PRECISE TIMING AND AIM
	EXPERIMENT AND TEST	EXPLOSIVE WITH PELLETT OR JET	1-SAME PELLETT OR JET USED IN WEAPON 2-VELOCITY TOO LOW BY INCREMENT DUE TO ENGAGEMENT VELOCITIES OF MISSILES
PASSIVE	WEAPON	AM MISSILE WITH PROJECTILES DISPERSED FROM WARHEAD	1-OPTIMUM PROJECTILE CONFIGURATION FOR KILL OF SPECIFIED TARGET 2-VELOCITY SUPPLIED BY ENGAGING MISSILES
	EXPERIMENT AND TEST	LIGHT-GAS GUN	1-SAME CONFIGURATION (MASS, MATERIALS, SHAPE) OF PROJECTILES USED IN WEAPON 2-VELOCITY TOO LOW, SINCE 6 TO 8 KM/SEC IS PRESENT MAXIMUM FOR COMPLEX PROJECTILE CONFIG

Figure 8 Accelerator Requirements for Missile Region of Military Missions

CRITIQUE OF ACCELERATOR TECHNIQUES

situation in his laboratory experiment - a highly desirable objective. The velocity may be lower in a static test than in an engagement, and how to make this up is one of the problems. Incidentally, it should be noted that a light-gas gun can be used as an alternate choice if test conditions preclude the use of explosives.

Consider, third, the passive attack with the accelerator used as a weapon. Here the "best choice" is a projectile, or rather, a group of projectiles dispersed from the warhead of an AM missile. This system takes advantage of the velocity of the ICBM and the high-speed missile, since the energy of the impact is supplied by the velocities of the missiles. Great subtlety and sophistication can be designed into the construction of the projectile so that it can be tailored to provide the most effective kill mechanism for the particular mission in question.

Consider, fourth, the passive attack with the accelerator used for **experiment and test. Here the "best choice" is a light-gas gun. Experience indicates that this is the only accelerator capable of firing projectiles with the complex shape and construction involved**

CRITIQUE OF ACCELERATOR TECHNIQUES

in the passive attack situation⁽⁴⁾. The problem is that the velocities of light-gas guns are a little low at the moment, since it is possible to fire complex projectiles at velocities from only 6 to 8 km/sec. Here is the challenge for further development.

Comments on the Performance of Light-Gas Guns

In order to illustrate the performance of light-gas guns and to thereby set up some standards for their selection, it is instructive to carry out a short design exercise, as follows: Design a gun for firing a 1 gm steel sphere to 8 km/sec. The procedure is sketched in Figure 9. The basic equation relates the kinetic energy to the work done. The maximum pressure is determined by the strengths of projectile and sabot; a value of 30,000 psi is possible. The ratio of average to maximum pressure is given by the ballistic efficiency of the gun; I have chosen an efficiency of 1/2, a high value for most guns. The area, A , is the cross-sectional area of the projectile. The diameter, D , is the caliber of the gun. The $\frac{L}{D}$ ratio is the length of the gun in calibers; experience indicates that a value of 300 is reasonable without incurring too severe losses from bore friction

PROBLEM
 DESIGN A GUN TO ACCELERATE A 1 GRAM
 STEEL SPHERE TO 8 KM/SEC

EQUATION

$$\frac{1}{2} m V^2 = \bar{p} A L = p_{\max} \left(\frac{\bar{p}}{p_{\max}} \right) A \left(\frac{L}{D} \right) D$$

GIVEN
 $m = 1$ gram
 $A = 0.31$ cm²
 $\frac{L}{D} = 300$
 $V = 8$ km/sec
 $p_{\max} = 30,000$ psi
 $\frac{p_{\max}}{p} = 2$

FIND
 D = GUN CALIBER

SOLUTION

$$D = \left(\frac{m V^2}{2 A p_{\max}} \right) \left(\frac{p_{\max}}{p} \right) \left(\frac{D}{L} \right)$$

D = 34 mm and L = 10 meters

Figure 9 Light-Gas Gun Design

CRITIQUE OF ACCELERATOR TECHNIQUES

and boundary layer effects. The problem is to determine the caliber of the gun, D .

The solution to the problem is indicated. The basic equation has been recast in suitable form. Putting in the given conditions, we obtain a caliber of 34 mm and a length of gun barrel of 10 meters.

From my experience, these gun dimensions are reasonable for firing a 1 gm steel sphere at 8 km/sec. They are in agreement with the general observation that a large gun is required to fire a small projectile with a high density of loading, that is, a high value of mass to area ratio due to high density or high fineness ratio.

It should be noted that the ballistic efficiency plays a controlling part in determining the gun's performance. The size of gun required to launch a particular projectile will vary inversely with the value of the ballistic efficiency. Conversely, if one has a given gun, the velocity with which he can fire a particular projectile will be a direct function of the gun's ballistic efficiency.

CRITIQUE OF ACCELERATOR TECHNIQUES

In our experience, the best choice of light-gas gun is the accelerated-reservoir gun. It has a high ballistic efficiency. Also, pressure is applied to the base of the projectile in a relatively gentle manner and this avoids shock waves being set up in the projectile itself. Our experience with accelerated-reservoir guns has been very favorable in this respect. We have been able to launch slender conical bodies at velocities of 6 km/sec without damage to the projectile. Other models, more rugged, although still relatively fragile, such as glass spheres, have been launched at velocities in excess of 8 km/sec.

Accelerator Requirements for Space Mission

The accelerator requirements for the space mission are shown in Figure 10. The projectiles for this region are the meteoroids. The task required of the accelerator is to fire simulated meteoroids at flight velocities up to 80 km/sec. In a certain sense, man is competing with nature and he finds this a challenging experience.

Only two types of accelerators to date have been able to penetrate this region. Explosives with fast jets have fired projectiles up to

CRITIQUE OF ACCELERATOR TECHNIQUES

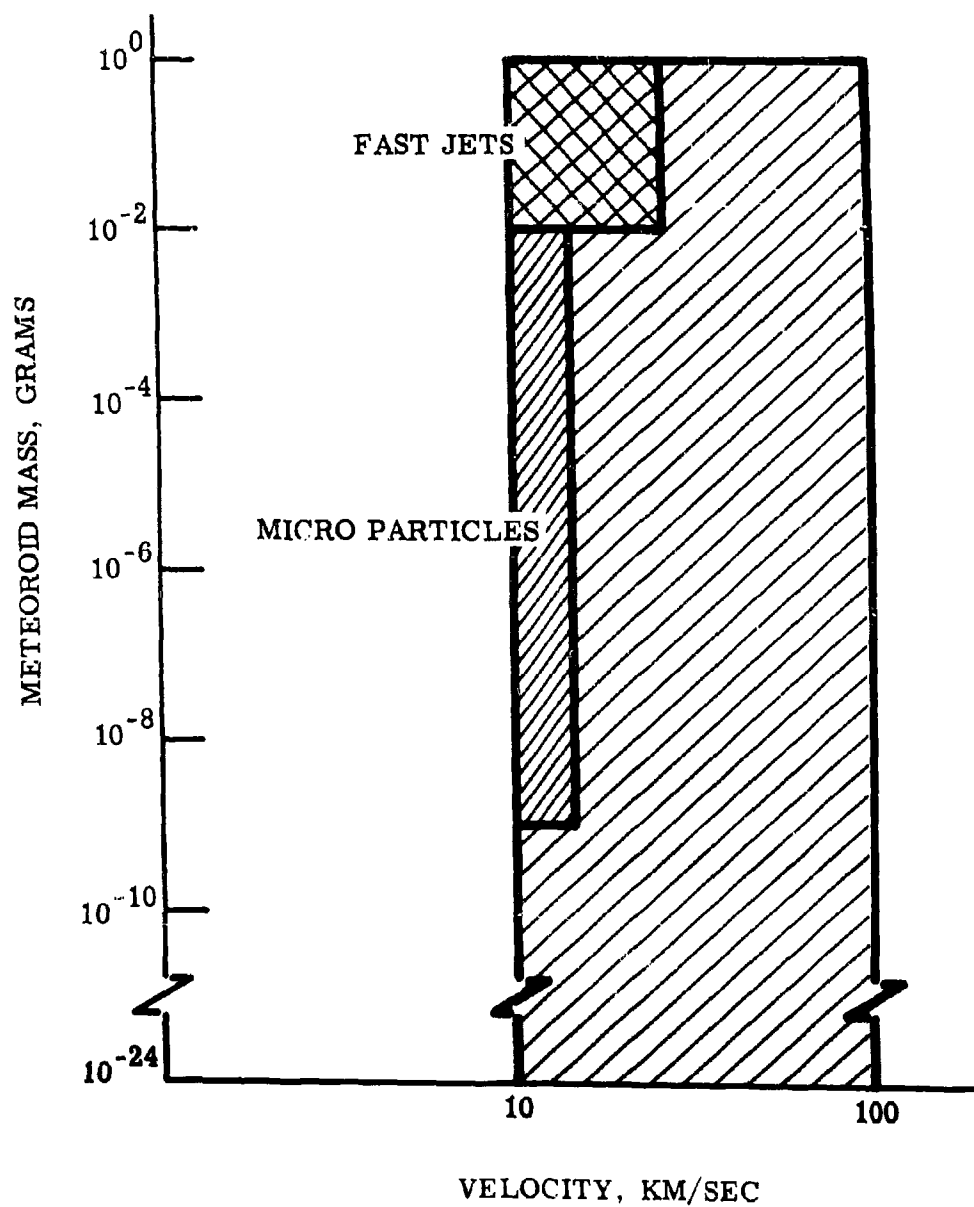


Figure 10 Accelerator Requirements for Space Missions

CRITIQUE OF ACCELERATOR TECHNIQUES

velocities of about 25 km/sec with masses ranging from 0.01 to 1.0 gm⁽⁷⁾. Other explosive devices have fired microparticles with masses from 10^{-9} to 10^{-2} gm at velocities up to 15 km/sec⁽⁸⁾.

Other types of accelerators for launching projectiles at meteoroid velocities are currently under development, such as the explosive foil gun⁽⁹⁾ and the electrostatic accelerator⁽¹⁰⁾. These devices show promise but at the moment they are still in the experimental stage. There are certain problems in their functioning and uncertainties in their results which must be overcome before they can be considered fully operational.

The development of an accelerator to study the meteoroid hazard is the most severe problem now facing the experimenter. The velocities of the fastest existing accelerators, the fast-jet explosives, must be tripled before the Spacecraft Region can be covered. Also, explosives are limited in the choice of materials which they can fire so that accelerators need to be developed which can handle projectiles of variable shape and density. It seems likely that these shape and density effects may be less important in the Spacecraft Region but a direct experiment is needed to test this point.

CRITIQUE OF ACCELERATOR TECHNIQUES

CONCLUDING REMARKS

To summarize, the picture with respect to the accelerators for military missions is reasonably bright. In the Armor Region, accelerators appear to be able to meet the requirements of mass and velocity, with improvements being desired in the traveling charge gun and in the spin compensation of shaped charge jets for use with artillery projectiles.

In the Missile Region, the status of accelerators is not quite as good as in the Armor Region, but the requirements here are not too far beyond the capabilities of existing accelerators. Explosives producing higher velocities are always desirable but perhaps the greatest improvement here is needed in the invention of devices for achieving better control of aim and timing of fire. Light-gas guns require further development in order to increase their performance to the point of firing complex projectiles at velocities of 10 km/sec and higher. Also, improvements in the design are desirable so that heavier projectiles can be fired without undue difficulty. Fortunately, the developments needed in this area fall almost within, or perhaps just beyond, the state-of-the-art.

CRITIQUE OF ACCELERATOR TECHNIQUES

The greatest challenge for the development of accelerators comes from the Spacecraft Region. To duplicate the flight characteristics of meteoroids has proven a difficult task indeed. At the moment, guns do not have velocities reaching into the Spacecraft Region, and, although improvements in velocity may be expected, they will probably be able to penetrate only the lower velocity part of the Spacecraft Region. Explosive accelerators have made some inroads on this region, but the maximum velocities are still low by a factor of 3. Also, they have limited capabilities for firing projectiles with variable shape and density. Other devices, such as the explosive foil gun and the electrostatic accelerator are under development but not yet fully operational. A vigorous effort will be needed to develop accelerators that are fully adequate to explore the conditions of impact significant to the meteoroid hazard to spacecraft.

In conclusion, let me remark that a balanced effort is desired in the development of improved accelerators. **The requirements for the space mission are the most challenging but those for the military missions are equally important. There are substantial rewards in both areas to be derived from the improvement of accelerators and the invention of new techniques.**

CRITIQUE OF ACCELERATOR TECHNIQUES

REFERENCES

1. Garrett Birkhoff, Duncan P. MacDougall, Emerson M. Pugh, and Sir Geoffrey Taylor, "Explosives with Lined Cavities," J. Appl. Phys., Vol. 19, No. 6, Jun. 1948, pp. 563-582.
2. C. J. Maiden, "Meteoroid Impact", General Motors Defense Research Laboratories, TM63-203, Apr. 1963.
3. A. C. Charters and J. L. Summers, "High Speed Impact of Metal Projectiles in Targets of Various Materials," Proc. of Third Hypervelocity Impact Symposium, 1960.
4. A. C. Charters and J. S. Curtis, "High Velocity Guns for Free-Flight Ranges," Chapter 19, The High Temperature Aspects of Hypersonic Flow, Pergamon Press (in press).
5. D. R. Christman, J. W. Gehring, K. N. Kreyenhagen, R. B. Mortenson, W. H. Dittrich, "Lethality of Hollow Spheres (U) (Secret)," Proc. of Sixth Hypervelocity Impact Symposium, 1963.
6. P. G. Baer and H. C. Smith, "Interior Ballistics of Hypervelocity Projectors Instrumented Light-Gas Gun and Traveling Charge Gun," Proc. of Fifth Hypervelocity Impact Symposium, 1962.
7. S. Kronman and J. H. Kineke, Jr., "Explosive Devices for Projecting Hypervelocity Pellets up to 21.0 km/sec (C)," Proc. of Fifth Hypervelocity Impact Symposium, 1962.
8. J. W. Gehring and L. G. Richards, "Further Studies of Micro-particle Cratering in a Variety of Target Materials," Proc. of Fourth Hypervelocity Impact Symposium, 1960. See also Ballistic Research Laboratories Report No.'s: 1134, 1286, and 1380.
9. Victor E. Scherrer, "Effects of Hypervelocity Impacts on Materials" Wright-Patterson Air Force Base, Air Force Systems Command, Aeronautical Systems Division, Directorate of Materials & Processes, ASD-TDR-62-762 (Prepared under contract No. AF 33(616)-8423), Aug. 1962.
10. J. F. Friichtenicht, "Experiments with a Two-Million Volt Electrostatic Accelerator," Proc. of Fifth Hypervelocity Impact Symposium, 1962.

EXPERIMENTAL AND THEORETICAL STUDIES ON THE INTERIOR BALLISTICS
OF LIGHT GAS GUNS

Paul G. Baer
Horace C. Smith

USA BALLISTIC RESEARCH LABORATORIES
ABERDEEN PROVING GROUND, MARYLAND

BALLISTICS OF LIGHT GAS GUNS

TABLE OF CONTENTS

Abstract	43
Introduction	44
Theoretical Task	44
Experimental Program	56
Experimental Results (Small Gun)	59
Large 37 mm .50 Cal Light Gas Gun	61
Discussion	63
References	64
Appendix I	65
Appendix II	71
Appendix III	74
Glossary	73

BALLISTICS OF LIGHT GAS GUNS

ABSTRACT

This paper reports the progress of a theoretical and experimental investigation designed to improve the performance of two stage light gas guns used as hypervelocity launchers. Two theories, which have been programmed for the BRLESC digital computer are discussed. Predictions resulting from the application of the two theories are compared with experimental results obtained from a small, highly instrumented light gas gun. The design of a longer, high performance light gas gun capable of accelerating one gram projectiles to velocities in excess of 20,000 f/s is discussed.

BALLISTICS OF LIGHT GAS GUNS

INTRODUCTION

This paper reports the progress of a theoretical and experimental interior ballistic program, being conducted in the Interior Ballistics Laboratory, which is designed to improve the performance of light gas guns used as hypervelocity launchers.

Two reports on this topic have been presented at the 4th and 5th Hypervelocity Impact Symposia^{1,2} respectively, thus this paper brings the developments reported at those two meetings up to date.

The current program being conducted by this laboratory is divided into two parallel tasks:

1. Task 1 has as its objective, the development of theoretical models of light gas guns; these models when set up on a digital computer will enable one to predict the performance of any size or type of light gas gun and in addition gain some insight into the performance capability of a particular model of gun. In addition these programs can be used to determine the upper velocity limit attainable in a light gas gun.
2. Task 2 has as its objective, the experimental confirmation of theoretical predictions obtained from these light gas gun models.

THEORETICAL TASK

As mentioned in the 5th Symposium Report², four mathematical models have been studied in this investigation. They are;

1. Charters method
2. Adiabatic compression model
3. Mass point model (Richtmyer Von Neuman "q" method)
4. Method of characteristics

All four of the models have been programmed for the ORDVAC and BRLESC digital computers, and many cases have been computed using each of the models. The assumptions used in each of the models are listed in Table 1 of the 5th Symposium Report².

BALLISTICS OF LIGHT GAS GUNS

Currently Charter's method is not being used in this program because of the limiting assumptions in the method. The method is good for a preliminary look at a large class of light gas guns, but for detailed studies, the method has its limitations.

The method of characteristics is a very powerful method for studying gas dynamics and has been used extensively by investigators in the past. Unfortunately, this essentially graphical method is difficult to program for a digital computer, and if any shock waves are formed in the process the programming becomes very difficult indeed. A characteristics program simulating a light gas gun was set up on the ORDVAC computer, but we were unable to complete the program because of lack of memory space due primarily to logical difficulties in locating the shock wave position.

The adiabatic compression model uses a set of simultaneous ordinary non-linear differential equations to simulate the light gas gun. These equations are integrated numerically with time as the independent variable on the computer to give a table of the variables of interest (pressure, displacement velocity, etc.) for even increments of time. The mathematical development of these equations and the assumptions used are discussed in Appendix I. This model has been used extensively to predict the performance of the laboratory's experimental light gas gun which is of the heavy piston type (piston velocity subsonic with respect to compressed gas.)

The mass point model, the most useful of the four systems discussed here, represents the gas column between the piston and the projectile by a series of mass points possessing volume, temperature and pressure characteristics. The equations used in this model have been derived from those used by Richtmyer and Von Neumann in the "q" method. These equations, their development, and the assumptions used are presented in Appendix II. Computer solutions to the problem describe the motion of the mass points as they are compressed and expanded in the light gas gun cycle. This model consequently accounts for pressure gradients and shock waves in the gas column.

It has been found that the adiabatic compression model is most closely applicable to light gas guns which use heavy pistons; that is the piston, for most of its travel in the pump tube, moves at a velocity which is subsonic to the velocity of sound in the gas being compressed. This has been confirmed in the close agreement between predicted and experimental results observed in guns of the heavy piston type.

BALLISTICS OF LIGHT GAS GUNS

The mass point model is applicable to light gas guns which use either light pistons (velocity of piston is generally supersonic with respect to the gas being compressed for a major portion of the compression cycle) or heavy pistons. Thus the model is of greater generality in simulating the flow of gas in the light gas gun and thus the overall performance of the gun.

It is interesting to compare the results obtained from the two models when the piston weight and propellant charge weight for a particular light gas gun configuration is changed such that the piston velocity changes from subsonic flow to supersonic flow. The particular gun chosen for this model study is the large 37 mm .50 cal light gas gun now under construction in this laboratory. Figure 1 is a sketch of the guns used in this model test. It will be noticed that gun used in the adiabatic model run does not have a tapered nozzle. This is because the mass flow rate through the nozzle used in this model depends only on the area ratio between the pump tube and launch tube. The guns are the same in that the initial pump tube volumes are equal.

The results of the computations using both the mass point model and the adiabatic compression model are shown in Figure 2. In this figure the maximum helium pressure developed in the pump tube and the muzzle velocity of the projectile are plotted as a function of piston weight and propellant charge weight.

In Table 1 additional information is given for these computer runs. It will be noticed that the difference between the mass point and adiabatic compression codes is slight at low propellant charge weights. In these runs the pressure gradients observed in the mass point method were slight. At the high propellant charge weight the piston velocity was higher and thus shock waves as well as severe pressure gradients should emphasize the difference between the mass point method and the adiabatic compression method as indeed it does.

The mass point method was also used in the design of the propellant burning chamber of the light gas gun currently under construction. Since it was proposed in the design of the gun to attain high temperatures in the light gas by shock heating, it was important to design a propellant burning chamber which would be capable of accelerating a light piston to a maximum velocity of 7000 - 8000 f/s. A modification of the mass point model was set up on the computer to examine the characteristics of propellant chambers of varying shape. This modification consisted of dividing the gas column between the breech end of the chamber and the base of the piston into 50 mass points. This

BALLISTICS OF LIGHT GAS GUNS

TABLE 1

Piston weight lb.	C _A lb.	P _{He} initial psi	Mass Point			Adiabatic Comp.		
			P _{max}	P _{He max}	V _{max} f/s	P _{max}	P _{He max}	V _{max} f/s
.5	.4	400	35,421	183,722	22,592	34,322	151,419	26,921
1.5	.4	400	40,602	209,614	20,015	40,385	232,131	30,619
3.0	.4	400	44,348	183,579	20,643	44,320	223,225	28,192
0.5	.1	400	7769	14,032	7879	7647	10,232	7,413
1.5	.1	400	8,427	14,590	8,816	8,400	10,713	8126
3.0	.1	400	8,918	13,050	8,578	8,882	10,422	8,003

BALLISTICS OF LIGHT GAS GUNS

gas column consisted of propellant gas which had burned out in the chamber before the piston started to move. At time zero the piston was allowed to move. Pressure and velocity profiles were computed in the gas column at each time step until the piston left the tube. This is admittedly an idealization of the actual case in which the propellant burns as the piston moves but it was thought that in this way the influence of chamber shape on performance of the gun could be studied.

It had been previously determined (see ref.9) that, in order to accelerate a 0.5 pound piston to a velocity of about 8000 f/s in a 37 mm pump tube, where the chamber pressure is limited to 100,000 psi or less, a chamber volume of 80 in³ is required.

Five chamber designs were studied using the mass point model. The characteristics of these chambers and the results of this breech chamber design study are shown in Table 11. It will be noticed that the velocity of the piston varies between 6568 and 7154 f/s after 120 inches of travel.

As a result of these computations Type IV chamber was chosen as the breech chamber for the light gas gun as it gave the highest velocity of the five chamber types studied.

The mass-point and adiabatic compression models can be used in a computer program for improving the performance of light gas guns. Of the two models, the mass-point model is of greater usefulness because it has fewer limiting assumptions. The use of this more favorable model is limited by longer computer running time; 15 minutes to 40 minutes as contrasted to 1 minute or less for the adiabatic compression method.

One method of improving the performance of light gas guns is to preheat the light gas to some temperature above ambient temperature before compressing the gas. Three methods have been used in preheating the light gas:

1. By electric discharge into the gas.^{3,4}
2. By preheating the pump tube with the light gas inside.
3. By preheating the gas outside the pump tube and rapidly injecting the hot gas into the cold pump tube prior to compression.²

All three methods result in contaminating the gas with metal vapor, either from the heaters or the electric discharge; however, it is expected that indirect heating, although more complicated, will result in less contamination to the gas.

BALLISTICS OF LIGHT GAS GUNS

TABLE II

Results of Light Gas Gun Breech Chamber Study

Chamber Type	Chamber Volume in. ³	Chamber Length in.	Nozzle Angle C	Straight Section Length in.	Piston Weight lb.	Max. Pressure psi	Muz. Vel. 120" Chamber Diameter f/s	Max. Chamber Diameter in.
I	80	20.2	2	0	.5	100,000	6802	2.91
II	80	15.9	3.5	0	.5	100,000	6812	3.45
III	80	7.44	30	5.27	.5	100,000	6374	4.0
IV	80	12.49	15	9.69	.5	100,000	7154	3.0
V	80	-5.27	0	-5.27	.5	100,000	6568	1.5

BALLISTICS OF LIGHT GAS GUNS

TABLE III

Light Gas Gun Model used to Predict Effects of Increasing Initial
Temperature of Light Gas

Length Pump Tube = 133"

I.D. Pump Tube = 1.5"

Length Launch Tube = 72"

Breech Chamber Volume = 40 in³

Piston Weight = .5 Lb.

Projectile Weight = 1 gram

Light Gas = Helium

Range of Initial Temperature Variation = 300^o to 1500^oK

Shot Start Pressure = 70,000 psi

Initial Helium Pressure = 400 psi

Transition Nozzle Angle = 30^o

Frictional Resistance:

Pump Tube = 500 psi

Launch Tube = 2000 psi

BALLISTICS OF LIGHT GAS GUNS

To assess the effect of preheating the gas, a gun model similar to that being constructed for the Interior Ballistics Laboratory Hypervelocity range was chosen. The characteristics of this gun are shown in Table III. In Figure 3 a plot of muzzle velocity vs. maximum pressure shows the effect of preheating the gas. The mass point model was used in all of the computations.

A more promising procedure, than preheating the light gas, is to so design the parameters of the light gas gun that constant pressure is applied to the base of the moving projectile for a portion of its travel down the launch tube. No reports, as yet, are available as to how this might be done but informally it has been reported that two methods are being tried experimentally. These are the following:

1. To determine the pressure profile needed to attain constant base pressure; and working backwards determine the motion of the piston necessary to attain this profile.

2. Extrude a rapidly moving flexible piston through a tapered nozzle such that the front end of the piston is moving more rapidly than the rear end. This rapidly moving piston face will act as a moving chamber for the projectile and thus for a portion of the travel keep an essentially constant pressure on the base of the projectile.

First let us determine the velocity attainable if a constant pressure is applied to the base of a projectile for its entire travel in a launch tube.

The performance of this type of gun can be computed from the well known relation between work and projectile kinetic energy:

$$1) \quad PAL = \frac{wv^2}{2g}$$

solving for velocity we obtain:

$$2) \quad v = \sqrt{\frac{2g PAL}{w}}$$

If we assume that the projectile is a right circular cylinder we can introduce some important simplifications into the above equation. Using the relation for projectile weight $w = \rho Al$ and substituting in the above equation we obtain:

$$3) \quad v = \sqrt{2g P \left(\frac{L}{\rho l} \right)}$$

BALLISTICS OF LIGHT GAS GUNS

TABLE IV
Launch Velocities from a Constant Base Pressure .50 Cal Gun

Projectile Density lb/in ³	Projectile Material	Barrel Length ft.	Projectile Length in.	Projectile Weight grams	Constant Base Pressure psi	$\frac{L}{\rho}$	Projectile Velocity f/s
.273	Steel	5.	.25	6.3	100,000	70.	21,000
.100	Aluminum	5.	.25	2.2	100,000	200	35,800
.010	Nylon	5.	.25	.9	100,000	500	56,700

BALLISTICS OF LIGHT GAS GUNS

In Figure 4 a plot of muzzle velocity vs the parameter $\frac{L}{\rho_1}$ as a function of pressure is presented. In this plot, pressures are varied from 10,000 to 500,000 psi and the parameter $\frac{L}{\rho_1}$ from 50 to 700. The upper limit on pressure is picked from a consideration that it is unlikely that pressure vessels can be made to withstand gas pressures in excess of 500,000 psi without considerable deformation. The last reported work on a high pressure vessel of this type was that of Utah Research and Development Corp⁶, who succeeded in making a pressure vessel which would hold 400,000 psi using stressed concentric cylinder construction.

Higher pressures up to about 4×10^6 psi could be obtained in a barrel by constructing it in concentric layers with annular spaces between the layers filled with high pressure gas or liquid such that the pressure on any one layer would not exceed the tensile strength of the layer. The ends of such an assembly would be held by hydraulic pistons of a type used by General Electric in their diamond making equipment. It is therefore assumed in this study that using monobloc construction 500,000 psi is an upper limit on attainable pressures. Higher pressures could be held but the cost and complexity of construction would increase rapidly.

Use of this plot is illustrated by three examples in Table IV in which projectiles of 3 different densities are launched from the same barrel at a constant base pressure of 100,000 psi. The result illustrates clearly the effect that changing projectile density has on the muzzle velocity. The above cases, however, represent a highly idealistic situation, other mechanism must be postulated which will account for deviation of the light gas gun from this ideal behavior.

One possible mechanism by which this may occur is to allow the piston face to move at a constant distance behind the accelerating projectile until a velocity is reached which is a portion of the final muzzle velocity. At this time the piston face will then move at a constant velocity until the projectile is ejected. Motion of the projectile when the piston face attains a constant velocity will follow a characteristic expansion relative to the moving face of the piston.

In appendix III the assumptions and derivations of the equations used in this theory are listed. A pictorial diagram of the events used in this theory is shown in Figure 8.

BALLISTICS OF LIGHT GAS GUNS

A parametric study was conducted on this problem using the same range of variables used on the constant base pressure gun. In addition, however, we have to specify the gas used, the temperature of the gas, and the portion of travel which the projectile moves under characteristic expansion processes. In the cases studied the gas used was hydrogen and the temperature of the gas varied from 3000°K to 30,000°K. Figure 5 to 7 show some of the results of this study. It will be noticed from these figures that at the low end of $L/\rho l$ there is very little velocity difference between operating the gun as a constant pressure gun or as a pure characteristic expansion gun. As $L/\rho l$ increases the differences between the two modes of firing increases. Increasing the final gas temperature improves the performance as does operating the gun as a constant pressure gun for a portion of its travel.

Means of attaining in a practical light gas gun constant base pressure for a portion of its travel vary:

- 1) Squeeze the chamber and barrel close behind the projectile by means of an accelerating detonation wave.
- 2) Rapidly accelerate the piston in the last portion of its travel by some means, rockets, high explosives, etc.
- 3) Squeeze a deformable piston through a tapered muzzle. During the deformation the piston face will travel faster than the piston base.

In this report we will discuss the last method only as having the most promise. The other two methods should be tried but probably would be very difficult to control.

The simplest case of the flow of a deformable piston through a nozzle is to assume the piston is incompressible; that is the total volume of the piston remains constant. This implies that the mass flow rate through the nozzle will be a constant, therefore we have:

- 4) Mass flow rate:

$$\frac{dm}{dt} = \frac{\rho A_1 dx_1}{dt} = \frac{\rho A_2 dx_2}{dt} = \text{Constant}$$

Rearranging:

$$5) \frac{dx_2}{dt} = \left(\frac{A_1}{A_2} \right) v_1 = \left(\frac{A_1}{A_2} \right) \frac{dx_1}{dt}$$

BALLISTICS OF LIGHT GAS GUNS

The acceleration equation for the piston is:

$$6) \frac{dv_1}{dt} = a_1 = \frac{F_1 - F_2}{m_p} = \frac{(P_b A_1 - P_r A_2) \epsilon}{v_p}$$

Figure 9 illustrates this relationship.

Two computer programs were set up to illustrate the results of integration of equation (5) and (6). In one program it was assumed that the piston by some means had attained a velocity and was just entering a nozzle of a known geometry. The piston was accelerated only by a base pressure P_b and opposed by a resistance pressure P_r ; the resistance pressure could be frictional or gas pressure ahead of the piston. Figure 10 illustrates the results of three of these computations. The cone in this case was fixed, only the piston lengths, weights, and initial velocities were varied. Looking at the motion of the front face of the piston it is noticed that there is an initial acceleration phase occurring over the length of the nozzle. This is followed by a constant velocity phase which is not terminated until the rear portion of the piston enters the nozzle. The face then undergoes a deceleration phase which is terminated when the base of the piston enters the launcher tube. The final velocity of the piston will be equal to the initial velocity of the piston minus any losses which might have occurred during the extrusion process. The first two phases are what is desired for a constant base pressure gun followed by a characteristic expansion; that is an acceleration phase for the face of the piston such that the volume of gas behind the accelerating projectile remains a constant. This is followed by a constant velocity phase in which the volume between the projectile and the piston face increases during the characteristic expansion. It is to be hoped that the projectile has left the launcher by the time the piston deceleration phase enters in.

Equations (5) and (6) were programmed into the mass point model so as to simulate the interior ballistics of a light gas gun with a deformable incompressible piston. The results of a number of computer runs indicated that the light gas pressure increased rapidly forward of the accelerating piston face. This increased pressure was not transmitted to the base of the rapidly moving projectile, because the projectile was moving faster than its local sonic speed. Further study will be required to determine the conditions necessary to obtain a velocity advantage from the extrudable piston technique.

BALLISTICS OF LIGHT GAS GUNS EXPERIMENTAL PROGRAM

The initial objective of the experimental program was to build a small 37 mm - .50 cal light gas gun out of available parts and fire it in a program which would serve to check out instrumentation to be used in a higher performance light gas gun. In addition, the results of the firings could be used to check the adequacy of theories developed in the parallel theoretical program. Knowledge gained in this program would be used to design and build a high performance 37 mm - .50 cal light gas gun.

The gun, as finally designed, launched 2.5 and 5 gram aluminum projectiles at velocities ranging from 6000 to 10,000 f/s. The pump tube for this gun consists of a smoothed bored 37 mm tank gun. To the muzzle of this gun is attached a three part high pressure section consisting of a two-diameter high pressure section, a gauging to hold the pressure gauge, and a transition section between the pump tube and the launch tube. To the transition section is attached a .50 cal smooth bore Mann barrel, which serves as the launch tube. The muzzle end of the launch tube has a vacuum adapter so that the tube may be evacuated. A thin nylon plastic disc is used in the vacuum adapter to seal off the bore. A sketch of the gun with dimensions is shown in Figure 14.

Initially the cartridge case used in the 37 mm gun was made of brass. After a few light gas gun firings it was evident that propellant gas leakage around the cartridge case limited the effectiveness of the gun. This cartridge case was then replaced by a steel cartridge case fitted with O-rings. Since then we have not observed any gas leakage from the breech end of the gun at the lower energy rounds.

The three-part, high pressure section is held together by a system of heavy steel flanges and bolts. The present design consists of 2 flanges 2-3/8 inches thick and 13-1/2 inches in diameter hardened to Rockwell 30/34. The flanges are held together by 6 bolts especially machined and hardened to reduce stress. This design which, is shown in Figure 12, represents the fourth try in the design of a clamping arrangement, three previous tries ending in catastrophic failures.

The two-diameter high pressure section was made initially to be used with scintillation counters; the counters were to be used to track a radioactive cobalt 60 source held in the base of the piston.

This approach was discussed in reference². The radioactive source-scintillation counter idea was abandoned when it was decided that the use of magnetic contacts would serve the same purpose at considerably less danger to the operator of the light gas gun.

BALLISTICS OF LIGHT GAS GUNS

Two types of pistons have been used in the light gas gun. For the initial firings a steel piston was used fitted with a copper cup obturator at one end (to seal off propellant gases) and a nylon buffer at the other end (to cushion the shock of the final impact of the piston against the transition section). A later design of the piston had $3/16$ " or $7/16$ " width grooves about $1/8$ " deep. These pistons were used in experiments with the magnetic contact. The aluminum projectiles and shear ring were machined in one piece out of aluminum bar stock. The two types of pistons and projectiles used are shown in Figures 13 and 14.

To obtain interior ballistic information from the light gas gun the following instruments were used:

- 1) Quartz crystal piezo pressure gauge - used to measure propellant gas pressure in the breech chamber of the pump tube.
- 2) Piston type strain gauge - used to measure helium pressure in the pump tube just before the transition section.
- 3) Magnetic contact - used to detect piston position as the piston passed under the contact.
- 4) Microwave interferometer - used to measure projectile displacement in the launch tube.

The quartz crystal piezo gauge is of a type used at the Ballistic Research Laboratories for the measurement of transient gun pressures for a period of about 20 years. When properly used the gauge has given quite reliable results.

The piston type strain gauge consists of a steel piston $1/4$ inches in diameter and $1-1/2$ inches long which has a strain patch cemented at its upper end. When the gauge was tested in a high pressure shock tube at about 1000 psi it gave a ringing frequency of 40 KC. This corresponds to a rise time of 15 microseconds. This type of gauge is quite rugged and has been used previously in light gas guns instrumentation systems.

The magnetic contact is a relatively new development in the field of light gas gun instrumentation, no published literature has been found concerning its use in light gas guns, however, it has been used in other fields, notably rocket launcher instrumentation. The magnetic contact used in the 37 mm .50 cal light gas gun consists of a magnetized cold-rolled steel bar $1/8$ inches diameter by $3/4$ inches long, wrapped with 140 turns of No. 35 copper wire. An aluminum cup-bearing combination protects the bar from the hot gases.

BALLISTICS OF LIGHT GAS GUNS

This cup in turn is supported by a steel hollow cylinder. A voltage signal is induced in the coil when the slotted piston passes underneath the contact.

A microwave interferometer is used to measure position of the projectile in the launcher as a function of time. The system used in the Interior Ballistics Laboratory has been described elsewhere¹ and only a brief description will be given here.

The principle on which it works is the same as that for an optical interferometer. A radar signal from a klystron is propagated through a hybrid junction into branches of a wave guide. The signal along one branch is directed to the muzzle by means of a horn and reflector, and then propagated along the bore of the barrel to the projectile face. The signal propagating along the other branch is directed to a fixed wave guide short. The reflected signals from both branches return to a junction and thence to a crystal detector. The output of the crystal is a constant D.C. voltage if the projectile is stationary; however, if the projectile moves, the crystal voltage changes in amplitude in a nearly sinusoidal wave, which goes from maximum to minimum for each quarter wave length change in projectile position. After being amplified, the signal is sent to an oscilloscope and is recorded on a General Radio camera and a rotating mirror camera. The rotating mirror camera is capable of recording frequencies up to about one megacycle. This is equivalent to a projectile velocity in the .50 cal barrel of about 30,000 f/s. The microwave equipment at the front of the launcher is shown in Figure 15.

A sketch of a portion of the high pressure section and the launcher tube of the light gas gun, together with the magnetic contact and the high pressure gauge is shown in Figure 16.

Muzzle velocity in the light gas gun is currently measured by timing the passage of the projectile between three printed circuit paper screens which are set about 5 feet apart. These screens, when broken by the projectile, start or stop electronic counters. Since these screens are in air the projectile experiences considerable aerodynamic drag and thus a velocity loss when passing between the screens. The muzzle velocity of the projectile is then determined by extrapolating the screen velocities back to the muzzle. For low velocities (less than 10,000 f/s) this is an acceptable method for measuring muzzle velocities, but for velocities greater than 10,000 f/s other means have to be used.

BALLISTICS OF LIGHT GAS GUNS

EXPERIMENTAL RESULTS (SMALL GUN)

A total of 52 rounds have been fired in the small 37 mm .50 cal light gas gun. A large number of these were fired to check out various modifications in light gas gun instrumentation so the results obtained from those rounds were either non-existent because of instrumental malfunction or only partially adequate. In other rounds, the instrumentation worked perfectly so these rounds were compared with the theoretical predictions described earlier. (See Table V). Both the adiabatic compression method and the mass point method were used in making predictions. The results from both of these predictions, since in general they do not agree, are listed separately.

The detailed interior ballistic trajectories for two rounds are shown in Figures 17 to 20 . The experimental results of these rounds are compared with the predictions from the mass point and the adiabatic compression methods.

The interior ballistic trajectory for round 26 gives fair agreement between the mass point method, the adiabatic compression method, and experimental results. However, the mass point method predicts higher pressures and velocities than observed experimentally. In round 40 the agreement is not as good. Again the mass point method predicts higher velocities and pressures than either the adiabatic compression method or the experimental results. Most of this error is probably due to predicted piston velocities being higher than that developed in the gun firing.

This discrepancy in piston velocities may be caused by the following:

1. Unforeseen frictional effects between the piston and the pump tube bore, for example:
 - a. The slightly eroded condition of the pump tube.
 - b. The "braking effect" caused by a compressible nylon buffer on the face of the piston.
2. Observed propellant gas leakage at the breech end of the system, particularly at the higher propellant charges.

It can be noticed that in both of these rounds the adiabatic compression method gives smooth helium pressure-time traces which is in contrast to the oscillatory pressure-time traces from both the experimental record and the mass point method. In general these pressure oscillations start with motion of the projectile and are due to shock waves formed by the rapid flow of gas in the transition section.

BALLISTICS OF LIGHT GAS GUNS

This is shown in Figure 21 which is a series of oscilloscope records of light gas rounds which vary widely in velocity. Shown in these records are helium pressure measured at the transition section and the interferometer record measuring projectile motion. In the one record no pressure oscillations are noted. This was a low velocity (4985 f/s) light gas gun round.

In successive rounds as the projectile velocity increases, the amplitude and frequency of oscillation increases; but, it will be noted in most cases, the oscillation starts after projectile start of motion. In the highest velocity case oscillations are noted before start of motion, but this is due to the formation of shock waves by the rapidly moving piston. All these phenomena can be predicted by the mass point method.

A typical light gas gun oscilloscope record is labeled in detail and shown in Figure 22. The projectile weighed 2.5 grams and the propellant charge weighed 60 grams. The muzzle velocity for this round was approximately 10,000 f/s.

BALLISTICS OF LIGHT GAS GUNS

LARGE 37 mm .50 CAL LIGHT GAS GUN:

A large and more massive 37 mm .50 cal light gas gun is now under design and construction. This gun has been designed to fire 1 gram projectiles in the 20,000 - 30,000 f/s velocity range, but will be used to obtain interior ballistic information on light gas guns operating under a wide variety of conditions. This gun represents the improvements in design suggested by the firing of the small gun. The large light gas gun has two 10 foot pump tubes which can be used separately or together giving a pump tube 20 foot long. The high pressure section which is 24 inches long is attached to the muzzle end of the pump tube. To the high pressure section in turn is attached the .50 cal launch tube 72 inches long.

The high pressure section is of mono bloc construction (unlike the small light gas gun) and consists of two concentric cylinders of 4140 steel which are water proofed for life. The inner cylinder is 1.5 inches I.D. by 4.5 inches O.D. and the outer cylinder is 4.5 inches I.D. by 6 inches O.D. The high pressure section is designed to withstand a maximum pressure of 200,000 psi. One complication in the design resulted from the presence of two holes into the bore of the high pressure section. One hole is for the high pressure gauge and the other for the magnetic contact. The hole for the high pressure gauge gives an unfavorable stress pattern at the point in the section which is subjected to maximum pressure so particular emphasis on the placement of this hole was made by the Engineering Laboratories of Watertown Arsenal (designers of the high pressure section) so that the stress in the high pressure section would be at a minimum. This resulted in the hole into the bore of the gun being off the axis of the gun.

The design of the breech section of the light gas gun has been described earlier. Briefly it consists of a cylinder of Potts Elastuf 44 steel 7.70 inches O.D. by 3 inches I.D. with a 30° nozzle between the 3 inch chamber and the bore of the pump tube. Three breech plugs can be used in this chamber to give chamber volume of 40, 60, and 80 cu. inches respectively. This allows one to vary the piston velocity over wide limits (up to a maximum velocity of 8,000 f/s with a .5 lb. piston) without exceeding the 100,000 psi pressure limit of the chamber.

Instrumentation similar to that used on the small light gas gun will be used on the large light gas gun. There will be one gauge which has been used on a previous small gun. The pressure instrumentation will be the same.

BALLISTICS OF LIGHT GAS GUNS

1) Propellant gas pressure in the breech of the gun will be measured by means of a HAT gauge inserted into the breech plug. The HAT gauge is a specially designed pressure transducer consisting of a hemispherical shell with strain patches bonded to the inner wall of the hemisphere. The transducer has a high frequency of response and a linear calibration. Further information on this transducer is contained in Reference 11.

2) Helium pressure will be measured by means of a piston type strain gauge similar to that used in the small gun. The laboratory is investigating other types of pressure transducers, but, so far, none have met our requirements.

3) Piston position and velocity will be measured by means of magnetic probes placed along the bore of the pump tube. Of importance will be the positions where the piston starts to move and the position where the piston stops or reverses its motion.

4) Projectile position will be measured by means of the microwave interferometer described earlier. Some effort will be expended in developing an interferometer which is capable of penetrating the layer of ionized gases which build up ahead of the projectile even when the launch tube is evacuated.

5) Muzzle velocity of the projectile will be determined in a specially designed vacuum range equipped with optical velocity measuring equipment. This range shown in Figure 23 is capable of being pumped down to a 15 micron vacuum. The range has five optical viewing ports, four of which are used with the optical velocity measuring equipment. This equipment similar to that described in Reference 8 uses a series of lights, lenses and mirrors to project shadows of the projectile on the film of a streak camera as it passes each viewing port.

Predicted performance of this gun using the mass point program has given indications that this gun is capable of accelerating 1 gram aluminum projectiles to velocities in the 20,000 - 30,000 f/s range without exceeding the 200,000 psi maximum pressure rating of the high pressure section. Later on in the program it is planned to use tapered transition sections and compressible pistons in an attempt to exceed the 30,000 f/s velocity mark.

BALLISTICS OF LIGHT GAS GUNS

DISCUSSION

Theoretical work on the Interior ballistics of light gas guns indicate that it is possible to attain projectile velocities higher than 30,000 f/s. Velocities of 40,000, 50,000 f/s or higher should be possible but only by greatly increasing the pressures and/or temperatures. The constant pressure followed by characteristic expansion theory needs to be backed up by computer runs using the mass point theory to give the former theory some connection with reality and to indicate to the engineer what type of gun would be needed to attain these supervelocities.

The mass point computer program needs further improvement in the removal of the ideal gas assumption, which works well for helium but would give unrealistic results for hydrogen. In addition some consideration should be taken in this program for heat loss from the hot gas by radiation and/or convection to the walls. This is expected to be of importance as the light gas temperature is increased.

Good agreement between the theoretical computer runs and experimental results have been obtained for the small low performance light gas gun. The mass point program has been particularly useful in predicting some of the complex pressure wave phenomenon observed in this gun. Replacement of the small gun with the larger higher performance light gas gun should enable one to extend the theory verification to higher performance guns. Any necessary modifications to the theory will be made in comparing theory with experimental results.

BALLISTICS OF LIGHT GAS GUNS

REFERENCES

1. Baer, P. G., "The Application of Interior Ballistic Theory in Predicting the Performance of Light Gas Hypervelocity Launchers," 4th Symposium on Hypervelocity Impact, APGC-TR-60-39 (II), (Sep 1960)
2. Baer, P. G. and Smith, H. C., "Interior Ballistics of Hypervelocity Projectors Instrumented Light Gas Gun and Traveling Charge Gun", 5th Symposium on Hypervelocity Impact", Vol. 1, Part 1, (April 1962)
3. Bloxom, D. Jr., "Experimental Production of Hypervelocity Pellets by Means of Condenser Discharge in Hydrogen", 4th Symposium on Hypervelocity Impact, APGC-TR-60-39(I), (Sep 1960)
4. Swift, H. F., "Electroballistic Techniques", Ibid.
5. Anderson, D. E., and Prince, M. D., "Design of Light Gas Model Launchers for Hypervelocity Research", AEDC-TR-62-97, (May 1962)
6. Brown, W. S., et al., "Construction of a High Pressure, High Temperature, Light Gas Gun", Hypervelocity Techniques Symposium, Denver, Colorado, (Oct 1960)
7. Vest, D. C., et al., "Ballistic Studies with a Microwave Interferometer, Part II", BRL Report No. 1006, (Feb 1957)
8. Bailey, S. O., et al., "Facilities and Instrumentation of NRL Hypervelocity Laboratory", 3rd Symposium on Hypervelocity Impact, Vol. 1, (Feb 1959)
9. Baer, P. G., and Frankle, J. M., "The Simulation of Interior Ballistic Performance of Guns by Digital Computer Program", BRL Report No. 1183, (Dec 1962)
10. Richtmyer, R. D., "Difference Methods for Initial Value Problems", Chapter X, pg. 215 - 222, Interscience Publishers, Inc., New York (1957)
11. Pfaff, S. P., "Measurement of Frequency Response of Pressure Gauges by a High Pressure Shock Tube Technique", BRL Memo Report No. 1179, (Nov 1958)

BALLISTICS OF LIGHT GAS GUNS

APPENDIX I

ADIABATIC COMPRESSOR MODEL

The assumptions used in this model are as follows:

- 1) Ideal gas with constant specific heat.
- 2) Frictional loss in the pump tube and launcher tube are considered to be a function varying with piston or projectile travel.
- 3) Frictional losses between the light gas and bore surfaces, including the transition section are assumed to be negligible.
- 4) Heat loss from the light gas to the pump tube, transition section, and launch tube is assumed negligible.
- 5) Pressure of the gas propelling the piston is governed by conventional interior ballistic equations.
- 6) Light gas velocity in the pump tube and launch tube is assumed to be some arbitrary fraction of the piston velocity and projectile velocity respectively.
- 7) Light gas velocity in the transition section between the pump tube and the launch tube is assumed to be either subsonic or sonic depending upon the pressure gradient between pump tube and launch tube.

In this model we set up three thermodynamic systems:

System 1:

This system includes the propellant gas and a moving piston of weight w_p . The piston does work against a frictional resistance pressure P_r and a light gas pressure P_g .

In this system it is assumed that conventional interior ballistic equations will hold.

System 2:

This system includes the light gas only from the face of the piston to the inlet of the nozzle. Work is done on the light gas by the motion of the piston. If the piston reverses, then the system will include the piston with the light gas doing work on the propellant gas. There are two limiting cases to this system:

- a. the light gas has a uniform velocity V (velocity of piston face) or--
- b. the light gas has no velocity ($V = 0$). When the projectile starts moving, heat and mass are lost through the nozzle.

BALLISTICS OF LIGHT GAS GUNS

System 3:

This system includes the light gas and projectile of weight w_p from the nozzle exit to the face of the projectile. As in System 2, there are two limiting cases to this system:

The light gas has a uniform velocity v_p (velocity of projectile) or the light gas has no velocity ($v_p = 0$). The light gas does work against a frictional resistance pressure $p_{r\ell}$

In the System 2 the energy relationship is:

$$\left[\begin{array}{l} \text{Change in kinetic energy} \\ \text{of system} \end{array} \right] + \left[\begin{array}{l} \text{Change in Internal} \\ \text{energy of system} \end{array} \right] - \left[\begin{array}{l} \text{Rate of work} \\ \text{done on system} \end{array} \right] \\ + \left[\begin{array}{l} \text{Rate of work} \\ \text{done by system} \end{array} \right] - \left[\begin{array}{l} \text{Rate of heat} \\ \text{lost from system} \end{array} \right]$$

In System 3 the energy relationship is:

$$\left[\begin{array}{l} \text{Change in kinetic} \\ \text{energy of system} \end{array} \right] + \left[\begin{array}{l} \text{Change in Internal} \\ \text{energy of system} \end{array} \right] + \left[\begin{array}{l} \text{Rate of work} \\ \text{done by system} \end{array} \right] \\ - \left[\begin{array}{l} \text{Rate of heat gained} \\ \text{by system} \end{array} \right]$$

In System 2:

$$\left[\begin{array}{l} \text{Change in kinetic energy} \\ \text{of system} \end{array} \right] = \frac{d}{dt} \left[\frac{m_p v^2}{2} \right] = \frac{1}{2} \frac{d}{dt} \left[v^2 \frac{dm_p}{dt} + 2m_p v \frac{dv}{dt} \right]$$

$$\left[\begin{array}{l} \text{Change in Internal energy} \\ \text{of system} \end{array} \right] = m_p J C_v \frac{dT_p}{dt} = \frac{m_p R}{(\gamma-1)M} \frac{dT_p}{dt}$$

$$\left[\begin{array}{l} \text{Rate of work} \\ \text{done on system} \end{array} \right] = A_p \frac{d}{dt} \left[\int_0^x p_g dx \right] = A_p p_g v$$

$$\left[\begin{array}{l} \text{Rate of work done} \\ \text{by system} \end{array} \right]$$

||

$$\left[\begin{array}{l} \text{Displacement through} \\ \text{nozzle} \end{array} \right] = \frac{p_g v_p}{m_p} \frac{dm_p}{dt}$$

+

BALLISTICS OF LIGHT GAS GUNS

$$\left[\begin{array}{l} \text{Piston motion on} \\ \text{reversal} \end{array} \right] = \frac{w_p V}{g} \frac{dV}{dt}$$

+

$$\left[\begin{array}{l} \text{Rate of work against propellant} \\ \text{pressure on reversal} \end{array} \right] = A_p p_p V$$

$$\left[\begin{array}{l} \text{Rate of heat lost by system} \\ \text{to launcher tube} \end{array} \right] = \frac{dm_\ell}{dt} J C_v T_p = \frac{-RT_p}{(\gamma-1)M} \frac{dm_\ell}{dt}$$

Writing out all the terms:

$$1) \frac{V^2}{2g} \frac{dm_p}{dt} + \frac{m_p}{g} V \frac{dV}{dt} + \frac{m_p R}{(\gamma-1)M} \frac{dT_p}{dt} - \frac{A_p p_p V}{g} + \frac{p_p V}{m_p} \frac{dm_\ell}{dt} + \left[\frac{w_p V}{g} \frac{dV}{dt} + A_p p_p V \right] = - \frac{RT_p}{(\gamma-1)M} \frac{dm_\ell}{dt}$$

upon reversal only

Rearranging the equation:

$$2) \frac{dT_p}{dt} = \frac{1}{m_p} \frac{dm_\ell}{dt} \left[T_p + \left(\frac{M(\gamma-1)}{R} \right) \left(\frac{\lambda V^2}{2g} - \frac{p_p V}{m_p} \right) + \frac{(\gamma-1)M}{R} \left[\frac{\lambda p_p V}{m_p} - \lambda \left(\frac{V}{g} \frac{dV}{dt} \right) - \frac{w_p V}{m_p g} \frac{dV}{dt} - \frac{A_p p_p V}{m_p} \right] \right]$$

upon piston reversal

A term λ has been added in equation (2) $0 \leq \lambda \leq 1$

if $\lambda = 0$ then the gas is not moving in the pump tube,

if $\lambda = 1$ then the gas in the pump is moving at the velocity of the piston.

BALLISTICS OF LIGHT GAS GUNS

In System 3:

$$\left[\begin{array}{l} \text{Change in kinetic} \\ \text{energy of system} \end{array} \right] = \lambda' \frac{v^2}{2g} \frac{dm_\ell}{dt} + \frac{v}{g} \frac{dv}{dt} \left[\lambda' m_\ell + w_\ell \right]$$

$$\left[\begin{array}{l} \text{Change in Internal} \\ \text{energy of system} \end{array} \right] = m_\ell J C_v \frac{dT_\ell}{dt} = \frac{m_\ell R}{(\gamma-1)M} \frac{dT_\ell}{dt}$$

$$\left[\begin{array}{l} \text{Rate of work done by} \\ \text{system on frictional resistance} \end{array} \right] = A_\ell P_{r_\ell} v$$

$$\left[\begin{array}{l} \text{Rate of heat gained by} \\ \text{system from pump tube} \end{array} \right] = \frac{dm_\ell}{dt} J C_v T_p = \frac{RT_p}{(\gamma-1)M} \frac{dm_\ell}{dt}$$

Writing out the entire equation:

$$\begin{aligned} 3) \quad & \lambda' \frac{v^2}{2g} \frac{dm_\ell}{dt} + \frac{v}{g} \frac{dv}{dt} \left[\lambda' m_\ell + w_\ell \right] + \frac{m_\ell R}{(\gamma-1)M} \frac{dT_\ell}{dt} + A_\ell P_{r_\ell} v \\ & = \frac{RT_p}{(\gamma-1)M} \frac{dm_\ell}{dt} \end{aligned}$$

Rearranging and solving for dT_ℓ/dt :

$$\begin{aligned} 4) \quad & \frac{dT_\ell}{dt} = \frac{1}{m_\ell} \frac{dT_\ell}{dt} \left[T_p - \frac{(\gamma-1)M}{R} \lambda' \frac{v^2}{2g} \right] - \frac{(\gamma-1)M}{m_\ell R} v \left\{ A_\ell P_{r_\ell} + \right. \\ & \left. \frac{1}{g} \frac{dv}{dt} \left[\lambda' m_\ell + w_\ell \right] \right\} \end{aligned}$$

Equation (4) thus is the energy equation used for system 3, the region between the end of the nozzle and the base of the projectile.

BALLISTICS OF LIGHT GAS GUNS

For the nozzle itself an equation is used to determine the mass flow rate of the gas between the pump tube and the launch tube. This mass flow rate depends upon the pressure at the pump tube side of the nozzle (upstream side) and the pressure in the launch tube (downstream side). It is assumed that the gas flow through the nozzle is similar to that through a rocket nozzle, that is, the flow is pseudo-steady state and that depending upon the pressure differential, flow is either subsonic or sonic.

The mass flow rate through a nozzle is:

$$5) \quad \frac{dm_l}{dt} = A_l P_g \sqrt{\left(\frac{2g}{R(\gamma-1)}\right) \left[\left(\frac{P_{l_t}}{P_g}\right)^{2/\gamma} - \left(\frac{P_{l_t}}{P_g}\right)^{\frac{\gamma+1}{\gamma}} \right]} \frac{1}{T_p}$$

for subsonic flow: $P_{l_t} = P_l > P^*$

for sonic flow: $P_{l_t} = P^* = P_g \left(\frac{2}{\gamma+1}\right)^{\frac{\gamma}{\gamma+1}}$

The complete set of equations used in the program are as follows:

For the pump tube:

Equation of energy:

$$6) \quad \frac{dT_p}{dt} = \frac{(\gamma-1)M}{R} \left[\frac{A P V}{P g m_p} - \lambda \left(\frac{V}{g} \frac{dv}{dt} \right) - \overbrace{\left(\frac{w_p}{g} \right) \frac{V}{m_p} \frac{dV}{dt} - \frac{A P V}{m_p}}^{\text{upon piston reversal}} \right]$$

$$+ \underbrace{\frac{dm_l}{dt} \left(\frac{1}{m_p} \right) \left[\frac{M(\gamma-1)}{R} \left(\frac{\lambda v^2}{2g} - \frac{P g v_p}{m_p} \right) - T_p \right]}_{\text{upon projectile motion}}$$

BALLISTICS OF LIGHT GAS GUNS

Equation of mass conservation:

$$7) \quad m_p = m_{p_0} - m_l$$

Equation of State:

$$8) \quad P_g = \frac{m T}{v_g} \left(\frac{R}{M} \right) \quad \text{where: } v_g = A_p (x_m - x)$$

Equation of Piston Motion:

$$9) \quad \frac{dv}{dt} = \frac{A_p g}{w_p} \left(P_b - P_r - P_g \right)$$

$$10) \quad \frac{dK}{dt} = v$$

For the launch Tube:

Equation of Energy:

$$11) \quad \frac{dT_l}{dt} = \frac{dm_l}{dt} \left(\frac{RT_l}{P_l v_l M} \right) \left[T_p - \frac{(\gamma-1)M}{R} \frac{\lambda^2 v^2}{2g} \right] -$$

$$\frac{(\gamma-1)T_l v}{P_l v_l} \left\{ A_l P_{r_l} + \frac{1}{g} \frac{dv}{dt} \left[\frac{\lambda^2 M P_l v_l}{RT_l} + w_l \right] \right\}$$

Equation of State:

$$12) \quad P_l = \frac{m_l T_l}{v_l} \left(\frac{R}{M} \right)$$

Equation of Motion:

$$13) \quad \frac{dv}{dt} = \frac{A_l g}{w_l} (P_l - P_{r_l}) \quad \frac{dx_l}{dt} = v$$

Equations (5) through (13) are used as an option in a general multigran gun program described in Ref. (9). Generally it can be said that computation on the light gas gun option takes place in the general program after motion of the piston is computed.

BALLISTICS OF LIGHT GAS GUNS

APPENDIX II

Mass Point Model (Richmyer-Von Neuman "q" Method)

The assumption used with this model are as follows:

- 1) Ideal gas with a constant specific heat.
- 2) Frictional losses in the pump tube and launcher tube are considered to be a function varying with piston or projectile travel.
- 3) Frictional losses between the light gas and bore surfaces, including the transition section are assumed to be negligible.
- 4) Heat loss from the light gas to pump tube, transition section, and launcher tube is assumed negligible.
- 5) Pressure of the gas propelling the piston is governed by conventional interior ballistics equations.

The partial differential equations used in describing the mass point flow have been described by Richmyer⁽¹⁰⁾ and will not be repeated here. These equations are converted to the following finite difference equations:

$$1) \quad u_j^{n+1} - u_j^n = \frac{x_j^{n+1} - x_j^n}{\Delta t}$$

$$2) \quad \frac{u_j^{n+1} - u_j^n}{\Delta t} = - \left(\frac{g}{\rho_0 A_0 \Delta z} \right) \Lambda(x) \left[p_{j+1/2}^n - p_j^n - 1/2 + q_{j+1/2}^n - u_{j-1/2}^n \right]$$

$$3) \quad v_{j+1/2}^{n+1} = \left(\frac{1}{\rho_0 A_0 \Delta z} \right) \Lambda(x) \left[x_{j+1}^{n+1} - x_j^{n+1} \right]$$

$$4) \quad q_{j+1/2}^{n+1} = \begin{cases} \frac{\left(\frac{2g^2}{g} \right) (u_{j+1}^{n+1} - u_j^{n+1})^2}{(v_{j+1/2}^{n+1} + v_{j+1/2}^n)} & \text{if } (u_{j+1}^{n+1} - u_j^{n+1}) \leq 0 \\ 0 & \text{if } (u_{j+1}^{n+1} - u_j^{n+1}) > 0 \end{cases}$$

BALLISTICS OF LIGHT GAS GUNS

$$5) E_{j+1/2}^{n+1} - E_{j+1/2}^n + \left(\frac{P_{j+1/2}^{n+1} + P_{j+1/2}^n}{2} + q_{j+1/2}^{n+1} \right)$$

$$(v_{j+1/2}^{n+1} - v_{j+1/2}^n) = 0$$

$$6) P_{j+1/2}^{n+1} = \frac{E_{j+1/2}^{n+1} (\gamma - 1)}{v_{j+1/2}^{n+1}}$$

Substituting Equation (6) into (5) and solving for $E_{j+1/2}^{n+1}$ gives:

$$7) E_{j+1/2}^{n+1} = \frac{E_{j+1/2}^n - (.5 P_{j+1/2}^n + q_{j+1/2}^{n+1}) (v_{j+1/2}^{n+1} - v_{j+1/2}^n)}{\left[1 + .5 (\gamma - 1) \left(1 - \frac{v_{j+1/2}^{n+1}}{v_{j+1/2}^n} \right) \right]}$$

To insure compatibility with the interior ballistic equations which are ordinary differential equations; equations (1) and (2) were converted into ordinary differential equations which then could be solved by a modified Euler integration technique. The new formulation for these equations are:

$$8) a_j^{n+1} = \frac{du_j^{n+1}}{dt} = \left(\frac{-\bar{g}}{\rho_o \Lambda_o \Lambda_j} \right) A(x) \left(P_{j+1/2}^n - P_{j-1/2}^n + q_{j+1/2}^n - q_{j-1/2}^n \right) \quad \text{for } j = 1, 2, \dots, J-1$$

$$9) \frac{dx_j^{n+1}}{dt} = u_j^{n+1} \quad \text{for } j = 0, 1, 2, \dots, J$$

We need two other equations to complete the boundary conditions. One of these is the piston equation:

$$10) a_o^{n+1} = \frac{A_o g \left[P_b - (P_r + P_{1/2}^n) \right]}{v_p}$$

The other is the projectile equation:

$$11) a_j^{n+1} = \frac{A_j g \left[P_{j-1/2}^n - P_r \right]}{v_k} \quad \text{when } P_{j-1/2}^n \geq P_{ss}$$

0

when $P_{j-1/2}^n < P_{ss}$

BALLISTICS OF LIGHT GAS GUNS

The time step used in the solution of these equations has to be redetermined at the end of each integration step so as to insure stability of the computations. The stability equation used is that recommended by Richmyer:

$$12) \Delta t = \frac{(L_f \rho_o) V_m^{n+1}}{c_o}$$

Where:

$$13) c_o = \sqrt{\gamma g P_m^{n+1} V_m^{n+1}} = \text{velocity of sound at maximum pressure.}$$

In the computer code the equations are solved in the following order: (10), (11), (8), (9), (3), (4), (7), (5). Equation (10) is the connecting link between the interior ballistic equations mentioned in reference (9) and the light gas gun equations mentioned here since P_b , the pressure on the base of the projectile has to be determined by the interior ballistic equations for a gun.

BALLISTICS OF LIGHT GAS GUNS

APPENDIX III

A Constant Base Pressure Gun Followed by Infinite Chamber

Adiabatic Expansion from a Moving Chamber

ASSUMPTIONS:

1. The gun chamber moves at the same velocity as the projectile up to a velocity v_1 . The chamber then maintains velocity v_1 until projectile ejection.

2. The motion of the projectile after attaining velocity v_1 , will follow that of a characteristic expansion (chamber appears to be of infinite extent to the projectile) until ejection from the gun barrel.

At v_1 the projectile has traveled a distance L_1 under constant pressure:

$$1) \quad L_1 = \frac{w \ell v_1^2}{2g PA} = \frac{\rho \ell v_1^2}{2g P} = \frac{\rho \ell v^2}{2g P}$$

At v_m (ejection velocity of the projectile) the base of the chamber will have moved:

$$2) \quad \Delta L = v_1 t \quad \text{where: } t = \text{time for base of projectile to move from } L_1 \text{ to } L$$

At ejection the projectile will have a velocity relative to the chamber base of v_r . Therefore ejection velocity relative to the barrel will be:

3) $v_m = v_r + v_1$ referring to figure 8 the total length L_t from face of chamber to muzzle of fire is initially

$$4) \quad L_p = L + L_c \quad \text{Where: } L = \text{projectile travel length}$$

$$L_c = \text{chamber length}$$

When the projectile is ejected with a velocity v_m :

BALLISTICS OF LIGHT GAS GUNS

$$14) \bar{t} = \left(\frac{\gamma - 1}{\gamma + 1} \right) \left\{ (1 - \bar{u}) - \left(\frac{\gamma + 1}{\gamma - 1} \right) - 1 \right\}$$

$$15) \alpha_0 = \frac{2a_0}{\gamma - 1} = \frac{2}{\gamma - 1} \sqrt{\frac{\gamma g R T}{M}}$$

Solving for v_1 :

$$16) v_1 = \sqrt{\frac{2g P L}{\rho l}} = \sqrt{2g P k_1 \left(\frac{L}{\rho l} \right)}$$

$$17) \bar{x} = \frac{P g x}{\rho l \alpha_0^2} = \frac{P g k_2}{\alpha_0^2} \left(\frac{L}{\rho l} \right)$$

$$\text{where: } k_2 = 1 - k_1 - k_2$$

$$18) \bar{u} = f(\bar{x}) \quad \bar{u} \text{ can be obtained by interpolating in a table of } \bar{u} \text{ and } \bar{x}$$

$$19) \bar{t} = f(\bar{u}) \quad \text{from equation (14)}$$

Now time of projectile motion during characteristic expansion is from equation (11) and (2):

$$20) t = \frac{\rho l \alpha_0 \bar{t}}{P g} = \frac{\Delta L}{v_1} = \frac{k_2 L}{v_1}$$

Solving for v_1 :

$$21) v_1 = \frac{k_2 P g}{\alpha_0 \bar{t}} \frac{L}{\rho l} = \sqrt{2g P k_1 \left(\frac{L}{\rho l} \right)}$$

After some manipulation:

$$22) k_2 = \frac{-1 + \sqrt{1 + 4 \left(\frac{a_0^2 L^2}{b_0} \right) k_0}}{2 \left(\frac{a_0^2 L^2}{b_0} \right)}$$

BALLISTICS OF LIGHT GAS GUNS

where: $k_0 = 1 - k_3$; $L^2 = \frac{L}{\rho l}$; $a_0 = \frac{Pg}{\alpha_0 t}$; $b_0 = 2 g P$

Then:

$$23) k_1 = k_0 - k_2$$

To solve this problem we have given: P , $\frac{L}{\rho l}$, T , γ , M , and k_3
We then solve equations (15), (17), (18), (19), (22), (23), (16), (10),
and (3) numerically in sequence:

If $k_3 = 0$ and $k_1 = 1.0$ we then have the limiting case of a
constant base pressure gun.

If $k_3 = 1$ we have the limiting case of a characteristic expansion
only.

BALLISTICS OF LIGHT GAS GUNS
GLOSSARY OF SYMBOLS

<u>Symbol</u>		<u>Units</u>	<u>Equations where found</u>
A	Cross sectional area of launcher bore	in ²	1
A ₁	Cross sectional area of piston base	in ²	1
A ₂	Cross sectional area of piston face	in ²	1
a ₁	Acceleration of piston base	ft/sec ²	
A _P	Cross sectional area of piston	in ²	I-1
A _ℓ	Cross sectional area of projectile	in ²	I-3
A ₀	Initial cross sectional area of pump tube	in ²	II-2
A(x)	Cross sectional area of gas segment, function of position	in ²	II-2
a	Viscous correction constant		II-4
a _j ⁿ	Acceleration of j gas segment at time n	in/sec ²	II-8
a ₀	Sound velocity		
C _v	Specific heat at constant volume		
E _j ⁿ	Internal energy of j segment at time n	$\frac{\text{in} \cdot \text{lb}}{\text{lb}}$	II-5
F ₁	Force on piston base	lb	
F ₂	Force on piston face	lb	
g	Gravitational constant	32.2 ft/sec ²	
j	Mechanical energy equivalent		
L	Length of launcher bore	ft.	
ℓ	Projectile length	in	
L _f	Courant number		II-12
m _P	Mass of piston	slugs	6
m _p	Mass of gas in pump tube	lb	I-1

BALLISTICS OF LIGHT GAS GUNS

<u>Symbol</u>		<u>Units</u>	<u>Equations where found</u>
m_p^0	Initial mass of gas in pump tube	lb	I-1
m_ℓ	Mass of gas in launch tube	lb	I-1
P	Pressure behind projectile	lb/in ²	
P_b	Pressure behind piston	lb/in ²	
P_r	Frictional pressure on piston	lb/in ²	
P_g	Pressure of gas in pump tube	psi	I-1
P_{r_ℓ}	Frictional resistance pressure on projectile in launch tube	$\frac{lb}{in^2}$	I-3
P_{ℓ_t}	Pressure in throat of transition section	$\frac{lb}{in^2}$	I-5
P_ℓ	Pressure in launch tube	lb/in ²	I-5
P^*	Pressure in throat of transition section at sonic velocity	$\frac{lb}{in^2}$	I-5
p_j^n	Pressure in j gas segment at time n	lb/in ²	II-2
P_{ss}	Shear pressure for projectile	psi	II-11
P_m^n	Maximum pressure in pressure profile at time n	psi	
q_j^n	Viscous pressure in j gas segment at time n	lb/in ²	II-2
R	Gas constant	$\frac{in - lb}{mole - ^\circ K}$	I-1
T_p	Temperature of gas in pump tube	$^\circ K$	I-1
T_ℓ	Temperature of gas in launch tube	$^\circ K$	I-3
Δt	Incremental time step	sec	II-1
t	Travel time for a projectile in characteristic expansion	sec	III-11
\bar{t}	Dimensionless travel time for a projectile in characteristic expansion		III-13

BALLISTICS OF LIGHT GAS GUNS

<u>Symbol</u>		<u>Units</u>	<u>Equations where found</u>
u_j^n	Velocity of j gas segment at time n	in/sec	II-1
v	Projectile velocity	f/s	
v_1	Velocity of piston base	f/s	
v_2	Velocity of piston face	f/s	
V	Piston velocity	in/sec	I-1
v	Projectile velocity	in/sec	I-3
v_g	Volume of gas in pump tube	in ³	I-8
V_j^n	Specific volume of j gas segment at time n	$\frac{\text{in}^3}{\text{lb}}$	II-3
V_m^n	Maximum specific volume in gas profile at time n	$\frac{\text{in}^3}{\text{lb}}$	II-13
v_r	Projectile velocity by a characteristic expansion	ft/sec	III-10
w	Projectile weight	lb	
w_p	Piston weight	lb	I-1
w_l	Projectile weight	lb	I-3
x_1	Travel of piston base	in	
x_2	Travel of piston face	in	
X	Piston travel	in	I-10
X_e	Projectile travel	in	I-13
x_j^n	Displacement of j gas segment at time n	in	II-1
\bar{x}	Dimensionless projectile travel under characteristic expansion		III-13

BALLISTICS OF LIGHT GAS GUNS

GREEK SYMBOLS

<u>Symbols</u>		<u>Units</u>	<u>Equations where found</u>
α_0	Escape speed of projectile under characteristic expansion	ft/sec	III-15
γ	Rate of specific heat of gas		
ρ	Projectile or piston density	lb/in ³	
ρ_0	Initial gas density in pump tube	lb/in ³	II-2
λ	Ratio of gas velocity in pump tube to piston velocity		I-2
λ^1	Ratio of gas velocity in launch tube of projectile velocity		I-2
Λ^3	Initial length of gas segment in pump tube	in	II-2

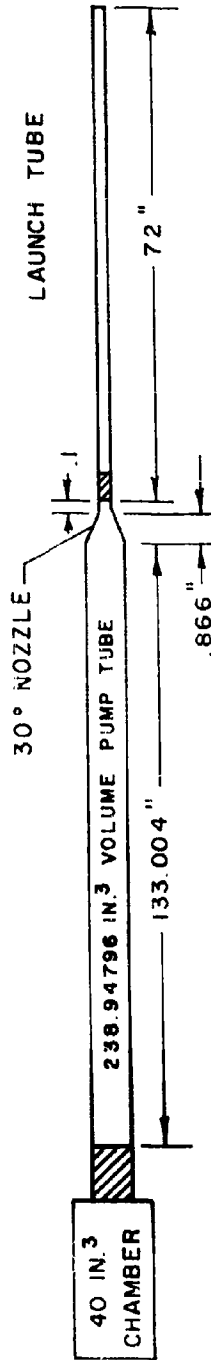
BALLISTICS OF LIGHT GAS GUNS

TABLE V

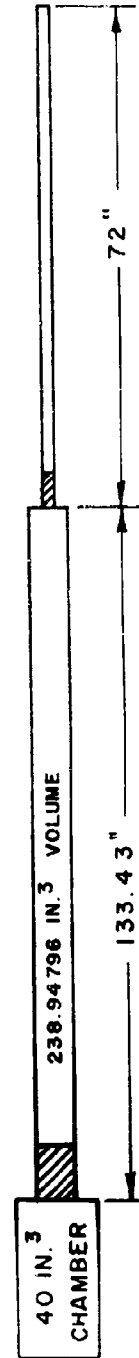
Round Number	Propellant Charge (GM)	Initial Helium Press (psi)	Projectile Shot Start Pressure (psi)			Projectile Weight (GM)	
			Shear	Exptl.	Theory	Exptl.	Theory
24	45.0	800.0	10000.	14000.	12200.	4.99	5.00
25	55.0	800.0	10000.	11000.	12200.	4.89	5.00
26	55.0	800.0	20000.	25023.	24400.	4.96	5.00
27	55.00	800.0	20000.	24451.	24400.	4.80	5.00
28	60.0	800.0	20000.	-----	24400.	4.93	5.00
29	60.0	800.0	20000.	23540.	24400.	4.86	5.00
30	65.0	800.0	20000.	23899.	24400.	4.92	5.00
10	65.0	800.0	20000.	21359.	24400.	4.92	5.00

Round Number	Muzzle Velocity (f/s)			Max. Propellant Pressure (psi)		Maximum Helium Pressure (psi)		
	Exptl.	Adiab.	Mass Pt.	Exptl.	Theory	Exptl.	Adiab.	Mass Pt.
24	4985.	5799.	-----	8022.	7176.	19665.	18422.	-----
25	5540.	6273.	-----	8770.	9045.	26936.	27238.	-----
26	6344.	7002.	7243.	9048.	9046.	31164.	31429.	46198.
27	-----	7002.	-----	9126.	9046.	31182.	31429.	-----
28	7124.	7304.	-----	9961.	10053.	42284.	36548.	-----
29	6874.	7304.	-----	15347.	10053.	40770.	36548.	-----
30	7494.	7585.	-----	19430.	11142.	39868.	42761.	-----
40	7573.	7731.	8765.	17964.	18169.	49690.	53885.	117457.

COMPUTER SIMULATION OF LIGHT GAS GUN



LIGHT GAS GUN MASS POINT MODEL



LIGHT GAS GUN ADIABATIC COMPRESSION MODEL

Figure 1

BALLISTICS OF LIGHT GAS GUNS

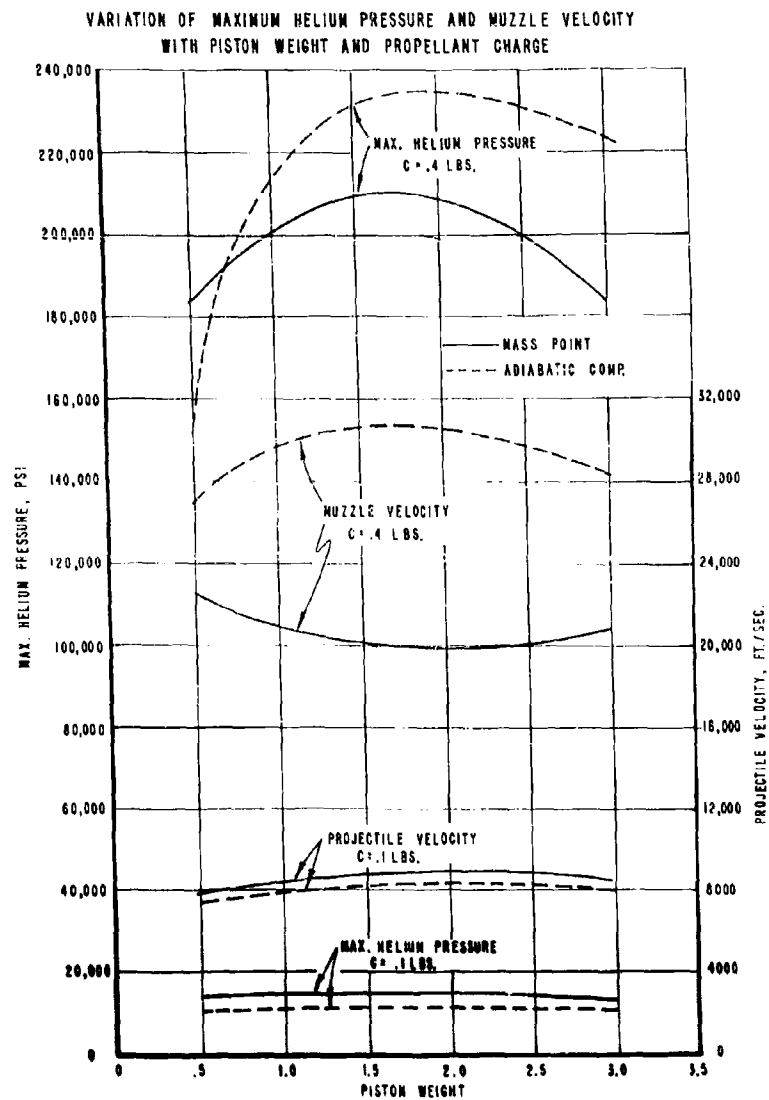


Figure 2

BALLISTICS OF LIGHT GAS GUNS

NUZZLE VELOCITIES OF LIGHT GAS GUN
USING PREHEATED HYDROGEN

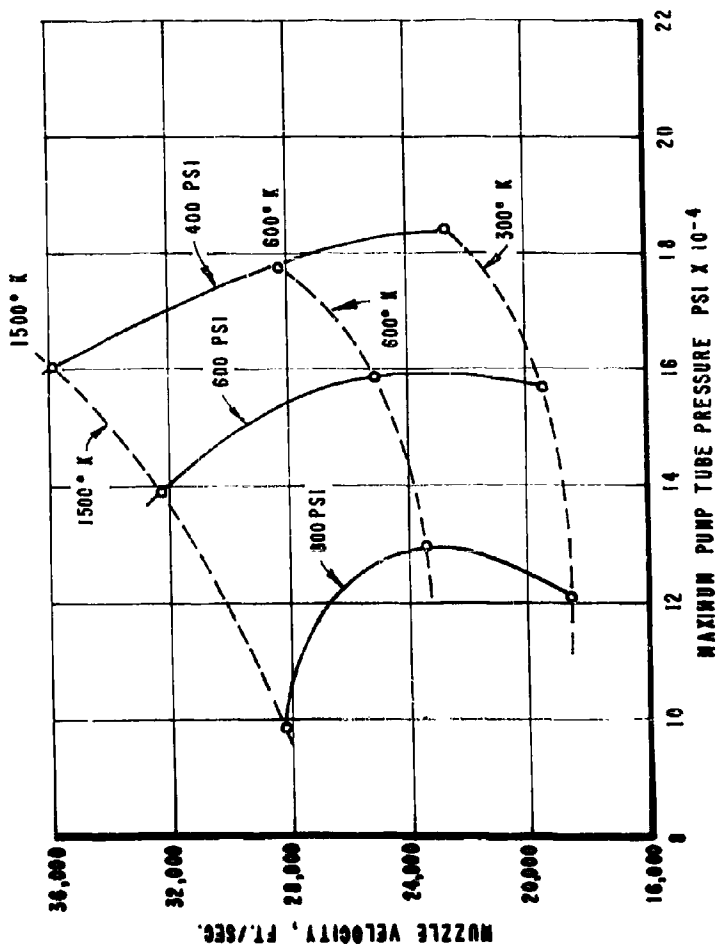


Figure 3

BALLISTICS OF LIGHT GAS GUNS

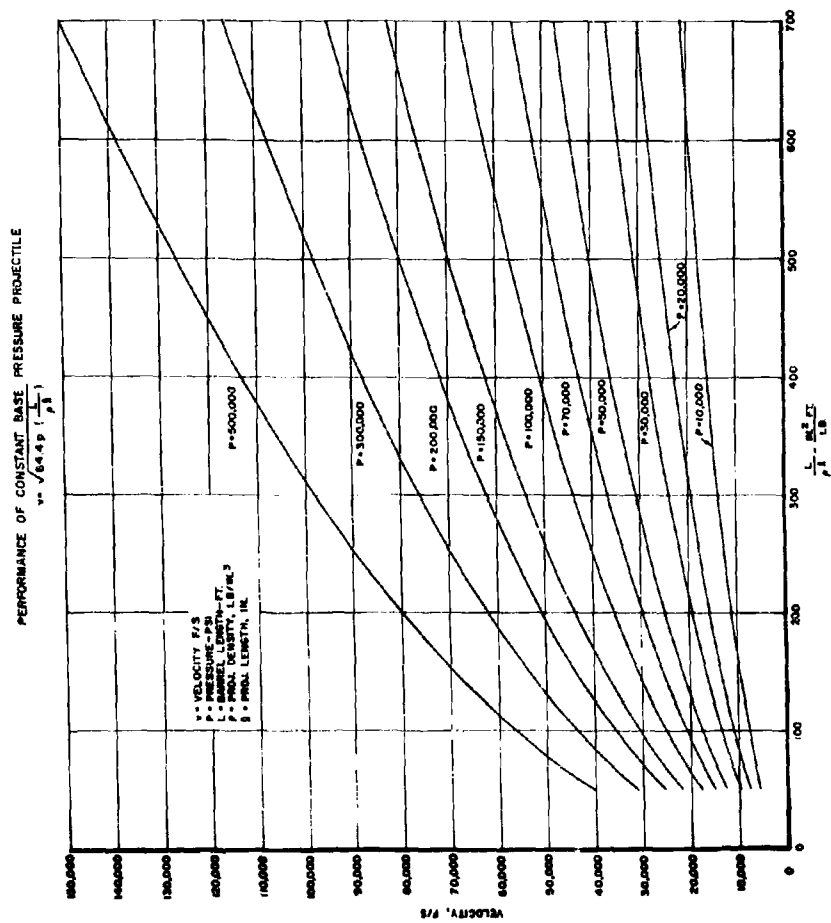


Figure 4

BALLISTICS OF LIGHT GAS GUNS

PROJECTILE VELOCITY
FOR
CONSTANT BASE PRESSURE FOLLOWED BY CHARACTERISTIC EXPANSION

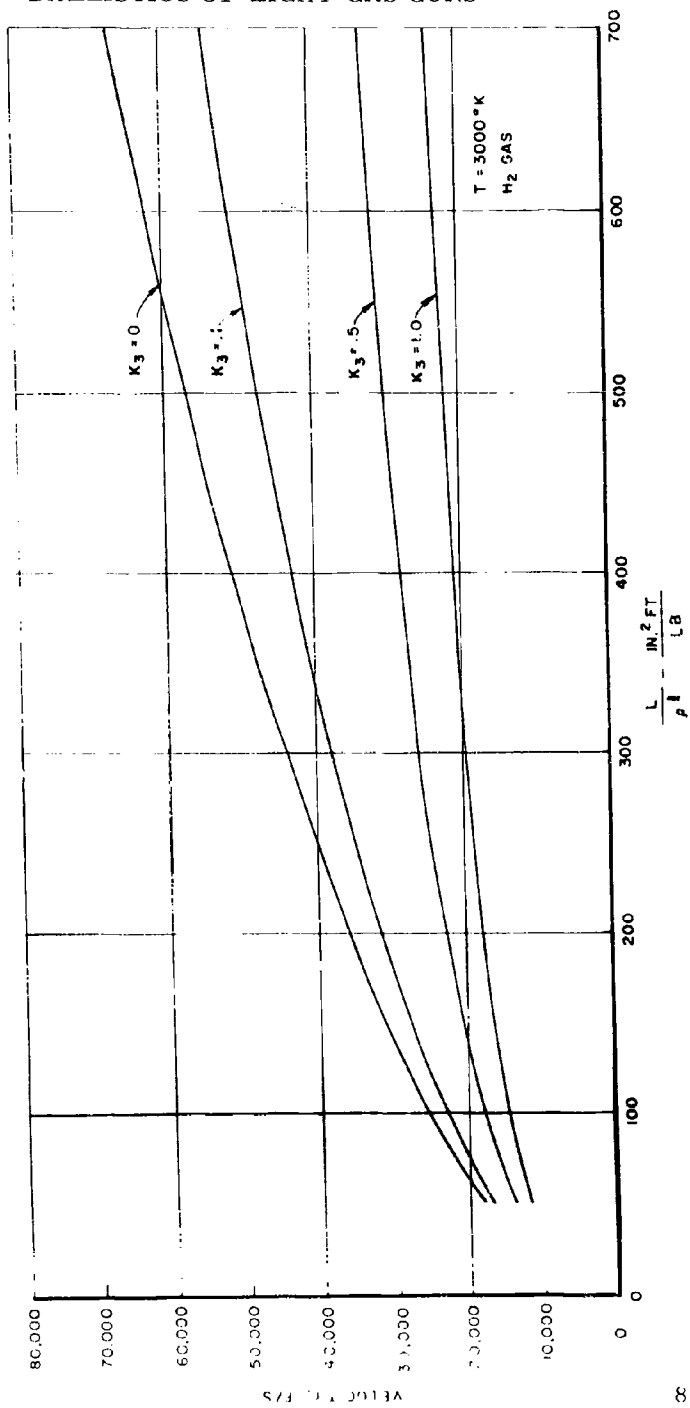


Figure 5

BALLISTICS OF LIGHT GAS GUNS

PROJECTILE VELOCITY
FOR
CONSTANT BASE PRESSURE FOLLOWED BY CHARACTERISTIC EXPANSION

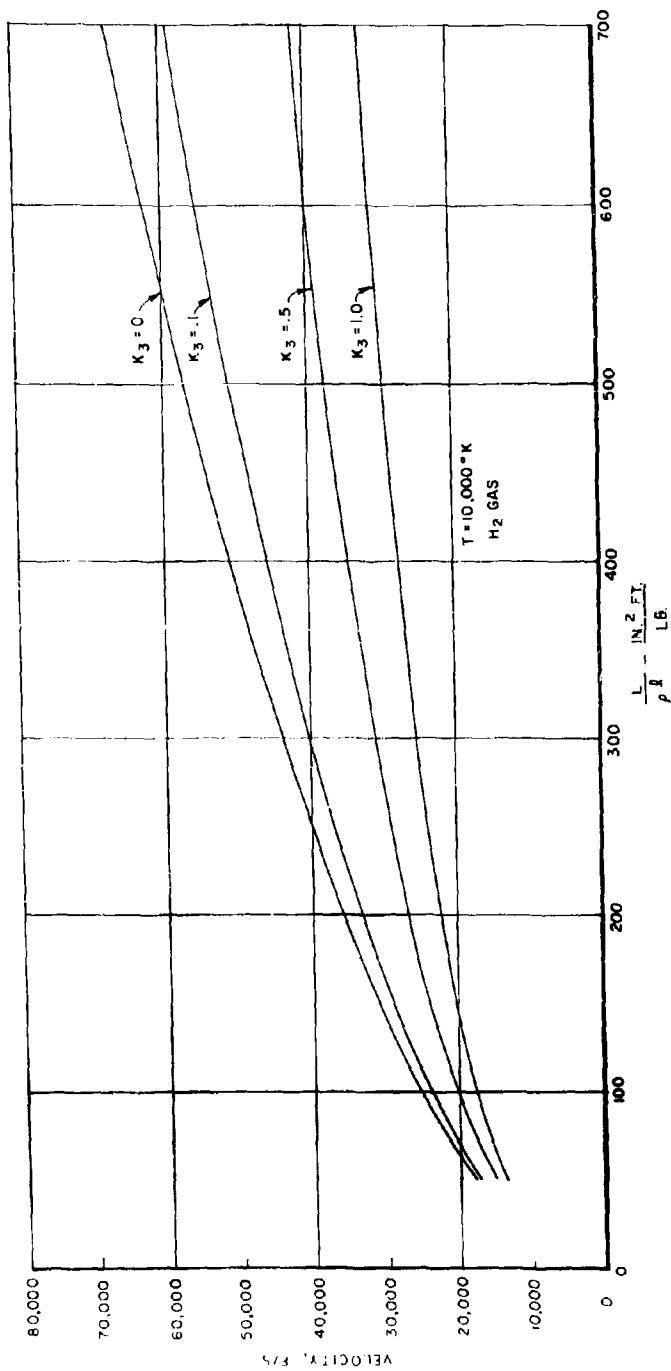


Figure 6

BALLISTICS OF LIGHT C.A.S GUNS

PROJECTILE VELOCITY
FOR
CONSTANT BASE PRESSURE FOLLOWED BY CHARACTERISTIC EXPANSION

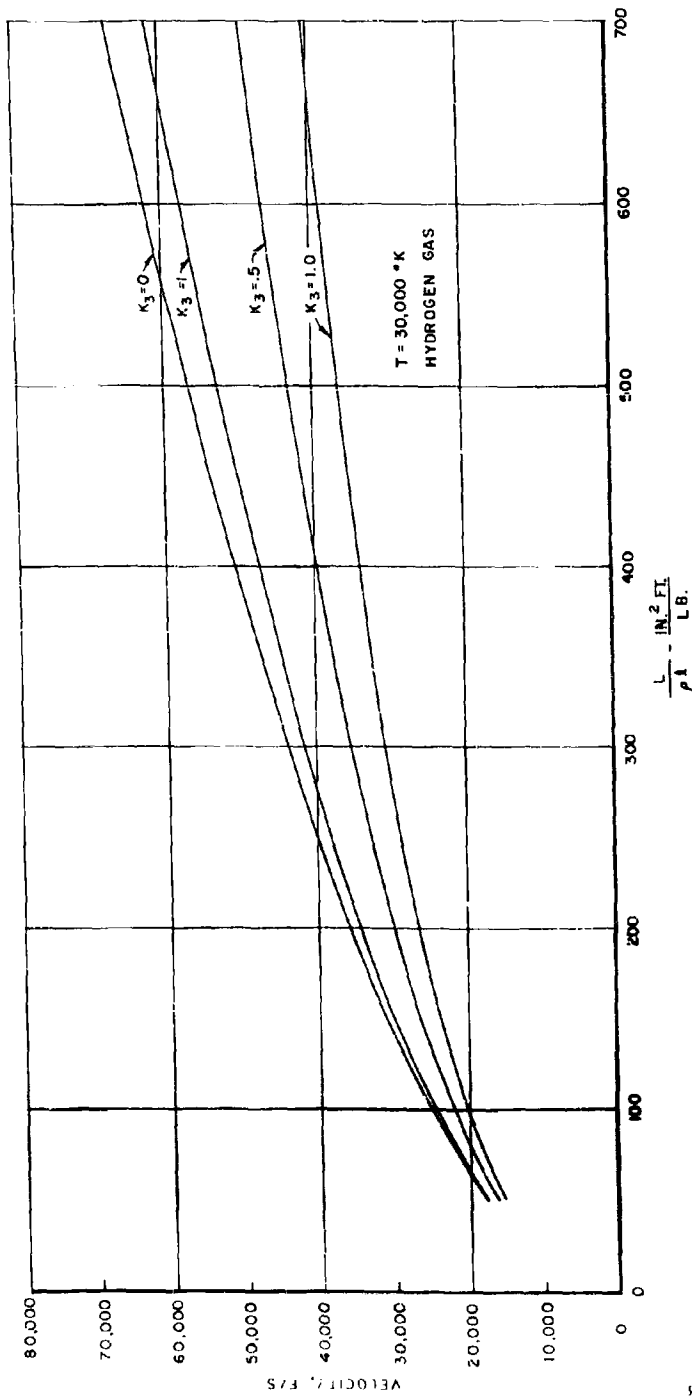


Figure 7

BALLISTICS OF LIGHT GAS GUNS

CONSTANT BASE PRESSURE LIGHT GAS GUN FOLLOWED BY CHARACTERISTIC EXPANSION

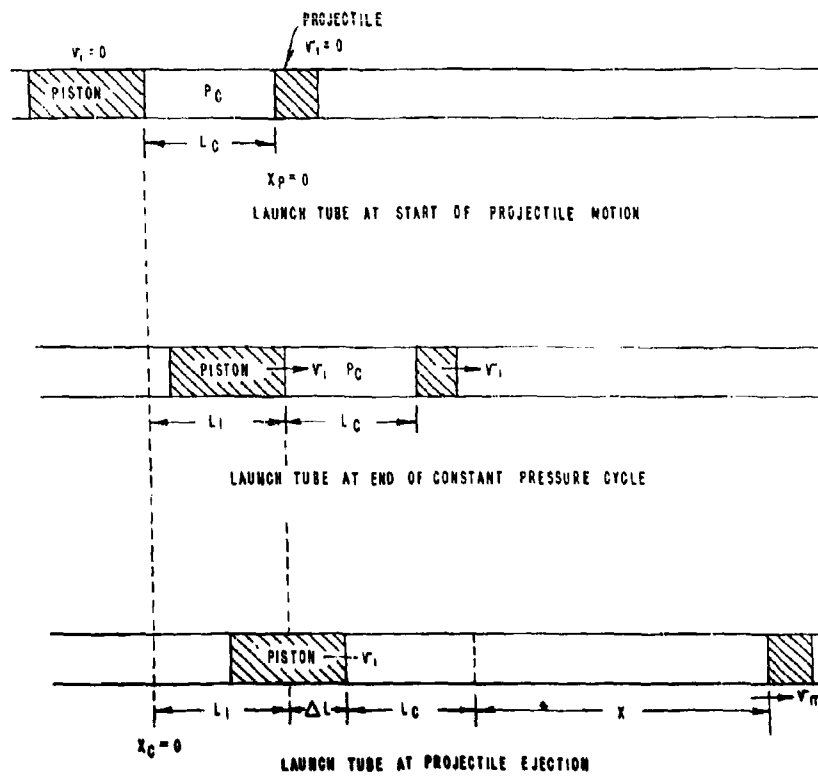
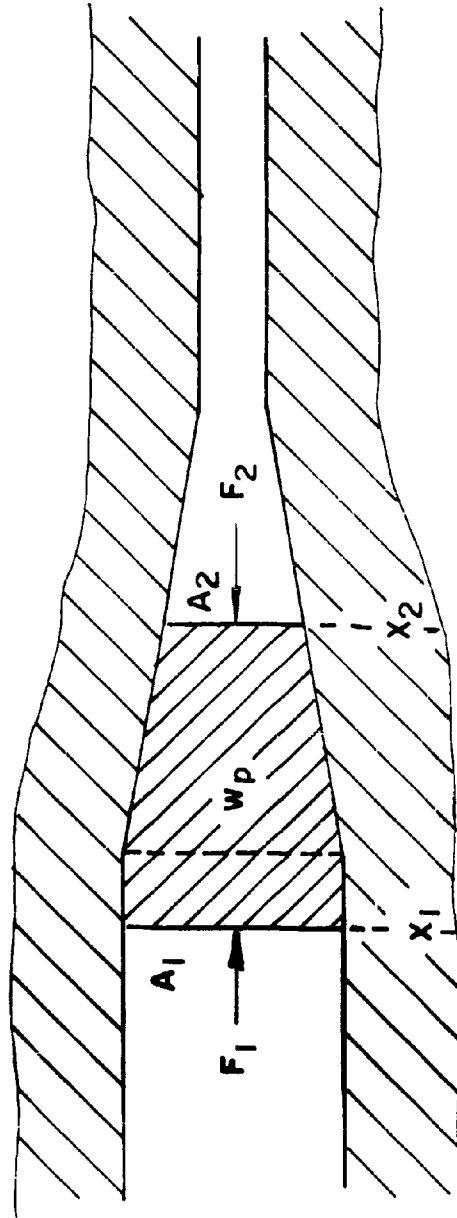


Figure 8



PISTON MOTION IN LIGHT GAS GUN NOZZLE

Figure 9

BALLISTICS OF LIGHT GAS GUNS

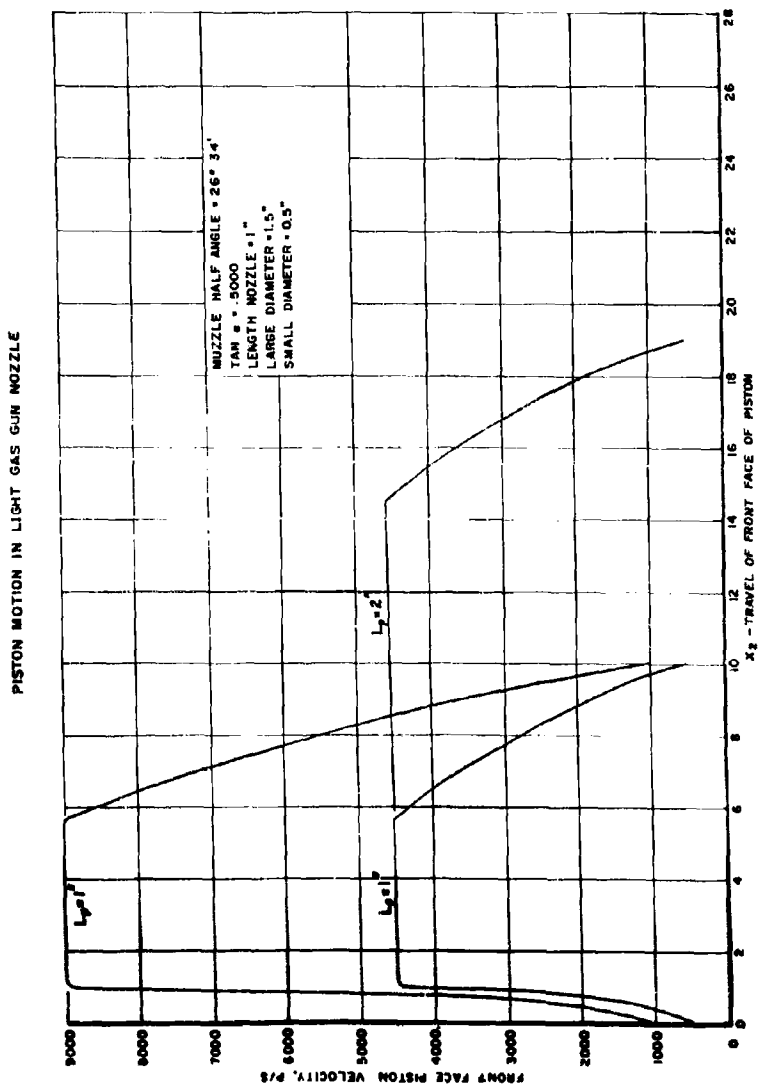
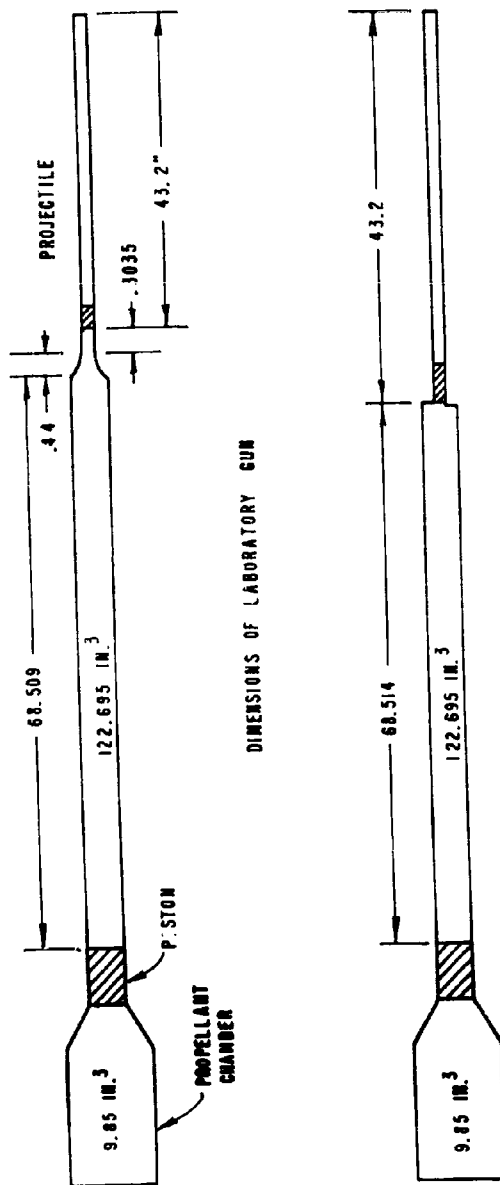


Figure 10

BALLISTICS OF LIGHT GAS GUNS



INTERIOR BALLISTIC LABORATORY LIGHT GAS GUN

Figure 11

BALLISTICS OF LIGHT GAS GUNS

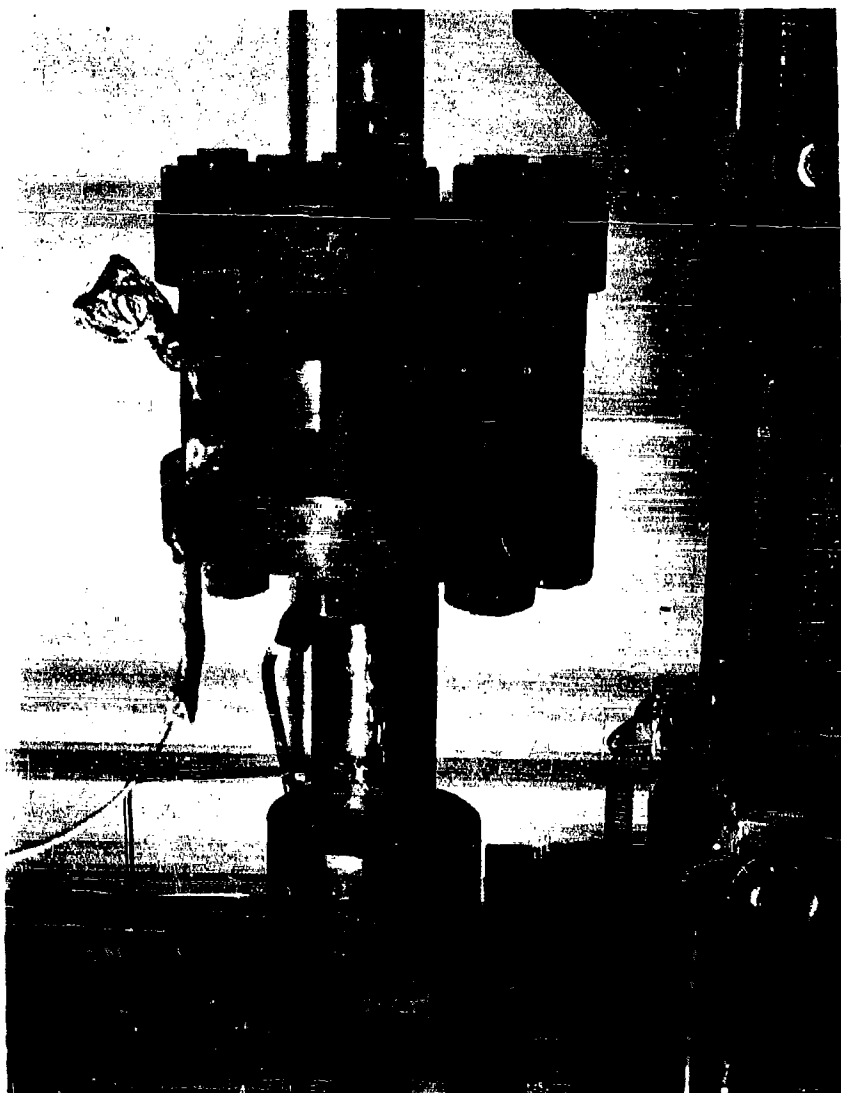


Figure 12

BALLISTICS OF LIGHT GAS GUNS

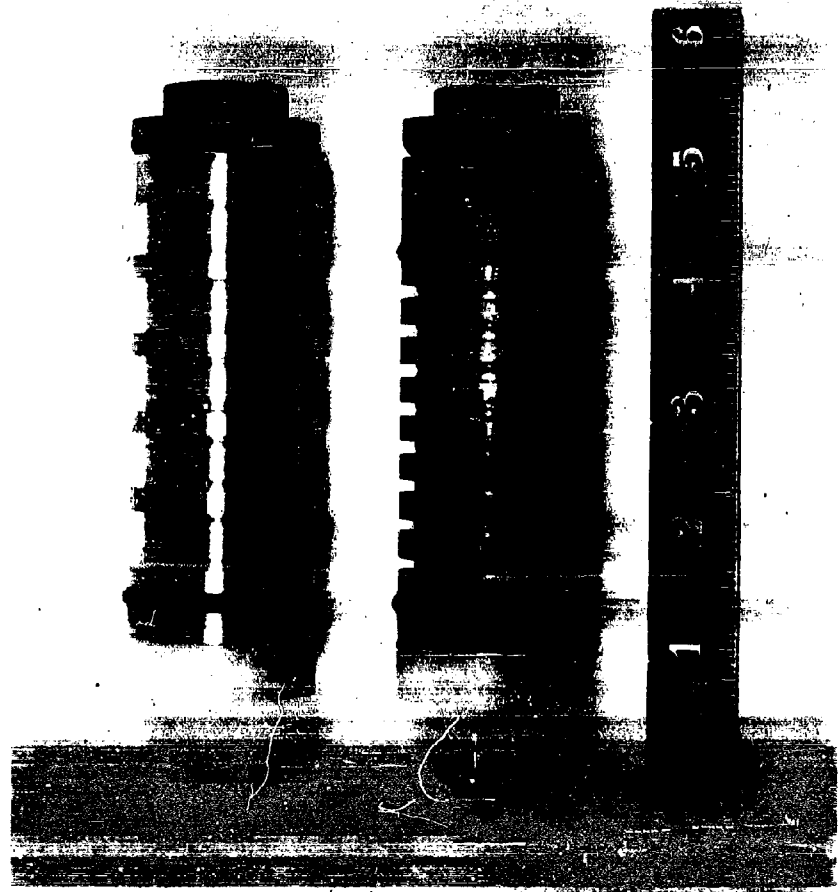


Figure 13

BALLISTICS OF LIGHT GAS GUNS



Figure 14

BALLISTICS OF LIGHT GAS GUNS

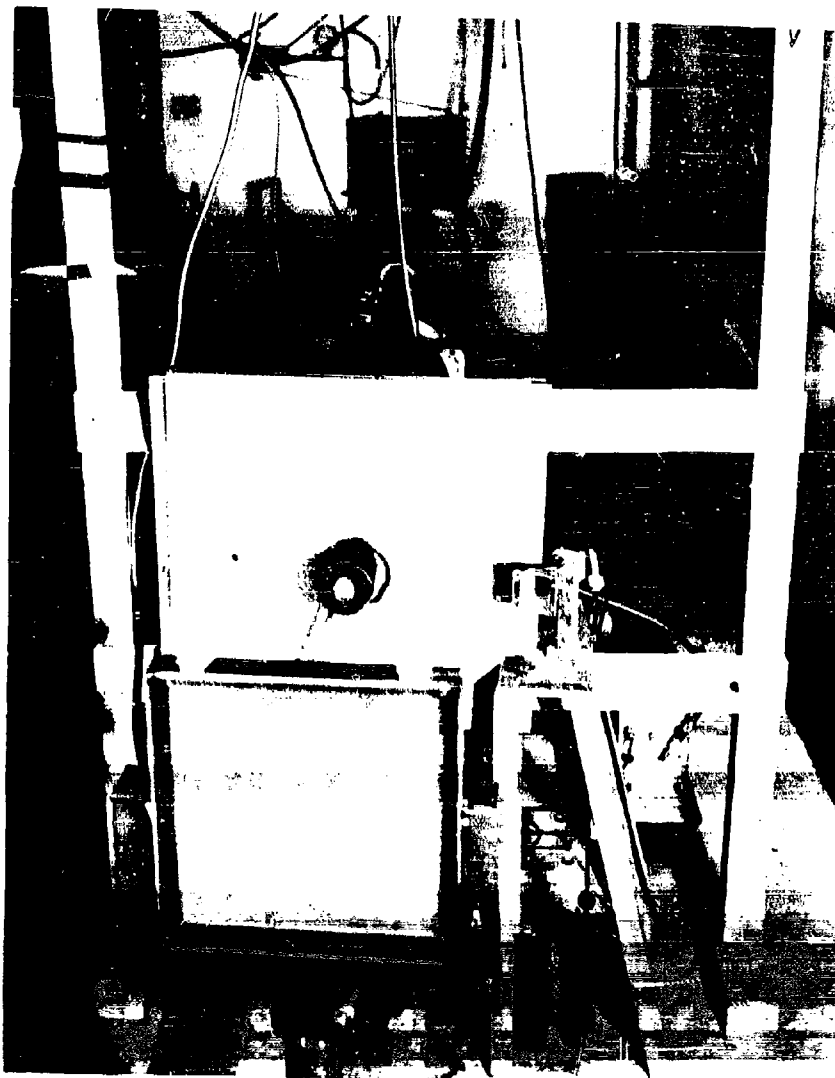
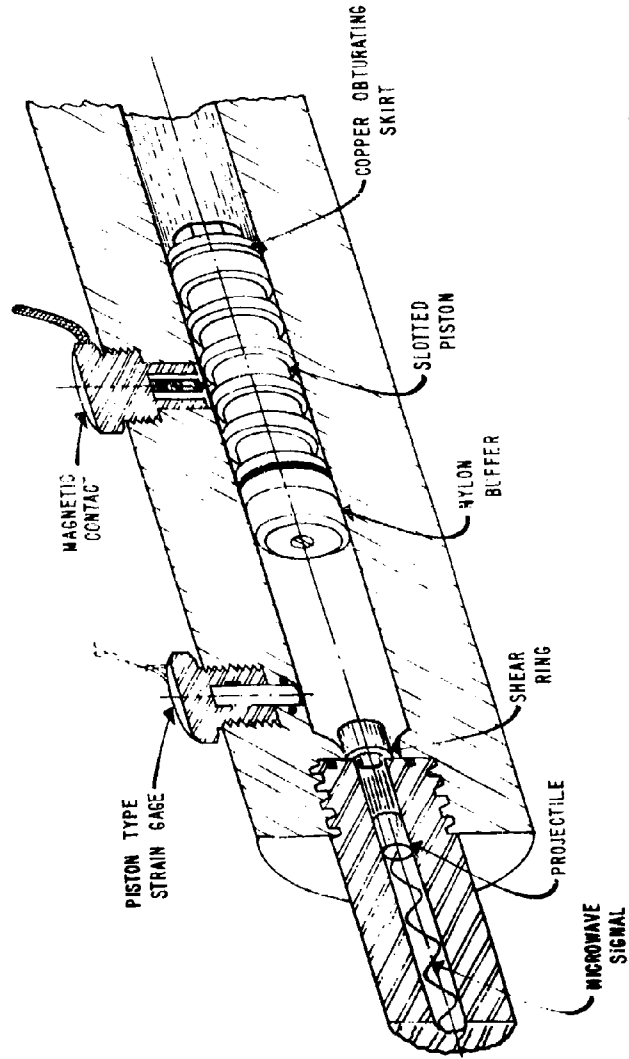


Figure 15

BALLISTICS OF LIGHT GAS GUNS



INSTRUMENTATION AT HIGH PRESSURE SECTION
OF
LIGHT GAS GUN

Figure 16

BALLISTICS OF LIGHT GAS GUNS

37 mm - 50 CAL LIGHT GAS GUN
 RD # 26
 COMPRESSION CYCLE
 INTERIOR BALLISTIC TRAJECTORY

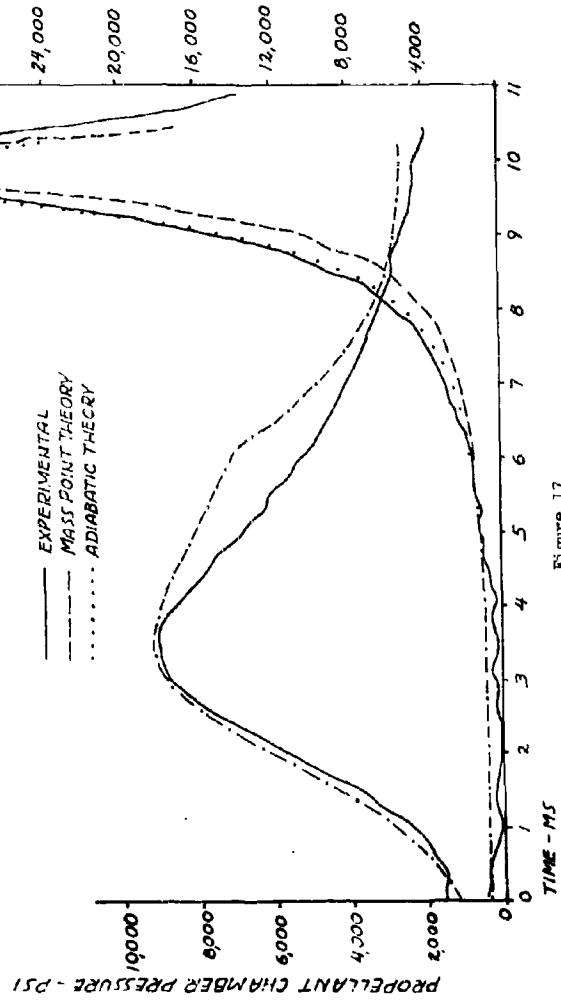


Figure 17

BALLISTICS OF LIGHT GAS GUNS

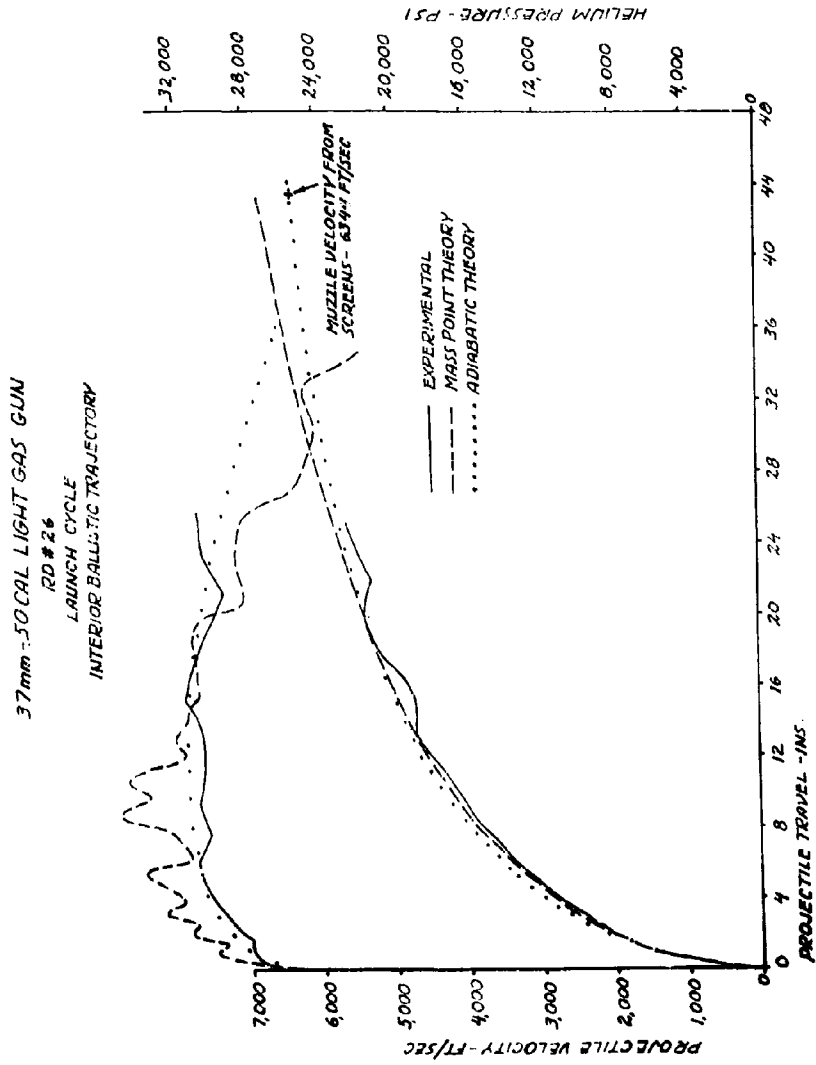


Figure 18

BALLISTICS OF LIGHT GAS GUNS

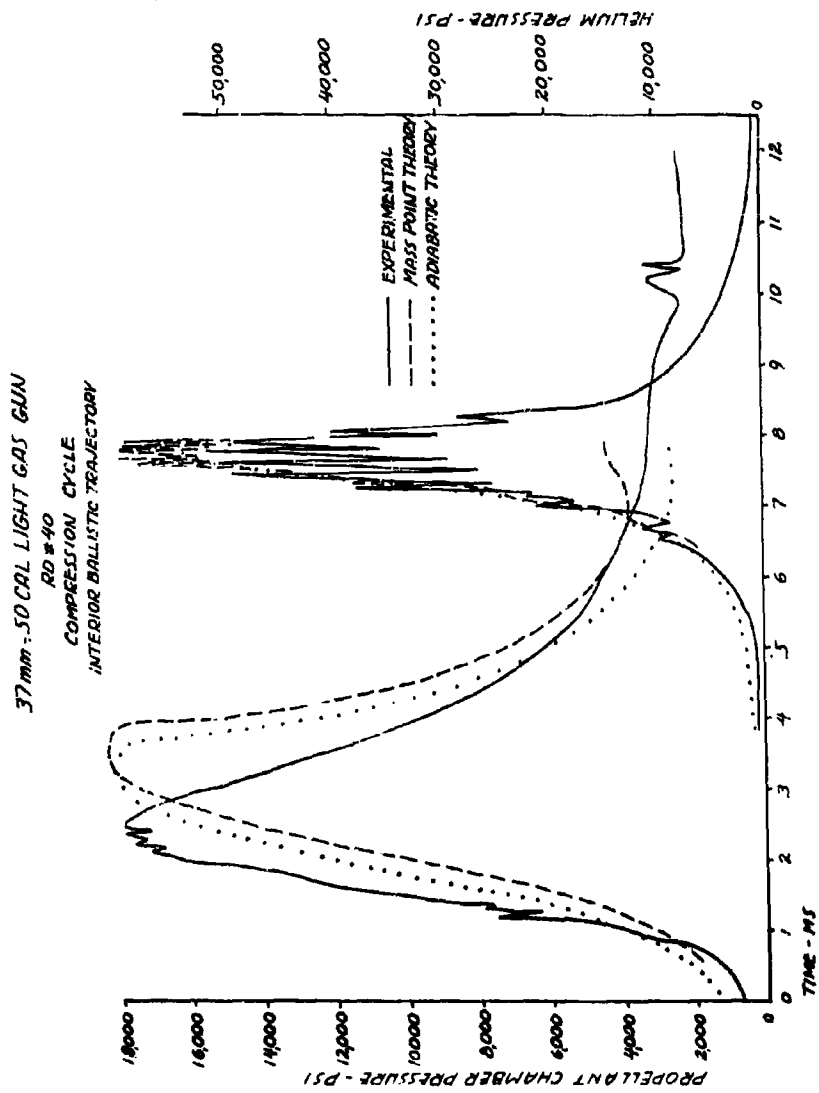


Figure 19

BALLISTICS OF LIGHT GAS GUNS

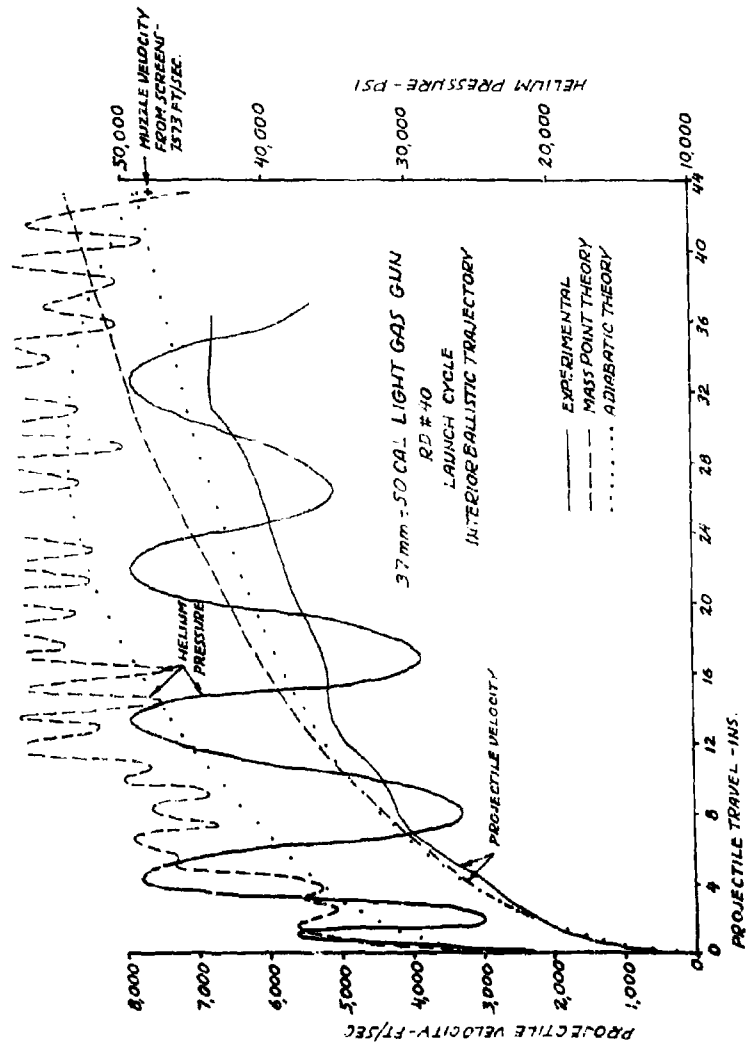


Figure 20

BALLISTICS OF LIGHT GAS GUNS

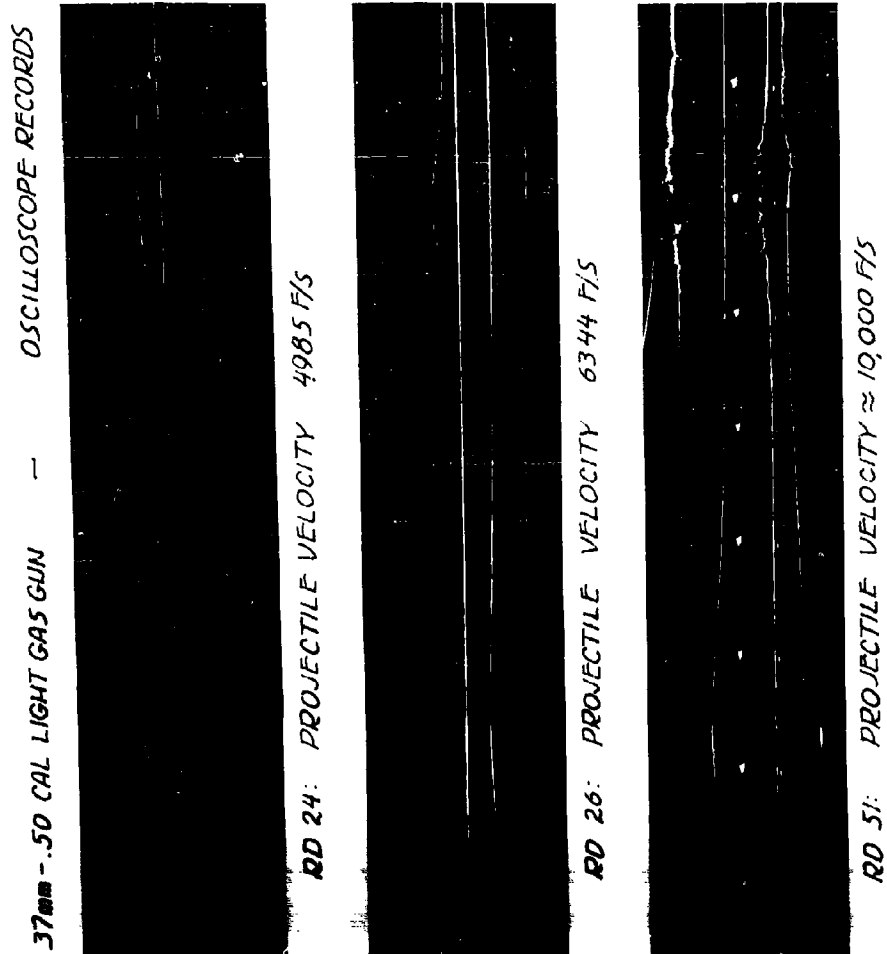


Figure 21

BALLISTICS OF LIGHT GAS GUNS

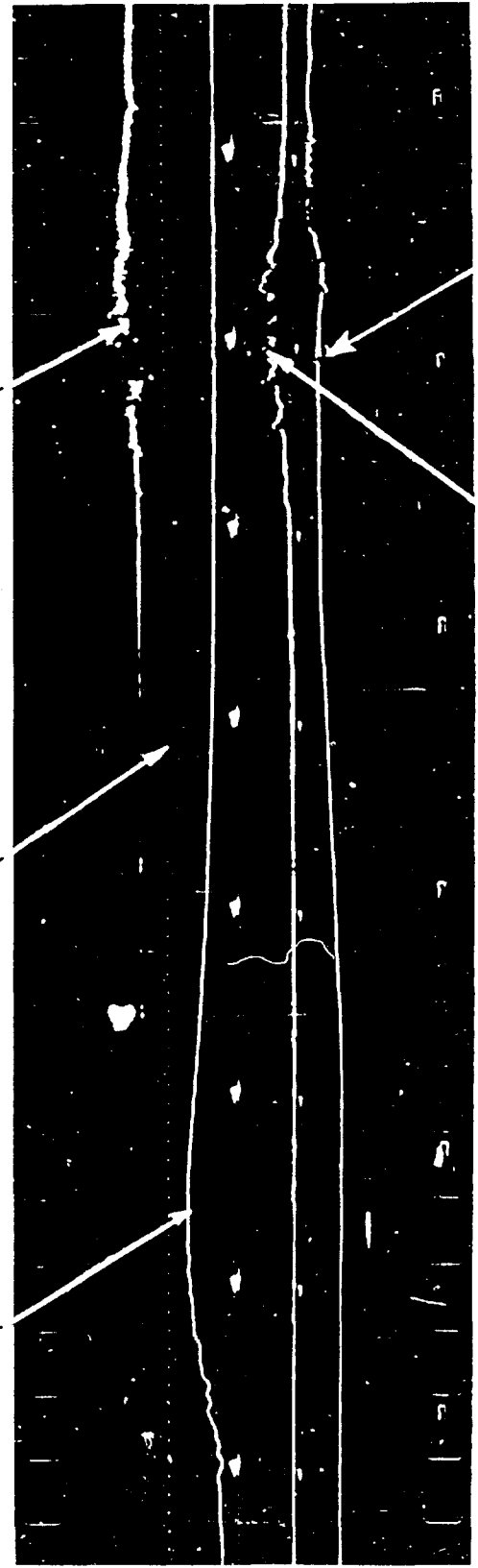
TYPICAL LIGHT GAS GUN OSCILLOSCOPE RECORD

RD. 51

0.1 MS. TIME MARKS

PROPELLANT PRESSURE

MAGNETIC CONTACT



HELIUM PRESSURE

INTERFEROMETER

Figure 22

BALLISTICS OF LIGHT GAS GUNS

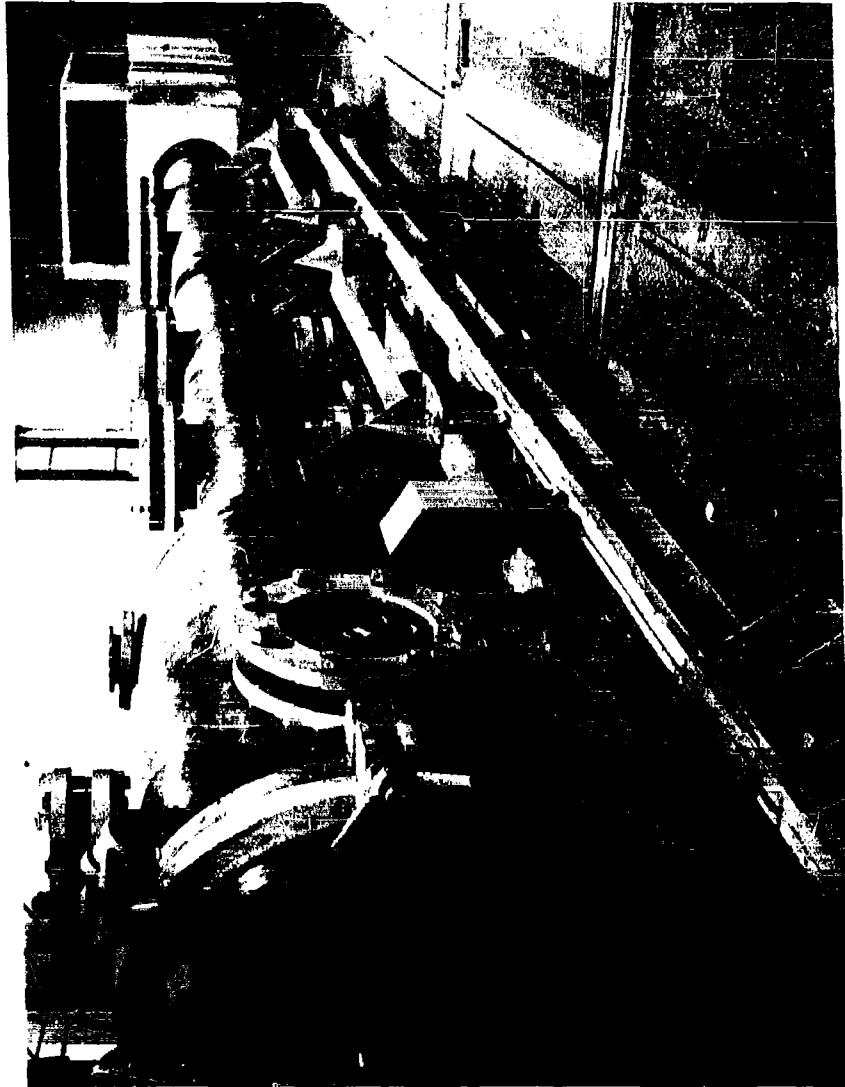


Figure 23

AN INVESTIGATION OF THE PERFORMANCE OF A
COMPRESSION HEATER FOR USE WITH GUN TUNNELS OR
HYPERVELOCITY LAUNCHERS

Bo Lemcke

Massachusetts Institute of Technology

March 1963

COMPRESSION HEATER PERFORMANCE

ABSTRACT

Two main modifications of the free piston compression heater have been considered for improving the performance of hypervelocity launchers and gun tunnels. To be able to predict the performance, analyses of the shock heating and the peak pressure generation including outflow of gas have been made. The conclusions from the analyses are that shock heating of hydrogen by means of a light piston at present seems very inefficient, that isentropic heating of the pump tube gas using a very high compression ratio would make it possible to launch very light projectiles at velocities of up to about 50,000 ft/sec, and that for gun tunnels, stagnation temperatures of up to about 5500 °K would be possible to obtain using hydrogen as driving gas.

COMPRESSION HEATER PERFORMANCE

Symbols

p	Pressure
ρ	Density
V	Specific volume
T	Absolute temperature
R	Universal gas constant
a	Sound speed
u	Particle velocity
U	Piston or projectile velocity
$\gamma = c_p/c_v$	Ratio of specific heats
\bar{n}	Number of kilomoles
M	Molecular weight
Z	Compressibility
H	Specific enthalpy per kilomole of initially undissociated gas
E	Specific energy
S	Specific entropy
x	Distance along tube
L	Length of tube
A	Cross-section area of tube
D	Diameter of tube
m	Mass of piston or projectile
t	Time
l	Length of gas layer that flows out of the chamber during time Δt

Indices

α	Driver gas
δ	Immediately behind the piston or the projectile
r	Properties of working gas at room temperature (290 °K) and atmospheric pressure
o	Initial conditions in main barrel, or physical properties of main barrel
10	Accelerating section

COMPRESSION HEATER PERFORMANCE

l	Launch tube, projectile
n	Conditions in main barrel after the passage of the n^{th} shock wave
∞	Conditions in front of the piston when this has come to rest with the same pressure on both sides
M	Peak conditions
$*$	Sonic conditions
p	Piston
s	When the projectile is released
t	When the projectile leaves the launch tube

Dimensionless Variables

\bar{U}	U/a_{α}
\bar{u}	u/a_{α}
\bar{a}	a/a_{α}
\bar{p}	p/p_{α}
\bar{T}	$T/T_r = T/290$
\bar{H}	H/RT
\bar{h}	$\bar{h} \cdot \bar{T} = H/RT_r$
\bar{E}	E/RT
\bar{e}	$\bar{e} \cdot \bar{T} = E/RT_r$
\bar{S}	S/R
$\bar{\sigma}_n$	p_n/p_{n-1}
\bar{x}	$(p_{\alpha} A_0 x)/(m_p \cdot a_{\alpha}^2)$
\bar{t}	$(p_{\alpha} A_0 t)/(m_p \cdot a_{\alpha})$
\bar{A}	A/A_0
Γ	$[2/(\gamma + 1)]^{(\gamma+1)/2(\gamma-1)}$
B	Average value of $(p/p_s)^{-(\gamma-1)/2\gamma}$

COMPRESSION HEATER PERFORMANCE

$$\begin{aligned}
 f & \quad \Gamma \bar{A}_f \bar{B} \bar{a}_s / (\bar{L}_0 - \bar{x}_s) \bar{P}_s \\
 F & \quad (2 - \gamma) \bar{A}_f^2 \Gamma^2 \bar{B}^2 \bar{a}_s^2 / (\bar{L}_0 - \bar{x}_s) \bar{P}_s \\
 \lambda & \quad 1 - \frac{1.5}{2 + \sqrt{\frac{2}{\gamma + 1}} (10)^{(\gamma - 1) / 2\gamma}}
 \end{aligned}$$

COMPRESSION HEATER PERFORMANCE

INTRODUCTION

Gas compression by means of a free piston has been used a long time for producing high pressure, high temperature gases. Two well-known applications of this technique are the gun tunnel and the two- (or three-) stage hypervelocity launcher. In the gun tunnel air is heated for driving a hypersonic nozzle; in the launcher, helium or hydrogen is compressed to form a driver for a light projectile. In both of these cases it is desirable to reach as high a temperature as possible. The reason for this is to be able to simulate real gas effects (dissociation) in the hypersonic flow for the gun tunnel operation, and to create higher sound speed which will give a higher projectile velocity in the launcher.

The main parameters that affect the final temperature during a rapid compression are the compression ratio p_f/p_0 , the piston velocity divided by the sound speed in the undisturbed gas, U/a_0 , and the initial temperature T_0 , where index f refers to the final state. For an isentropic compression of a perfect gas, the final temperature is given by $T_f = T_0 (p_f/p_0)^{(\gamma-1)/\gamma}$. If the piston velocity is high enough to create a shock wave, the entropy will increase and the final temperature will become higher than for the isentropic compression with the same value of p_f/p_0 and T_0 .

Two main factors will limit the temperature that can be obtained by free piston compression. First, the shock formation process, discussed below and in Refs. 1 and 2, makes it impossible to fully exploit the advantage of shock compression in a conventional free-piston compression heater. For high piston velocities the final temperature can be considerably lower than would be expected from theories not taking this effect into account. Second, due to the kinetic energy of the piston, a pressure peak will occur in the working gas when the piston is brought to rest at the end of the barrel. This peak

COMPRESSION HEATER PERFORMANCE

pressure must be limited from a structural point of view. Also, the piston strength itself might put a limit to the peak pressure, as has been the case in all gun tunnels so far, where this peak value has been considerably lower than reasonable design considerations of the facility would indicate. Thus certain restrictions have to be made on the different parameters that affect the performance of a compression heater.

A modified use of the compression heater is suggested in this paper to eliminate the entropy gradient in front of the piston and to be able to use peak pressures in gun tunnels of the same order as those currently achieved in launchers. Calculations of the performance indicate that final temperatures of about 5000 °K could be obtained in gun tunnels, using helium at 2000 atm as the driving gas. For launchers employing hydrogen as working gas it is shown that it is unrealistic to consider shock heating by means of a piston. By using preheated hydrogen and high pressure ratios, the calculations indicate that velocities of up to 50,000 ft/sec could be obtained with light projectiles.

CONSIDERED MODIFICATIONS OF THE COMPRESSION HEATER

If the piston is accelerated directly into the working gas, see Fig. 1, a shock wave with increasing strength will be formed ahead of the piston. A lamina in the working gas will be heated first non-isentropically through the shock wave and then isentropically through the compression waves from the accelerating piston, see Refs. 1 and 2. Thus an axial entropy gradient with a corresponding temperature gradient will be produced in the working gas. The higher the piston velocity becomes, the greater this entropy gradient will be. This means that the advantage of shock compression cannot be fully exploited. In Ref. 1 an evacuated accelerating section was suggested for the piston to eliminate the entropy gradient in the working gas. This modification of the compression heater will

COMPRESSION HEATER PERFORMANCE

be considered here in connection with the launcher and the gun tunnel.

In gun tunnels the strength of the piston has been the main limiting factor of the performance. For those light pistons that have been used in gun tunnels the peak pressure has destroyed the pistons at pressures of the order of 500 to 1000 atm. A modified operation of the gun tunnel will be considered in this paper using solid heavy pistons. Such pistons will be able to withstand very high peak pressures (50,000 atm). The end of the barrel must then be reinforced to the same degree. The modified compression heater is shown in Fig. 2 with corresponding piston and shock-wave histories.

To be able to predict the performance of the modified compression heater certain details of the history have to be worked out; namely, the acceleration of the piston into vacuum, the shock heating and isentropic heating of a real gas, and the generation of the peak pressure including the outflow of gas from the high pressure section. These problems will be dealt with in the following sections.

PISTON ACCELERATION

In the modified compression heater, the piston is first accelerated into an evacuated section which is separated from the main barrel by a thin diaphragm (see Fig. 2). The required length of the accelerating section for different driving gases, driving pressures, piston masses, and piston velocities will be given in this section. This has been done in many papers before, but the final results will be presented for use later on.

The equation of motion for the piston is

$$\frac{d^2x}{dt^2} = \frac{A_0 p_0}{m_p} \quad (1)$$

COMPRESSION HEATER PERFORMANCE

or in dimensionless variables

$$\frac{d^2 \bar{x}}{dt^2} = \bar{p}_6 \quad (2)$$

where the pressure in front of the piston has been neglected as well as the friction force at the barrel walls. For a driver with a large cross section, the pressure behind the piston, if the driving gas is treated as a perfect gas, is given by

$$\bar{p}_6 = \left(1 - \frac{\gamma_\alpha - 1}{2} \bar{U}_p^2 \right)^{\frac{\gamma_\alpha}{\gamma_\alpha - 1}} \quad \text{for } \bar{U}_p \leq \sqrt{\frac{2}{\gamma_\alpha + 1}} \quad (3)$$

$$\bar{p}_6 = \left(\sqrt{\frac{\gamma_\alpha + 1}{2}} - \frac{\gamma_\alpha - 1}{2} \bar{U}_p \right)^{\frac{2\gamma_\alpha}{\gamma_\alpha - 1}} \quad \text{for } \bar{U}_p \geq \sqrt{\frac{2}{\gamma_\alpha + 1}}$$

Integration of Eq. (2), using Eq. (3) gives for $\bar{U}_p \geq \sqrt{2/(\gamma_\alpha + 1)}$

$$\begin{aligned} \bar{x} = & \frac{\bar{U}_p - \sqrt{\frac{2}{\gamma_\alpha + 1}}}{\left(\sqrt{\frac{\gamma_\alpha + 1}{2}} - \frac{\gamma_\alpha - 1}{2} \bar{U}_p \right)^{(\gamma_\alpha + 1)/(\gamma_\alpha - 1)}} + \\ & + \left(\frac{\gamma_\alpha + 1}{2} \right)^{\frac{1}{\gamma_\alpha - 1}} - 1 \end{aligned} \quad (4)$$

Figure 3 shows \bar{x} as a function of \bar{U}_p for $\gamma_\alpha = 1.40$ and 1.66. The corresponding driving gases are assumed to be air or

COMPRESSION HEATER PERFORMANCE

hydrogen, and helium, respectively.

SHOCK COMPRESSION

Equations and curves will now be worked out from which the pressure and temperature change through a shock wave moving into a gas of known state can be iterated. The curves will concern air and hydrogen.

The conservation equations for the transition through a plane shock wave are, if (n - 1) indicates conditions in front of the wave and (n) conditions behind the wave

$$\frac{H_n - H_{n-1}}{M_r} = \frac{(u_n - u_{n-1})^2}{2} \cdot \frac{\rho_n + \rho_{n-1}}{\rho_n - \rho_{n-1}} \quad (5)$$

$$p_n - p_{n-1} = (u_n - u_{n-1})^2 \cdot \frac{\rho_n \rho_{n-1}}{\rho_n - \rho_{n-1}} \quad (6)$$

In addition to these an equation of state is needed which will be written

$$p = \frac{R}{M_r} \rho T \quad (7)$$

To simplify Eqs. (5) and (6) the perfect gas expression of the sound speed at room temperature and atmospheric pressure will also be used

$$a_r^2 = \gamma_r \frac{R}{M_r} T_r \quad (8)$$

where $T_r = 290$ °K. Elimination of ρ_n and ρ_{n-1} between Eqs. (5), (6) and (7) and Eqs. (6) and (7), respectively, gives in nondimensional variables

$$\bar{H}_n = \bar{H}_{n-1} - \frac{\gamma_r}{2} \left(\frac{\bar{u}_n - \bar{u}_{n-1}}{\bar{a}_r} \right)^2 + (\bar{\sigma}_n - 1) z_{n-1} T_{n-1} \quad (9)$$

COMPRESSION HEATER PERFORMANCE

$$\sigma_n = \frac{1}{2} \left[C + \sqrt{C^2 - 4 \frac{Z_n \bar{T}_n}{Z_{n-1} \bar{T}_{n-1}}} \right] \quad (10)$$

where

$$C = 1 + \frac{\gamma_r \left(\frac{\bar{u}_n - \bar{u}_{n-1}}{\bar{a}_r} \right)^2 + Z_n \bar{T}_n}{Z_{n-1} \bar{T}_{n-1}}$$

Equations (9) and (10) may be written

$$h_n = h_n(\bar{h}_{n-1}, \gamma_r, \bar{u}_n - \bar{u}_{n-1}, \bar{a}_r, \bar{\sigma}_n, Z_{n-1} \bar{T}_{n-1})$$

where $\bar{u}_n - \bar{u}_{n-1}$ and $\bar{\sigma}_n$ are the unknown variables, and

$$\sigma_n = \sigma_n(\gamma_r, \bar{u}_n - \bar{u}_{n-1}, \bar{a}_r, Z_{n-1} \bar{T}_{n-1}, Z_n \bar{T}_n)$$

where $\bar{u}_n - \bar{u}_{n-1}$ and $Z_n \bar{T}_n$ are the unknown variables. Now, from the definition of \bar{h} and Z , it is known that

$$\bar{h} = \bar{h}(T, p) \quad (11)$$

and

$$Z\bar{T} = Z\bar{T}(T, p) \quad (12)$$

i.e., \bar{h} and $Z\bar{T}$ are functions of the state in the gas and can be found with the aid of a table of thermodynamic properties of the particular gas of interest.

Equations (9) and (10) and curves from Eqs. (11) and (12) have been used for iterating values of p_n/p_0 and \bar{T}_n for repeatedly reflected shock waves in air and hydrogen according to the following scheme, starting with $n = 1$:

- (a) Choose a value of $(\bar{u}_n - \bar{u}_{n-1})/\bar{a}_r$ and p_0
- (b) Compute \bar{h}_n from Eq. (9) with the perfect gas value of $\bar{\sigma}_n$
- (c) Determine $Z_n \bar{T}_n$ from Eqs. (11) and (12)

COMPRESSION HEATER PERFORMANCE

- (d) Compute $\bar{\sigma}_n$ from Eq. (10) and go back to (b)
- (e) Repeat until the desired accuracy is obtained.

Determine \bar{T}_n from Eq. (12)

The corresponding curves to Eqs. (11) and (12) were prepared from data by Gilmore (Ref. 3), Hilsenrath and Beckett (Ref. 4), and Rosenbaum and Levitt (Ref. 5). For air, Gilmore's tables were used whenever possible and Hilsenrath and Beckett's only when needed (for lower pressures). For hydrogen the tables were extended to higher pressures using the equations and curves of Ref. 5.

The results of the calculations are given in Figs. 4 and 5. Figure 4 shows the pressure and temperature behind successive shock waves in air for different initial pressures and temperatures. The same data for hydrogen with the initial temperature equal to 290 °K are shown in Fig. 5. Figure 4a and b have been compared with curves prepared by Stollery (Ref. 6) and a reasonably good agreement is found. The deviations are probably due to the high pressure effects that are included in Gilmore's tables and thus do not show up in Stollery's results.

PEAK PRESSURE WITH OUTFLOW OF GAS

Due to the kinetic energy of the piston, a peak pressure will be produced in the working gas when the piston is brought to rest at the end of the barrel. This peak pressure is of great importance both from a structural point of view as well as for the launching conditions in a launcher.

In Ref. 8 the peak pressure in a launcher has been predicted by augmenting the energy in the working gas when the piston has its maximum velocity with the kinetic energy of the piston at this moment. This process can be described mathematically by

COMPRESSION HEATER PERFORMANCE

$$\frac{1}{2} m_p U_p^2 = - \int_{S=\text{const.}}^{(M)} p d(\bar{n}V) = - \bar{n}_r \int_{S=\text{const.}}^{(M)} p dV \quad (13)$$

where it is assumed that the entropy remains constant during the deceleration of the piston and that the contribution to the peak pressure from the driving gas can be neglected. It is also understood that the mass of the energy absorbing gas, $\bar{n} \cdot M$, remains constant throughout the process.

Two different approaches will be made to improve Eq. (13). First, the energy of the driving gas will be taken into account; second, the outflow of gas will be included, neglecting the driving gas.

In Eq. (13) an extra term will be required to take the energy of the driving gas into account and this term will be assumed to be a constant, independent of U. Thus

$$\text{const.} + \frac{1}{2} m_p U_p^2 = - \bar{n}_r \int_{S=\text{const.}}^{(M)} p dV \quad (14)$$

To determine the constant the case of $m_p = 0$ will be suitable. In this case it is known that the maximum pressure will be equal to

$$P_M = \left(\frac{\gamma_\alpha + 1}{2} \right)^{\frac{\gamma_\alpha}{\gamma_\alpha - 1}} P_\alpha = P_\infty$$

for a large area driver. It is then found that

$$\text{const.} = - \bar{n}_r \int_{S=\text{const.}}^{(\infty)} p dV$$

COMPRESSION HEATER PERFORMANCE

and

$$\frac{1}{2} m_p U_p^2 = - \bar{n}_r \int_{(\infty)}^{(M)} p dV \quad (15)$$

S=const.

From the first law of thermodynamics it is seen that

$$p dV = - dE$$

since $dQ = 0$. Furthermore, the mass contained in the barrel is $\bar{n}_0 M_0 = \bar{n}_r M_r$ or $L_0 \Lambda_0 \rho_0$ from which

$$\bar{n}_r = \frac{L_0 \Lambda_0 \rho_0}{M_r} = \frac{L_0 \Lambda_0 \rho_0}{R Z_0 T_0} \cdot \frac{M_0}{M_r}$$

where the equation of state has also been used. If the initial temperature and pressure, T_0 and p_0 , are not too high it is possible to write

$$Z_0 = 1.0 \text{ and } M_0 = M_r$$

Equation (15) can then be rewritten

$$\frac{1}{2} m_p U_p^2 = \frac{L_0 \Lambda_0 \rho_0}{R T_0} \int_{(\infty)}^{(M)} dE = \frac{L_0 \Lambda_0 \rho_0}{R T_0} (E_M - E_\infty) \quad (16)$$

S=const.

or in dimensionless form

$$(\bar{e}_M - \bar{e}_\infty)_{\bar{S}=\text{const.}} = \frac{\bar{U}_p^2 \bar{T}_0}{2 \bar{L}_0 \bar{p}_0} \quad (16)$$

Equation (13) can, in the same way, be written

$$(\bar{e}_M - \bar{e}_2)_{\bar{S}=\text{const.}} = \frac{\bar{U}_p^2 \bar{T}_0}{2 \bar{L}_0 \bar{p}_0} \quad (17)$$

COMPRESSION HEATER PERFORMANCE

The dimensionless energy $\bar{e} = E/RT_r$ is a state function and is plotted vs entropy for air and hydrogen in Figs. 6 and 7, respectively.

To show the importance of the difference between Eq. (17) and Eq. (16) a simple example will be worked out. If it is assumed that hydrogen at 2000 atm is used as a driving gas, hydrogen initially at 30 atm and 290 °K is used as a working gas, a maximum piston velocity of 1800 m/sec and a value of 11.8 of the right-hand side of Eq. (16), then a peak pressure of 20,000 atm will be given by Eq. (13) and 33,000 atm by Eq. (16). Thus for high driving pressures, when the outflow of gas can be neglected the, until now, estimated peak pressures are believed to be too small by a considerable amount.

In a launcher the area of the launch tube is not negligible when compared to that of the pump tube. A considerable outflow of gas will thus generally occur during the retardation of the piston and it is not obvious that this will have been brought to rest before it reaches the end of the pump tube. To get a better understanding of this problem, a perfect gas model will be worked out for the pressure rise in the working gas where, for simplicity, the pressure behind the piston is neglected during the retardation.

Figure 3 shows the changes in the working gas during a time element Δt . If it is assumed that the piston position and velocity at time t are x and U_p , respectively, and that the pressure at the same time is p , the adiabatic compression of the working gas minus what is escaping through the hole at the end of the barrel, for a perfect gas can be written

$$\frac{p + \Delta p}{p} = \left(\frac{L_0 - x - \Delta x}{L_0 - x - l} \right)^{-\gamma} \quad (18)$$

where l is the thickness of the gas layer that will flow out

COMPRESSION HEATER PERFORMANCE

during the time Δt , see Fig. 8. At the same time the motion of the piston is given by

$$\frac{d^2x}{dt^2} = -p \frac{A_0}{m_p} \quad (19)$$

For a small Δt , Eq. (18) can be simplified

$$1 + \frac{\Delta p}{p} = \left(1 - \frac{L_0 - x - \ell}{L_0 - x - \ell} \right)^{-\gamma} \approx 1 + \gamma \frac{\Delta x - \ell}{L_0 - x - \ell}$$

or

$$\frac{1}{p} \frac{\Delta p}{\Delta t} = \gamma \frac{\frac{L_0 - x - \ell}{\Delta t} - \frac{\ell}{\Delta t}}{L_0 - x - \ell} \quad (20)$$

If it is assumed that the outflow into the tube or the nozzle always occurs at sonic speed, the following expression is found for ℓ

$$\ell = \frac{1}{A_0 \rho} A_\ell a_* \rho_* \ell t$$

or, with perfect gas expressions for a_* and ρ_*

$$\frac{\ell}{\ell t} = \frac{A_\ell}{A_0} \left(\frac{2}{\gamma + 1} \right)^{\frac{\gamma+1}{2(\gamma-1)}} \left(\frac{p}{p_s} \right)^{\frac{\gamma-1}{2\gamma}} a_s = \bar{A}_\ell \Gamma a_s \left(\frac{p}{p_s} \right)^{\frac{\gamma-1}{2\gamma}}$$

where index (s) indicates conditions in the working gas at some reference point, for instance when the projectile is released and the outflow begins. Thus Eq. (20) becomes

$$\frac{dp}{dt} = \frac{\gamma p}{L - x} \left[U_p - \bar{A}_\ell \Gamma a_s \left(\frac{p}{p_s} \right)^{\frac{\gamma-1}{2\gamma}} \right] \quad (21)$$

With the transformation

$$y = p(L_0 - x)^\gamma$$

COMPRESSION HEATER PERFORMANCE

Equation (21) reduces to

$$y^{\frac{1}{\gamma}-1} \frac{dy}{dt} = -\gamma \bar{A}_p \Gamma a_s p_s \frac{1}{y} \left(\frac{p}{p_s} \right)^{\frac{\gamma+1}{2\gamma}} \quad (22)$$

If p/p_s ranges from 1 to 10 and $\gamma = 1.2$ it is found that

$$1 \leq \left(\frac{p}{p_s} \right)^{\frac{\gamma+1}{2\gamma}} \leq 8.3$$

Thus the following approximation is justified

$$\left(\frac{p}{p_s} \right)^{\frac{\gamma+1}{2\gamma}} = B \left(\frac{p}{p_s} \right)$$

where, for $\gamma = 1.2$, the constant B could be given the value of 0.91 to make the maximum relative deviation as small as possible. With this approximation Eq. (22) becomes

$$y^{\frac{1}{\gamma}-1} \frac{dy}{dt} = -\gamma \bar{A}_p \Gamma a_s p_s \frac{1}{y} B p \quad (23)$$

Since, from Eq. (19)

$$p = -\frac{m_p}{A_0} \frac{d^2 x}{dt^2} = -\frac{m_p}{A_0} \frac{dU_p}{dt}$$

it is found that

$$y^{\frac{1}{\gamma}-1} \frac{dy}{dt} = \frac{\gamma m_p}{A_0} \Gamma \bar{A}_p B a_s p_s \frac{1}{y} \frac{dU_p}{dt}$$

This equation is easily integrated giving, after going back to the initial variables

$$p = (L_0 - x)^{-\gamma} \left(\frac{m_p}{A_0} \Gamma \bar{A}_p B a_s p_s \frac{1}{y} U_p + D \right)^\gamma \quad (24)$$

COMPRESSION HEATER PERFORMANCE

where, from the boundary condition $U_p = U_s$, $x = x_s$, $p = p_s$

$$D = p_s^{\frac{1}{\gamma}} (L_o - x_s) - \frac{m_p}{A_o} \Gamma \bar{A}_l B a_s p_s^{\frac{1}{\gamma-1}} U_s$$

or, in dimensionless form

$$\bar{p} = \bar{p}_s \left(\frac{\bar{L}_o - \bar{x}_s}{\bar{L}_o - \bar{x}} \right)^{\gamma} \left[f(\bar{U}_p - \bar{U}_s) + 1 \right]^{\gamma} \quad (25)$$

where

$$f = \frac{\Gamma \bar{A}_l \bar{B} a_s}{(\bar{L}_o - \bar{x}_s) \bar{p}_s}$$

Again Eq. (19) is used, now written in the form

$$\bar{p} = -\bar{U}_p \frac{d\bar{U}_p}{d\bar{x}}$$

Integration of Eq. (25) then gives

$$\bar{L}_o - \bar{x} = (\bar{L}_o - \bar{x}_s)^{\frac{1}{F\gamma-1}} \left\{ F - (2-\gamma) f \bar{U}_s + 1 - \right. \\ \left. - [(\gamma-1) f \bar{U}_p - f \bar{U}_s + 1] [f(\bar{U}_p - \bar{U}_s) + 1]^{1-\gamma} \right\}^{\frac{1}{1-\gamma}} \quad (26)$$

where

$$F = (2-\gamma) \frac{\bar{A}_l^2 \Gamma^2 B^2 a_s^2}{(\bar{L}_o - \bar{x}_s) \bar{p}_s}$$

The pressure is found in terms of \bar{U}_p as

COMPRESSION HEATER PERFORMANCE

$$\bar{p} = \bar{p}_s F^{\frac{\gamma}{1-\gamma}} \left\{ [F - (2 - \gamma)f\bar{U}_s + 1][f(\bar{U}_p - \bar{U}_s) + 1]^{\gamma-1} - [(\gamma - 1)f\bar{U}_p - f\bar{U}_s + 1]^{\frac{\gamma}{\gamma-1}} \right\} \quad (27)$$

Further integration of Eq. (26) has not been possible to perform analytically. The time dependence of \bar{x} and \bar{p} can be obtained from a numerical evaluation, however, by making use of the fact that

$$d\bar{t} = \frac{d\bar{x}}{\bar{U}}$$

If the initial conditions are chosen in such a way that \bar{U}_p becomes zero before or when the piston strikes the end of the tube, it can be found that the pressure will reach a peak and then drop again. If \bar{U}_p is sufficiently large when the piston reaches the end, the pressure will increase all the time.

LAUNCHER PERFORMANCE

The main interest in the performance of a hypervelocity launcher will here be devoted to the problem of how to reach as high a projectile velocity as possible regardless of the size and shape of the projectile. There are certain obvious requirements that have to be fulfilled, namely to have

- (1) As long an accelerating distance (launch tube) as possible
- (2) As light a projectile as possible
- (3) As high an accelerating pressure as possible over the whole accelerating distance

Condition (3) implies that

COMPRESSION HEATER PERFORMANCE

- (4) The peak pressure and temperature in the chamber should be as high as possible.

It is understood, furthermore, that hydrogen is used in the pump tube.

Due to the limited strength of the gun components, viscous effects in the gases etc., all of these quantities must be given finite values. The limiting values that will be used throughout this section are as follows:

- (1) the length to diameter ratio of the launch tube is 300
- (2) the projectile mass is $(D_g/2)A_g\rho_g$, where the density is $\rho_g = 1700 \text{ kg/m}^3$
- (3) the accelerating pressure is $\leq 5000 \text{ atm}$
- (4) the peak pressure is 50,000 atm (which is about equal to the highest report value found, see Ref. 8)

The peak temperature cannot be arbitrarily given but has to be worked out from the performance of the compression heater.

The limitation in the peak pressure will put a limit to $m_p U_p^2/p_0$, see Eq. (16), for a particular gun. To create strong shock waves, high values of U_p are needed and thus m_p has to be made small and p_0 large. Again, there is a limit to how small m_p can be made and thus the matching of the peak pressure to the initial shock strength has to be done by varying U_p and p_0 .

To show the important characteristics of the peak conditions, two numerical examples will be analyzed where, for convenience, Eq. (17) will be used for the peak pressure. The right-hand side of Eq. (17) is

COMPRESSION HEATER PERFORMANCE

$$\frac{\bar{U}_p^2 \bar{T}_0}{2 \bar{L}_0 \bar{p}_0} = \frac{m U_p^2}{2 L_0 A_0 p_0} \cdot \frac{T_0}{T_r}$$

The lightest piston that has been found in the literature that can withstand a peak pressure of more than 20,000 atm is one with a mass of 86 grams for a 40-mm diameter pump tube (Ref. 7). Using this value, m_p can be written

$$m_p = 1700 A_0 D_0 \text{ kg}$$

L_0 will be given the value $150 D_0$, which is a reasonable average of what is in use, and T_0 will be assumed to be equal to T_r . Thus it is found that

$$\frac{\Delta \bar{e}}{\bar{S}} = \text{const.} = \frac{17}{3} \cdot \frac{U_p^2}{p_0}$$

with U_p in m/sec and p_0 in N/m^2 . Two different velocities will be considered, namely: 2000 m/sec which is about equal to the highest velocity presently in use and 4000 m/sec. If it is assumed that the piston has been accelerated to these velocities in an evacuated section, uniform conditions will be valid in the working gas when the first shock reflection occurs at the piston. If conditions in front of the piston at this moment are given index (2), and the initial pressure in the working gas, p_0 , is adjusted so as to give peak pressures around 20,000 atm, the results shown in the following table are obtained. In these calculations, p_2 and T_2 were found from Fig. 5, \bar{e}_2 , \bar{S}_2 , p_M and T_M from Fig. 7. In Fig. 9 the paths in the $\bar{e} - \bar{S}$ -plane have been plotted for two cases from each piston velocity. It is immediately seen that the entropy gain through the first two shock waves, which are the strongest ones, is very small, comparable to the entropy difference from the mere change in initial pressure. It is also seen that the higher piston velocity does not produce a sig-

COMPRESSION HEATER PERFORMANCE

TABLE I

U m/sec	P ₀ atm	P ₂ atm	T ₂ °K	\bar{e}_2	\bar{s}_2	$\Delta\bar{e}$	\bar{e}_M	P _M atm	T _M °K
2000	10	237	895	7.3	13.95	22.7	30.0	32,000	3050
	15	356	895	7.3	13.60	15.1	22.4	16,500	2400
	20	474	895	7.3	13.30	11.3	18.6	12,000	2050
4000	50	5350	2150	19.7	14.30	18.1	37.8	56,000	3700
	100	10700	2150	19.7	13.60	9.1	28.8	40,000	2950
	200	21400	2150	19.7	12.85	4.5	24.2	46,000	2550

nificantly higher peak temperature. The reason for this is that the higher piston velocity requires a higher initial pressure to keep the peak pressure down. In fact it does not seem possible to get a peak pressure below 20,000 atm in this case.

Thus the following conclusion can be drawn: at present, shock compression of hydrogen does not appear to be an efficient way of reaching high peak temperatures, even if very high piston velocities are used. If higher peak temperatures are to be obtained, which is a necessary condition for reaching higher projectile velocities, another fundamental way of heating must be considered. Thus the accelerating section, mentioned above, would not provide any improvement to a launcher, and as a consequence will not be employed in the launchers considered below.

From Fig. 9 it is seen that the most obvious way of reaching a higher temperature at the same peak pressure is to use a lower initial pressure and a higher initial temperature. If the initial pressure and temperature were 1 atm and 870 °K, respectively, the final temperature at 20,000 atm would be \approx 7500 °K. The highest temperature obtained in hydrogen so far is about 3500 °K and thus an increase in peak sound speed of about 50% together with a smaller value of γ would be obtained, both of which tend to increase the projectile velocity. It is realized that for a given pump tube the size of the projectile

COMPRESSION HEATER PERFORMANCE

must be made smaller with this type of operation but it is assumed that the higher velocities that can be reached will justify this disadvantage.

To optimize the performance of the launcher, Eqs. (26) and (27) will be used where values for the launch tube area, the maximum piston velocity, and the piston mass must be found. For finding these parameters the following assumptions and conditions will be employed:

- (a) The piston will transfer 85% of its energy to the working gas, i.e. the piston velocity is $0.4 U_s$ when it strikes the end of the tube. The barrel is assumed to absorb no energy.
- (b) The pressure will reach a maximum equal to $10 p_g$ when $U_p = 0.4 U_s$.
- (c) The time for the piston to decelerate from U_p to $0.4 U_p$ plus the time it takes for the first rarefaction wave from the entrance to the launch tube to reach the projectile is about equal to the time for the projectile to travel through the launch tube. The maximum projectile velocity is assumed to be three times larger than the sound speed in the working gas at the release pressure. At this velocity the base pressure on the projectile has decreased to about 70% of the release pressure for $\gamma = 1.2$.

The maximum pressure is found by differentiating Eq. (27) and putting the derivative equal to zero. The resulting piston velocity and peak pressure are, respectively

$$U_M = U_s + \frac{[F \approx (2 - \gamma)f\bar{U}_s + 1] \frac{1}{2-\gamma} - 1}{f} \quad (28)$$

COMPRESSION HEATER PERFORMANCE

$$\bar{p}_M = \bar{p}_s \left(\frac{2-\gamma}{F} \right)^{\frac{\gamma}{\gamma-1}} \left\{ [F - (2-\gamma)f\bar{U}_s + 1]^{\frac{1}{2-\gamma}} + f\bar{U}_s - 1 \right\}^{\frac{\gamma}{\gamma-1}} \quad (29)$$

Thus, from (a) and (b) it is found that

$$F = (2-\gamma)f\bar{U}_s - 1 + (1 - 0.6 f\bar{U}_s)^{2-\gamma} \quad (30)$$

and

$$[F - (2-\gamma)f\bar{U}_s + 1]^{\frac{1}{2-\gamma}} = \frac{10^{\frac{\gamma-1}{\gamma}} F}{2-\gamma} + 1 - f\bar{U}_s \quad (31)$$

Elimination of F between Eqs. (30) and (31) gives

$$(1 - 0.6 f\bar{U}_s)^{2-\gamma} = 1 - (2-\gamma) \left[1 - 0.4 \left(10^{\frac{1-\gamma}{\gamma}} \right) \right] f\bar{U}_s \quad (32)$$

and then

$$F = (2-\gamma) 0.4 \left(10^{\frac{1-\gamma}{\gamma}} \right) f\bar{U}_s \quad (33)$$

For given γ , $f\bar{U}_s$ can be determined from Eq. (32) and then F from Eq. (33). The definition of f gives

$$\frac{\bar{A} \bar{U}_s}{\bar{L}_o - \bar{x}_s} = f\bar{U}_s \frac{\bar{F}_s}{\Gamma B \bar{a}_s} \quad (34)$$

where the right-hand side is determined from Eq. (32) and the given launch conditions. From Eq. (33) and the definition of F it is found in the same way that

$$\frac{\bar{A} \bar{U}_s}{\bar{L}_o - \bar{x}_s} = F \frac{\bar{p}_s}{(2-\gamma) \Gamma^2 B^2 \bar{a}_s^2} \quad (35)$$

Thus two relations are found between the three parameters.

COMPRESSION HEATER PERFORMANCE

The third relation will be found from condition (c).

The time to reach the peak pressure can be approximated by

$$\bar{t}_M - \bar{t}_s \approx \frac{\bar{L}_o - \bar{x}_s}{\frac{2\bar{U}_s + 0.4 \bar{U}_s}{3}} = \frac{\bar{L}_o - \bar{x}_s}{0.8 \bar{U}_s} \quad (36)$$

where a weighed mean value of \bar{U}_p has been used.

With the given assumptions, the pressure on the base of the projectile will be fairly constant, equal to p_s , throughout the launch. Thus it is found that

$$\bar{U}_\ell = 3\bar{a}_s = \frac{\bar{A}_\ell \bar{p}_s}{m_\ell} (\bar{t}_t - \bar{t}_s) \quad (37)$$

and

$$\bar{x}_t = \bar{L}_\ell = \frac{\bar{A}_\ell \bar{p}_s}{2m_\ell} (\bar{t}_t - \bar{t}_s)^2 = \frac{9}{2} \frac{\bar{m}_\ell \bar{a}_s^2}{\bar{A}_\ell \bar{p}_s} \quad (38)$$

The slope of the first rarefaction wave from the piston at the projectile is

$$3\bar{a}_s + \bar{a}_s = 4\bar{a}_s$$

and at the entrance to the launch tube

$$\begin{aligned} \bar{u}_* + \bar{a}_* &\approx 2 \sqrt{\frac{2}{\gamma+1}} \bar{a}_M \approx 2 \sqrt{\frac{2}{\gamma+1}} \left(\frac{\bar{p}_M}{\bar{p}_s} \right)^{\frac{\gamma-1}{2\gamma}} \bar{a}_s = \\ &= 2 \sqrt{\frac{2}{\gamma+1}} (10)^{\frac{\gamma-1}{2\gamma}} \bar{a}_s \end{aligned} \quad (10)$$

COMPRESSION HEATER PERFORMANCE

Thus the mean value of the slope can be approximated by

$$\frac{4\bar{a}_s + 2\sqrt{\frac{2}{\gamma+1}} (10)^{\frac{\gamma-1}{2\gamma}} \bar{a}_s}{2}$$

which gives

$$\bar{t}_c - \bar{t}_M \approx \frac{\bar{L}_\ell}{2\bar{a}_s + \sqrt{\frac{2}{\gamma+1}} (10)^{\frac{\gamma-1}{2\gamma}} \bar{a}_s} = \quad (39)$$

$$= \frac{\frac{9}{2} \frac{\bar{m}_\ell \bar{a}_s}{\bar{A}_\ell \bar{p}_s}}{2 + \sqrt{\frac{2}{\gamma+1}} (10)^{\frac{\gamma-1}{2\gamma}}}$$

It is then found from Eqs. (36), (37) and (39) that

$$\frac{(1 - \bar{x}_s) \bar{A}_\ell}{\bar{U}_s} = \frac{2.4 \bar{a}_s \bar{m}_\ell}{\bar{p}_s} \left\{ 1 - \frac{1.5}{2 + \sqrt{\frac{2}{\gamma+1}} (10)^{\frac{\gamma-1}{2\gamma}}} \right\} = \quad (40)$$

$$= \frac{2.4 \lambda \bar{a}_s \bar{m}_\ell}{\bar{p}_s}$$

Finally, the ratio between the projectile mass and that of the piston can be written

$$\bar{m}_\ell = \frac{m_\ell}{m_p} = \frac{p_\alpha A_0 L_0}{a_\alpha^2 m_p} \cdot \frac{a_\alpha^2 m_\ell}{p_\alpha A_0 L_0} = \bar{L}_0 \frac{a_\alpha^2}{p_\alpha} \frac{m_\ell}{A_0 L_0} = \frac{8.5}{3} \cdot \frac{a_\alpha^2}{p_\alpha} \bar{L}_0 \bar{A}_\ell^{3/2}$$

COMPRESSION HEATER PERFORMANCE

where the values $m_\ell = (\pi_\ell/2)(1700 A_\ell)$ and $L_0 = 300 D_0$ have been used. Inserted in Eq. (40) this gives

$$\frac{\bar{L}_0 - \bar{x}_s}{\bar{L}_0} \cdot \frac{1}{\bar{U}_s \sqrt{\bar{A}_\ell}} = 6.8\lambda \frac{a_\alpha a_s}{P_s} \quad (41)$$

with a in meters/sec and p_s in N/m^2 . Since the first factor in the left-hand side of Eq. (41) is equal to the volume ratio V_s/V_0 it is found from the equation of state that

$$\bar{U}_s \sqrt{\bar{A}_\ell} = \frac{1}{6.8\lambda} \frac{Z_s \bar{T}_s}{\bar{T}_0} \frac{P_0}{a_\alpha a_s} \quad (42)$$

This is then the third relationship between the three parameters to be determined. The assumptions for the three relations are based on the following: viscous effects in the gases, friction between the walls and the piston and the projectile, and heat losses are negligible; the launch tube is initially evacuated.

A particular example will now be worked out to find the final velocity of a projectile using the three relations. In this calculation, after finding the pressure variation in the chamber, the launch process will be solved by the method of characteristics to give the pressure variation at the base of the pellet and the terminal velocity after 300 diameters accelerating distance.

The initial conditions will be given as follows: $p_0 = 1$ atm, $T_0 = 870$ °K, $p_s = 5000$ atm, $p_M = 50,000$ atm, $L_0 = 300 D_0$, and the reference values $p_\alpha = 100$ atm, $a_\alpha = 1000$ m/sec. From Fig. 7 it is seen that $T_s = 5575$ °K and $T_M = 8800$ °K. It can then be found that $\gamma_s = 1.20$, $\gamma_M = 1.33$, $a_s = 5580$ m/sec and $a_M = 7900$ m/sec. During the increase in pressure from p_s to p_M , γ will change. Since the pressure level is very high it is reasonable to expect that the expansion into the launch

COMPRESSION HEATER PERFORMANCE

tube will occur in thermodynamic equilibrium and thus γ will change back to the value corresponding to the base pressure of the projectile. Since this pressure will stay fairly constant during the launch, which will be seen from the characteristics solution, it is reasonable to make the approximation that γ is equal to γ_s , during the whole compression-expansion process. This value of γ gives $a_M = a_s (p_M/p_s)^{(\gamma_s-1)/2\gamma_s} = 6760$ m/sec. According to the three relationships mentioned above it is now easily deduced that

$$\bar{A}_\ell = 0.0260; U_s = 290 \text{ m/sec}; m_p = 11.8(A_0 D_0 1700) \text{ kg}$$

From the equation for the peak pressure without outflow, Eq. (17), the maximum piston velocity is calculated and found to be 385 m/sec, a value that is easily obtained with, for instance, helium at 100 atm as driving gas. This relatively low driving pressure will give only a very small contribution to the peak pressure and neglecting the driving gas in this example is thus justified. The value of $\bar{A}_\ell = 0.0260$ means that the diameter ratio between pump tube and launch tube is 6.2.

The variation of pressure, sound speed and piston position with time are shown in Fig. 10. Using the result in Fig. 10 as the chamber conditions, and assuming that the flow at the entrance to the launch tube is not sonic until the downstream conditions for this to take place are fulfilled, the characteristics solution gives a final velocity of 17.2 km/sec = 56,500 ft/sec compared to 18.70 km/sec for the case of a constant accelerating pressure of 5000 atm. The pressure variation at the base of the projectile is shown in Fig. 11 and can be seen to oscillate within about 20% of the desired value. By launching the projectile at a slightly earlier moment, the over-ride in the base pressure can probably be avoided. A reduced terminal velocity of the projectile might then be expected. To check the accuracy of the theoretical

COMPRESSION HEATER PERFORMANCE

model, the calculation of the launching conditions according to Eqs. (26) and (27) plus the characteristics solution of the launch was then applied to a particular case where the muzzle velocity had been measured to 29,500 ft/sec. The theoretically found value was 32,500 ft/sec. The data for this example were taken from Ref. 8 where the piston velocity was not measured, however. From the given value of the peak pressure the piston velocity was calculated from Eq. (17).

The close agreement between the calculated projectile velocity and the measured one makes it possible to predict that a velocity of 45,000 to 50,000 ft/sec would be possible by using a configuration as discussed earlier in this section.

GUN-TUNNEL PERFORMANCE

In the gun tunnel air is generally used as the working gas and shock compression becomes important at piston velocities that are considerably lower than those considered for shock compression of hydrogen. At the same time the non-dimensional internal energy, \bar{e} , is of the same order for air and hydrogen. This means that the peak pressure would be about the same in these gases for the same piston velocity, initial pressure, and temperature. Thus shock compression of air by means of a piston can be of great importance for the production of high temperature, high pressure air. To take advantage of shock compression and yet preserve uniform stagnation conditions during a run, the accelerating section is believed to be a valuable feature of the gun tunnel.

In computing the peak pressure in a gun tunnel the outflow of gas can be neglected since the cross-sectional area of the entrance to the nozzle will generally be very small compared with the pump tube area. Thus Eq. (16) together with Fig. 6 will be used for finding the peak pressure.

COMPRESSION HEATER PERFORMANCE

From Fig. 6 the final temperature is also found at the point where $p = p_{\infty}$ at $\bar{S} = \bar{S}_2$. Using the results for piston acceleration, shock compression and peak pressure from the previous sections, the following table was prepared to show the effect of various driving conditions and piston masses where the total length of the accelerating section and the main barrel is equal to $300 D_0$.

TABLE II

Driving gas	p_a atm	$m/A_0 D_0$ kg/m ³	T_0 °K	P_0 atm	$\frac{L_{10}}{D_0}$	P_{∞} atm	T_{∞} °K	P_M atm	
Air	200	1700	290	1.10	165	350	1870	20,000	
			1700	580	1.60	180	350	2650	20,000
			200	290	0.30	59	350	2760	1,350
			200	580	0.55	55	350	3330	1,350
	2000		1700	290	1.75	100	3500	3260	20,000
			1700	580	1.90	120	3500	4030	20,000
			300	290	2.00	14	3500	3000	5,500
			300	580	2.00	21	3500	4000	5,500
He	200	1700	290	2.1	120	350	2480	20,000	
			1700	580	3.8	130	350	2780	20,000
			200	290	0.65	43	350	3570	1,350
			200	580	1.2	44	350	3780	1,350
	2000		1700	290	3.1	68	3500	4250	20,000
			1700	580	5.6	71	3500	4660	20,000
			300	290	3.0	12	3500	4310	5,500
			300	580	4.0	17	3500	5140	5,500
H ₂	200	1700	290	2.4	100	350	2720	20,000	
			1700	580	4.5	105	350	3000	20,000
			200	290	0.80	39	350	4240	1,350
			200	580	1.45	42	350	4550	1,350
	2000		1700	290	4.8	54	3500	4800	20,000
			1700	580	9.0	56	3500	5320	20,000
			300	290	4.7	9.6	3500	4850	5,500
			300	580	8.0	11	3500	5600	5,500

In Table II the driving gas is assumed to be at 290 °K.
The different piston masses correspond to

COMPRESSION HEATER PERFORMANCE

- (a) a solid piston of one diameter length with a density of 1.7 g/cm^3 when $m/A_0D_0 = 1700$
- (b) a light piston (Ref. 2) that can withstand a pressure difference of 1000 atm when $m/A_0D_0 = 200$
- (c) a light piston that can withstand a pressure difference of 2000 atm when $m/A_0D_0 = 300$.

The final pressure p_{∞} was taken as $1.75 p_u$ which, according to experimental data, is a reasonable value for a large area driver. The peak pressure for the light pistons was then given as p_{∞} plus the allowed pressure difference across the piston and found by using Eq. (16). For the solid piston the peak pressure was given the value 20,000 atm using Eq. (17); the reason for neglecting the energy of the driving gas during the deceleration was that air data for pressures higher than 20,000 atm were not available. Thus, for solid pistons, the same computing method and limit for the peak pressure was used as in Ref. 7. The procedure for finding the final conditions was to try different values of p_0 until the peak pressure was equal to the prescribed value. The piston velocity was always adjusted so that the pressure became equal on both of the sides of the piston when it had broken through the second diaphragm. The highest piston velocity considered was 2190 m/sec occurring in the last example.

Some interesting conclusions can be drawn from the result of Table II. It is seen that preheating of the working gas by a factor of 2 gives, for air as driving gas, an increase in the final temperature of 20 to 40%, while for helium or hydrogen as driving gas, the increase is only 5 to 20%. It is also seen that the use of a heavy, strong piston generally results in a lower temperature. Thus the light

COMPRESSION HEATER PERFORMANCE

piston is definitely more attractive, since it also reduces the peak pressure which is favorable for the design problems as well as for any possible instrumentation in the high pressure section of the barrel. The increase in driving pressure from 200 atm to 2000 atm does not give a significant increase in final temperature for the lighter pistons but, on the other hand, the higher pressure level is probably desirable for reducing the nonequilibrium effects in the expansion process in the nozzle. Thus, the most significant ways to increase the stagnation temperature in a gun tunnel appear to be to use light gases for driving the piston in combination with an accelerating section and to take advantage of a good piston design.

COMPRESSION HEATER PERFORMANCE

REFERENCES

1. Lemcke, B. "Determination of final temperature in a gun tunnel." J. Aero. Sci., Vol. 28, No. 10, p. 827 - 828, October, 1961.
2. Lemcke, B. "An investigation of the stagnation conditions in the shock-compression heater of a gun tunnel. ARI (Sweden) Report 90, 1962.
3. Gilmore, F. R. "Additional values for the equilibrium composition and thermodynamic properties of air." Rand Corporation, Research Memorandum RM-2328, Dec. 1959.
4. Hilsenrath, J. and Beckett, C.W. "Table of thermodynamic properties of argon-free air to 15,000 °K." Arnold Engineering Development Center, Rep. AEDC-TN-56-12, Sept. 1956.
5. Rosenbaum, B. M. and Levitt, L. "Thermodynamic properties of hydrogen from room temperature to 100,000 °K." NASA TN D-1107, Jan. 1962.
6. Stollery, J. L. and Maul, D. J. "A note on the compression of air through repeated shock waves." J. Fluid Mech., Vol. 4, Part 6, p. 650-654, November, 1958.
7. Andersson, D. E. and Prince, M. D. "Design of light-gas model launchers for hypervelocity research." Proceedings of the Second Symposium on Hypervelocity Techniques, March 1962.
8. Charters, A. C. and Curtis, J. S. "High velocity guns for free-flight ranges." Paper presented to AGARD specialist's meeting, "High temperature aspects of hypersonic flow." April 1962.

COMPRESSION HEATER PERFORMANCE

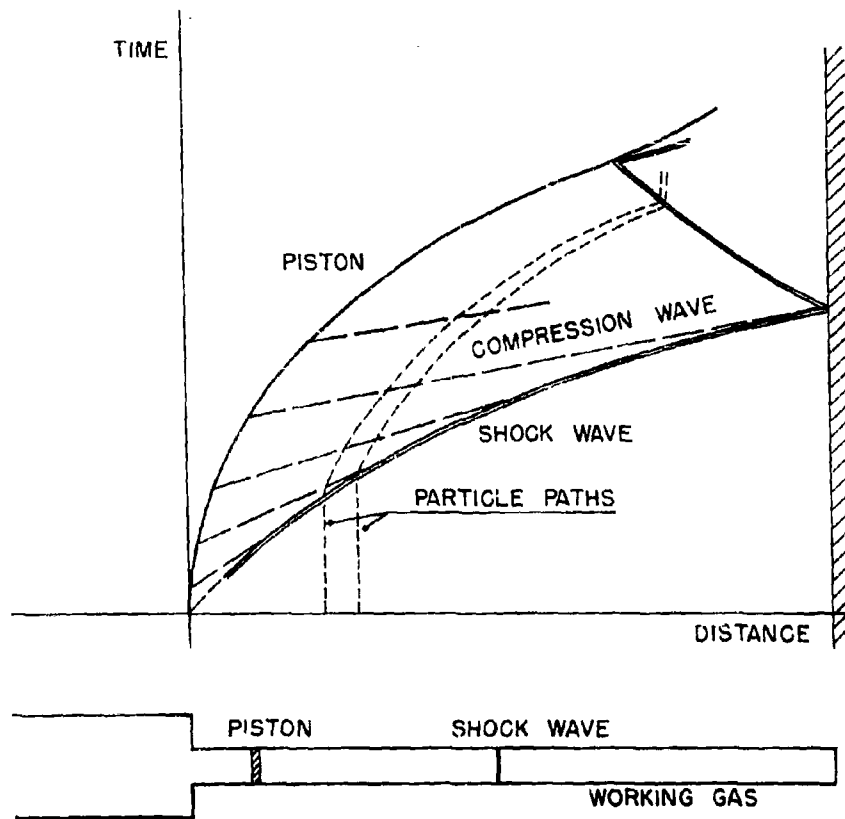


Fig. 1. Piston acceleration and shock formation

COMPRESSION HEATER PERFORMANCE

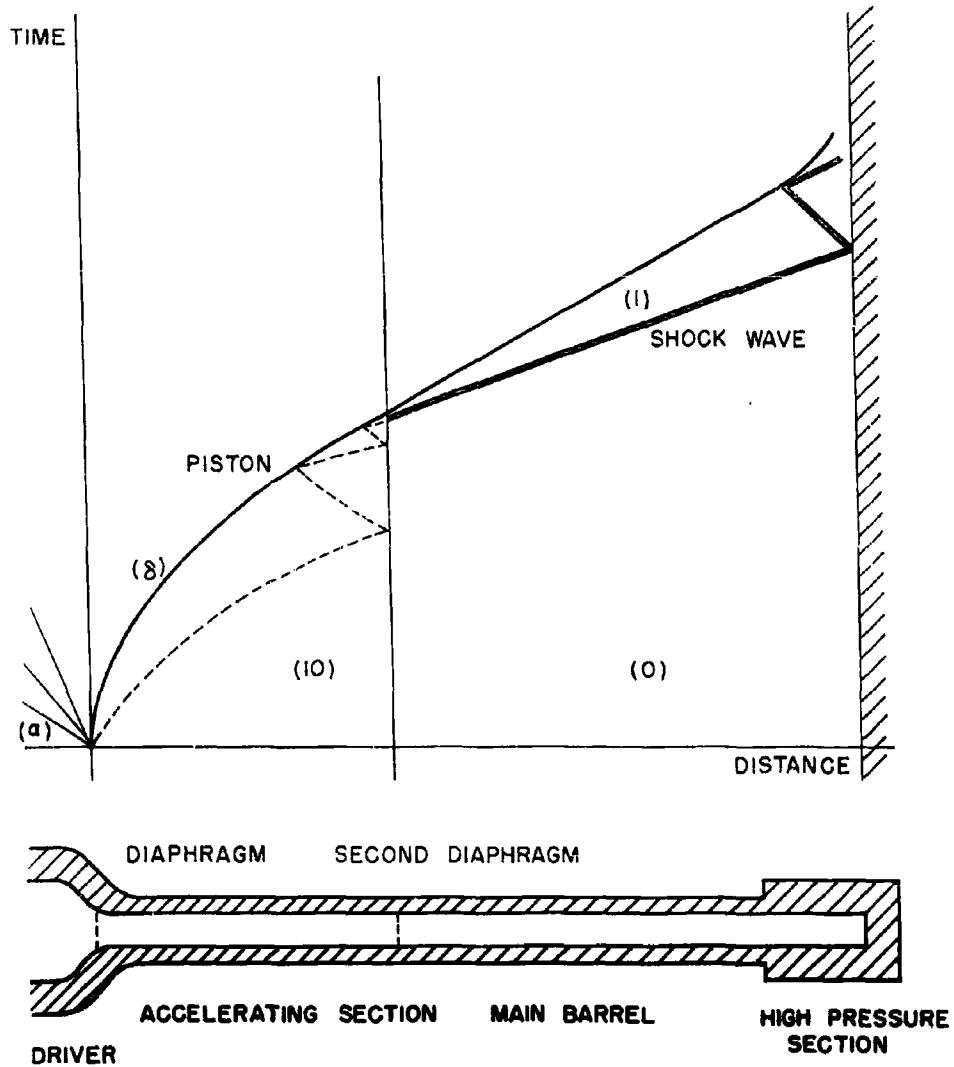


Fig. 2. Piston acceleration and shock generation in modified shock-compression heater

COMPRESSION HEATER PERFORMANCE

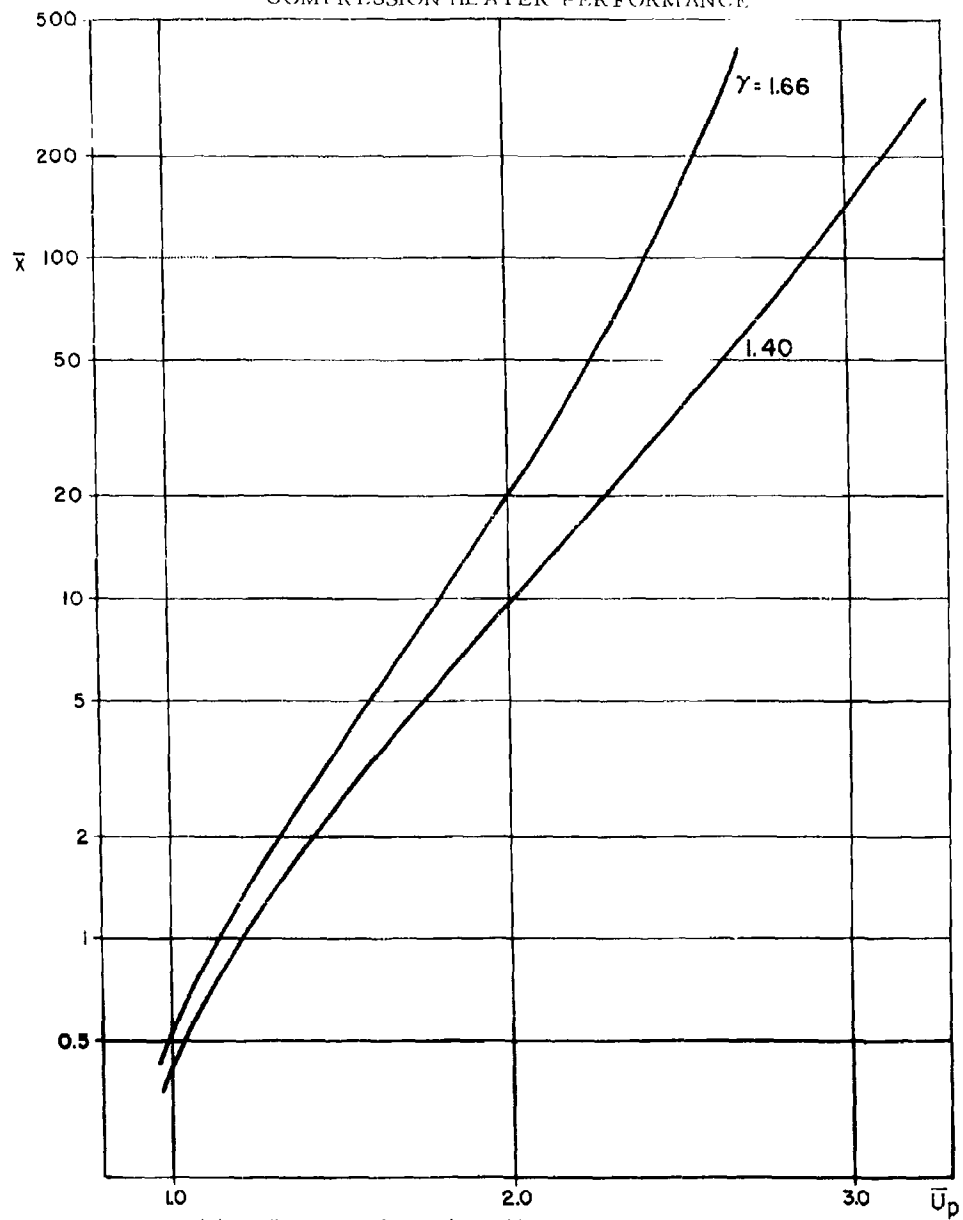


Fig. 3. Accelerating distance vs piston velocity

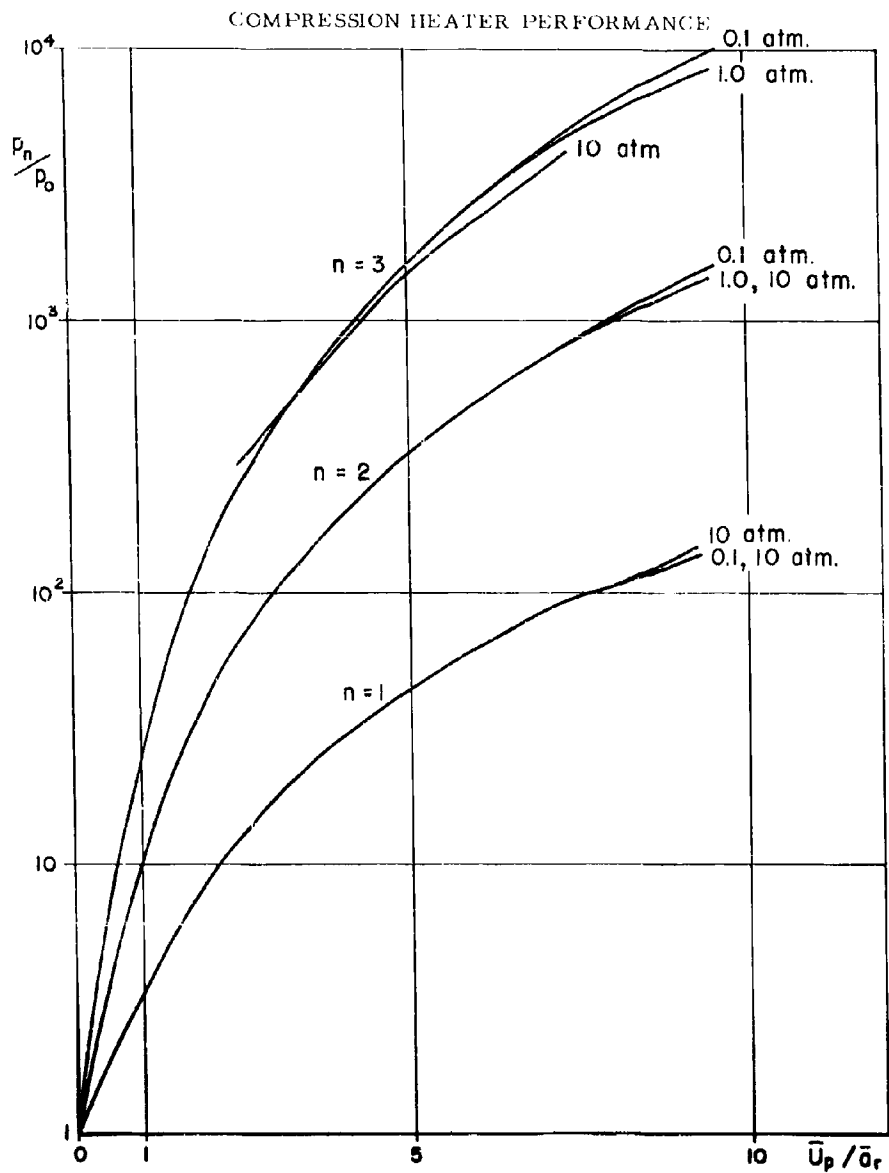


Fig. 4a. Pressure jump through repeated shock waves in air, $T_0 = 290^\circ\text{K}$

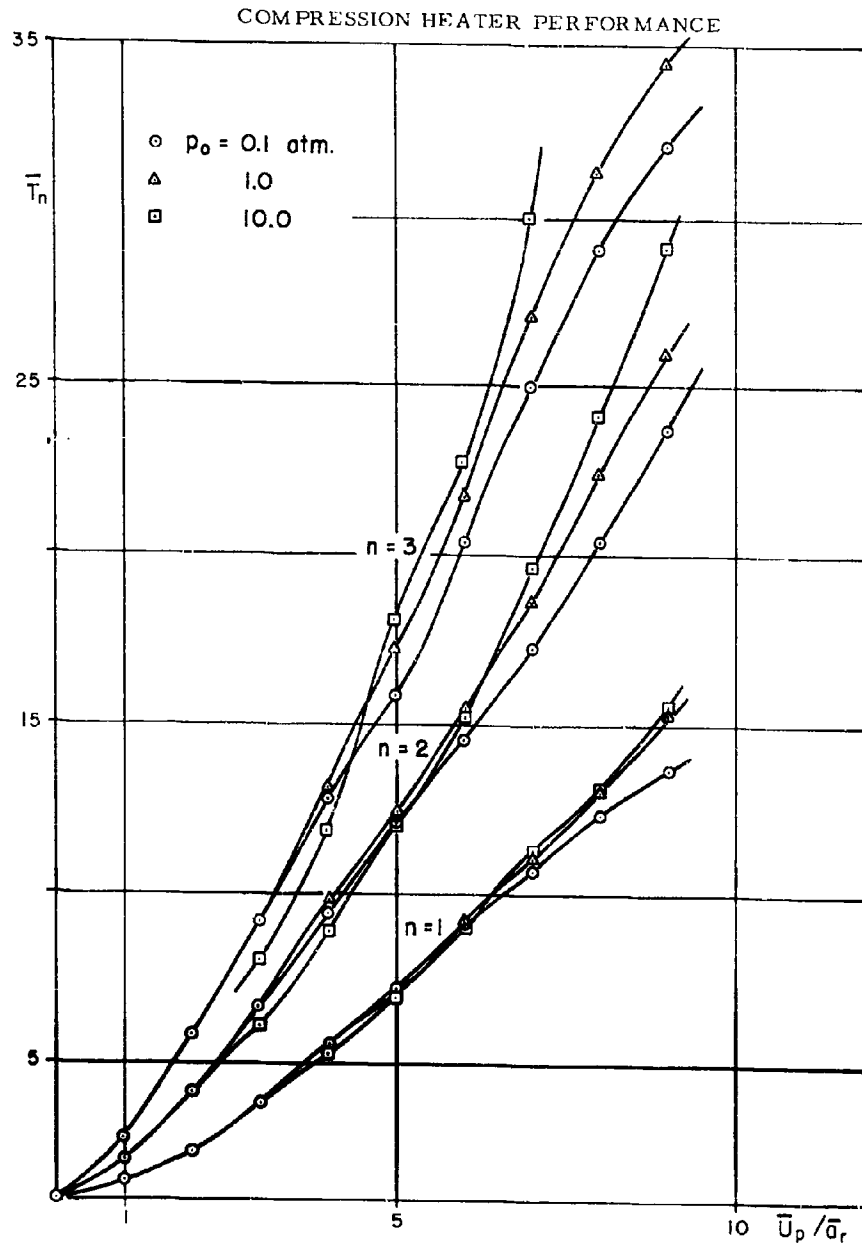


Fig. 4b. Temperature jump through repeated shock waves in air, $T_0 = 290$ °K

COMPRESSION HEATER PERFORMANCE

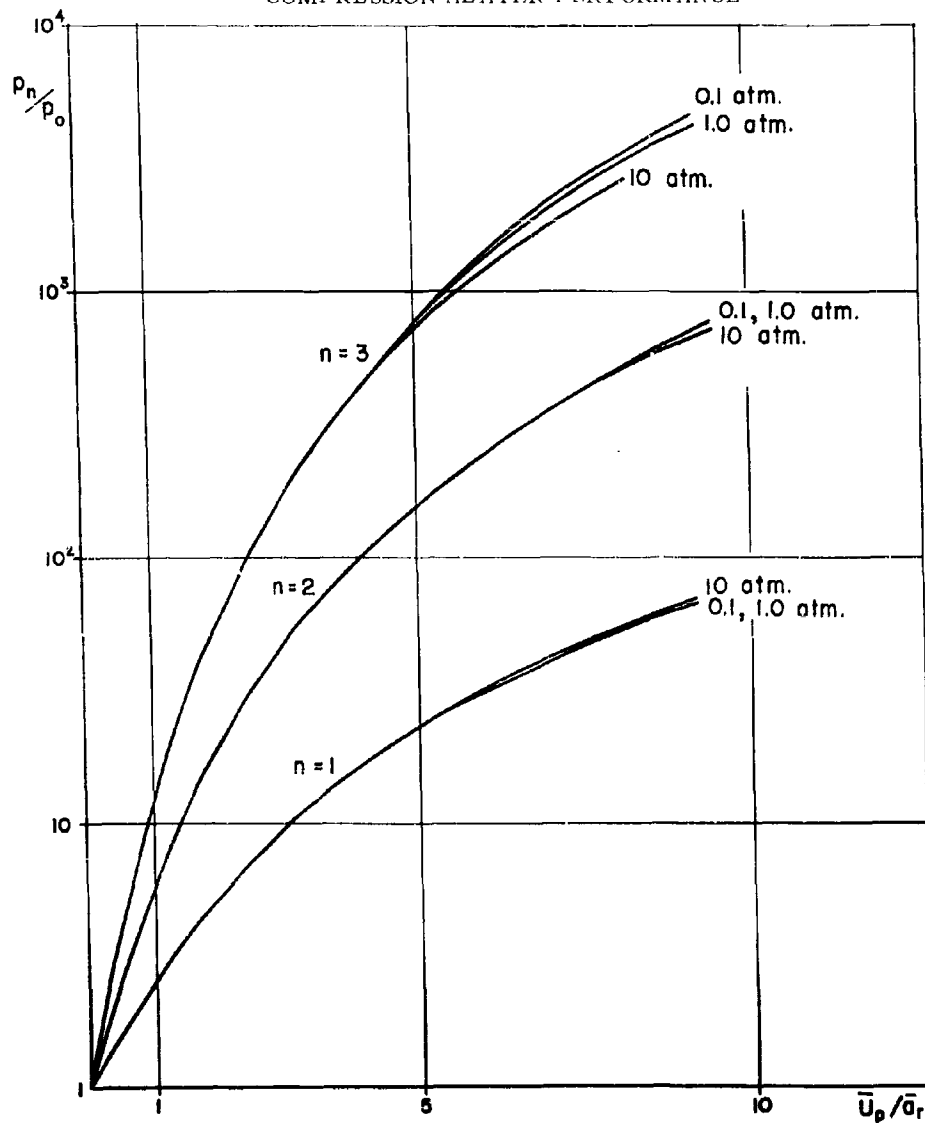


Fig. 4c. Pressure jump through repeated shock waves in air, $T_0 = 580$ °K

COMPRESSION HEATER PERFORMANCE

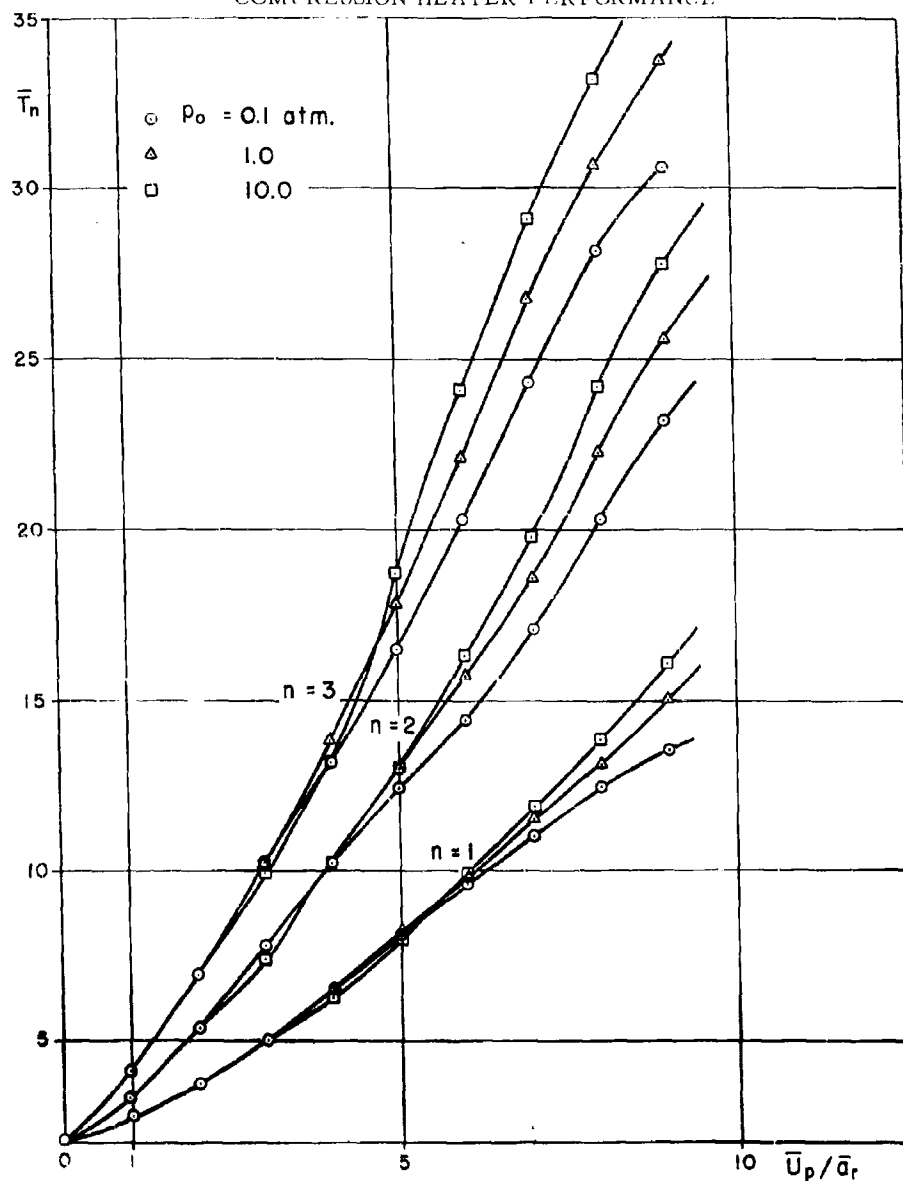


Fig. 4d. Temperature jump through repeated shock waves in air, $T_0 = 580^\circ\text{K}$

COMPRESSION HEATER PERFORMANCE

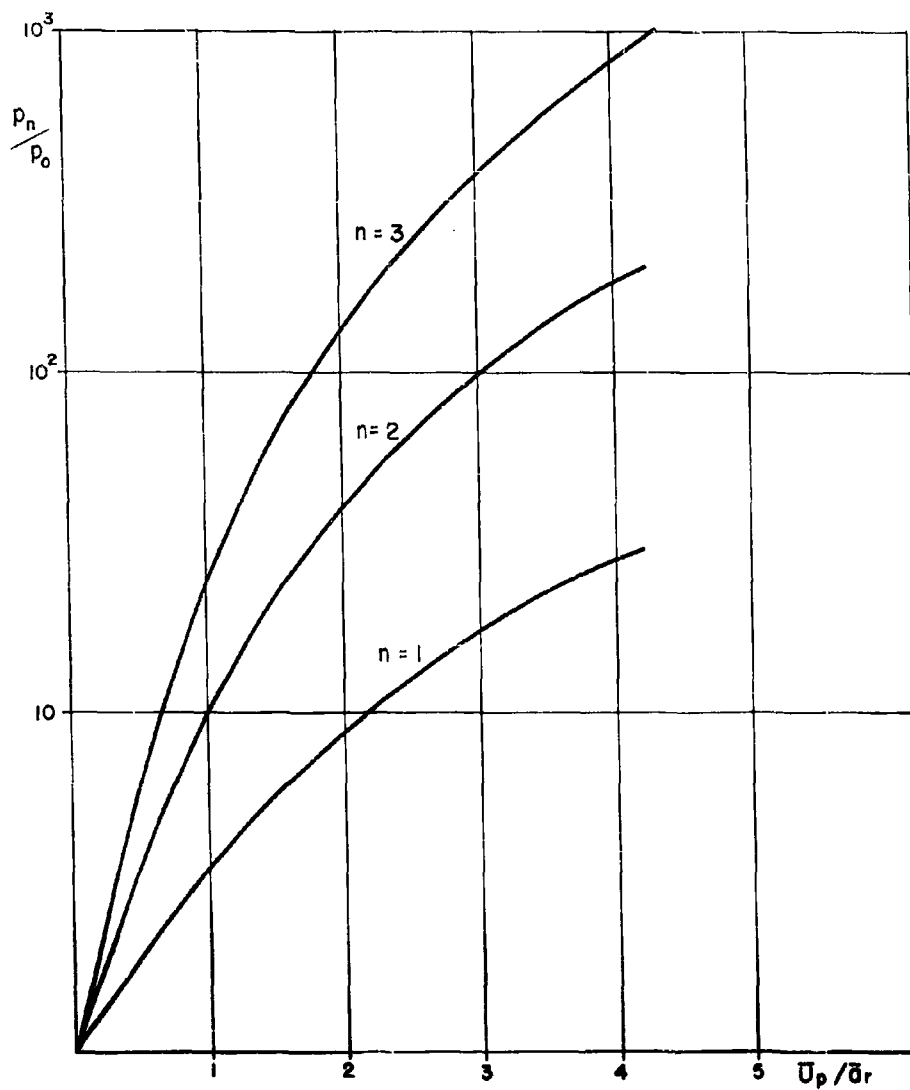


Fig. 5a. Pressure jump through repeated shock waves in hydrogen $T_0 = 290 \text{ }^\circ\text{K}$

COMPRESSION HEATER PERFORMANCE

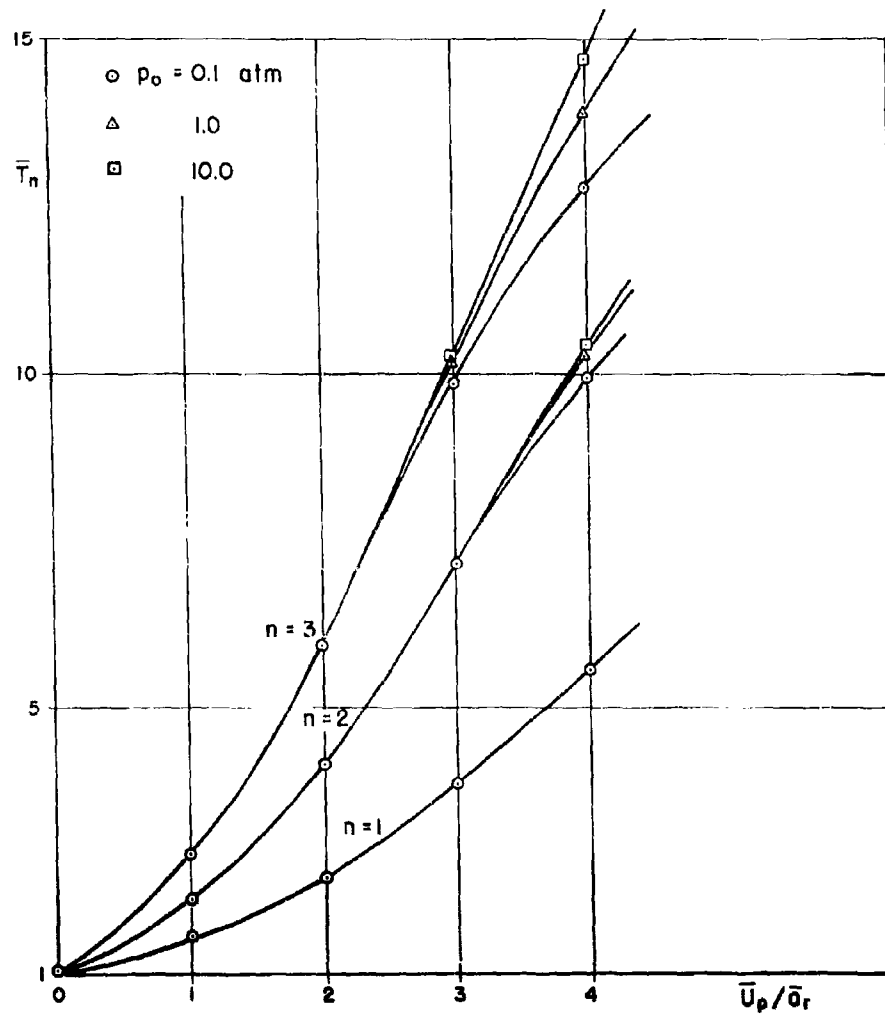


Fig. 5b. Temperature jump through repeated shock waves in hydrogen, $T_0 = 290^\circ\text{K}$

COMPRESSION HEATER PERFORMANCE

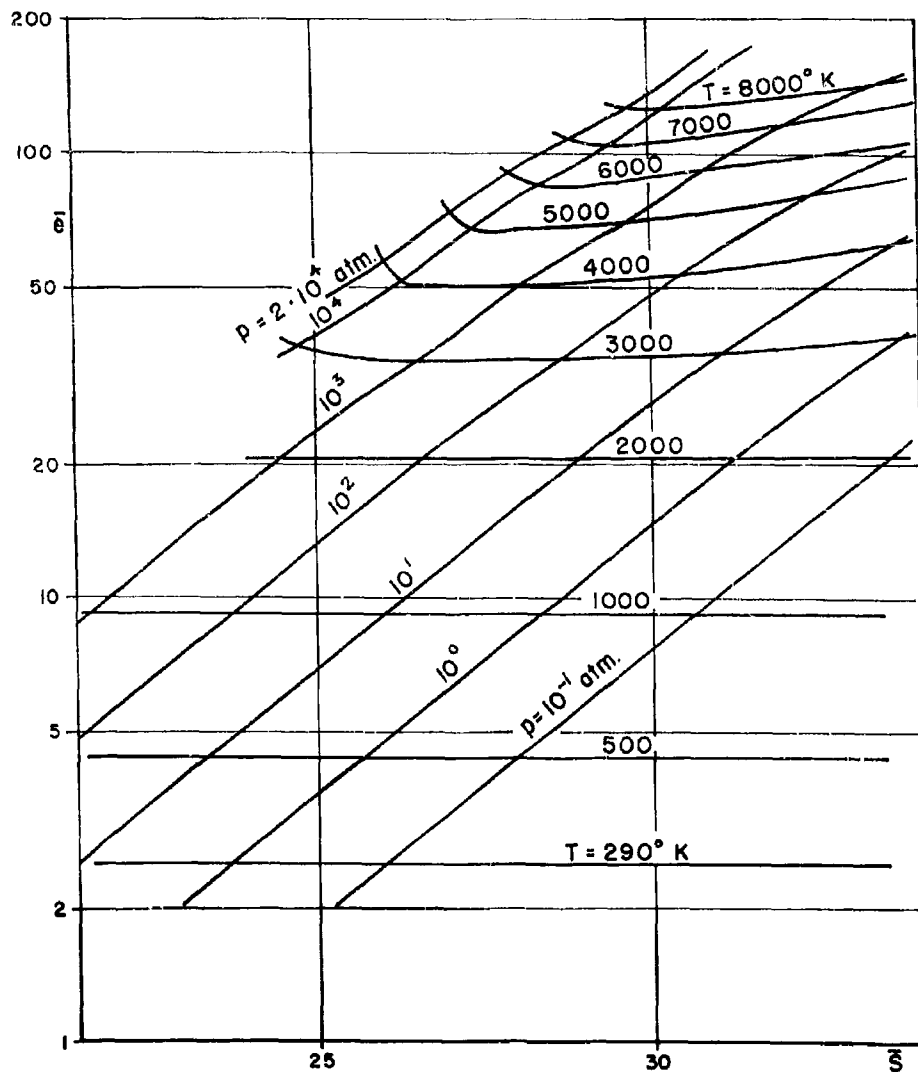


Fig. 6. Dimensionless energy as a function of entropy for air

COMPRESSION HEATER PERFORMANCE

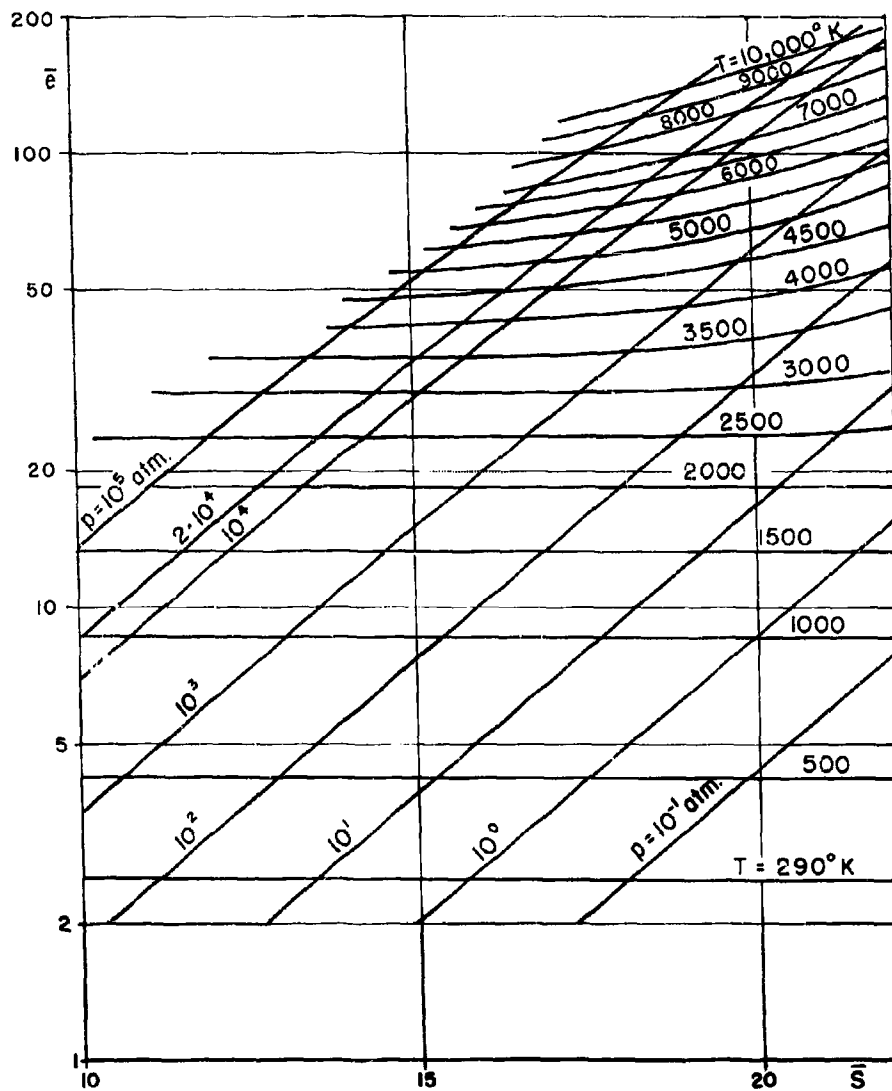


Fig. 7. Dimensionless energy as a function of entropy for hydrogen

COMPRESSION HEATER PERFORMANCE

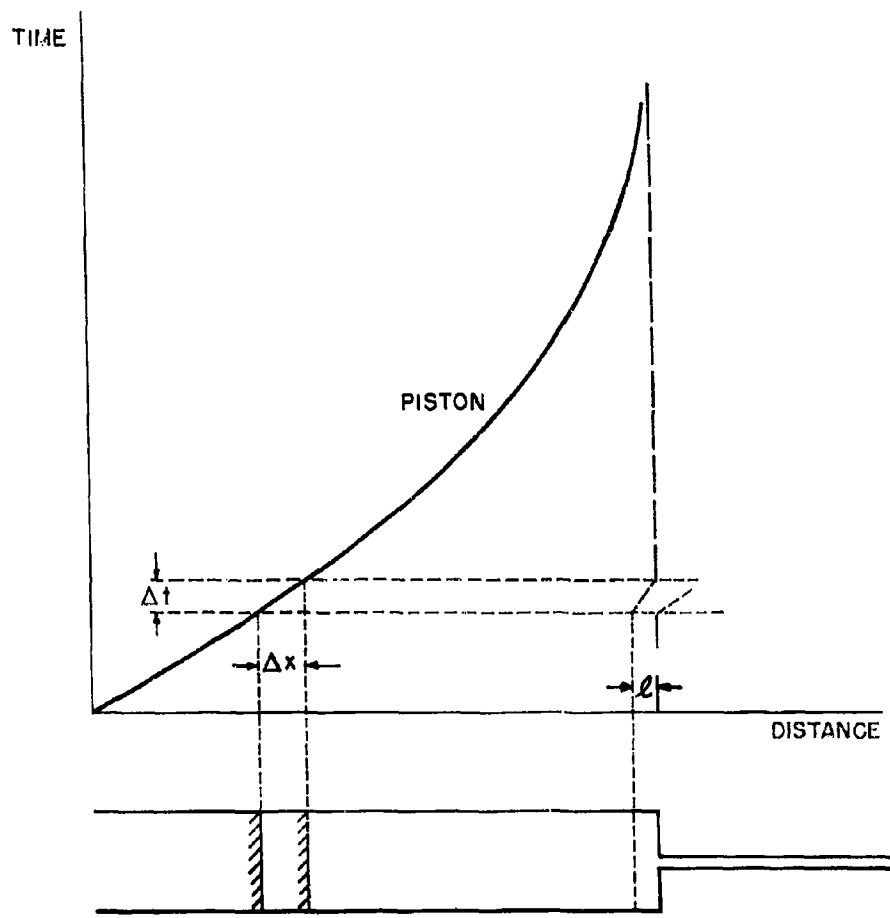


Fig. 8. Compression and outflow of gas during the time element Δt

COMPRESSION HEATER PERFORMANCE

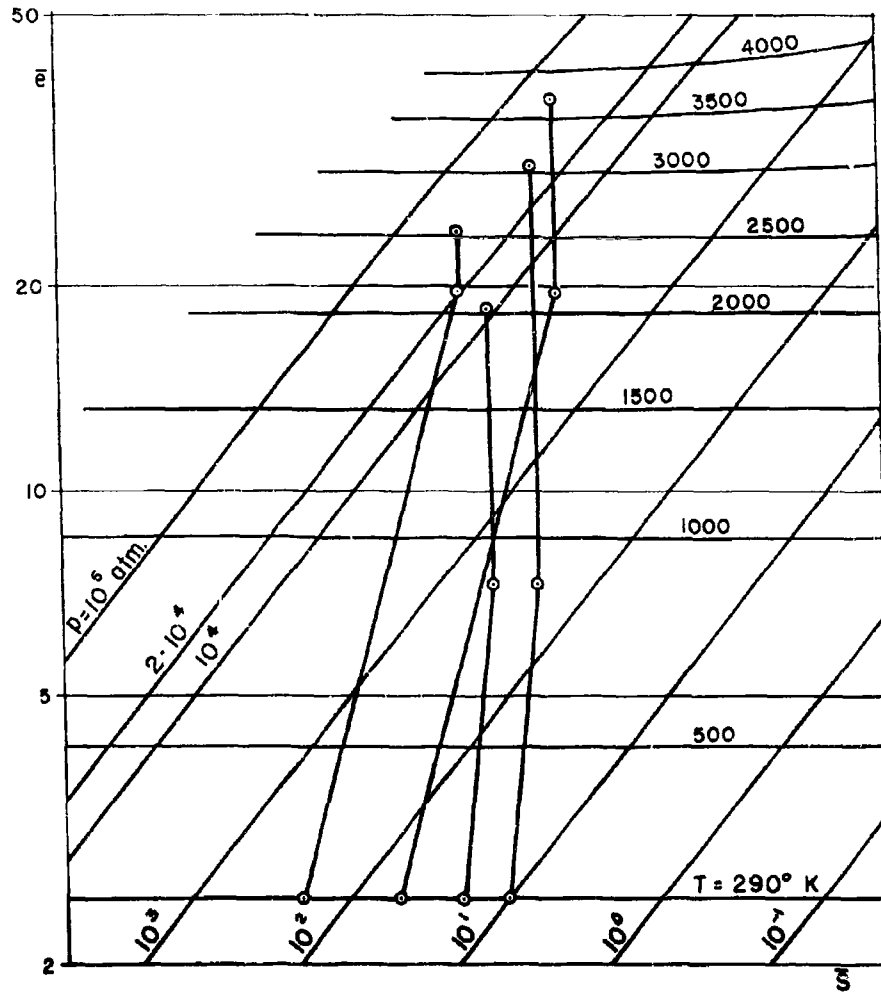


Fig. 9. Transitions to the peak pressure in hydrogen for different initial conditions

COMPRESSION HEATER PERFORMANCE

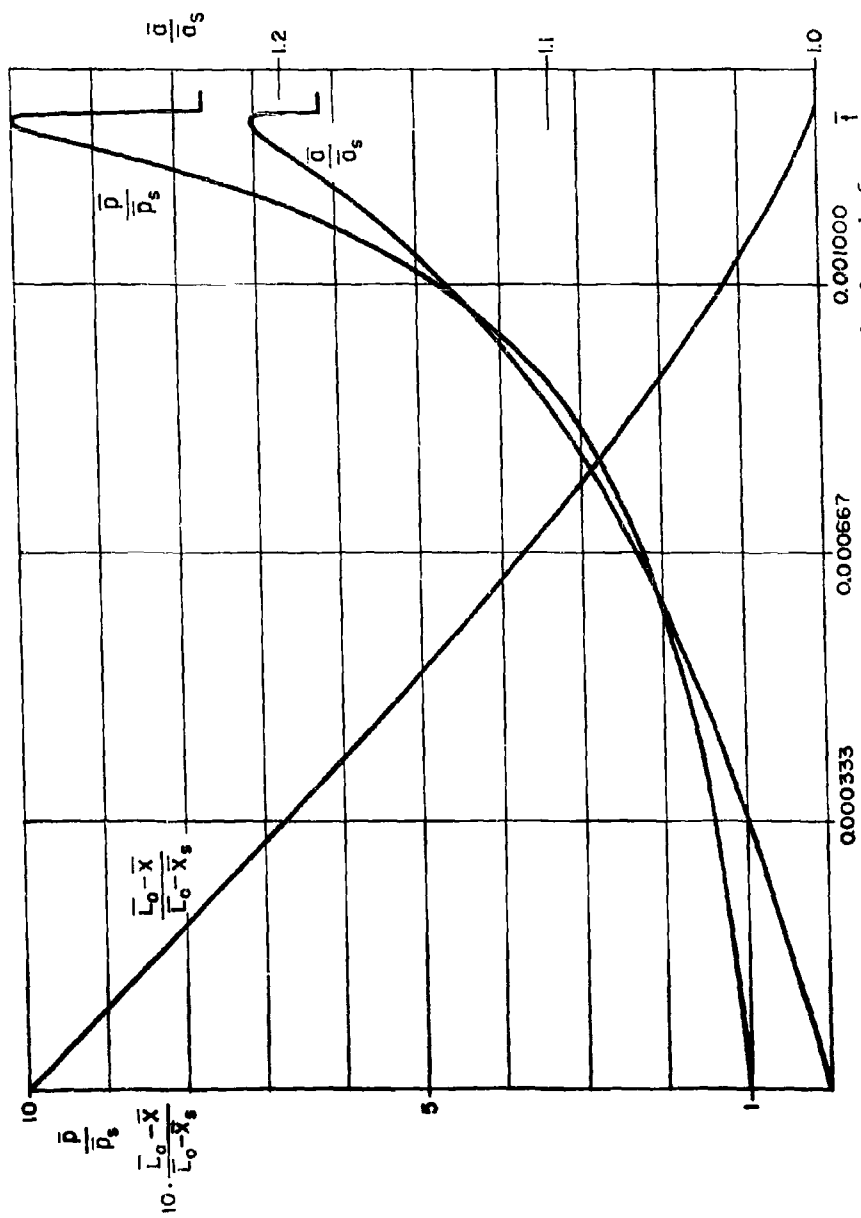


Fig. 10. Variation of chamber conditions during the launch for $\lambda_0 = 0.0260$, $U_s = 0.287$, $L_0 = 0.150$

COMPRESSION HEATER PERFORMANCE

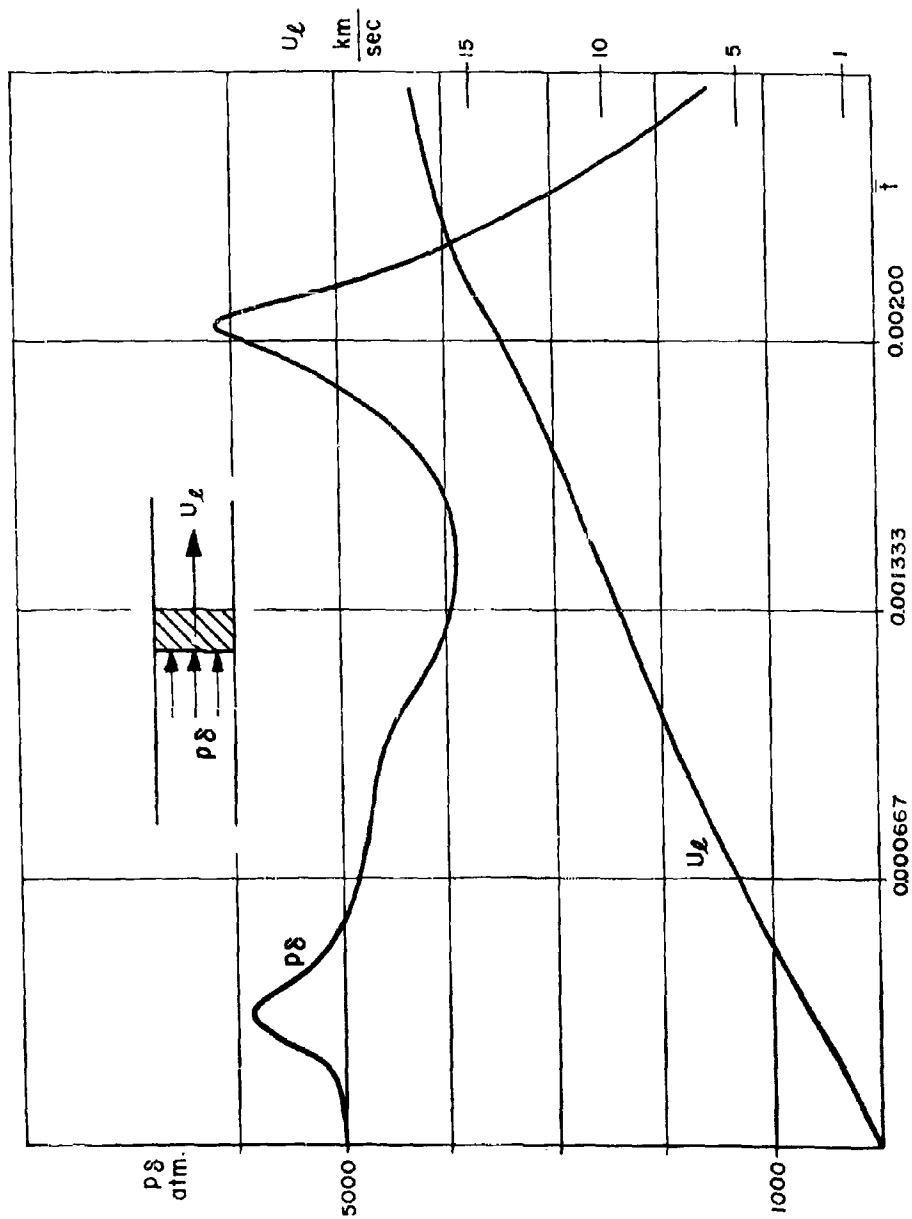


Fig. 11. Base pressure and velocity of projectile during the launch for $A_j = 0.0260$, $U_s = 0.287$, $I_0 = 0.150$

COMPUTER ANALYSIS OF TWO-STAGE
HYPERVELOCITY MODEL LAUNCHERS

By

R. Piacesi, D. F. Gates, and A. E. Seigel

Ballistics Department
U. S. Naval Ordnance Laboratory
White Oak, Silver Spring, Maryland

COMPUTER ANALYSIS OF TWO-STAGE
HYPERVELOCITY MODEL LAUNCHERS

By

R. Piacesi, D. F. Gates, and A. E. Seigel

ABSTRACT: A computer study for predicting high-speed launcher performance was conducted using a one-dimensional hydrodynamics computer code. This computer code uses the Lagrangian scheme, and is based on the "q" method as devised by Von Neumann and Richtmyer. These calculations provide understanding for the proper variation of the launcher parameters for optimization of launcher performance. A series of calculations for the 2-in. Two-Stage Hypervelocity Model Launcher, which is in use in the NOL 1,000-ft. Hyperballistics Range No. 4, are presented and are compared with the actual performance of the launcher.

COMPUTER ANALYSIS OF TWO-STAGE
HYPERVELOCITY MODEL LAUNCHERS

By

R. Piacesi, D. F. Gates, and A. E. Seigel

Introduction

To make possible the study of hypervelocity phenomena in the laboratory, two-stage hypervelocity model launchers have been developed to propel projectiles at velocities presently as high as 34,000 feet per second (this velocity has been achieved at the NASA Laboratory at Ames). Due to the multiple number of phenomena occurring in a two-stage launcher, it becomes very difficult to predict launching velocities and virtually impossible to determine how to vary the launcher parameters to maximize the velocity capability of the launcher. Maximizing the velocity capability while maintaining a moderate pressure behind the projectile is particularly difficult; this has been a problem of interest for the Naval Ordnance Laboratory Launchers which have been used to launch scale models that cannot withstand high accelerations. To overcome the tediousness of hand calculations and the inaccuracies of approximate analyses (see for example, ref. (1)), calculations of the performance of a two-stage model launcher were done numerically by the authors, utilizing an IBM 7090 computer. The method of calculation and some results are described below.

Description of the Computer Code

The computer code is a one-dimensional hydrodynamic program, using the Lagrangian scheme, and is based on the "q" method as devised by Von Neumann and Richtmyer (refs. (2) and (3)). The code solves quasi-one-dimensional hydrodynamic problems, i.e., it will handle cases of one-dimensional flow through ducts of varying cross section. Automatic treatment of the shock by the "q" method lends itself nicely to the solution of multiple shock systems such as occur in the two-stage light-gas launchers.

The computer program, which is written in FORTRAN for the IBM 704 and 7090 computers (refs. (4) and (5)), is a modification of a program prepared by W. A. Walker of the Explosion Dynamics Division of the Naval Ordnance Laboratory. The code is similar, in many respects, to an earlier non-FORTRAN program obtained from the Lawrence Radiation Laboratory, Livermore, California, in 1957.

In the Lagrangian scheme the system is divided into regions, each having its own equation of state,* and each

* The equation of state may be that of solids, liquids or ideal and non-ideal gases.

TWO-STAGE MODEL LAUNCHERS

region being further subdivided into zones. Mass points containing one-half the mass of each of two adjacent zones are assumed at the interface of these two zones. These mass points are labeled initially (see fig. 1) and carry these labels throughout the entire computation. The hydrodynamic equations of motion and conservation of energy are put into finite difference form. These, along with a suitable stability calculation, are then solved numerically to determine the subsequent motion of these weighted interfaces.

Initial values of the internal energy E_0 , the density ρ_0 , the specific volume V_0 , the pressure p_0 and the velocity u_0 are given for each zone. The new values of these variables and the new positions of the mass points are calculated by numerically integrating the hydrodynamic equations. An appropriate variable time increment is calculated for the numerical integration at each computation cycle to assure stability of the finite difference equations. At each time step, the pressure differential at each interface is used in the equation of motion to determine the acceleration of the mass points. Using the accelerations, the new velocities are computed. Knowing the position of its interfaces, the volume of a zone is computed. The pressure and internal energy are then obtained by a single iteration of the equation of state and the energy equation. In this manner the scheme provides a complete history of the position and velocity of the mass points and of the volume, pressure, and internal energy of the zones.

The code uses the following hydrodynamic equations:

Energy equation for isentropic flow

$$\frac{\partial E}{\partial t} = - p \frac{\partial V}{\partial t} \quad (1)$$

Equation of state

$$p = p(E, V) \quad (2)$$

Equation of motion

$$\frac{\partial u}{\partial t} = - \frac{\partial p}{\partial M} \cdot A(x) \quad (3)$$

TWO-STAGE MODEL LAUNCHERS

where M , the mass, is defined in the equation

$$M = \int_0^X \rho(x) A(x) dx \quad (4)$$

In the "q" method, equations (1) and (3) are rewritten as:

$$\frac{\partial E}{\partial t} = -(p+q) \frac{\partial v}{\partial t} \quad (5)$$

$$\frac{\partial u}{\partial t} = -\frac{\partial(p+q)}{\partial x} \cdot \frac{1}{M} \cdot A(x) \quad (6)$$

where

$$q = \begin{cases} \frac{C_0^2}{V} \left(\frac{\partial u}{\partial j} \right)^2, & \frac{\partial u}{\partial j} < 0 \\ 0, & \frac{\partial u}{\partial j} \geq 0 \end{cases} \quad (7)$$

$$(8)$$

The term q , which is added to the pressure in equations (5) and (6), acts as an artificial dissipative mechanism giving the correct entropy change across the shock and allows the hydrodynamic variables to be continuous across the shock front. C_0 is a constant which can be adjusted to spread the shock over a desired number of zones.

Equations (5), (6), (7), and (8) appear below in differenced form along with the other necessary equations in logical sequence as used in the program

$$\left(\frac{\partial u}{\partial t} \right)^n = \frac{(p_{j-\frac{1}{2}}^n + q_{j-\frac{1}{2}}^n) - (p_{j+\frac{1}{2}}^n + q_{j+\frac{1}{2}}^n)}{\frac{1}{2} (\Delta M_{j-\frac{1}{2}} + \Delta M_{j+\frac{1}{2}})} \cdot A(x) \quad (9)$$

$$u_j^{n+\frac{1}{2}} = u_j^{n-\frac{1}{2}} + \left(\frac{\partial u}{\partial t} \right)_j^n \Delta t^n \quad (10)$$

TWO-STAGE MODEL LAUNCHERS

$$X_j^{n+1} = X_j^n + u_j^{n+\frac{1}{2}} \cdot \Delta t^{n+\frac{1}{2}} \quad (11)$$

$$V_{j+\frac{1}{2}}^{n+1} = \frac{p_{j+\frac{1}{2}}^n}{(\Delta M)_{j+\frac{1}{2}}} \int_{X_j^{n+1}}^{X_{j+1}^{n+1}} A(x)_j^{n+1} dx \quad (12)$$

$$g_{j+\frac{1}{2}}^{n+\frac{1}{2}} = \begin{cases} \frac{2c_0^2 p_{j+\frac{1}{2}}^n}{V_{j+\frac{1}{2}}^n + V_{j+\frac{1}{2}}^{n+1}} \left[u_{j+1}^{n+\frac{1}{2}} - u_j^{n+\frac{1}{2}} \right]^2, & u_{j+1}^{n+\frac{1}{2}} < u_j^{n+\frac{1}{2}} \quad (13) \\ 0, & u_{j+1}^{n+\frac{1}{2}} \geq u_j^{n+\frac{1}{2}} \quad (14) \end{cases}$$

$$\epsilon_{j+1}^{n+1} = \epsilon_j^n \cdot \left[\frac{p_{j+\frac{1}{2}}^{n+1} + p_{j+\frac{1}{2}}^n}{2} + g_{j+\frac{1}{2}}^{n+\frac{1}{2}} \right] \left[\frac{V_{j+\frac{1}{2}}^{n+1}}{V_{j+\frac{1}{2}}^n} \right] \quad (15)$$

$$p_{j+\frac{1}{2}}^n = p \left(\epsilon_{j+\frac{1}{2}}^{n+1}, V_{j+\frac{1}{2}}^{n+1} \right) \quad (16)$$

$$j = 1, 2, 3 \dots J_{\max}$$

$$n = 0, 1, 2$$

$$\Delta t^{n+1/2} = t^{n+1} - t^n$$

$$\Delta t^n = \frac{t^{n+1/2} + t^{n-1/2}}{2}$$

$$\Delta M_{j+1/2} = \text{zone mass}$$

$$A(x)_j^n = \text{cross-sectional area at } x$$

Here j refers to the mass point number and n the time cycle number.

Two-Stage Gun Process

It is known that for an isentropically expanding gas pushing a projectile, the pressure drop behind the projectile may be decreased by using a propellant gas with a high initial sound speed, a_0 , and a low specific heat ratio γ . Since γ for gases does not differ widely, much effort is given to obtain a high initial sound speed for the driver gas.

TWO-STAGE MODEL LAUNCHERS

One method of obtaining a high sound speed driver is the two-stage gun. The events occurring in the operation of a two-stage gun can be described in the following way.

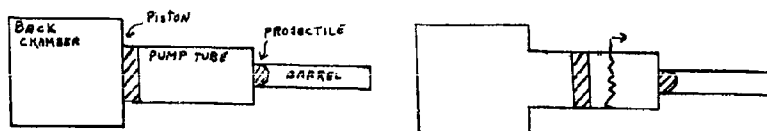


Fig. A

Fig. B

The back chamber contains a propellant which is burned to a high pressure. The front chamber or "pump tube" contains a low-molecular-weight gas such as hydrogen or helium initially at a much lower pressure than the peak pressure of the back chamber gas (fig. A). The diaphragm separating the back and front chambers is opened near the back chamber peak pressure, causing the piston to be accelerated. A shock precedes the piston down the pump tube which reflects between the piston and the end of the pump tube several times, raising the temperature and pressure of the light gas (fig. B). The resulting high temperature, along with the low molecular weight of the gas produces a much higher sound speed for the pump tube gas than was possible to attain for the back chamber driver.

Although the drop in pressure behind a projectile may be decreased by increasing the sound speed in the driver gas, the increase in sound speed practically attainable is insufficient in itself to maintain the pressure at the desired constant value. What is required is that the reservoir pressure in the pump tube be increased during the movement of the projectile. By so doing the tendency of the pressure behind the projectile to drop is overcome. The higher the sound speed of the driver gas, the less is the required reservoir pressure increase to maintain the pressure behind the projectile constant. In practice the reservoir pressure would be required to rise perhaps a factor of 10 or more times the value of the pressure behind the projectile to maintain it constant.

The two-stage gun provides the possibility of increasing the reservoir pressure in the pump tube by means of the piston in the pump tube which, by its movement, compresses the reservoir gas, thus effecting the required increase of pressure.

TWO-STAGE MODEL LAUNCHERS

Therefore, the condition desired in the two-stage gun is a constant pressure behind the projectile as a result of the proper increase of pump tube reservoir pressure. The selection of the variables required to attain this condition is almost impossible by means of hand calculations. The electronic computing machine offers a means for selection of the required parameters.

The processes occurring in the two-stage gun are readily seen in the plots of information as obtained from the electronic computer. Figure 2 is a typical calculated distance-time plot showing the trajectories of shocks between the piston and projectile, the piston trajectory, and the projectile trajectory. Figure 3 is a plot of calculated pressure behind the model as a function of distance along the barrel. Figure 4 is a calculated velocity-time plot of the projectile and shows clearly the effect of shock impingements on the back of the model.

Calculations and Results

Many calculations were made to determine optimum gun operating conditions for various NOL Hypervelocity Facilities. As mentioned above, the problem of optimum performance is complex due to the number of parameters involved. For a given gun geometry these parameters are the initial back-chamber conditions, the initial front-chamber conditions, the weight of the piston, the weight of the projectile and the projectile release pressure. There are certain physical restrictions existing on the facility and the projectile; these being, a limiting pressure that the gun can contain without damage being done, and a maximum acceleration that the projectile can withstand without breaking up. In addition, it may be desired to vary the gun geometry itself (length and diameter of launch tube, etc.) to obtain an optimum model launcher. By adjusting the above parameters, keeping in mind the physical limitations, optimum operating conditions can be determined.

A typical set of computer calculated results for the 2-in. Two-Stage Hypervelocity Model Launcher, which is in use in the NOL 1,000-ft. Hyperballistics Range No. 4, are shown in tables 1, 2, and 3. Figure 5 shows the dimensions of the 2-in. two-stage facility. A large portion of the success of this facility in presently firing sabot models of various aerodynamic configurations over 17,000 feet per second is attributed to these calculations (ref. (6)). Figure 6 is a spark photograph of a 10° total angle cone fired in the range at 17,600 feet per second. The computer calculation showed that the highest pressure the projectile would feel was 25,000 psi.

The calculations assume the back-chamber propellant is preburned and is an ideal gas with a constant specific heat

TWO-STAGE MODEL LAUNCHERS

ratio γ . A constant γ is also used for the pump tube gas. Co-volume effects in the pump tube gas were taken into account for the 2-in. two-stage calculations.*

The calculations for the 2-in. two-stage launcher for the higher velocity cases ($> 15,000$ feet per second) predict higher velocities (about 10 percent higher) than are obtained experimentally. Figure 7 shows a comparison of the theoretical calculations and the experimental results.** For smaller bore launchers the deviation appears more serious. This is not disturbing in that one is still guided in the direction to vary the parameters for optimizing the performance. The difference in predicted velocities and experimental velocities is attributed largely to frictional effects. The frictional effects can be accounted for, but only at the expense of computer time which is costly. When optimum conditions are obtained, losses due to friction can be taken into account for that set of conditions (ref. (7)).

Conclusion

Two stage gun performance calculations were made using a one-dimensional hydrodynamics computer code. This code takes account of the gas dynamic processes occurring including the shocks which are reflected back and forth both in the pump tube and in the barrel. The true equations of state are used for the gases as well as for the piston and projectile. Although the code is one-dimensional, it had been previously demonstrated experimentally that the one-dimensional approximation is excellent for unsteady flows between tubes of different diameters (ref. (8)). Friction effects can also be taken into account in this code.

Predictions by approximate methods of computations for the pressure experienced by the model have been found to be in error by a factor which may be as high as 4 since the sharp pressure peaks which occur are not accounted for by these approximate methods. Without the computer code it becomes virtually impossible to select conditions for launching fragile models (such as the cone shown in fig. 6) at relatively high velocities without failure of the model. A common experience in attempting to launch such a small angle cone in ballistic range facilities is the emergence of the cone with the nose tip broken off (spalled). On the basis of the experience gained with the NOL Two-Stage Launchers, it is felt that successful launching of fragile models at high velocities can only be achieved without the necessity for many trials with a computer program of this type which accurately calculates the conditions occurring during the firing.

* As noted before, any equation of state may be used for the gas.

** The experimental firings were made with the barrel evacuated.

TWO-STAGE MODEL LAUNCHERS

References

- (1) Seigel, A. E., "Method of Calculating Pre-Burned Propellant Gun Performance with Special Application to Two-Stage Guns," NOLTR 61-29, Jun 1961
- (2) Von Neumann, I. and Richtmyer, R. D., "A Method for the Numerical Calculation of Hydrodynamic Shocks," J. Appl. Phys., Vol. 21, p. 232, 1932
- (3) Richtmyer, R. D., "Difference Methods for Initial Value Problems," Interscience Publishers, Inc., New York, 1957
- (4) Piacesi, D. and Sternberg, H. M., "The Application of the "q" Method to the Solution of Hypervelocity Gun Problems," Proceedings of the Fifth Symposium on Hypervelocity Impact, Vol. II, Apr 1962
- (5) Piacesi, D and Sternberg, H. M., "Hydrodynamic "q" Method Calculations for High Explosive Systems Designed to Accelerate Pellets to High Velocities," NOLTR 62-40 (in preparation)
- (6) Carter, H. L., Oakes, D. A., Piacesi, R., and Shepard, B. M., "The Design and Testing of the Naval Ordnance Laboratory's 2-in. Two-Stage Gun," NOLTR 62-112, Jun 1962
- (7) Seigel, A. E. and Piacesi, R., "The Effect of Gas Friction and Heat Transfer on High-Speed Gun Performance," NOLTR 62-169 (in preparation)
- (8) Seigel, A. E. and Dawson, V. C. D., "Results of Chambrage Experiments on Guns with Effectively Infinite Length Chambers," NavOrd Report 3636, Apr 1954

TABLE 1
COMPUTER PERFORMANCE CALCULATIONS FOR 240-GRAM PROJECTILE

Back Chamber Pressure (psi)	Pump Tube Pressure (psi H ₂)	Piston Weight (gm)	Projectile Release Pressure (psi)	Pressure Felt By Projectile (psi)	Maximum Pressure In Taper (psi)	Velocity 240 Calibers (ft./sec)
20,000	750	5,540	5,000	82,000	125,000	18,200
20,000	500	5,540	5,000	175,000	195,000	18,730*
20,000	750	1,000	5,000	116,900	116,600	14,600
20,000	750	2,700	5,000	91,350	121,200	17,400*
20,000	750	5,540	5,000	82,000	125,000	18,200
20,000	750	9,000	5,000	91,840	123,650	18,500
20,000	1,000	1,000	5,000	111,900	122,900	15,900
20,000	1,000	5,000	5,000	63,000	107,300	17,350
20,000	1,000	9,000	5,000	64,600	112,300	17,600
20,000	1,500	1,000	5,000	61,500	82,600	12,650
20,000	1,500	5,000	5,000	59,450	78,900	15,200
20,000	1,500	9,000	5,000	29,800	81,400	15,000
30,000	1,500	9,000	5,000	69,300	155,700	19,200
30,000	2,000	9,000	5,000	52,000	129,200	17,200
30,000	1,500	18,000	10,000	53,700	128,600	18,500
30,000	2,000	18,000	10,000	42,700	112,500	17,100
30,000	2,000	18,000	5,000	32,000	115,350	14,900
40,000	2,000	2,000	5,000	107,500	136,700	17,400
40,000	1,500	9,000	5,000	114,000	246,500	23,650
40,000	2,500	9,000	5,000	76,400	173,600	18,700

* (200 Cal.)
Initial pump tube temperature 300°K

TABLE 2

COMPUTER PERFORMANCE CALCULATIONS FOR 120-GRAM PROJECTILE

Back Chamber Pressure (psi)	Pump Tube Pressure (psi H ₂)	piston Weight (gm)	Projectile Release Pressure (psi)	Pressure Felt By Projectile (psi)	Maximum Pressure In Taper (psi)	Velocity 240 Calibers (ft/sec)
20,000	100	2,000	5,000	178,000	213,000	22,800
20,000	200	9,000	5,000	63,000	125,100	20,000
20,000	300	9,000	5,000	57,300	101,200	20,600
20,000	500	2,000	5,000	87,000	121,700	22,300
20,000	500	5,000	5,000	68,000	126,300	22,000
20,000	500	9,000	5,000	56,400	121,600	20,600
20,000	750	2,000	5,000	54,250	98,200	20,400
20,000	500	18,000	5,000	21,750	64,300	17,500
30,000	500	18,000	5,000	41,600	105,800	20,700
20,000	1,000	18,000	5,000	15,600	30,600	17,100
20,000	1,000	18,000	20,000	41,800	87,400	19,300
20,000	1,000	1,000	5,000	42,000	67,900	17,500
20,000	1,000	5,000	5,000	37,700	106,700	19,900
20,000	1,000	9,000	5,000	23,000	102,500	19,500
20,000	1,500	18,000	5,000	9,300	68,000	12,600

TWO-STAGE MODEL LAUNCHERS

Initial pump tube temperature 300°K

TWO-STAGE MODEL LAUNCHERS

TABLE 3
COMPUTER PERFORMANCE CALCULATIONS FOR 50-GRAM PROJECTILE

Back Chamber Pressure (psi)	Pump Tube Pressure (psi H ₂)	Piston Weight (gm)	Projectile Release Pressure (psi)	Pressure Felt By Projectile (psi)	Maximum Pressure In Taper (psi)	Velocity 240 Calibers (ft/sec)
20,000	100	500	5,000	49,000	72,000	25,600
20,000	100	1,000	5,000	69,600	83,000	25,700
20,000	100	9,000	20,000	90,000	127,000	23,200
20,000	300	500	5,000	76,000	101,200	25,300
20,000	300	1,000	5,000	117,700	117,700	27,000
20,000	300	9,000	5,000	35,670	95,300	24,400
20,000	500	9,000	5,000	35,200	117,700	25,200
20,000	1,000	9,000	5,000	13,600	104,000	19,700
20,000	1,000	9,000	20,000	28,700	98,300	20,900
20,000	1,500	9,000	5,000	29,000	161,700	20,100
30,000	1,500	9,000	5,000	8,700	82,600	12,600

Initial pump tube temperature 300°K

TWO-STAGE MODEL LAUNCHERS

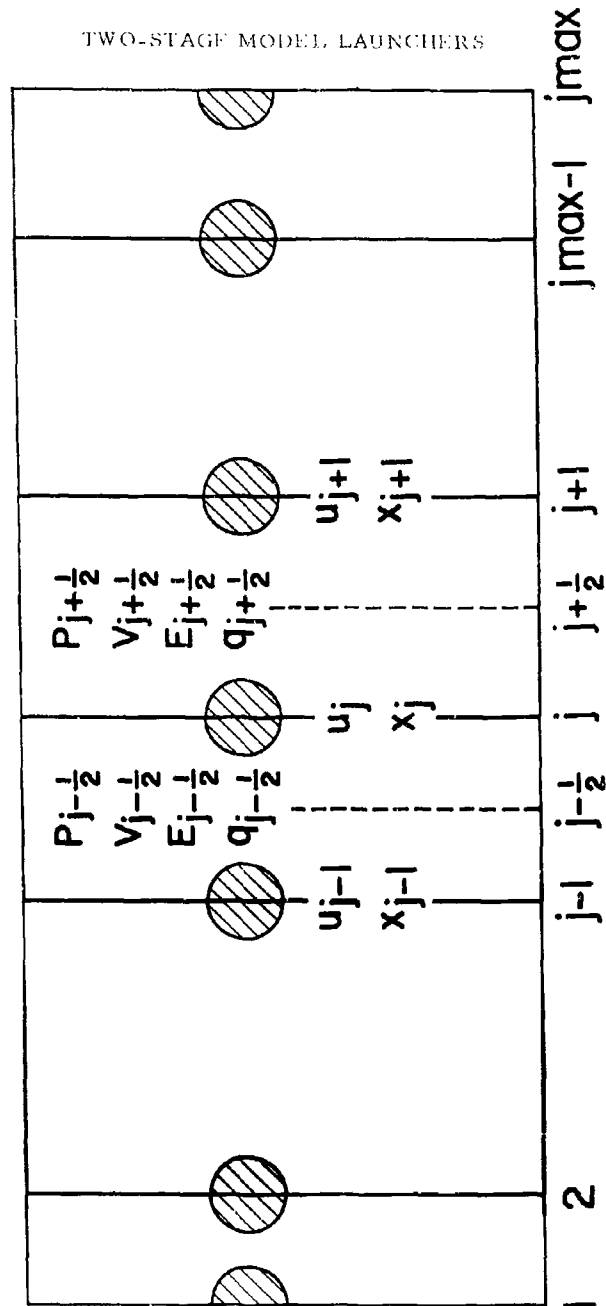


FIG.1

TWO-STAGE MODEL LAUNCHERS

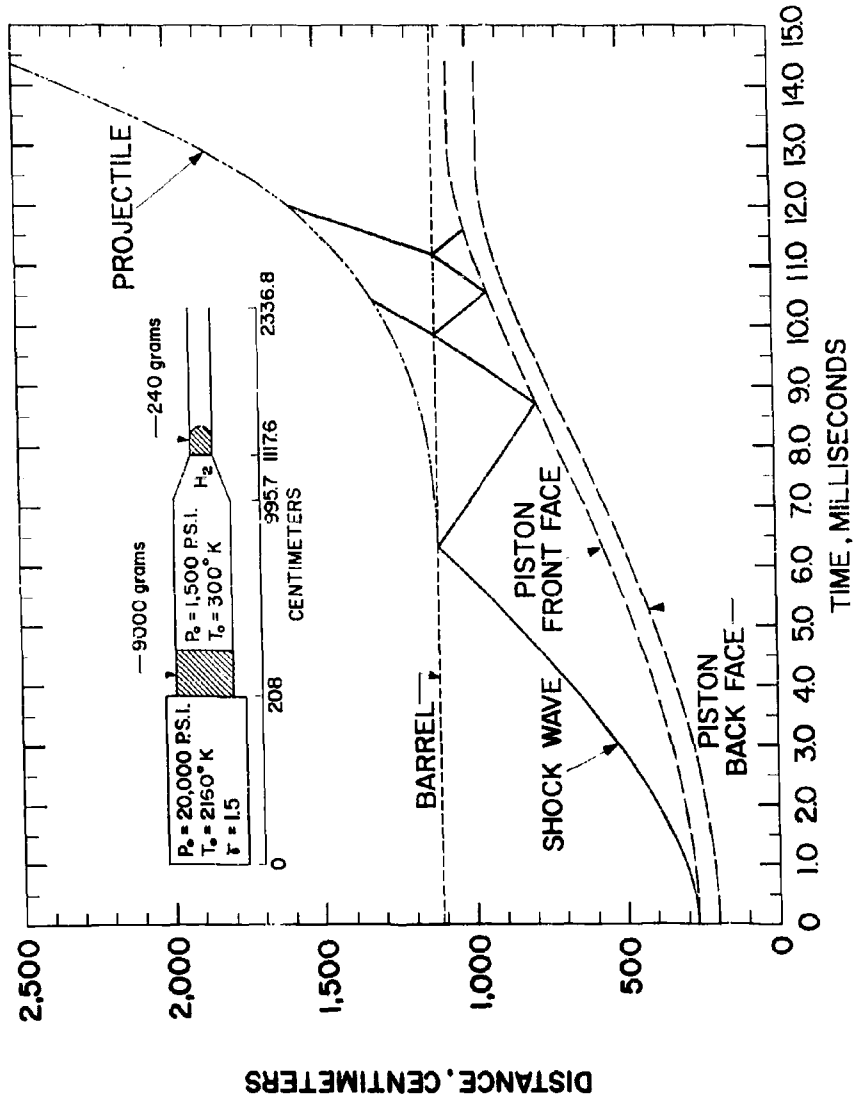


FIG. 2 TWO-STAGE GUN, TIME-DISTANCE PLOT

TWO-STAGE MODEL LAUNCHERS

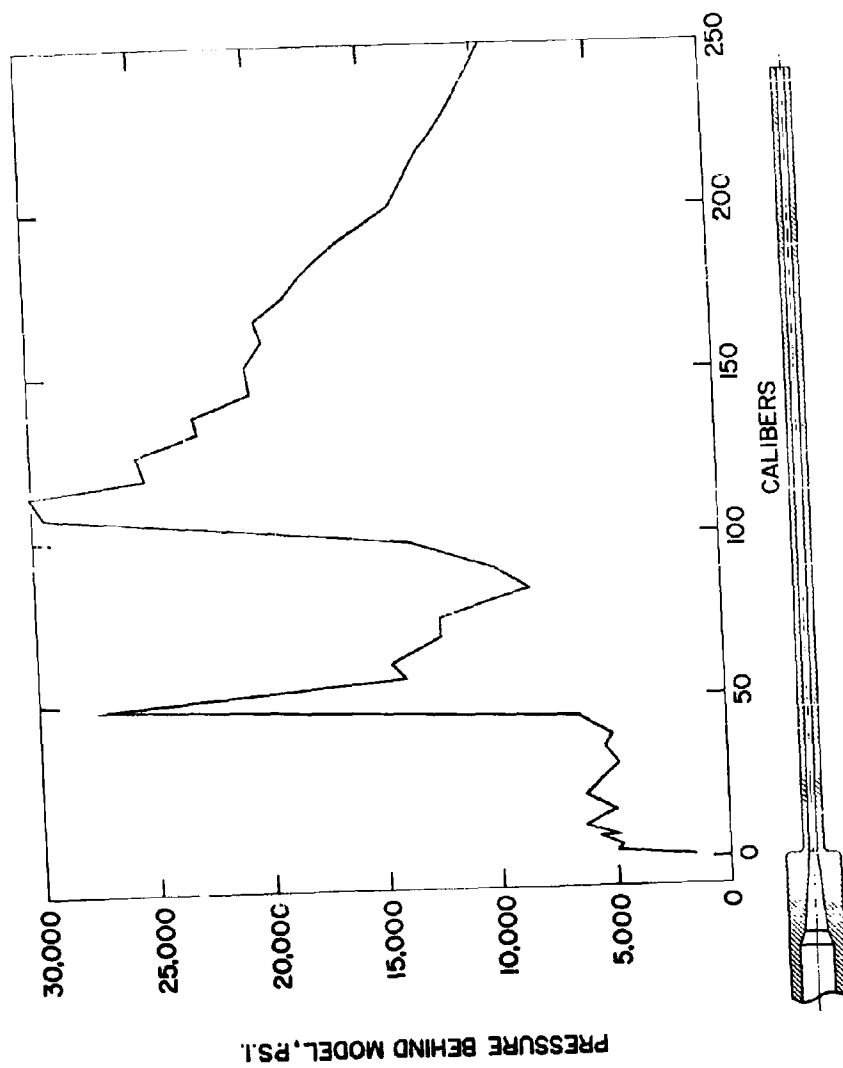
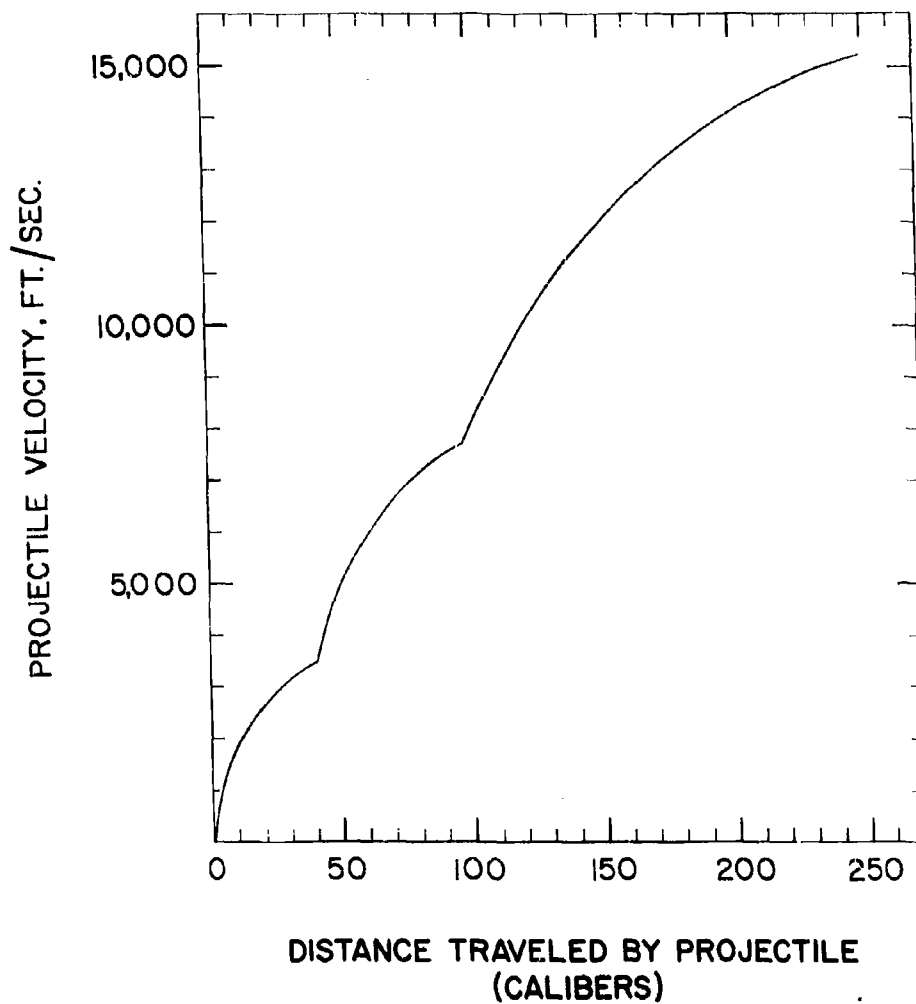


FIG.3 PRESSURE BEHIND MODEL VS BORE TRAVEL IN CALIBERS

TWO-STAGE MODEL LAUNCHERS



**FIG.4 PROJECTILE VELOCITY VS
BORE TRAVEL IN CALIBERS**

TWO-STAGE MODEL LAUNCHERS

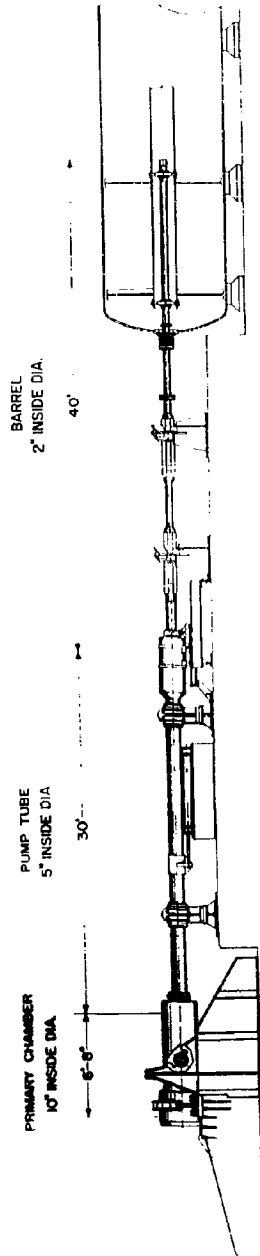


FIG.5 TWO-INCH TWO-STAGE LIGHT GAS GUN

TWO-STAGE MODEL LAUNCHERS

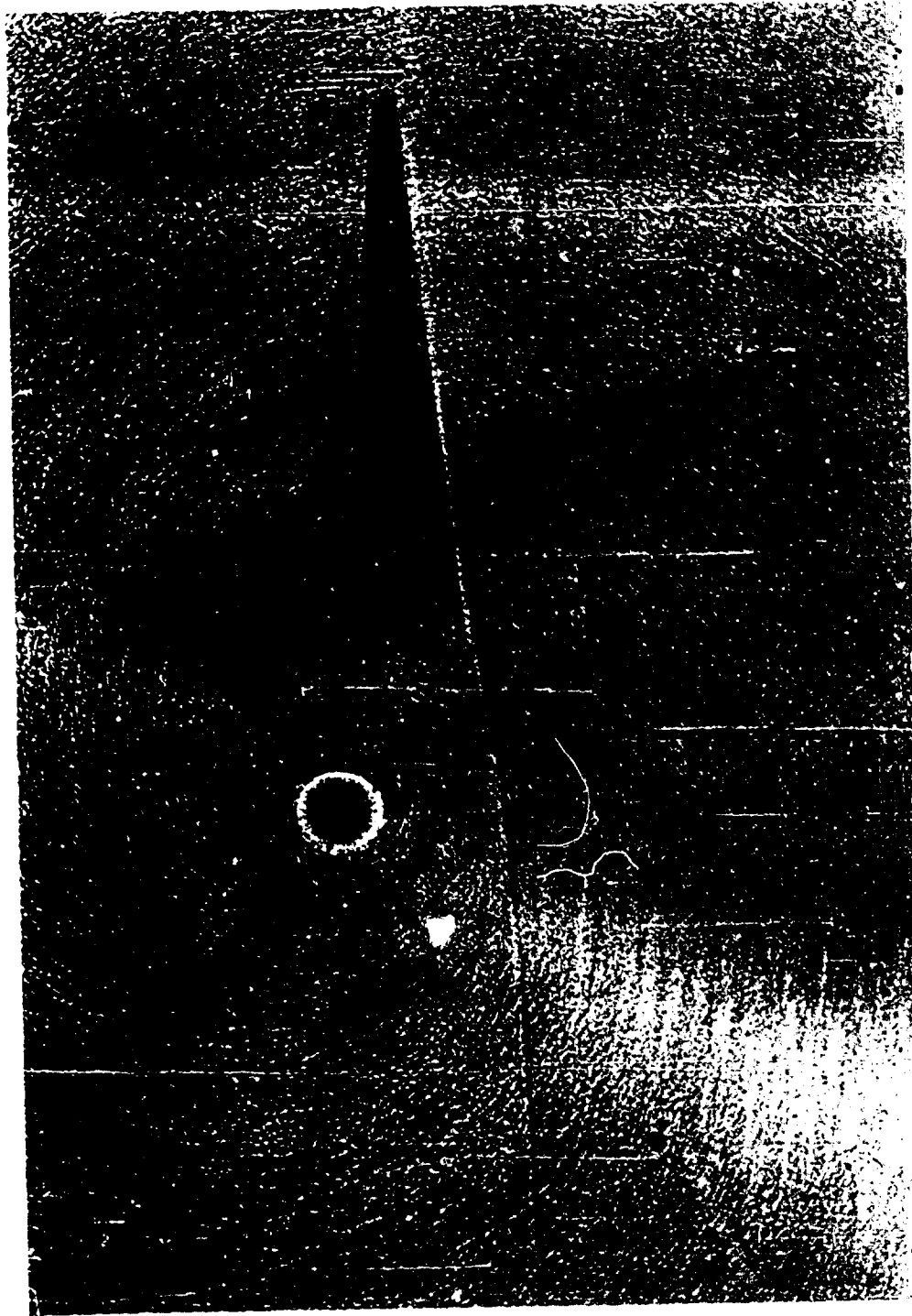


FIG. 6 10° TOTAL ANGLE CONE $V=17,600$ FT./SEC.

TWO-STAGE MODEL LAUNCHERS

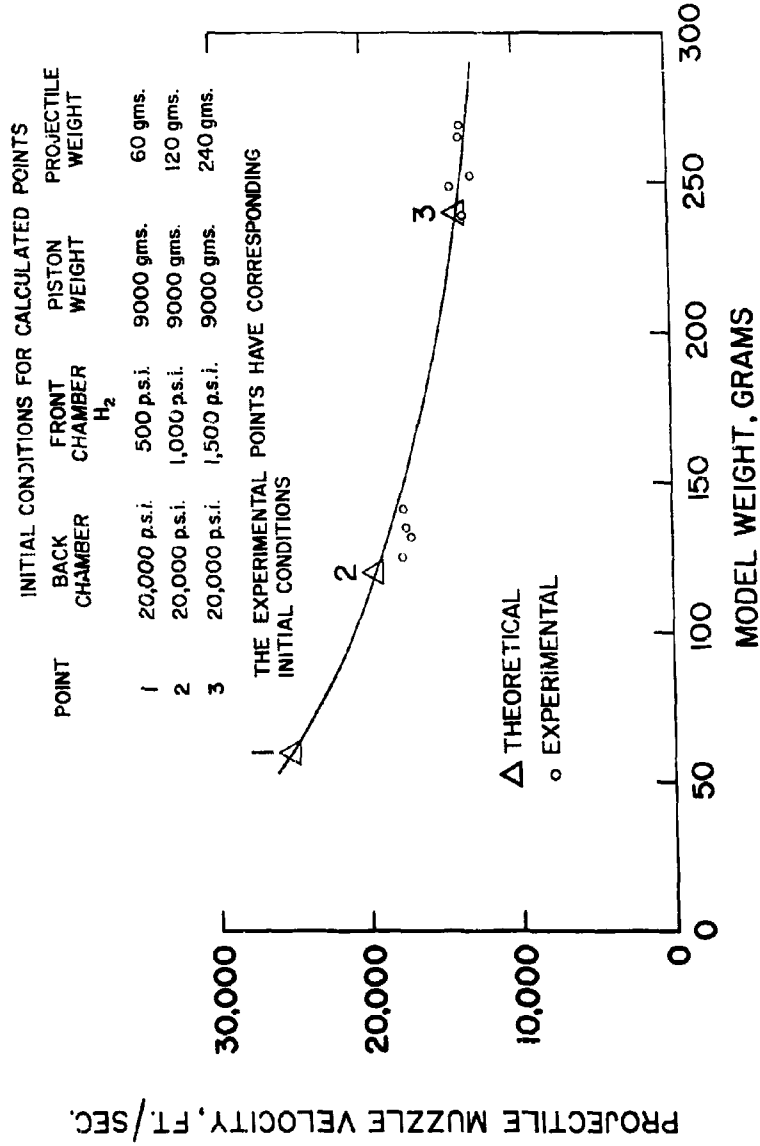


FIG. 7 COMPARISON OF THEORETICAL CALCULATIONS AND EXPERIMENTAL RESULTS FOR NOL TWO-INCH TWO-STAGE LAUNCHER

NRL HYPERVELOCITY ACCELERATOR DEVELOPMENT

by

H. F. Swift, C. D. Porter,
J. J. Condon, and J. R. Baker

Sponsored by

Advanced Research Projects Agency
Ballistic Missile Defense Systems Branch
ARPA ORDER NO. 70
ARPA ORDER NO. 149

U. S. Naval Research Laboratory
Washington 25, D. C.

NRL ACCELERATOR DEVELOPMENT

CONTENTS

ABSTRACT	177
INTRODUCTION	178
LIGHT-GAS-GUN DEVELOPMENT	178
Operating Guns	179
Related Gun Studies	189
LIGHT-GAS-GUN COMPUTER ANALYSIS	198
Gun Simulation Program	198
Systematic Variation of Parameters	205
Results of Firing Parameter Variation	208
Comparison with Experimental Results	221
Future Development	222
ELECTROBALLISTIC STUDIES	223
Constant-Volume-Gun Development	223
Electrocompression Gun Development	225
Electrical Plate Accelerator	241
REFERENCES	245

NRL ACCELERATOR DEVELOPMENT

ABSTRACT

The U. S. Naval Research Laboratory is engaged in a continuing program to develop hypervelocity-accelerator capability. Present accelerators are light-gas guns of the semiexpansible-central-breech design which vary in size from 0.830", .30" units to an 8.2", 2.5" gun. The current launch capability of the facility ranges from 0.1 gram at 9.35 km/sec to 250 grams at 5.6 km/sec. The operation of gas guns is being studied theoretically with a computer program. An experimental study of various aspects of gun operation including projectile release, driver gas leakage, projectile-bore friction and sabot breakup is also being conducted. The feasibility of electrically energizing hypervelocity accelerators has been experimentally and theoretically studied. The addition of electrical energy to the driver gas of a standard light-gas gun operating under reduced parameters has generated a 33% increase in gun performance. Electrical pulses have also been used to generate sheets of dense plasma that have accelerated thin plastic plates to velocities above 9 km/sec.

NRL ACCELERATOR DEVELOPMENT INTRODUCTION

The U. S. Naval Research Laboratory is engaged in a program to study hypervelocity impact phenomena. The results of these studies are being applied to many problems, i.e., those associated with impact damage to space probing vehicles. In order to carry out these studies effectively, space vehicle impacts must be accurately simulated under laboratory conditions.

A continuing program to develop hypervelocity acceleration facilities for simulating such impacts has therefore been maintained. The program consists of the development of new gas guns, theoretical and experimental studies of their operation, studies of new techniques to extend the operating range of gas guns, and the development of associated acceleration techniques.

During the last 18 months, two relatively large gas-gun facilities have been installed. One contains a 3.25", .83" gas gun of the expendable central breech design which is used to launch packages weighing between 5 grams and 60 grams. The other uses an 8.2", 2.5" gas-gun with a semicxpendable central breech to launch packages weighing between 200 grams and 1000 grams.

A study of the operation of these light-gas guns and other smaller units is centered around a computer program which uses an iterative process to compute a complete set of parameters that describe gun conditions during a firing sequence from initial motion of the piston to exit of the projectile from the muzzle of the launch tube. Since computation runs take only 10 minutes each, the program can be used to examine the performance of operational guns and those under design. A series of experimental studies is being carried out to measure selected firing parameters for comparison with predicted values. The results of these comparisons will be used to establish the validity of the computer program and possibly to formulate empirical correction terms for increasing overall accuracy.

Investigations are also being conducted to determine the feasibility of using electrical energy pulses for hypervelocity acceleration. These include both electrical discharges into a reservoir of light gas within the gas gun in order to increase the temperature developed during gas compression, and the electrical explosion of metallic foils to accelerate thin plates to hypervelocities.

LIGHT-GAS-GUN DEVELOPMENT

The ballistic launching capability of the NRL hypervelocity facility has been sharply increased during the past 18 months. Two large gun ranges have been constructed and the performance of the older gas gun systems improved. All of the range systems are being used primarily for terminal ballistic studies that require the launching of sabot packages

NRL ACCELERATOR DEVELOPMENT

containing high density projectiles covering a wide range of mass, size, and velocity. Since all material launched with the projectile must be removed from the trajectory the ability of sabot packages to withstand high acceleration and to separate adequately after launch is of prime importance. Several sabot configurations have been designed and tested because a wide range of projectiles and projectile velocities are needed for the impact investigations. An example of one of the sabots used frequently is a five-piece design originally developed at the U. S. Naval Ordnance Laboratory (1). The material used for this design has been primarily Lexan* and glass-filled Lexan. The front section of the sabot consists of four quadrants of a cylinder that are centrally relieved to form a cavity for the launched model. The rear of the sabot is a cap that holds the front segments in position during launch from a gas gun. Five piece sabots have been designed and used with .30", .60", and .83" launch tubes and have successfully launched such models as steel spheres, titanium aerodynamic models, and aluminum rods with L/D ratios up to 10. New sabot materials for all the present designs are continually being searched for and new designs investigated.

All of the gas-guns presently in operation at NRL use semicompactable central breeches and are operated both in the adiabatic compression and shock heated modes. Projectiles are released by shearout disks, petal type diaphragms or slide valves, depending upon the particular shot requirements. Since several of the guns are set up to use interchangeable launch tubes of several diameters, each gun is referred to by the diameter of its compression tube. The particular gas-gun configurations are referred to by specifying the compression tube diameter and the launch tube diameter, e.g., 1.625", .60".

Table I lists the gun configurations presently being used at NRL. Other combinations are being considered.

The firing capabilities of all these gun combinations are presented in Table II and selected gun configurations are presented graphically in Fig. 1. The areas under the solid lines represent proven capability and the dotted lines enclose areas of expected performance capability.

Operating Guns

Two guns using the 1.14", .30" configuration have proven especially effective within their velocity-mass regime. The experience of several years has demonstrated that these guns are capable of successfully launching relatively delicate sabot packages when fired near the limit of their capability. This effect has allowed 3/16" steel spheres to be launched at 6.0 km/sec, 1/4" aluminum spheres at 6.93 km/sec, and 1/4" steel spheres

*Trade name for polycarbonate, a thermoplastic supplied by Fiberfil, Inc.

NRL ACCELERATOR DEVELOPMENT

Table I
NRL Light-Gas-Gun Configurations

No. of guns	Compression Tube diameter	Launch Tube diameter	Overall length
2	.830" (20mm)	.30"	8 ft
2	1.14"	.30"	13 ft
		.50"	15 ft
2	1.625" (40mm)	.22"	14 ft
		.30"	13 ft
		.50"	14 ft
		.60"	15 ft
1	3.25"	.83"	35 ft
1	8.2"	2.50"	100 ft

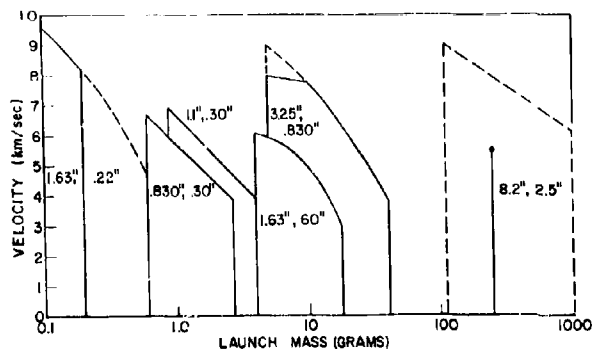


Figure 1 - Present and expected capabilities of NRL light-gas guns

NRL ACCELERATOR DEVELOPMENT

Table II
Present Capability of NRL Light-gas Guns

Compression Tube (in.)	Launch Tube (in.)	Total Launch Mass (gms)	Value Type	Proj. Type	Velocity (km/sec)	Remarks
.83	.30	.60	slider	cyl.	6.71	
	.30	1.00	slider	cyl.	5.64	
	.30	2.70	slider	cyl.	3.90	
1.14	.30	.89	shear	1/4" Al sphere	6.94	saboted
	.30	1.00	shear	3/16" Fe sphere	6.00	saboted
	.30	1.47	shear	cyl.	5.94	saboted
	.30	1.60	shear	cyl.	5.67	saboted
	.30	2.15	shear	cyl.	5.01	
	.30	4.00	shear	cyl.	3.90	
	1.14	.50	2.00	shear	cyl.	
	.50	3.10	shear	cyl.	4.82	
	1.63	.22	.10	slider	cyl.	
1.63	.22	.15	slider	cyl.	8.84	
	.22	.20	shear	cyl.	8.14	
	.30	.63	shear	cyl.	6.92	
1.63	.30	2.10	shear	cyl.	5.09	
	.60	4.10	shear	cyl.	6.00	
3.25	.60	6.90	shear	cyl.	5.61	
	.60	18.00	shear	cyl.	3.05	
	.83	5.20	shear	cyl.	7.99	
8.2	.83	9.60	shear	cyl.	7.80	saboted
	.83	15.40	shear	cyl.	6.92	
	.83	19.60	shear	cyl.	5.79	
	.83	42.50	shear	cyl.	3.81	
8.2	2.50	253.25	slider	cyl.	5.58	

NRL ACCELERATOR DEVELOPMENT

at 5.5 km/sec. This gun system has also launched spheres as small as 1/64" and long rods (L/D = 10). The launch tubes used with this gun system can be reused more than 100 times with some sacrifice in performance. The reliability of these range systems is also exceptionally high. A total reliability of 90% for 180 consecutive rounds was established, with a shot being considered successful only when all terminal ballistic requirements were met. Considerable sabot development took place during this sequence of firings.

The 1.625" guns have been in operation for a relatively long time and were reported earlier (2). Their performance has been optimized during the past 18 months to the point where several firings can be made with a central breech before it must be expended. Maximum capability has not yet been reached with this gun for the case of high density sabot projectiles. Present capability includes 5/16" steel spheres launched at slightly over 5 km/sec when .60-cal launch tubes were used. A 40-mm, .22-cal configuration is being used to launch 0.1-gram plastic cylinders at velocities as high as 9.54 km/sec, which is the highest velocity yet achieved at NRL.

The 3.25", .830" gas gun range is shown in Figure 2. This system was designed to increase mass-throwing capacity to the point where severe damage may be inflicted upon realistic space-vehicle structures and was designed for general impact studies. For this reason, both sabot and unsabot firings are required for terminal ballistic studies. Sabot problems have been especially critical with this gun when high mass packages containing steel pellets are launched. Despite this problem the results from the 3.25", .830" gun have been good, and much critical information on high-mass impacts has been obtained. Special sabot designs with titanium floors are being investigated and have achieved several promising results. The central breeches used with this gun are reused on a routine basis for from four to six times. Studies are now being made to determine the feasibility of extending breech life indefinitely without sacrificing gun performance.

The 8.2", 2.5" gas gun facility was constructed to accelerate projectile packages weighing from 1/4 to 2 pounds to maximum velocities between 6.1 and 9.2 km/sec.

After much theoretical program analysis related to the gun's firing parameters, to material reconnaissance and acquisition, prototype development, and design assembly work, the present 8.2", 2.5" hypervelocity gun was designed. The gun structure, which is approximately 100 feet long and weighs 150 tons, is made up of a compression tube, a high pressure section, and a launch tube. (See Figures 3 and 4).

The compression tube consists of two 8-inch guns smooth-bored to 8.2 inches in diameter and flange-connected muzzle to muzzle. The rear

NRL ACCELERATOR DEVELOPMENT



Figure 2 - Medium size range facility with a 3.25", .830" light-gas gun

NRL ACCELERATOR DEVELOPMENT

barrel is a modified MK VI and is connected to a modified M1. The M1 is threaded and screwed into the high pressure case, which is a modified breech end of a 16-inch gun. The compression tube is reinforced longitudinally by two 24-inch I-beams which are pretensioned in order to pre-compress the compression tube. This precompression of the compression tube decreases any tensile forces in the tube due to firing reactions. The tube alone could not withstand these forces.

The high pressure section, consisting of the high pressure case and the semidisposable core, is designed to withstand pressures up to 400,000 psi with no damage to the high pressure case and minimum damage to the core. The core is composed of sixteen pieces of 4340 alloy steel heat-treated to a yield of 120,000 psi, any part of which may be replaced. The

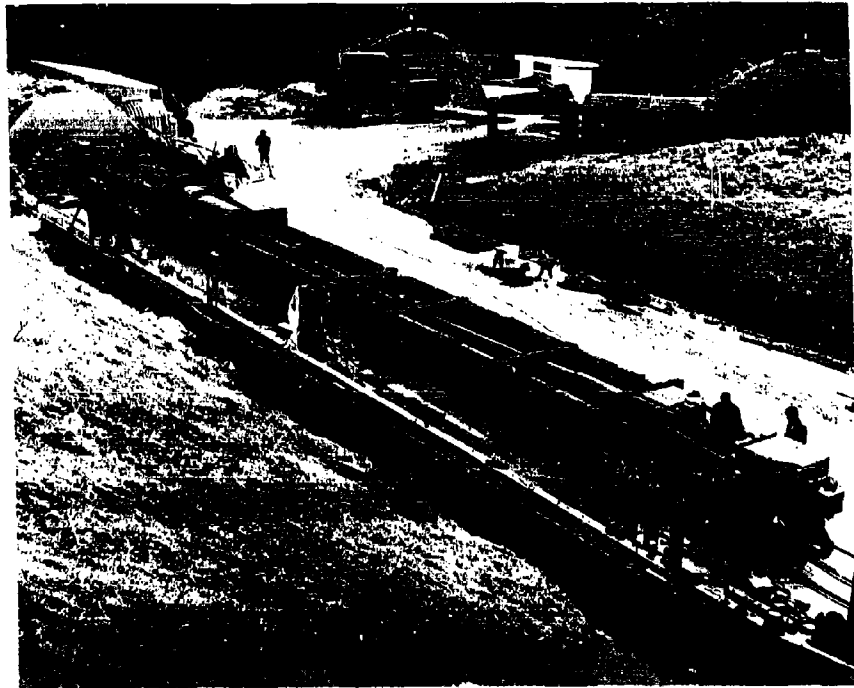


Figure 3 - Large range facility with a 8.2", 2.5" light-gas gun

NRL ACCELERATOR DEVELOPMENT

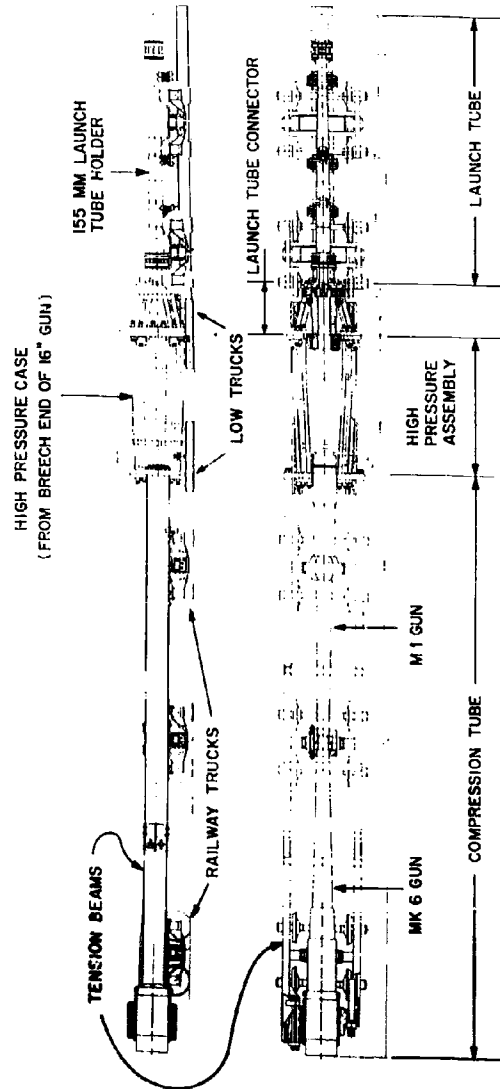


Figure 4 - Overall view of the 8.2, 2.5" light-gas gun

NRL ACCELERATOR DEVELOPMENT

core assembly is placed in a mold in order to cast a fluted lead cover varying from 0.20 to 0.30 inch thick around it. The lead covered core is then pressed into the high pressure case, which has an inside taper varying from 18.6 to 18.4 inches in diameter. The purpose of the lead cover is to prevent permanent damage to the high pressure case, and to eliminate the possibility of locking the core in the high pressure case due to core expansion. Should the core be permanently expanded due to piston impact or high pressures, the fluted lead would prevent full transmission of the radial forces by flowing into the slots. When extraction forces are applied to the core the lead will creep and give way allowing the core to be removed.

The holding mechanism which compresses and holds the core in place during the shot is comprised of a 16-inch-gun breech block and a backup system consisting of flanges and rods. (Figure 5.) The longitudinal elements have been designed to withstand 21,000,000 lbs of force. The breech block alone compresses the core 0.060 inch over a total length of 126.7 inches. This compression greatly reduces the possibility of leakage between the core joints. The rods of the back-up system are then pretensioned to as high as 8,000,000 lbs.

The quick opening valve is located within the core at the end of a section, containing two tapers. The 8.2" tube first tapers very slowly to 7.6" and then more rapidly to 2.5" in a total of 112". The core is adaptable to the slider type, shear diaphragms or petal type valve. Following the valve is the 2.5-inch launch tube in which the projectile is placed. The first section of the launch tube, called the launch tube connector, is comprised of several inner disposable tubes. The launch tube proper is made of two 3-inch gun barrel blanks which have been bored to 2.5 inches and encased in a 155-mm gun tube that serves as a launch tube holder. The total projectile travel as measured from the valve to the launch-tube muzzle is 34 feet or 163 calibers.

The entire gun structure is mounted on wheels and rails allowing movement in either direction along the longitudinal axis of the gun. This type of mount eliminates the necessity for large lifting equipment to separate gun components. A second advantage of the rail system is that it eliminates the chance of transmitting ground shock to nearby installations.

Following the gun is a blast tank, a viewing section, and a target chamber. The blast tank is 23 feet long, 9-3/4 feet in diameter, and contains a series of eight baffle plates with trajectory holes varying from 4-1/2 to 10 inches in diameter. The viewing section contains three sets of horizontal and two sets of vertical optical ports. Here the projectile velocity measurements are taken using the Hall-shadowgraph method (3). The target chamber is a steel-walled tank constructed to contain the gas blast and debris associated with target impacts.

NRL ACCELERATOR DEVELOPMENT

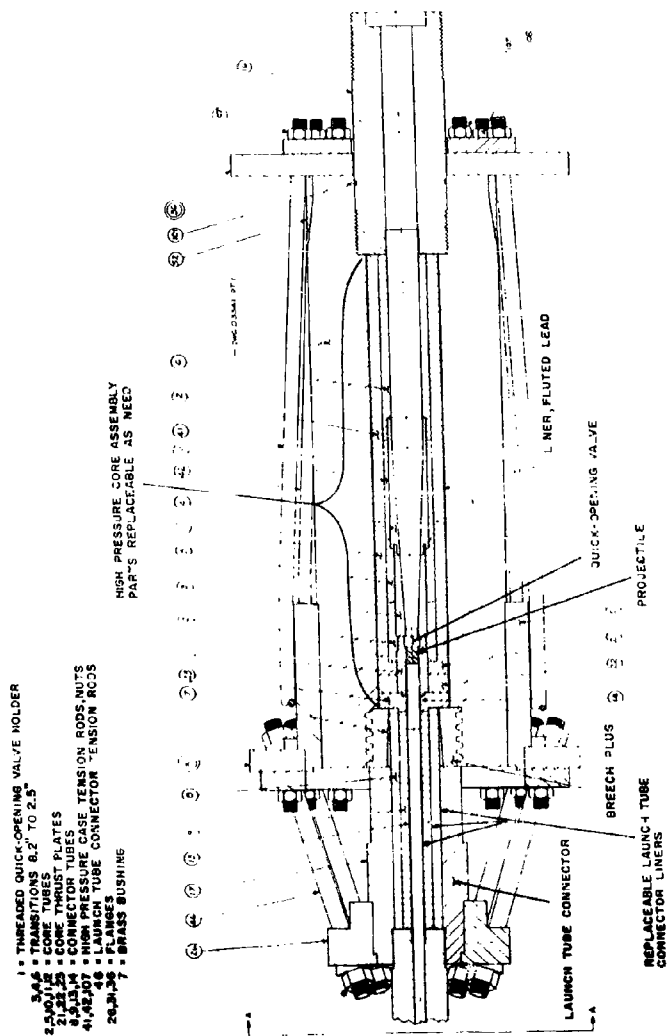


Figure 5 - High pressure assembly of the 8.2", 2.5" light-gas gun

NRL ACCELERATOR DEVELOPMENT

The gun is fired by a pulse from the shadowgraph camera counter which actuates a solenoid-controlled firing pin.

Two vacuum fore pumps and a booster with a high pumping rate but limited vacuum capability are required to draw and maintain the necessary vacuum extending from the quick opening valve through the launch tube, blast tank, viewing section, and target chamber. The time required to obtain an adequate vacuum is approximately two hours.

The NRL 8.2", 2.5" hypervelocity gun was fired for the first time on March 9, 1963. A piston of polyethylene and water (Figure 6) weighing 70-1/2 pounds was used to compress the driver gas (hydrogen). The initial gas pressure was 197 psig. A slider-type quick-opening valve made of 7075-T6 aluminum was used for the first shot. The center of the valve is slotted and drilled to break at a predetermined pressure. A Lexan projectile weighing 253.25 gm (8.93 oz), 2.5 inches in diameter and 2.75 inches long was used. It was a true cylinder except for a slight cup on the high pressure end.

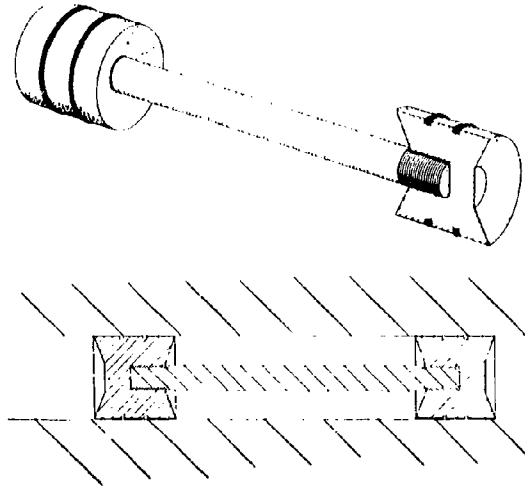


Figure 6 - Polyethylene-water piston for the 8.2", 2.5" light-gas gun

NRL ACCELERATOR DEVELOPMENT

The shot was fired at approximately one-half maximum piston energy and proved highly successful since the projectile attained a planned velocity of 18,300 ft/sec and hit the target on trajectory. The axial movement of the gun was less than 1/2-inch in the direction of the breech end. The gun structure suffered no damage and the core damage was minimal. Although the core expanded somewhat in the tapered section, it is reusable except for the replacement of the valve and two sections of 2.5-inch tubing (Core Pt.'s 13, 14 - Figure 5). The core expansion caused the lead to flow into the slots over a length of approximately 6 inches. The core was extracted from the high pressure case at approximately the same load that was required to press it in, however.

Future shots are planned which will make full use of the capability of the gun and facility. Changes which can and will be made on individual shots are powder loading, piston weight and design, gas loading, valve type and break pressure, launch tube diameter, the type, weight, and size of projectile, and instrumentation. The gun is designed to shoot projectiles of several types including cylinders, sabots, and traveling explosive charges. The blast tank and auxiliary chamber are designed for installation of a sabot stopper which will permit only the projectile to pass through the viewing section and into the target chamber. The target chamber is designed to accommodate a ballistic pendulum which may be installed for measuring projectile mass.

Related Gun Studies

A development program to support the operation of light-gas guns at NRL has been in operation for several years. The basic aim of this research is to design components for use with light-gas guns and to develop instrumentation capability for monitoring the internal operation of gas guns.

Petal Valve Development

One of the most critical phases of a light-gas-gun firing sequence is the release of the projectile package. The position of the compression piston and the local gas pressure at the time of projectile release strongly affect peak projectile acceleration levels and velocity performance of the gun. Shearout diaphragms have long been used for projectile release valves and are highly reliable, but the sheared disk which must be accelerated with the projectile package adds to the total launch weight and must be deflected after launch. Slide valves have also been developed for projectile release applications and were reported earlier (4).

Petal-type projectile release diaphragms patterned after similar units in operation at the Naval Ordnance Laboratory (5) have been developed for use in several light-gas guns during the last year. A disk of stainless

NRL ACCELERATOR DEVELOPMENT

steel is scored with two crossed grooves and is mounted between the launch tube and compression tube of a light-gas gun. The diaphragm bulges and then tears along the grooves as the driver-gas pressure increases. After tearing apart, the segments (petals) are bent against the wall of a retainer by the high pressure gas, which then has an unobstructed flow path into the launch tube. The initial petal diaphragms were constructed for the 3.25", .830" gas gun using design data from NOL and performed as expected both when tested statically in an hydraulic facility and in the gas gun. A series of petal diaphragms has also been designed for the 1.63", .22", the 1.63", .30", and the 1.63", .60" gun configurations where maximum projectile release pressures as high as 100,000 psi are required. The initial design parameters were computed from pressure and size extrapolations of the data obtained from the 0.83" diaphragm development and the static test results were within $\pm 5\%$ of the predicted release pressures. Diaphragms constructed using second approximations deviated less than $\pm 1.5\%$ from expected release pressures.

The possibility exists that any of the projectile release mechanisms presently in use may not open at the same pressure when dynamically loaded in a gas gun as they do in the hydraulic facility, in which pressure loads are applied slowly. Two phenomena that could cause deviations between static and dynamic operation are differences between the static and dynamic strengths of the materials used in the release mechanisms and the finite growth rate of deformations of the release mechanisms which occur before opening.

Gas Dynamic Pressure Generator

It has been reasoned that an adequate dynamic test of release mechanisms would be to subject them to a rapidly changing pressure pulse whose time derivative at release is the same as that encountered within the gun. The pressure measured at the opening time of the release mechanism during a test ought to be a close approximation of the projectile release pressure in a gas-gun firing. A gas dynamic pressure generator has been constructed using a 37-mm chamber and an adaptor that contains mounting fixtures for projectile release mechanisms and a dynamic pressure sensor (Figure 7). Both the sensor and the release mechanism are mounted at right angles to the axis of the 37-mm chamber to eliminate measurement errors caused by pressure gradients along the gas column. A test is started by igniting a calibrated charge of powder in the 37-mm gun chamber. The resulting gas pressure rise is monitored by the pressure sensor and opening of the release mechanism is detected by a sharp reduction in gas pressure as shown on a photographic oscillogram of the pressure-time profile.

NRL ACCELERATOR DEVELOPMENT

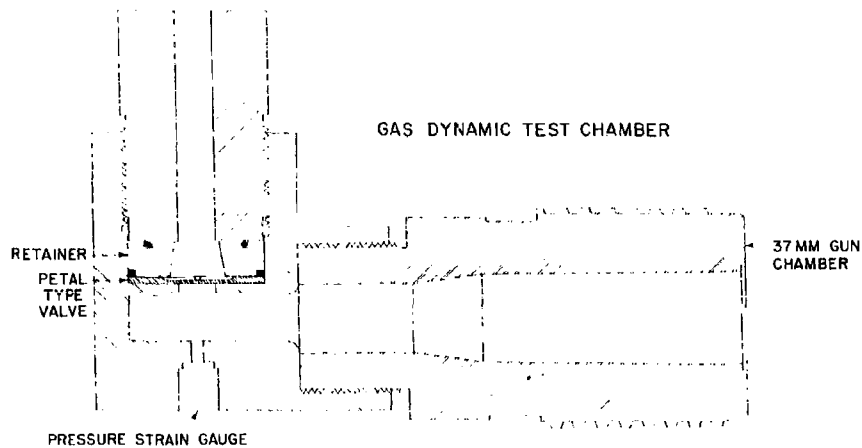


Figure 7 - Gas-dynamic test chamber for studying projectile release mechanisms

Preliminary tests of shearout and petal diaphragms have been made with the gas dynamic pressure system using pressure increase rates that both simulate and exceed values predicted for gas-gun firing situations. The results indicate that no significant difference exists between static and dynamic pressures required to actuate either mechanism for release pressures up to 40,000 psi.

Piston Leakage

The various analyses of light-gas gun firings assume ideal operation of some phases of the gun-firing sequence. Since each of the presently available techniques has limited capability to predict the firing results of light-gas guns, the possibility exists that some of these assumptions are not adequate. Two of the most common of these assumptions are that no leakage of the driver gas occurs around the piston during its compression stroke and that projectile bore friction is negligible. An attempt has been made to evaluate these assumptions experimentally for the case of a .830", .30" light-gas gun.

The experimental arrangement used to investigate piston leakage is shown in Figures 8 and 9. The aim of this experiment is to obtain a sample of the powder gas that was used to accelerate the compression piston and determine the concentration of driver gas (helium) contained in it.

NRL ACCELERATOR DEVELOPMENT

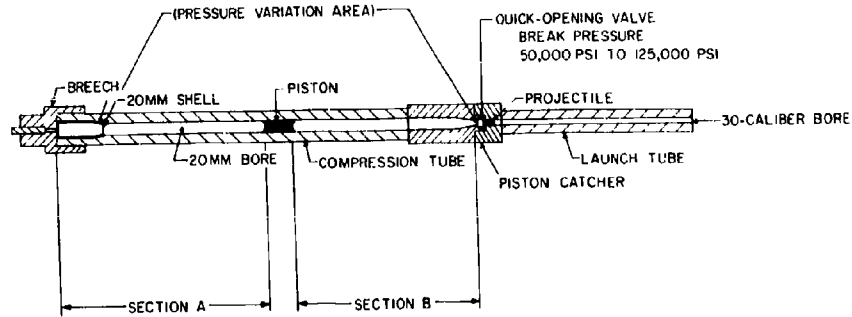


Figure 8 - Cross section of a .830" (20mm), .30" light-gas gun

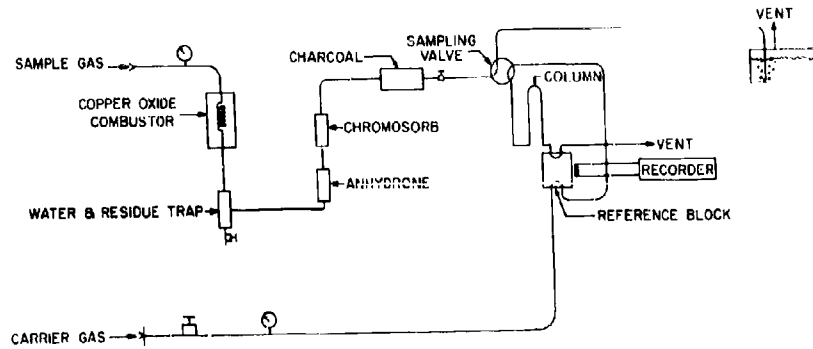


Figure 9 - Fractometer setup used for measuring gas leakage around the compression piston of a light-gas gun

NRL ACCELERATOR DEVELOPMENT

After a test shot, a sample of gas is taken from Section A (Figure 8) and passed through a vapor-phase fractometer having a molecular-sieve partitioning column and employing nitrogen as a carrier gas (Figure 9). Any traces of helium in the sample gas is converted to the output voltage of a resistance bridge, because of the differences in thermal conductivity of the two gases. The bridge output is recorded on a standard time-vs-voltage recorder in the form of a continuous curve. The area under the peak caused by the helium is directly proportional to the total amount of helium which passed through the detection cell of the fractometer.

One of the problems encountered in this experiment was the presence of large amounts of hydrogen as well as helium in the gas samples, which the available fractometer equipment was not able to separate. The use of a copper-oxide furnace ahead of the column allowed the hydrogen to react with oxygen and form water, which was disposed of easily.

Calibration curves showing the percent of helium in relation to total volume can be obtained by setting up a closed system in the actual pump tube, loading with predetermined pressures of helium and firing the standard charge of propellant into the helium without a separating piston. The amount of helium present, in the calibration, is determined from the equation of state:

$$P = \rho RT$$

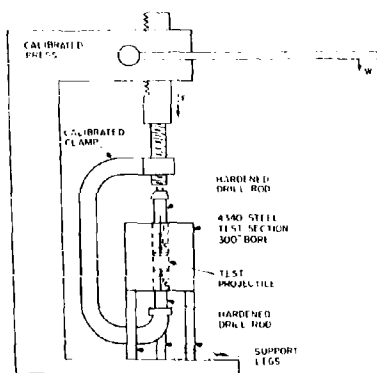
where P is the pressure, R is the gas constant in terms of energy per unit mass, and T is the absolute temperature. Once the density ρ is computed, the mass of helium can be computed from the known tube volume. A calibration curve is then made where the fractometer reading, in square inches, is related to the computed mass of helium present. Fractogram readings from shots may then be referred to this curve to determine the helium present.

In tests conducted with a .830", .30" gun and a piston of polyethylene backed up with aluminum showed a 23% leakage. Projectile velocity of this shot was 18,000 fps. Another shot with a Lexan piston, in which no significant leakage was detected, had the projectile velocity raised to 22,000 fps. Both tests were conducted under identical conditions, except for piston material and design.

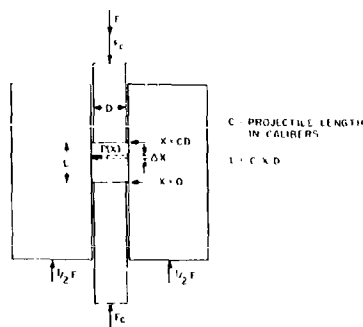
Projectile-Bore Friction

The projectile-bore friction forces generated during the early phases of a gas-gun launch have been partially simulated under laboratory conditions. Figure 10 shows the experimental setup. A test projectile is placed in a short length of launch tube and is held in place with two lengths

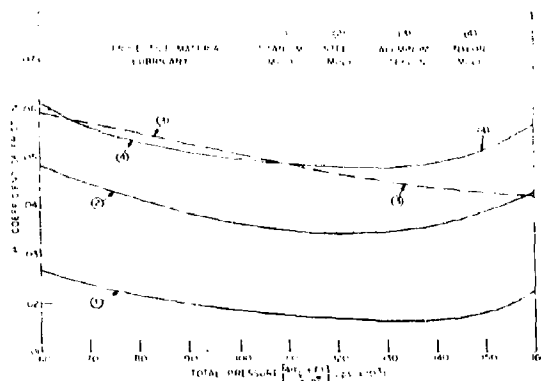
NRL ACCELERATOR DEVELOPMENT



Experimental setup for determining the coefficients of friction of test projectiles and lubricants



Theoretical model for bore friction study



Variation of projectile coefficient of friction with applied pressure (μ_s coefficient of friction of 4340, 0.300 in. I.D. steel bore; obtained from experiments and calculated by using Equation (4))

Figure 10 - Laboratory simulation of projectile-bore friction

NRL ACCELERATOR DEVELOPMENT

of hardened drill rod. A calibrated clamp that engages the drill rods is used to compressively load the test projectile to a predetermined pressure. A calibrated press is then used to slowly force the test projectile along the launch tube and the required force F is related to the bore friction during a projectile launch by the following analysis based on Figure 10.

In the light-gas gun, pressures several times the yield strength of the projectile are developed. To simplify the problem, it is assumed that the material retains its shear modulus, and that pressures developed in any projectile lamina are transmitted undiminished to the bore wall.

Since the acceleration used to determine F is infinitesimally small, the only pressure gradient in the projectile is the result of the friction developed in any projectile lamina of thickness ΔX . The elemental friction force ΔF in this lamina is given by utilizing the elementary definition of μ , the coefficient of friction.

$\Delta F = P(X)\mu nD\Delta X$, where n is the diameter of projectile and bore. By the assumptions about transmission of internal pressures $P(X)$ to the wall,

$$\frac{\partial P(X)}{\partial X} \sim \frac{4 \partial F}{nD^2 \Delta X} = \frac{4\mu}{D} P(X). \quad (1)$$

Solving Equation (1) for $P(X)$ yields

$$P(X) = B \left[e^{(4\mu X/D)} \right] \quad (2)$$

where B is an arbitrary constant. By applying boundary conditions as shown in Figure 10,

($F_c =$ clamping force)

$$P(X=0) = \frac{4F_c}{nD^2} = B; \quad (3)$$

$$P(X=CD) = \frac{4(F+F_c)}{nD^2} = \frac{4F_c}{nD^2} e^{4\mu C}. \quad (4)$$

NRL ACCELERATOR DEVELOPMENT

The ratio of the clamping force to the total force is then

$$p = \frac{F_c}{F + F_c} = e^{-4\mu C} \quad (5)$$

Taking the logarithm of Equation (5),

$$\mu = -\frac{\ln p}{4C} \quad (6)$$

Five sabot materials were tested in combination with five lubricants. The results for four of the combinations having the lowest coefficient of friction are plotted in Figure 10. The curves were computed from Equation (6).

Dusting the projectile and bore with molybdenum disulphide powder (MOLY) was highly effective in reducing friction at pressures above 10,000 psi when both steel and titanium projectiles were tested. With a 1020 steel projectile in the 4340 steel bore (0.300 in. I.D.), the coefficient of friction was reduced from 0.122 (no lubrication) to a minimum of 0.034 at 125,000 psi with the use of MOLY as the lubricant. The material having the lowest coefficient of friction (0.016) with MOLY lubricant was titanium alloy CPDE-Y-720 (sp. gr., 4.6; hardness, Rockwell C 40-45).

A 2024-T4 aluminum projectile coated with Teflon had a minimum coefficient of friction of 0.042 at 160,000 psi, the highest pressure used. The nylon projectile, with half of the surface relieved 0.005 in. in the center position, did not respond significantly to any of the lubricants which were tested (MOLY-grease, MOLY-oil, MOLY-powder, grease, or Teflon) but exhibited a minimum coefficient of friction of about 0.048 at about 125,000 psi. While the coefficient of friction is low compared to values in standard determinations, it is in fair agreement with dynamic friction studies made in hypervelocity firings of 0.30-in. (O.D.) Teflon-coated aluminum projectiles (9).

Sabot Breakup Studies

Considerable difficulty was experienced during the development of sabots with sabot fragments following the projectile along the trajectory and destroying target impact data. It was first reasoned that the sabots were functioning properly within the gun but were not separating adequately after launch. This problem was investigated by placing a velocity measurement port of a Hall optical system as close to the muzzle of the gun as possible (5 ft for the 1.63" gun; 10 ft for the 3.25" gun). The Hall

NRL ACCELERATOR DEVELOPMENT

system is continuously sensitive for 0.1 sec and generates shadowgram images of all objects passing the port during that time. Photographic results showed that sabot fragments almost always preceded the launched pellet in cases where the target was ruined by secondary impacts. This result indicates the sabot fragment left the muzzle before the launched pellet and therefore that the sabot mechanically failed during launch.

A flash x-ray source* with a pulse duration of less than 10^{-7} sec was then set up to radiograph the sabot package as it left the launch tube. The x-ray source is triggered by placing a thin aluminum foil (.001" thick) across the end of the launch tube and viewing the foil with a photo pickup. The impact flash caused by the sabot package striking the foil initiates a set time delay which triggers the x-ray source. The system has worked reliably when the sabot package remains intact during the launch but is triggered early when the sabot fails due to early rupture of the aluminum foil by fragments or escaping gas. Figure 11 is a radiograph of a successful sabot launch of a 5/16" steel sphere ($V = 4.95$ km/sec). Measurements have shown that the sabot has been deformed but not fractured.



Figure 11 - Radiograph of a sabot steel sphere (5/16" dia) near the muzzle of a 1.63", .60" gas gun ($V = 4.95$ km/sec)

Instrumentation to Support Computer Studies

Various instrumentation elements have been installed on the light-gas guns to provide information for the NAREC computer program. Powder chamber pressures are being measured with Ferrule and hot strain gauge sensors developed at Ballistics Research Laboratory (6). Piston velocities and accelerations are being measured with electrically insulated probes that can withstand pressures over 30,000 psi. All projectile velocities are measured with the Hall velocity measuring system using two independent sets of timing marks for measuring film velocity. A 10-kc primary system with an accuracy of $\pm 0.1\%$ is backed up by a 1-kc system with an accuracy of $\pm 0.5\%$.

*Field Emission Corp. Mod 235.

NRL ACCELERATOR DEVELOPMENT
LIGHT-GAS-GUN COMPUTER ANALYSIS

In order to fully exploit light-gas gun capability, it is necessary to evaluate the interrelation of the variables affecting gun performance. These variables may be classified into two categories. They are: (1) the gun parameters (such as the length and diameter of the compression tube and of the launch tube), which relate to the geometry of the gun and are relatively fixed, and (2) the firing parameters (that is, piston mass, projectile mass, powder load, type of gas, initial light-gas temperature and pressure, and the projectile release pressure), which can be readily varied from each shot to the next. The gun performance is usually determined by maximum projectile velocity and acceleration, maximum light-gas pressure and temperature, and piston motion (either bounce or impact into the high pressure section). The effect on the gun performance of varying the firing and gun parameters could be determined empirically. However, in most cases, this would be extremely costly both in time and money. A much more reasonable approach is to simulate on a high-speed digital computer the processes of a light-gas gun firing. Since the computer can "shoot" more frequently than a real gun, a larger number of gun configurations can be examined and the gun parameters can be altered more readily. Also, the cost per shot is generally much lower than for a real gun.

The purpose of a light-gas gun computer study is to enable the determination of that gun configuration which will produce a desired performance with the minimum possible stress on the gun and projectile. In other words, given a projectile mass and a desired velocity, the computer can determine the firing parameters which will achieve this with the least light-gas pressure, projectile acceleration, etc. This computer study is programmed for the NRL NAREC high-speed digital computer and is a continuation of previous computer studies of light-gas guns (7,8,9).

Gun Simulation Program

The geometry of the theoretical gun is illustrated in Figure 12. The program provides for altering any of the dimensions of the gun. The most significant simplification made in the gun geometry is the elimination of a taper at the end of the compression section. The presence of a taper at the end of the compression section has been demonstrated experimentally (10) to increase projectile velocity. This is probably due to the geometrical effect that deformation of the piston into the taper decreases the cross-sectional area of the piston, which decreases the total refarding force on the piston for a given gas pressure. Consequently the piston will have a higher velocity than it would in a flat-bottomed compression section and will impart a higher velocity to the projectile. In any future work with this program, provision will be made to include this effect of the taper.

NRL ACCELERATOR DEVELOPMENT

Table III
List of Symbols

A_1	= $\pi D_1^2/4$
A_2	= $\pi D_2^2/4$
a	= projectile acceleration
D_1	= launch tube diameter
D_2	= compression tube diameter
Δ	= incremental change
E	= energy or work done
g	= acceleration of gravity at the earth's surface
γ	= ratio of specific heats
L_1	= launch tube length
L_2	= compression tube length (effective distance of piston travel)
L_{3s}	= standard gun length = $78.8 \sqrt{A_2}$
M_1	= projectile mass
M_2	= piston mass
m	= light-gas molecular weight
P	= light-gas pressure
\bar{P}	= average light-gas pressure
R	= universal gas constant
T	= light-gas temperature
t	= time
τ	= t/L_2
u	= piston velocity

NRL ACCELERATOR DEVELOPMENT

Table III (Continued)
List of Symbols

- \bar{u} = average piston velocity
- v = free light-gas volume (in units of $\Lambda_2 L_2$) = $x + \frac{\Lambda_1}{\Lambda_2} y - v_c$
- v_c = light-gas covolume (in units of $\Lambda_2 L_2$) = bP_0 / RT_0
- w = projectile velocity
- \bar{w} = average projectile velocity
- x = piston position
- X = piston position (in units of L_2) = $\frac{x}{L_2}$
- y = projectile position
- Y = projectile position (in units of L_2) = y/L_2 (with the important exception that in the computer output, Y is in units of L_1)
- 0 = initial condition
- 1 = projectile or launch tube
- 2 = piston or compression tube
- j = beginning of interval
- k = end of interval
- r = projectile release
- p = powder gas

Constants

van der Waal's constants:

hydrogen - $a = 2.48 \times 10^{11}$ dyne-cm⁴/(gm-mole)²

$b = 26.61$ cm³/gm-mole

helium - $a = 3.44 \times 10^{10}$ dyne-cm⁴/(gm-mole)²

$b = 23.4$ cm³/gm-mole

NRL ACCELERATOR DEVELOPMENT

Table III (Continued)
List of Symbols

$\gamma = 5/3$ (helium)

$K_s =$ powder gas pressure constant = 0.376 (3.25-inch gun)

$\kappa = 980$ cm/sec²

$R = 0.8315 \times 10^8$ ergs/mole °K

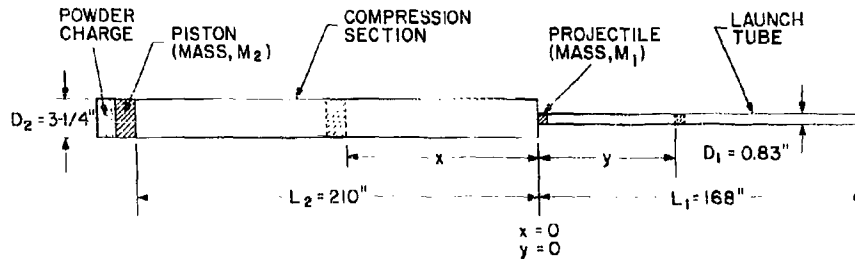


Figure 12 - Theoretical gun geometry

Another basic simplification is made in the treatment of the initial piston motion and powder gas pressure. Until the powder burns out, the piston motion is described by an empirical equation which relates the instantaneous piston position and its free muzzle velocity, u_f , to its instantaneous velocity. The free muzzle velocity of a piston is the velocity the piston would attain with the given powder load if fired into a vacuum from a standard open-ended powder gun of the same diameter as the compression section. The free muzzle velocity must therefore be

NRL ACCELERATOR DEVELOPMENT

empirically related to the powder load for a given gun. The powder is considered to have burned out when the piston is approximately 86% of the way down the compression section. At this point, the powder gas pressure is empirically related to u_f and is hereafter varied by adiabatic expansion using $\gamma = 1.23$. The use of these empirical approximations was originally dictated by the limited storage capacity of the NAREC computer. While this is no longer the case, their continued use is warranted by the considerable savings in computation time.

In describing the light-gas gun, van der Waal's equations are used to determine temperature and pressure. This takes into account the effect of the gas covolume (the volume occupied by the gas molecules) and the intermolecular potential energy, which becomes significant when the gas is highly compressed. Except for the Mach correction to the pressure at the base of the projectile, the light gas is assumed to have uniform pressure and temperature throughout its volume. The value of the ratio of specific heats, γ , for hydrogen is obtained from an empirical equation as a function of temperature (11):

$$\gamma = 1.28 \left[1 + \exp(-2.27 - 1.581 \times 10^{-7} T^{1.8}) \right].$$

This equation was obtained for a pressure of one atmosphere. While pressures in the gun go considerably above this, it is nevertheless the best description of γ available and is somewhat more realistic than keeping γ constant.

Finally, it should be noted that in this program no provision is made for shock waves in the light gas or for the constriction of the gas flow from the compression tube into the launch tube. These effects are unquestionably present, and perhaps significant, but are omitted mainly because of the speed limitations of the NAREC computer.

The shot calculations proceed in four, generally consecutive, phases: (1) from the beginning of powder burning to powder burnout, (2) from powder burnout to projectile launch, (3) from projectile launch to piston bounce or impact, and (4) from piston bounce or impact until the projectile leaves the muzzle. The calculations are done by a reiterative process in which the variables are altered by small increments. The equations and procedures of each phase are as follows:

- (1) A small increment of piston position $\Delta x_{p,i}$ is arbitrarily selected.* Using a Taylor expansion, the average piston velocity over the interval,

*The symbols are defined in Table III.

NRL ACCELERATOR DEVELOPMENT

u_{jk} is calculated. The time increment is then $\Delta t_{jk} = \Delta X_{jk} / u_{jk}$. The empirical equation for piston velocity is

$$u_k = 1.02 u_f \left[1 - \exp \left(-\frac{L_2}{20 A_2} (X_k - 1) \right) \right]$$

where the piston position, X_k , initially equals 1 and goes to zero at the end of the compression section. The gas volume is

$$V_k = X_k + \frac{A_1}{A_2} Y_k - V_c,$$

where the projectile position, Y_k , initially equals zero. Then using van der Waal's equations for adiabatic compression, the light-gas temperature and pressure are given by

$$T_k = T_1 (V_1 / V_k)^{\gamma+1};$$

$$P_k = \left[T_k - \left(\frac{a P_0}{k T_0} \right) \frac{V_k}{(V_k + V_c)^2} \right] \frac{P_0}{V_k T_0}.$$

The total work done by the light gas on the piston is

$$E = \sum_{jk} P_{jk} \Delta X_{jk}$$

where P_{jk} is the average light-gas pressure over the interval.

(2) At the point of powder burnout the piston energy is reduced by the work done on the light gas,

$$u'_k = \sqrt{u_k^2 - \frac{2A_2 L_2}{M_2} E}.$$

Pressure behind the piston is determined by the empirical equation

$$P_{pk} = K_1 \frac{M_2 u_f^2}{2A_2 L_2} \left[\frac{0.86 L_2}{L_2 (1 - X_k)} \right]^{1.23}$$

where K_1 is an empirically determined constant and L_2 is the length of the standard powder gun corresponding to the compression tube diameter;

NRL ACCELERATOR DEVELOPMENT

and is given by $L_s = 78.8 \lambda_2$. The change in piston energy is now calculated by

$$\Delta E_{2jk} = (P_{pk} - \bar{P}_{jk}) \Delta X_{jk}$$

and the resulting piston velocity is

$$u_k = \sqrt{u_j^2 + \frac{2A_2 L_2}{M_2} \Delta E_{2jk}}$$

Other calculations proceed as for phase (1).

(3) Once the projectile launches the time increment Δt_{jk} is fixed and the piston and projectile average velocities, \bar{u}_{jk} and \bar{w}_{jk} , are extrapolated using Taylor expansions so that the position increments are $\Delta X_{jk} = \bar{u}_{jk} \Delta t_{jk}$ and $\Delta Y_{jk} = \bar{w}_{jk} \Delta t_{jk}$, respectively. The increment of work done on the projectile by the light gas is calculated using a Mach correction for the pressure at the base of the projectile and is given by

$$\Delta E_{1jk} = \bar{P}_{jk} \left[1 - \left(\frac{\gamma-1}{\gamma} \frac{m w_{jk}^2}{2 P T_k} \right)^{\gamma-1} \right] \Delta Y_{jk}$$

The resulting projectile velocity is

$$w_k = \sqrt{w_j^2 + \frac{2A_1 L_2}{M_1} \Delta E_{1jk}}$$

and the projectile acceleration is $a_{jk} = (w_k - w_j) / \Delta t_{jk} L_2$. Other calculations proceed as for phase (1).

(4) (a) If the piston bounces, the piston velocity equation is altered to

$$u_k = \sqrt{u_j^2 + \frac{2A_2 L_2}{M_2} \Delta E_{2jk}}$$

(b) If the piston impacts into the end of the compression section, then the piston position and velocity are set equal to zero and further piston calculations are eliminated. Increments of projectile position are now chosen arbitrarily and the time increments are calculated by

$$\Delta t_{jk} = \Delta Y_{jk} / \bar{w}_{jk}$$

Other calculations proceed as for phase (1).

NRL ACCELERATOR DEVELOPMENT

The computer performs the calculations in cgs units; however, for convenience, the input and output data are supplied in mixed units. The input data consist of:

- projectile mass* (gm)
- piston mass (lbs)
- initial light-gas pressure (psia)
- projectile release pressure (psia)
- initial light-gas temperature (°K)
- free piston velocity (km/sec)
- light-gas molecular mass (gm)
- compression tube and launch tube length† and diameter (inches).

The output data are:

- piston and projectile position (in units of compression tube and launch tube length respectively)
- piston and projectile velocity (km/sec)
- projectile acceleration (10^6 g)
- light-gas pressure (psia) and temperature (°K)
- time (μ sec) (see Figure 13 for sample input/output data).

The computer also produces tapes for automatically plotting the piston and projectile velocities, the projectile acceleration, and the light-gas pressure vs time from the beginning of the projectile launch until the end of the shot. A sample of these curves is presented in Figure 14.

Systematic Variation of Parameters

The specific study considered here is of the 3.25" NRL light-gas gun. This gun has a compression section 210" long and 3.25" in diameter, and a launch tube 168" long and 0.83" in diameter. These gun parameters were constant throughout the study. While the program is capable of taking into account simple frictional effects and radiation heat losses, friction has been omitted for the sake of simplicity and clarity, and radiation heat losses have been omitted because recent computations showed them to be negligible. Also, in order to reduce the number of variables, preheat was not considered at this time. The initial light-gas temperature for all shots was taken as 300°K.

*Projectile mass means the entire mass of the package accelerated down the launch tube. This includes any sabot and shear disk masses as well as the actual projectile.

†Compression tube length means the effective distance of piston travel.

NRL ACCELERATOR DEVELOPMENT

CODE

LIGHT-GAS GUN ANALYSIS

```

INPUT DATA
M1 +14.00 (GM)
M2 +4000.0 (GM)
L1 +160.00 (IN)
L2 +210.00 (IN)
D1 +.630 (IN)
D2 +3.250 (IN)
P1 +10000. (PSI)
P +250. (PSI)
T +300. (F)
UF +.9144 (CM/SEC)
GAS HYDROGEN
    
```

X	Y	U (CM/SEC)	V (CM/SEC)	P (PSI)	TK	T (USEC)	A (MG/CM)
+0.9900	+0.0000	+0.134	+0.000	+250.	+300.	+0.	+0.00
+0.8484	+0.0000	+0.365	+0.000	+316.	+320.	+4588.5	+0.00
+0.7275	+0.0000	+0.5723	+0.000	+398.	+341.	+5890.0	+0.00
+0.6242	+0.0000	+0.6957	+0.000	+497.	+364.	+6755.8	+0.00
+0.5359	+0.0000	+0.7600	+0.000	+519.	+388.	+7444.0	+0.00
+0.4605	+0.0000	+0.822	+0.000	+573.	+414.	+7985.1	+0.00
+0.3961	+0.0000	+0.8795	+0.000	+644.	+442.	+8314.8	+0.00
+0.3410	+0.0000	+0.9303	+0.000	+727.	+471.	+8545.9	+0.00
+0.2940	+0.0000	+0.9716	+0.000	+819.	+503.	+8690.1	+0.00
+0.2539	+0.0000	+0.9713	+0.000	+9170.	+536.	+8728.4	+0.00
+0.2188	+0.0000	+0.9785	+0.000	+2331.	+571.	+8648.5	+0.00
+0.1892	+0.0000	+0.964	+0.000	+2906.	+609.	+8412.0	+0.00
+0.1652	+0.0000	+0.9482	+0.000	+3623.	+649.	+8141.7	+0.00
+0.1520	+0.0000	+0.9471	+0.000	+4134.	+675.	+8043.1	+0.00

N +170. +.8884 PISTON VELOCITY (CM/SEC)

+0.1492	+0.0000	+0.8451	+0.000	+4258.	+650.	+8040.6	+0.00
+0.1405	+0.0000	+0.8442	+0.000	+4385.	+684.	+8072.7	+0.00
+0.1221	+0.0000	+0.8435	+0.000	+4591.	+719.	+8090.0	+0.00
+0.1074	+0.0000	+0.8414	+0.000	+4790.	+754.	+8105.4	+0.00
+0.9834	+0.0000	+0.8421	+0.000	+4994.	+777.	+8121.0	+0.00

N +152. +0.8123 PISTON VELOCITY (CM/SEC)

+0.8494	+0.0000	+0.8473	+0.000	+11176.	+874.	+8121.0	+0.00
---------	---------	---------	--------	---------	-------	---------	-------

N +152. +0.8226 PISTON VELOCITY (CM/SEC)

+0.8094	+0.0000	+0.8428	+0.000	+11174.	+874.	+8121.0	+0.00
+0.8887	+0.0000	+0.8427	+0.000	+11147.	+874.	+8121.0	+0.00
+0.9880	+0.0000	+0.8423	+0.000	+11202.	+874.	+8121.0	+0.00
+0.0800	+0.0000	+0.8434	+0.000	+11948.	+914.	+8411.0	+0.00
+0.0718	+0.0000	+0.8404	+0.000	+14741.	+947.	+8205.0	+0.00
+0.0664	+0.0000	+0.8444	+0.321	+16943.	+1012.	+8441.7	+0.00
+0.0599	+0.0000	+0.8479	+0.465	+20866.	+1074.	+8680.9	+0.00
+0.0530	+0.0189	+0.8498	+0.642	+26492.	+1149.	+8914.1	+0.00
+0.0481	+0.0209	+0.8481	+0.849	+34124.	+1241.	+9141.4	+0.00
+0.0394	+0.0325	+0.8470	+1.157	+44876.	+1364.	+9291.8	+0.00
+0.0320	+0.0478	+0.8462	+1.556	+57378.	+1524.	+9371.8	+0.00
+0.0266	+0.0671	+0.8454	+2.020	+71422.	+1741.	+9411.0	+0.00
+0.0207	+0.0939	+0.8447	+3.001	+87187.	+2014.	+9411.0	+0.00
+0.0157	+0.1322	+0.8440	+4.294	+105330.	+2348.	+9371.8	+0.00
+0.0140	+0.1418	+0.8434	+4.983	+125732.	+2622.	+9151.5	+0.00
+0.0129	+0.1713	+0.8427	+5.347	+147155.	+2773.	+8611.4	+0.00
+0.0117	+0.2309	+0.8421	+5.954	+180375.	+2873.	+8011.0	+0.00

N +290. +0.8441 PISTON VELOCITY (CM/SEC)

+0.0109	+0.2815	+0.8419	+6.081	+223363.	+2943.	+8211.5	+0.00
---------	---------	---------	--------	----------	--------	---------	-------

N +290. +0.8400 PISTON VELOCITY (CM/SEC)

+0.0100	+0.2937	+0.8417	+6.007	+210291.	+2910.	+8111.0	+0.00
+0.0112	+0.3047	+0.8417	+6.113	+122792.	+2740.	+8211.5	+0.00
+0.0120	+0.4249	+0.8410	+6.110	+80348.	+2546.	+7711.4	+0.00
+0.0131	+0.4843	+0.8410	+6.110	+56890.	+2407.	+7441.7	+0.00
+0.0143	+0.5941	+0.8401	+6.110	+42868.	+2299.	+8111.9	+0.00
+0.0197	+0.8130	+0.8404	+6.110	+33390.	+2181.	+8971.1	+0.00
+0.0172	+0.8648	+0.8410	+6.110	+24998.	+2142.	+8711.3	+0.00
+0.0188	+0.7447	+0.8405	+6.110	+22370.	+2103.	+8471.5	+0.00
+0.0204	+0.8139	+0.8410	+6.110	+18918.	+2033.	+9921.8	+0.00
+0.0221	+0.8743	+0.8410	+6.110	+15244.	+1919.	+9111.0	+0.00
+0.0238	+0.9442	+0.8410	+6.110	+14173.	+1951.	+1083.2	+0.00
+0.0255	+1.0015	+0.8410	+6.110	+12845.	+1921.	+1173.0	+0.00

N +404.

Figure 13 - Sample computer printout

NRL ACCELERATOR DEVELOPMENT

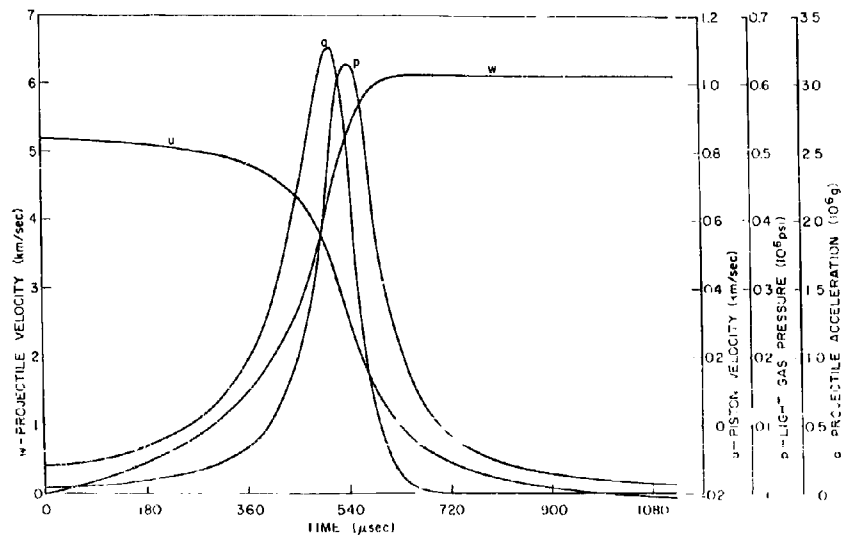


Figure 14 - Gun performance curves

The remaining firing parameters were given the following range of values:

projectile mass - 7, 14, 21 gm
 piston mass - 4.5, 9, 13.5 lbs
 free piston velocity - 2500, 3000, 3500 fps
 projectile release pressure - 5,000, 10,000, 20,000 psia
 initial light-gas pressure - 150, 200, 250, 300, 350 psia
 light gas - hydrogen, helium.

These particular values and ranges were selected as a compromise between the requirements of a thorough, systematic study and the current practical operation of the 3.25" gun. Taking all the possible combinations of these parameters results in 405 shots for each gas, or 810 shots total. In order to reduce this to a manageable number for a preliminary analysis, attention is focused on the shot whose parameters lie at the center of the ranges studied. The effects of variations away from this central shot are then examined. The conditions of this central shot are 14 gm projectile, 9 lb piston, 3000 fps free piston velocity, 10,000 psia projectile release pressure, and 250 psia initial light-gas pressure.

NRL ACCELERATOR DEVELOPMENT

Results of Firing Parameter Variation

The analysis emphasizes maximum projectile acceleration and maximum light-gas pressure as a function of maximum projectile velocity, and the variations in these relationships as the firing parameters are varied. These relationships can be readily examined by such curves as Figures 15 and 16. From these and similar graphs, one can decide on the gun configuration necessary to achieve a desired projectile velocity with the lowest maximum projectile acceleration and light-gas pressure.

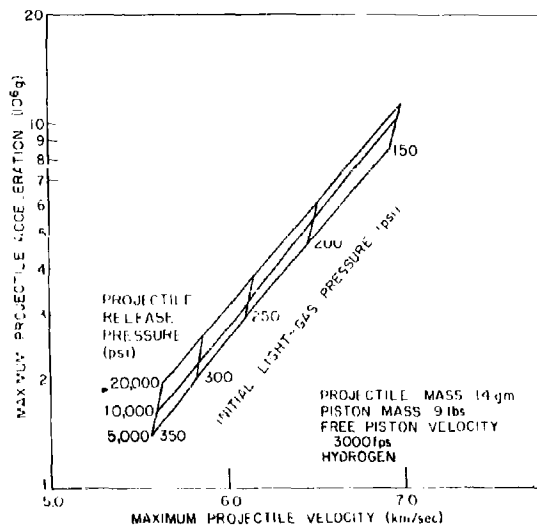


Figure 15 - Maximum projectile acceleration vs maximum projectile velocity as a function of initial and projectile release pressures

The effect on the maximum projectile velocity of the variations in projectile mass, piston mass, and free piston velocity is also examined. The initial light-gas pressure and projectile release pressure are held constant at 250 psia and 10,000 psia respectively.

NRL ACCELERATOR DEVELOPMENT

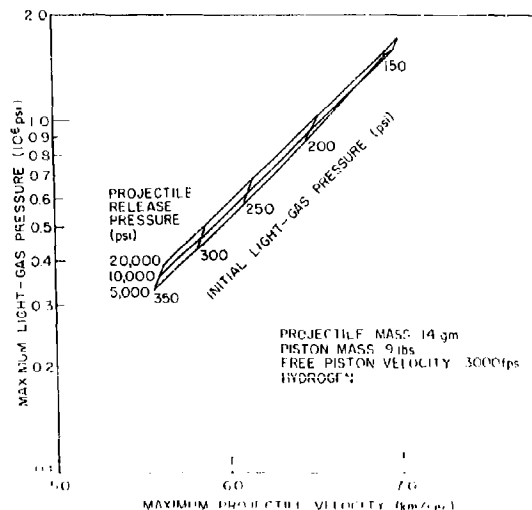


Figure 16 - Maximum light-gas pressure vs maximum projectile velocity

The following discussion will refer to the results for the hydrogen shots unless otherwise noted. Any discussion of the effect of the variation of a parameter presupposes that all other parameters remain constant. This requires some caution in regard to the free piston velocity and the piston mass as they relate to the powder charge. For example, as the piston mass is decreased, in order to maintain the same free piston velocity, the powder load must be decreased accordingly.

1. Initial Light-Gas and Projectile Release Pressure Variation

From Figure 15 it can be seen that changing the projectile release pressure has virtually no effect on the maximum projectile velocity and has a small effect on the maximum projectile acceleration. The acceleration increases slightly as the launch pressure increases. The initial light-gas pressure, however, has a marked effect on both the maximum projectile velocity and acceleration. These both increase as the initial

NRL ACCELERATOR DEVELOPMENT

light-gas pressure is decreased. The lower the initial light-gas pressure, the more rapid the rate of increase of maximum projectile acceleration. These trends hold generally throughout the range of parameters. For a heavy, fast piston, however, the trend is inverted so that the projectile release pressure strongly affects the maximum velocity and has little effect on the maximum acceleration. The trend for the effects of the initial light-gas pressure remains the same.

The results are essentially the same for helium. The absolute values of both velocity and acceleration are lower and the acceleration does not increase as rapidly as it does for hydrogen.

The maximum light-gas pressure shows the same trends as the maximum projectile acceleration (see Figure 16).

2. Piston Mass and Free Piston Velocity Variation

Figures 17 and 18 show that as the piston mass or the free piston velocity increases, the maximum projectile velocity, maximum projectile acceleration and the maximum light-gas pressure are increased. It is preferable, however, to increase the piston mass rather than the free piston velocity in order to achieve higher maximum projectile velocity. This will produce a velocity increase with a lesser increase in projectile acceleration and light-gas pressure. This is also more or less the case as one deviates away from the central shot configuration.

The same gun configuration for helium shows a reversal of this relationship. For the central shot using helium, it is apparently preferable to increase the free piston velocity rather than the piston mass in order to achieve higher projectile velocities.

3a. Projectile Velocity vs Projectile Mass

Maximum projectile velocity changes linearly decreasing by 0.5 to 1 km/sec as the projectile mass increases from 7 to 21 gm (Figure 19).

For helium, this decrease is nonlinear and is most pronounced for the heavy, slow piston. The decrease is very slight for either the heavy, fast piston or the light, slow piston. For the light, fast piston the velocity shows a maximum for a projectile mass of approximately 14 gm.

3b. Projectile Velocity vs Piston Mass

Maximum projectile velocity increases by about 2 km/sec as the piston mass is increased from 4.5 to 13.5 lbs. The increase becomes

NRL ACCELERATOR DEVELOPMENT

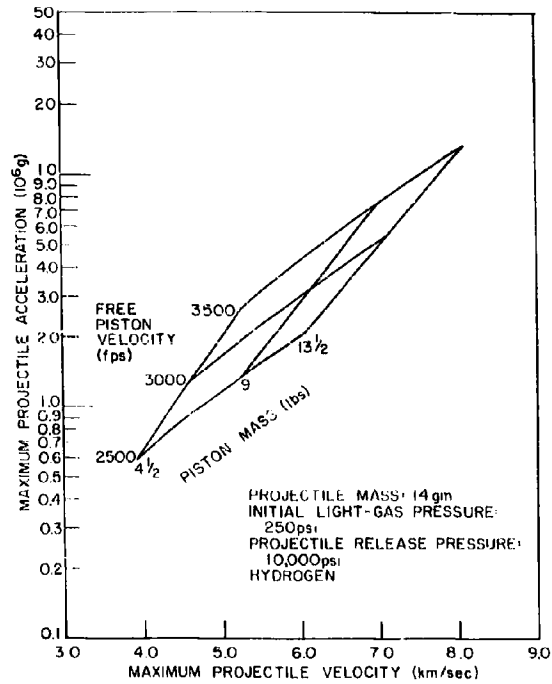


Figure 17 - Maximum projectile acceleration vs maximum projectile velocity as a function of piston mass and velocity

NRL ACCELERATOR DEVELOPMENT

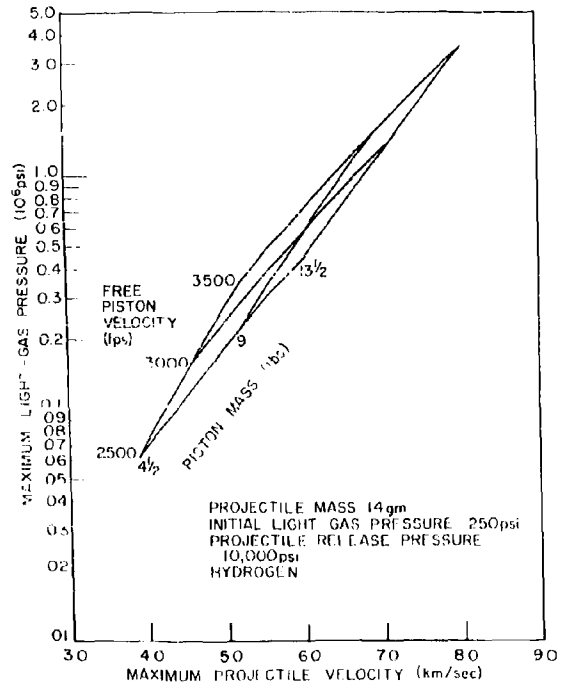


Figure 18 - Maximum light-gas pressure vs maximum projectile velocity as a function of piston mass and velocity

NRL ACCELERATOR DEVELOPMENT

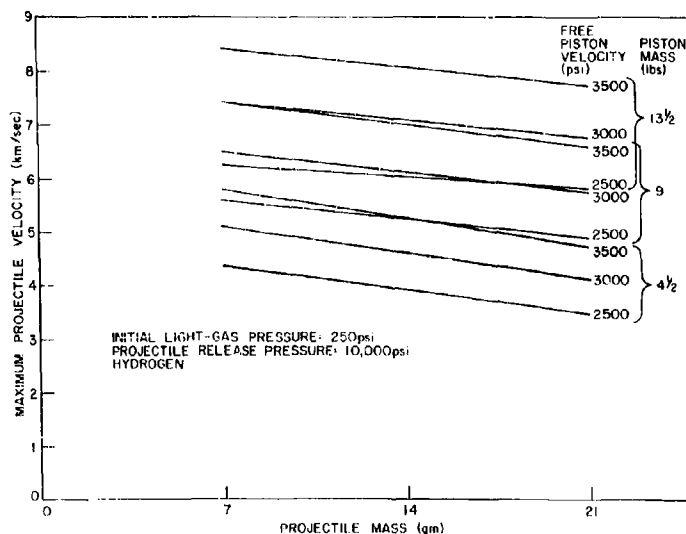


Figure 19 - Maximum projectile velocity vs projectile mass

progressively less for the higher piston masses (Figure 20). Helium shows similar trends, except that the absolute values of the velocity and the increases in the velocity are smaller than for hydrogen.

3c. Projectile Velocity vs Free Piston Velocity

Maximum projectile velocity increases linearly by as much as 1 to 2 km/sec as the free piston velocity is increased from 2500 to 3500 fps (Figure 21). Helium produces essentially the same trend.

4a. Projectile Acceleration vs Projectile Mass

The heavier and faster the piston, the more rapidly the maximum projectile acceleration increases as the projectile mass increases. As the piston becomes light and slow, however, this increase becomes less

NRL ACCELERATOR DEVELOPMENT

rapid, until for the 4.5 lb 2500 fps piston the maximum projectile acceleration actually decreases slightly as the projectile mass increases (Figure 22).

4b. Projectile Acceleration vs Piston Mass

The maximum projectile acceleration also increases as the piston mass is increased. The rate of this increase is lower for the lighter projectiles (Figure 23).

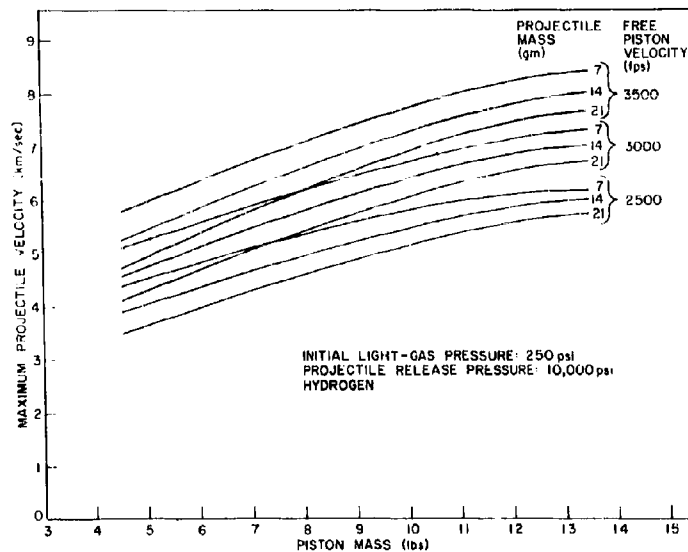


Figure 20 - Maximum projectile velocity vs piston mass

NRL ACCELERATOR DEVELOPMENT

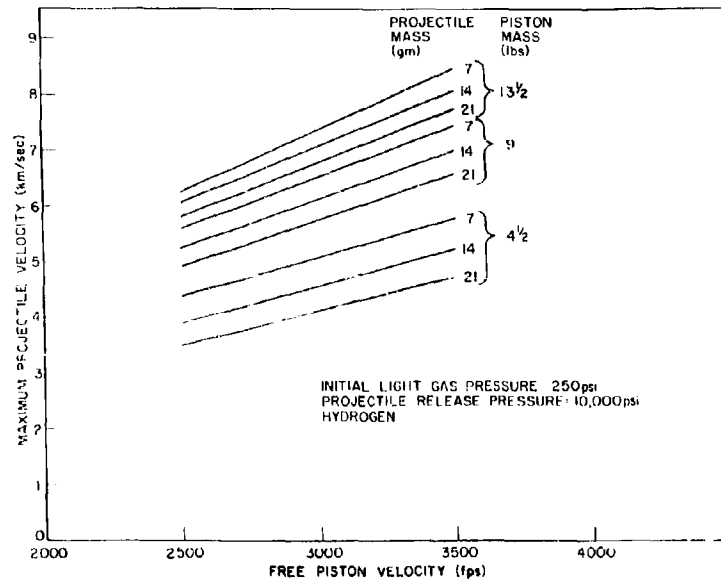


Figure 21 - Maximum projectile velocity vs free piston velocity

NRL ACCELERATOR DEVELOPMENT

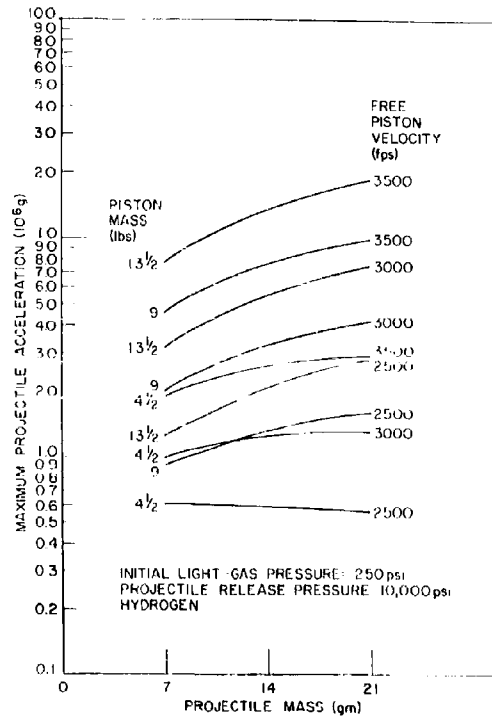


Figure 22 - Maximum projectile acceleration vs projectile mass

NRL ACCELERATOR DEVELOPMENT

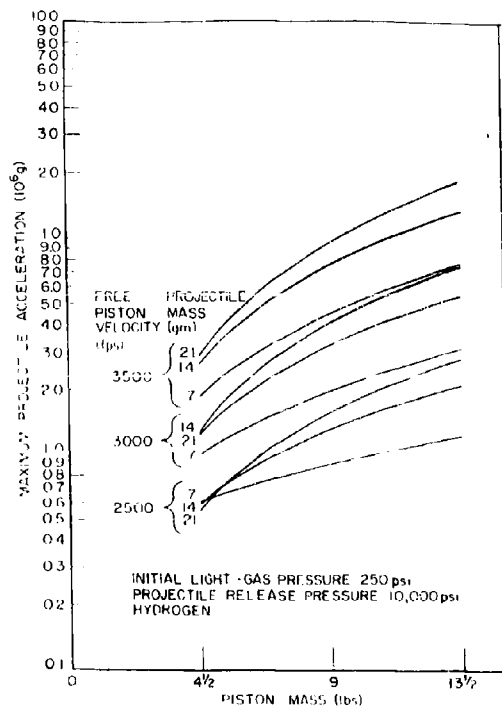


Figure 23 - Maximum projectile acceleration vs piston mass

NRL ACCELERATOR DEVELOPMENT

4c. Projectile Acceleration vs Free Piston Velocity

The maximum projectile acceleration increases even more rapidly with an increase in the free piston velocity than with an increase in the piston mass (Figure 24).

The variations indicated in 4a to 4c are generally the same for helium.

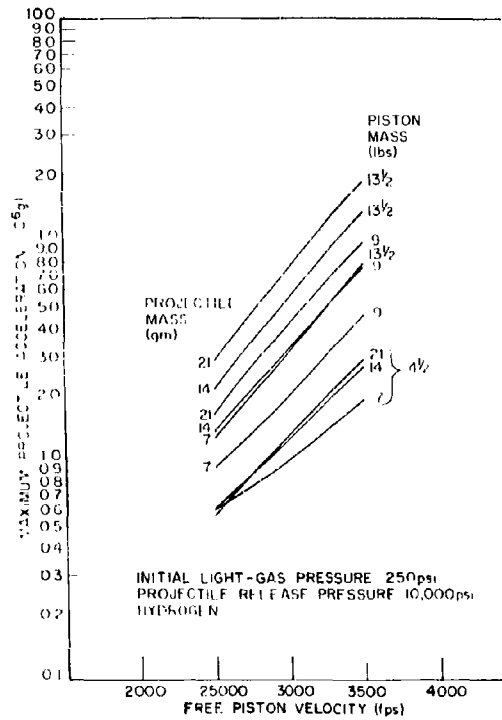


Figure 24 - Maximum projectile acceleration vs free piston velocity

NRL ACCELERATOR DEVELOPMENT

5. Maximum Light-Gas Pressure

The maximum light-gas pressure increases with an increase in projectile mass, piston mass, or free piston velocity throughout the range of the other firing parameters. The rate of this increase becomes progressively greater for the larger values of these parameters (Figures 25 to 27).

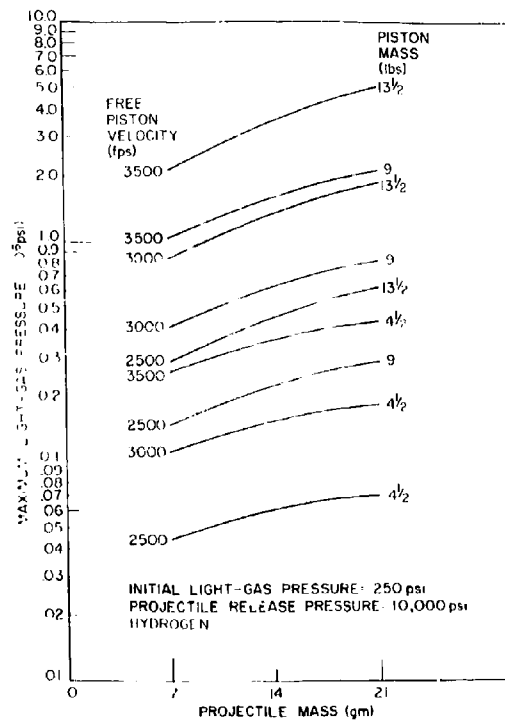


Figure 25 - Maximum light-gas pressure vs projectile mass

NRL ACCELERATOR DEVELOPMENT

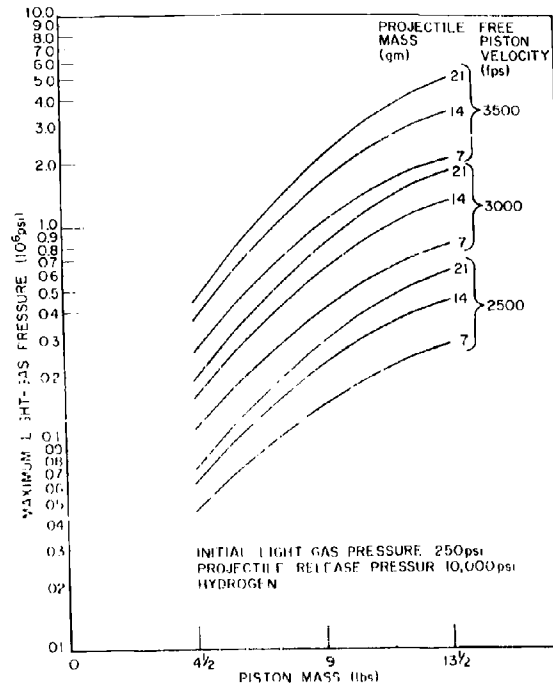


Figure 26 - Maximum light-gas pressure vs piston mass

NRL ACCELERATOR DEVELOPMENT

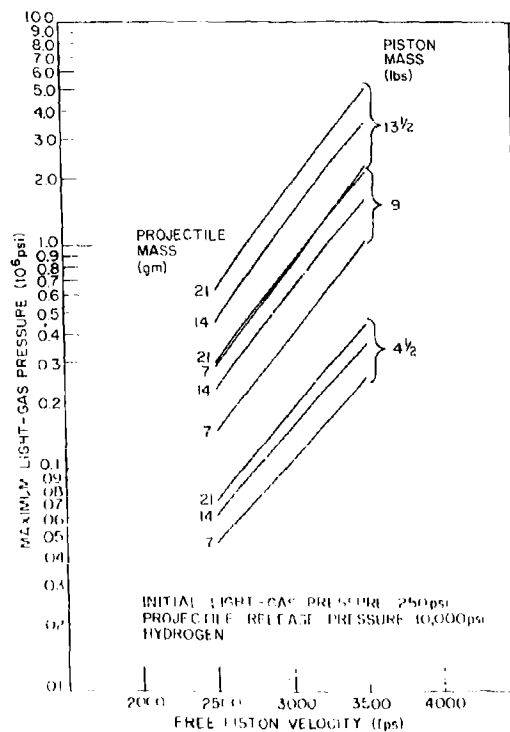


Figure 27 - Maximum light-gas pressure vs free piston velocity

Comparison with Experimental Results

In most cases, the projectile velocity is the only point of comparison between the computer output and an actual light-gas-gun shot. In conjunction with the computer study of the 3.25" NRL light-gas gun, however, provision was also made to measure the piston velocity just before the high pressure catcher section, and to obtain a time history of the powder gas pressure behind the piston. Preliminary results of these latter measurements indicate that the computer results agree with the actual dynamics of the piston to within 5% or better.

NRL ACCELERATOR DEVELOPMENT

Comparison of the actual and computed projectile velocity in the preliminary testing procedures showed discrepancies on the order of 5 to 10%. More recent evidence, however, indicated that the sabot package in those shots had broken up in the launch tube, which would invalidate comparison with computed results. Recent shots made with unsaboted projectiles have been compared with the computer study by interpolation between the selected values of the firing parameters. The results are shown in Table IV and indicate deviations between actual and computed velocities on the order of 20%.

Table IV
Comparison of Experimental and Theoretical
Results for Hydrogen

Initial Loading Pressure	Piston Mass	Free Piston Velocity	Proj. Release Pressure	Proj. Mass	Proj. Velocity Experimental	Proj. Velocity Theoretical	Error
(psia)	(lb)	(fps)	(psia)	(gm)	(km/sec)	(km/sec)	(%)
315	8.91	3150	24,700	9.6	7.69	6.15	-20.0
235	9.00	2750	3,950	15.5	6.90	5.73	-17.0
235	9.00	2750	3,950	15.5	6.91	5.73	-17.0
235	9.00	2750	3,950	14.3	7.06	5.75	-18.6
235	9.00	2750	3,950	11.9	7.36	5.85	-20.5

Future Development

Two improvements which can quite readily be included in the computer program are the effects of the taper, and piston and projectile friction. Previous studies have shown light-gas preheating to be effective in increasing projectile velocities; hence this effect too will be studied in detail. Introduction of shock effects will require the use of a much faster computer. This will be considered if other improvements in the program do not secure sufficiently accurate results.

Once the computer program is deemed satisfactory, it can then be used to evaluate and optimize the operation of the NRL light-gas guns. In addition, by examining the effects of variations in the gun parameters, it may be possible to improve light-gas-gun design.

NRL ACCELERATOR DEVELOPMENT

ELECTROBALLISTIC STUDIES

One important phase of the hypervelocity gun development program at NRL is the study of methods for electrically heating the gas used to accelerate projectiles. It is generally agreed that the overall firing efficiency and peak performance of gas guns are strongly affected by the maximum temperature reached by the driver gas. Recent increases in peak gun performance have been achieved by increases in maximum driver gas temperature.

The use of electrical energy for increasing gas temperature has several very attractive features: (1) there is no fundamental limit to the amount of electrical energy that can be added to a gas reservoir, and therefore very high gas temperatures can be readily attained; (2) electrical heating of a gas reservoir enables peak temperatures to be directly controlled and varied over a wide range for studying the effects of gas-temperature increases on gun performance; (3) the rate of gas heating and the time of energy insertion are controllable (12).

Thus far, electrical pulses have been used to energize three types of ballistic accelerators. Constant-volume guns have been constructed such that electrical pulses are used to preheat small reservoirs of light-gas to temperatures and pressures needed for ballistic launches. Electrical probes have been installed in standard light-gas guns and used to preheat the driver gas in order to reach very high operating temperatures. Thin plates have also been launched by exposing them to the high temperature and pressure plasma generated during the electrical explosion of thin metallic foils.

Constant-Volume-Gun Development

Because of its basic simplicity, the constant-volume electric gun was chosen for initial development. The basic form consists of a high strength gas chamber separated from a launch tube by a diaphragm and a projectile. After initially charging the chamber with a low-molecular-weight gas, i.e., H_2 or He, the energy stored in a capacitor bank is discharged into the chamber through a high-intensity electrical arc. The resultant heating of the chamber gas increases the chamber pressure which causes the diaphragm to rupture and the projectile to be accelerated down the launch tube.

A variety of gun designs has been tested with chamber volumes varying between 10 cm^3 and 30 cm^3 at electrical energy levels as high as 10^5 joules. Initial gas loading pressure has been held at 100 atmospheres. Projectiles weighing between 0.1 and 0.5 gm have been fired in .22" and .30" launch tubes at peak velocities of 5.4 km/sec.

NRL ACCELERATOR DEVELOPMENT

The most successful design for a constant-volume gun is shown in Figure 28. It consists of a massive steel breech block enclosing the chamber with an insulated hot electrode at one end and a threaded launch tube at the other. A fixture mounted in the chamber sidewall is used to admit the light-gas charge through a check valve. The front of the chamber consists of a grounded ring electrode and a transition section between the chamber and launch tube.

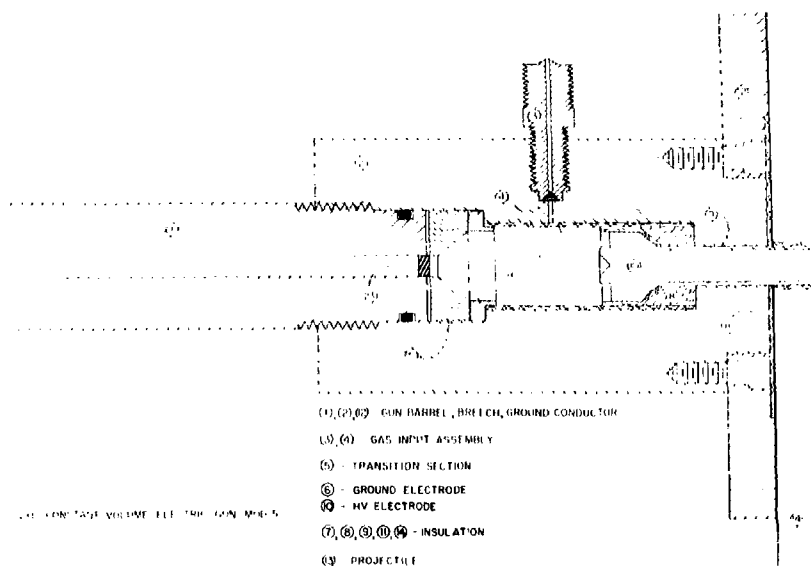


Figure 28 - Electrically powered gun with a constant volume gas reservoir

Electrical energy is transmitted from a parallel-plate transmission line to the shaft of the hot electrode, by which it is conducted into the chamber. A length of a 0.02-inch-wide, 0.002-inch-thick aluminum foil is stretched between the hot and ground electrodes. During the initial phase of the discharge, the foil explodes, thereby generating an ion path

NRL ACCELERATOR DEVELOPMENT

for the main energy surge. The large gas pressure increase caused by the energy transfer from the electrical arc to the chamber gas causes the hot electrode to move back into its insulating sheath, thereby generating a gas seal. The seal is strengthened as the gas pressure increases in accordance with the Bridgman principle. The increased gas pressure also causes the forward diaphragm to rupture, allowing the driver gas to flow through the transition section into the launch tube, where it accelerates the projectile.

The extreme gas-dynamic conditions within the transition section, i.e., high gas density, temperature, turbulence, and velocity, have caused very severe erosion of all transition section materials tested. Erosion at the transition section is especially critical to gun performance because the resulting gas mixes with the driver gas and increases its mean molecular weight. Such an increase substantially reduces the effectiveness of the driver gas as a hypervelocity projectile accelerant. All metals tested, including high strength steel, various tungsten-copper alloys, and molybdenum, have proven unsuccessful for this application. Teflon has shown marginal erosion properties, but it lacks sufficient mechanical strength to withstand the pressure impulse. Several other materials including hard fluoroplastics and machinable ceramic materials failed under the severe mechanical forces developed during a firing. A satisfactory transition section material must be composed of fairly low atomic weight constituents and have a high initial phase-change point, low thermal conductivity, and high impact strength.

Two conclusions have been drawn from the constant-volume-gun study. First, it is possible to transfer stored electrical energy from a capacitor bank to a low-molecular-weight gas in a small chamber with reasonably high efficiency and successfully contain the gas until it has accelerated a projectile. Second, all present light-gas guns totally powered by electrical energy are limited in performance by driver-gas contamination caused by the erosion of their electrodes and transition elements. Unless a significant breakthrough in the gas-contamination problem area is achieved, it is doubtful that peak projectile velocities above 6.5 km/sec to 7 km/sec can be achieved using such devices. For these reasons, the constant-volume-gun program has been suspended and emphasis has been placed upon other electroballistic techniques.

Electrocompression Gun Development

The extreme gas dynamic conditions that led to the serious erosion problems associated with the constant-volume-gun firings were brought about by the need for very high electrical-energy input densities. Large energy densities are required because the peak gas pressures needed for hypervelocity ballistic acceleration can be achieved only through large temperature increases of the fixed-density driver gas. The requirement

NRL ACCELERATOR DEVELOPMENT

for high electrical-energy densities can be largely eliminated, and with it much of the contamination problem, if the electrical energy were added to a low density gas reservoir which is then compressed until ballistically usable pressures and temperatures are achieved. These conditions can be realized in a standard light-gas gun in which the electrical energy is added to the driver gas by an arc initiated in the pump tube early in the compression cycle. In this way, the electrical energy can be added to a large volume of gas at relatively low pressures without generating extreme temperatures. As compression continues, the gas temperature increases at a slower rate than the pressure until maximum pressures are reached when the driver gas is near liquid density. The final gas temperature-to-pressure ratio can be readily controlled over a very wide range, and higher values of this ratio can be reached than are possible using gas compression alone by judicious choices of initial gas density and energy input level. Both basic gun analysis and detailed studies with the NAREC ballistic computer program have demonstrated that very high ratios of driver gas temperature to pressure are required for increasing the velocity capabilities of gas guns beyond presently attainable values. A related advantage is that high temperature-to-pressure ratios significantly reduce the peak acceleration level experienced by a model as it is launched to a particular velocity.

The above concepts were used in the design of an electrically augmented 1.63", .22" gas gun of the expendable central breech type. An electrical energy insertion section (Figure 29) may be inserted either at the center of the compression tube or at the junction between the compression tube and the central breech. The section is a heavy-walled extension of the compression tube with an electrical probe installed flush with the bore. The probe is held in place with a nut, and an overall gas seal is generated by drawing the probe tightly against its electrical insulator with a second nut that engages threads at the upper end of the probe (not shown in Figure 29). A capacitor bank is connected between the insulated probe and the body of the insertion section and is discharged through an exploding wire that electrically connects the probe face to the inner wall of the insertion section.

The insertion of the bank energy into the exploding wire arc causes intense localized heating of the metallic vapor, and some mechanism must be provided for efficiently transferring this energy to the remainder of the light-gas reservoir. An operating hypotheses concerning this process has been established after reviewing the possible phenomena responsible for transmitting the energy. The release of a pulse of electrical energy within the compression tube creates a strong shock disturbance which propagates in both directions along the barrel. Initially, the wave is cylindrical and hence the maximum pressure associated with it decreases linearly with distance as it moves away from the arc channel. The wave rapidly becomes planar, however, as it propagates down the cylindrical pump tube because of the constriction of the walls and undergoes no more

NRL ACCELERATOR DEVELOPMENT

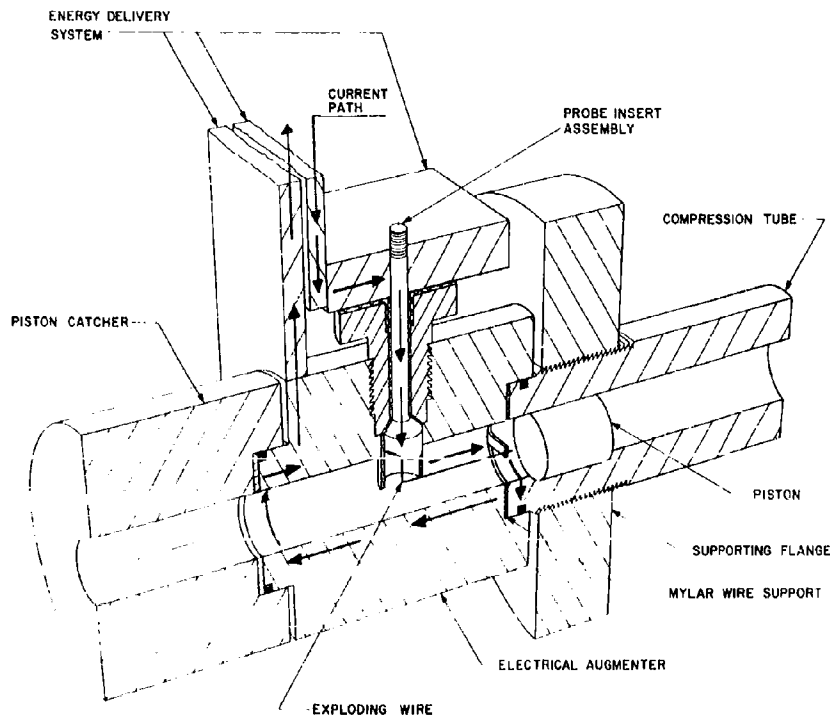


Figure 29 - Electrical energy insertion section for a 1.63",
.22" light-gas gun

reduction in intensity due to geometric factors. For this reason, the shock waves can propagate up and down the compression tube several times while their energy is slowly absorbed by the driver gas, which is thereby heated. Shock wave heating is advantageous for the electrocompression experiment because it generates a relatively uniform temperature rise of the driver gas. Experimental evidence to substantiate the shock heating hypotheses is to be presented in a later section. The operation of the gas-gun proceeds in a normal manner after the insertion of the electrical energy and may be examined directly with the NAREC computer program.

NRL ACCELERATOR DEVELOPMENT

Analysis

An analysis of the energy insertion mechanism must be made in order to determine the operating criteria of an energy storage and delivery circuit that would be effective for preheating the gas reservoir of the 1.63", .22" gas gun. The first step is to determine the amount of energy that must be added to the gas reservoir to effect a particular temperature increase. The computations were carried out using ideal monatomic and diatomic gas assumptions which were justified by the relatively low gas densities existing in a gas gun prior to compression. The derived expressions are as follows:

$$\text{for } \gamma = 1.4, \quad \Delta T = \frac{2E}{5nR}$$

$$\text{for } \gamma = 1.66, \quad \Delta T = \frac{2E}{3nR}$$

where ΔT is the increase in the gas temperature, E is the energy input to the gas, n is the number of moles of gas, R is the universal gas constant and γ is the ratio of the specific heat of the gas at constant pressure to that at constant volume.

A plot of ΔT vs E for the range of values of n likely to be encountered during gas gun firings is presented in Figure 30. The temperature increase experienced by other quantities of gas lying within the range of the values presented can be interpolated in a straightforward manner.

The next problem to be considered is the rate of heat loss suffered by the gas after electrical heating and compression. The following assumptions were made in computing the gas cooling effects: (13)

1. The gas is a perfect diatomic gas.
2. All heat-loss from the gas to the barrel wall is radiative.
3. The barrel wall is a blackbody.
4. The temperature change of the barrel wall is small with respect to the temperature change of the gas.
5. The gas heating time is short with respect to gas cooling times.
6. The energy reradiated from the walls to the gas is negligible.

NRL ACCELERATOR DEVELOPMENT

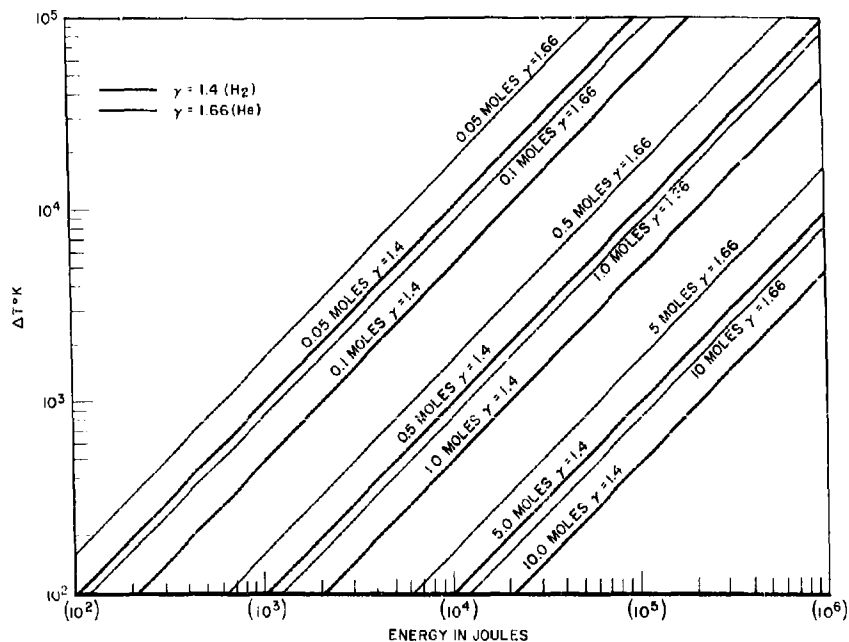


Figure 30 - Temperature increase of various amounts of ideal gas vs input energy

Experience with the NAREC ballistic computer program indicates that these assumptions are good for temperatures up to 3000 $^{\circ}\text{K}$. These assumptions will be better as the gas temperature is increased because of the T^4 term in the expression for blackbody radiation.

The computations were carried out in a standard manner and an equation relating gas cooling time to temperature reduction was derived:

$$t = \frac{nC_v}{3\sigma A\theta_0^3} \left[\frac{1 - T^3}{T^3} \right] \quad (7)$$

NRL ACCELERATOR DEVELOPMENT

where t is the time elapsed after gas heating, c_v is the specific heat of the gas at constant volume, σ is the Stefan-Boltzmann constant, A is the area of the gas radiation surface, T_0 is the initial gas temperature, z is T/T_0 , and t_k is the gas temperature at time t .

$$t_k = \frac{3\sigma A c_v}{3\sigma A c_v} \cdot \frac{1-z^3}{z^3} \quad (8)$$

Here, t_k is the time required for the gas to cool to the characteristic fraction of its original temperature, i.e., the time required to cool to 79.4% of its initial temperature.

A graph of Equation (8) is presented in Figure 31. The time taken for the gas to reach 1/2 its initial temperature, i.e. ($z = 0.5$) can readily be seen to be $7t_k$. The half-temperature times for a number of initial gas conditions have been computed, and the results indicate that these times are greater than 0.1 sec for gas densities normally used in gas-gun firings with initial temperatures less than 10 times room temperature. Thus a very wide latitude of bank-triggering techniques can be utilized without serious loss in overall efficiency since precise synchronization between the bank-discharge and piston-motion parameters is not needed to prevent serious gas heat-loss.

The next quantity to evaluate is the efficiency of energy transfer between the capacitor bank and the gas. In order to analytically study the energy transfer phenomena between the capacitor bank and the gas-heating arc, the high current discharge circuit must be treated as an RLC circuit. The differential equation for the current in an RLC circuit has been set up and solved using an analog computer (14). The initial conditions were a charged capacitor that is switched into the remainder of the circuit at time = 0. A family of curves was constructed that represent the current variation vs time for 48 different values of resistance ranging from 0 to ten times the critical damping resistance.* Curves of power input to the resistance vs time were then generated for each of the 48 cases by forming i^2R and plotting the results vs time. Finally curves of energy input to the total circuit resistance vs time were generated by electronically integrating the power vs time curves.

*The critical damping resistance of an RLC circuit is the resistance required to just prevent oscillations. It was chosen for normalizing the resistance values since it may be readily computed, $R_c = 2\sqrt{LC}$.

NRL ACCELERATOR DEVELOPMENT

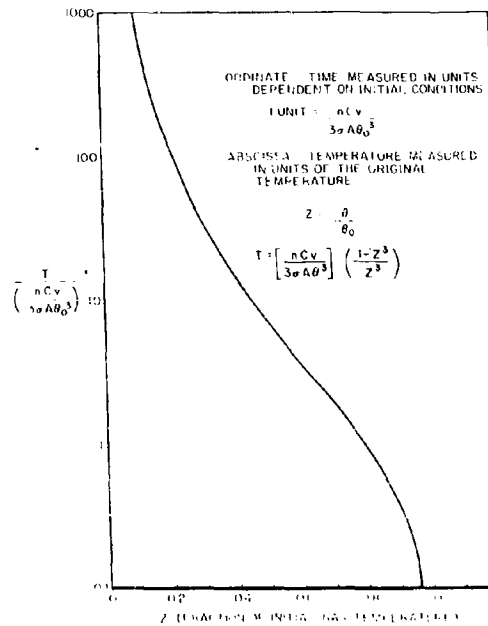


Figure 31 - Radiative cooling curve for a reservoir of ideal gas

Partial results of all the energy input curves are presented in Figure 32. The ordinate is time presented in units of $\sqrt{LC} = t_c$ and the abscissa is the total circuit resistance presented in units of the critical damping resistance $2\sqrt{L/C} = R_c$. The lines represent the fraction of energy initially stored in the capacitor that has been expended in the resistance. For example consider the time required for 90% of the energy stored in a capacitor to be expended in the resistive elements of an RLC circuit if the circuit is critically damped. Move along the 0.9E line from left to right until the abscissa $R/R_c = 1$ is reached. The ordinate of this point shows the time to be $2.7\sqrt{LC}$. This time can be evaluated if both L and C are known.

NRL ACCELERATOR DEVELOPMENT

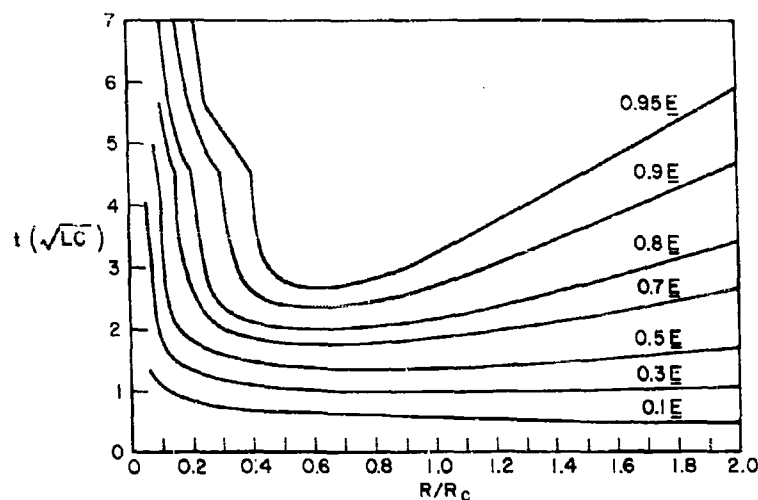


Figure 32 - Time required for an RLC circuit to dissipate selected fractions of total stored energy vs R/R_c .

This analysis may be used to evaluate the energy input to the arc within a gas gun if R , L , and C of the discharge circuit can be evaluated and the ratio of total circuit resistance to arc resistance is known. In addition, it must be assumed that R , L , and C remain constant throughout the discharge. The parameters of the discharge circuit are determined for each electroballistic shot by recording oscillograms of current vs time during each electroballistic firing (inductive pickup techniques have been used at NRL). Circuit inductance is determined by the frequency of the discharge, and total circuit resistance is computed from the damping rate of the oscillations. These parameters are sufficient to determine the energy delivery rate to the total resistance in the discharge circuit. The energy is divided between the various resistance elements as $E = E_{tot} R/R_{tot}$, where R is the resistance of an element and R_{tot} is the total circuit resistance. The ratio of the arc resistance to the total resistance is evaluated by discharging the circuit several times and measuring the change in total resistance caused by insertion and removal of the arc from the discharge circuit.

NRL ACCELERATOR DEVELOPMENT

Results of these studies show that considerably more than 50% of the stored energy in a capacitor bank may be delivered to the gas-heating arc when exterior switching is used and that 70% to 80% efficiency can be achieved using internal switching. It was also found that arc resistance often varies over a factor of two during a discharge; therefore the above analysis can yield only approximate results.

A modification of the above analytical technique has made it possible to determine the energy input rates to the gas-heating arc and to establish the variation of arc resistance with time. Basically, the oscillogram of the discharge current vs time is used to determine the local damping rate of successive pairs of positive and negative current peaks. These damping values are then used to determine average values of the total circuit resistance for each succeeding half cycle of the oscillation. Plots of these values vs median time yield smooth curves that are taken as representations of total circuit resistance vs time. Similar curves generated with no arc in the circuit are used to determine arc resistance vs time by subtracting them from the curves obtained with the arc in the circuit. Incremental power and energy input curves are then generated as before. Figure 33 is a summary of such an analysis performed for an electroballistic firing. Note that slightly over 50% of the energy was inserted into the arc (load) in 186 μ sec, i.e., 3.1%.

The problem of predicting the efficiency of energy transfer by shock waves between the gas-heating arc and the driver gas has not yet been solved; therefore, an experimental program is being set up to determine this value by measuring gas pressure within the compression tube before and after energy insertion. If the volume remains constant (the piston is not launched) and perfect gas assumptions are applied, the following expression for energy input to the gas may be derived:

$$E = \frac{3}{2} V \Delta P \text{ for monatomic gas}$$

$$E = \frac{5}{2} V \Delta P \text{ for diatomic gas.}$$

where E is the energy input, V is the chamber volume, and ΔP is the pressure change. Studies of electrically powered constant-volume guns and initial electrocompression results indicate that these efficiencies should exceed 50% for most cases of interest.

The above analysis was used to choose tentative initial operating parameters for the 1.63", .22" augmented gun. The compression tube of the gun has a volume of approximately three liters and NAREC computer results indicated that initial gas loading pressures between 4 and 8

NRL ACCELERATOR DEVELOPMENT

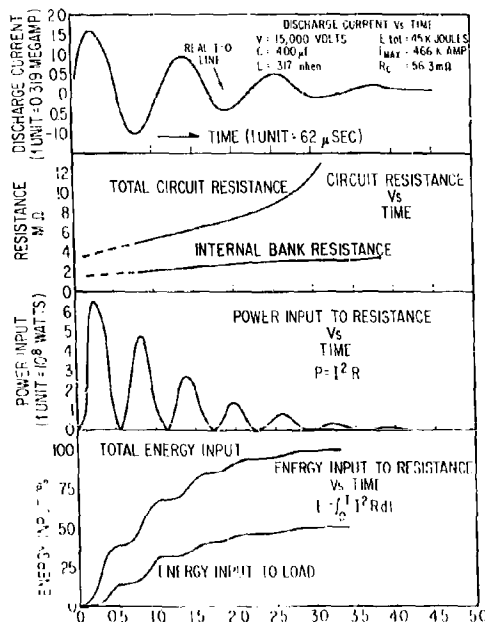


Figure 33 - Operation of an RLC circuit with variable resistance

atmospheres would be needed for high performance launches. Such loads would require between 0.5 and 1.25 moles of gas. It was estimated that the minimum advantageous temperature increases would be 300°K (twice room temperature) which would require approximately 8 kilojoules of energy to be added to hydrogen or 4.3 kilojoules to helium. The analysis presented above indicates that overall efficiencies of 25% might be expected when exterior switching is used, and 35% to 40% efficiencies might be obtained by using internal switching. Thus, a 20-kilojoule capacitor bank should produce marginal results. Since such a bank was available, initial experiments were carried out at this energy level.

NRL ACCELERATOR DEVELOPMENT

Experimental Results

A series of firings was made with the 1.63", .22" light-gas gun to determine its maximum performance capability without electrical energy addition. The maximum velocity achieved was 9.55 km/sec with an 0.1-gram Lexan cylinder. The firing conditions were:

Round 88 1.63", .22"-cal Gas Gun

Date 8/10/62

Firing Parameters

Powder - IMR 8436, 285 gm

Piston - Steel with Forward Nylon Seal-960 gm

Driver Gas - Hydrogen, 100 psia

Projectile Release - Quick opening valve release, 65000 psia

Projectile - Lexan cylinder
0.217" diam × 0.136" long
M = 0.100 gm

Velocity - 9.35 km/sec.

Gun Parameters

Compression Tube - 10' (effective length) × 1.625" diam

Transition Section - 6"-diam expendable unit with 30° conical transition section between the compression and launch tubes

Launch Tube - 0.217" ID × 41" long (189 calibers)

The electrical augmentation unit was then installed and the 20-kilojoule, 20-kv capacitor bank was connected to it using a minimum inductance configuration. Test discharges showed that 90% of the electrical energy could be dissipated in 7 μsec when a piston triggering mode was used. The gas gun was then fired using firing parameters equal to those used when 9.55 km/sec was achieved. The resulting projectile velocity was 4.1 km/sec. The compression piston bounced and was retrieved from the compression tube 4 feet from the transition section. Optimized shots where electrical energy was not added resulted in the piston being lodged in the transition section. A comparison of these results showed that a large amount of energy had been added to the gas during the augmented shot since it had changed the gas pressure profile enough to strongly affect piston motion.

Both theory and experimental results show that the performance of a light-gas gun is reduced when the driver-gas pressure is increased to the point where piston bounce occurs. Therefore a series of electrically augmented shots was fired with the initial gas pressure systematically reduced until piston bounce was eliminated. Projectile velocity increased steadily during these firings but reached a maximum value of only 6.1 km/sec.

NRL ACCELERATOR DEVELOPMENT

Several of the shots fired during this sequence had to be repeated because of shattering of the projectile. It is felt that the shattering was caused by shock waves in the driver gas.

At this point, a hypothesis was proposed that the shock waves generated by the arc propagated back and forth along the pump tube and were successively reflected at the ends during gas compression. Reflections from the face of the oncoming piston increased the wave amplitude as compression continued until it reached a value capable of fracturing the projectile-release mechanism when the average gas pressure was considerably below that required for maximum gun performance.

An experimental study was set up to test the above hypothesis. A closed bomb was constructed for studying wire explosions under conditions closely simulating those in the gun. The closed bomb used for the exploding wire study is a slight modification of the central portion of the gas gun. An expendable connector and the electrical insertion section have been coupled and the two ends of the section are sealed with plugs to make a gas-tight chamber. It was planned to charge the bomb with light gas (H_2 or He) until the density is the same as that in an operational gun at a point in the firing sequence when the electrical discharge occurs (i.e., when the piston is about to enter the energy insertion section). Thus, all the operating conditions of the gun except the piston velocity could be reproduced in a closed bomb system. Several attempts were made to discharge the bank into the bomb. In all cases the electrical arc was quenched before the energy stored in the bank could be delivered. It was then decided to reproduce these shots in the gun since there was obviously some difference between the bomb and the gun experiments. The augmented gun was assembled, as if to fire, and charged with driver gas to the same pressure as was used in the bomb (this was considerably more pressure than is usable for firing). A series of five discharges were fired without evidence of arc-quenching. It appears that the plug covering the end of the bomb (located 3 inches from the arc) reflected an electrically generated shock wave back onto the arc, thereby quenching it. For this effect to occur a shock-wave velocity greater than 12 km/sec (Mach 8) is required. Such a shock wave is extremely powerful and potentially capable of generating the effects attributed to it by the original hypothesis.

The second phase of this study is an attempt to establish that premature release of projectiles was occurring in electrically augmented firings. An experiment was conducted to measure the piston position at the time of projectile release. The average pressure within the gas can be computed from loading parameters and the piston position; therefore, the piston position at projectile release can be computed by using the design break-pressure if no significant shock waves are present. If the piston has not yet reached its expected position when the valve opens, the existence of a shock disturbance is strongly indicated. This procedure can also be checked out by firing the gun without electrical augmentation and comparing the results with an augmented shot.

NRL ACCELERATOR DEVELOPMENT

A number of techniques were considered for the measurement of both piston position and the time of projectile release. Piston position is now being measured by placing a series of probes in the barrel that are successively short circuited by the oncoming piston. Small capacitors (0.01 μ f) at each probe are charged to 6 volts and are discharged across 50-ohm resistors as the piston passes to produce sharp pulses. These pulses are presented on oscilloscopes and photographed to produce a lasting record of the piston velocity and deceleration. The NAREC ballistic computer program was used to predict the gas pressure as a function of time for pressures up to the maximum values required for projectile release.

Probe techniques for determining the time of projectile release are not feasible because peak pressures in the region of the projectile-release mechanism are too large to be sealed by electrically insulating materials. For this reason an all optical method has been developed for determining projectile-release times. Since the Lexan projectile is optically clear, the driver-gas chamber can be viewed by an optical instrument mounted in front of the gun and aligned with the launch tube axis. The launch tube opening into the relatively large diameter high pressure section approximately satisfies the conditions required for a blackbody radiation source whose radiative power is easily computed. With the assumption that the gas temperature at projectile release is 1500°K (a minimal value) the power output of the chamber in the visible region as seen from the launch tube is approximately .03 watt. (The optical power of the chamber will increase sharply as the gas temperature exceeds 1500°K.) Such light sources can be radially detected at distances of up to several hundred feet by photomultiplier tubes. Since the light output of the gun is beamed along the trajectory, photomultiplier equipment used to detect projectile release must be protected from the projectile. This has been accomplished by using an optically clear target (Plexiglas) and mounting the photomultiplier unit behind it and outside the vacuum tank. A window assembly in the rear of the tank allows the detector to view the muzzle of the gas gun.

Several gun firings have been made to date with both the piston-position and projectile-release instrumentation functioning properly. The results indicate that when electrical energy is added to the system, the projectile release mechanism is activated before the gas has reached its desired projectile release pressure.

Since the experiments discussed above have provided at least a strong indication that the shock-wave hypothesis is correct, a series of experiments was devised for counteracting shock waves in the driver gas. The simplest of these consisted of firing the gas gun with electrical augmentation, the arc being initiated by the pulse used to ignite the powder charge. A 25 millisecond delay is thus generated between arc-initiation and the passage of the piston over the energy insertion probe. It was reasoned

NRL ACCELERATOR DEVELOPMENT

that arc-generated shock waves would be dissipated in the driver gas before the piston was accelerated to a sufficient velocity to maintain or amplify them. Gas radiation computations discussed previously show that cooling losses do not become serious until at least 0.1 second has passed.

Several augmented firings have been made using exterior arc-triggering, and the total efficiency of electrical-energy transfer has not suffered appreciably. Poor gun performance and projectile shattering have indicated, however, that the shock waves still exist after this relatively long delay.

Another method for eliminating augmentation of this shock wave at the piston face is to reduce the peak pressure associated with the wave to the point where attenuation factors become dominant and the shock waves are damped out. The duration of the shock waves must be increased to maintain the total energy content of the waves, if such a mode of operation is attempted. Both of these effects can be realized by increasing the duration of the gas heating arc by increasing the inductance associated with the electrical discharge circuit as is shown below. The electrical parameters of the discharge circuit used for initial electrocompression experiments where circuit inductance was held to the minimum feasible value were as follows:

Bank Capacitance	$C = 100 \mu f$
Bank Voltage	$V = 20,000 v$
Total Inductance	$L_0 = 60 \text{ m}\mu h$
Period of Oscillation	$P = 15.4 \mu\text{-sec}$
Circuit Resistance	$R = 3 \text{ milliohms}$
Critical Damping Res.	$R_c = 49 \text{ milliohms}$
$R/R_c = N$	$N = .0625$
Maximum Current	$I_{Max} = .717 \text{ megamps}$
Maximum Power Input to resistance elements	$P_{Max} = 1.67 \text{ billion watts}$
Time to dissipate 50% of bank energy	$T_{50\%} = 13.5 \mu\text{-sec}$
Time to reach maximum power	$T_{PM} = 5.2 \mu\text{-sec}$
Characteristic Time ($t_c = \sqrt{LC}$)	$t = 2.45 \mu\text{sec}$

The above quantities were computed from oscillograms of the discharge current vs time taken during an actual firing as discussed above.

NRL ACCELERATOR DEVELOPMENT

The RLC equation was then solved for the conditions discussed on the previous page and the effect of inductance increases upon the circuit parameters was investigated. The parameters, I_{MAX} , P_{MAX} , $T_{50\%}$, and $T_{P_{MAX}}$ were computed and are presented in Figure 34 after being normalized with respect to the given conditions. Presentation of results in this way allows the curves to be used for many other arc discharge situations once a set of standard conditions has been determined.

The above results were used to design experiments to evaluate the effects of various shock wave configurations on driver-gas heating and projectile release mechanisms. The peak pressure of an electrically generated shock wave is controlled by the maximum power delivered to the arc channel and the rate of power rise as well as by various gas and geometric parameters. Information about the above electrical parameters

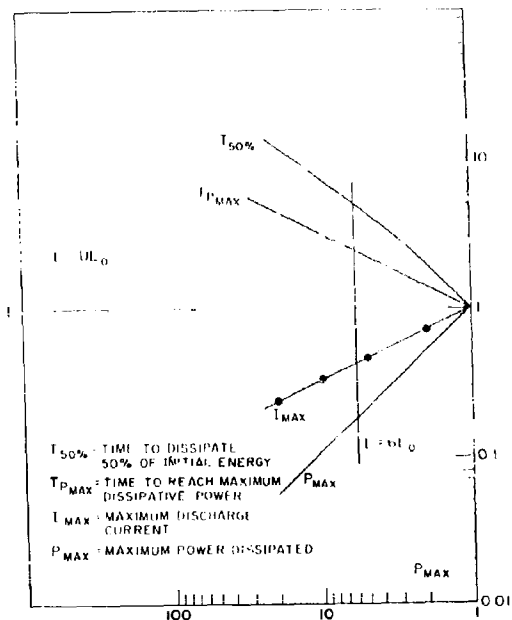


Figure 34 - Deviation of time, current, and power of an RLC circuit vs increase of inductance

NRL ACCELERATOR DEVELOPMENT

is contained in the $T_{P_{Max}}$ and P_{Max} curves. The length of the shock waves, as well as the average energy density within them, is a function of the time required to discharge half the energy into the channel ($T_{50\%}$), and the electrical resistance of the arc channel is dependent upon I_{Max} .

An analysis technique is currently under development that will allow the prediction of the effects $T_{50\%}$, $T_{P_{Max}}$, and P_{Max} upon shock-wave parameters. In order to test this technique, and to determine whether increased inductance will remove the shock-wave difficulties a series of experiments was carried out concerning the effects of inductance shifts on discharge circuit performance and gun operation. A 300-muhenry inductor was added to the circuit, which increases total circuit inductance by a factor of six. The following Table V shows the computed new parameters and their relationship to the original ones:

Table V
Deviation of Selected Parameters of an RLC Circuit
Occurring When Inductance is Increased by a
Factor of 6

Quantities	Deviation Factor From Given Conditions	New Value
I_{Max}	.425	$.318 \times 10^6$ amp
P_{Max}	.185	$.309 \times 10^9$ watts
$T_{50\%}$	4.95	67.0×10^{-6} sec
$T_{P_{Max}}$	2.45	9.02×10^{-6} sec

The shift of all parameters from original conditions is greater than a factor of two but less than a factor of six for $L = 6L_0$. The results of this study have indicated that increased inductance within the RLC discharge circuit can reduce the effects of shock-wave pressure disturbances without causing large reductions in gas heating efficiency.

Augmented firings were resumed at this point, but the 1.63", .22" gas gun had to be fired at reduced piston energy because faults had been discovered in the supply of transition sections then on hand. Maximum projectile velocity without augmentation was found to be 6.1 km/sec. When 20 kilojoules of energy were added through the high inductance circuitry, peak velocities were increased to 6.5 km/sec. It was decided to try to exploit this small positive result by increasing the electrical energy input to 42.5 kilojoules. Firings at this level resulted in maximum velocities of 8.5 km/sec, clearly indicating that a substantial increase of gas gun performance had been achieved by electrically heating the driver gas.

NRL ACCELERATOR DEVELOPMENT

Electrical Energy Added (joules)	0.1-gram-Projectile Velocity (km/sec)
0	6.1
20,000	6.5
42,500	8.5

Transition sections without faults have become available, and augmentation experiments have recently been initiated at maximum gun performance levels. Thus far 0.15-gram plastic cylinders have been fired at 8.85 km/sec. It appears that the amount of energy added to the driver gas of a gas gun is quite critical (note the reduced energy firing results) and therefore more energy may deliver significantly increased results. Experiments at still higher energy levels (60 to 120 kilojoules) are planned for the near future. In addition instrument studies will be carried on to complete the efficiency evaluation of the energy insertion mechanism and to study the effects of electrically generated shock waves in the driver gas.

Electrical Plate Accelerator

The electroballistic group at NRL has initiated a project to extend a technique previously developed at AFSWC* for launching thin plates of plastics and low density metals to hypervelocities using the plasma from electrically exploded foils (15). The plate launcher (Figure 35) consists of a sheet of thin aluminum foil (.00025") which is contained in a plastic holder that supports it massively on one side. A thin plate is held against the free surface of the aluminum foil and is launched by the violent foil explosion caused by an electrical pulse from a low inductance capacitor bank. The resulting plasma expands against the rear of the plate and accelerates it to hypervelocities. The motion of the plate is inherently unstable but the total trajectory is made sufficiently short (1 inch or less) to prevent instability effects from becoming important. Initial experiments utilized a 4700-joule capacitor bank to launch 1" x 2" x .0075" Mylar sheets to 2.03 km/sec (6670 ft/sec), yielding an overall efficiency of 22%. Similar experiments performed at AFSWC resulted in efficiencies of up to 50%. It was determined that this discrepancy was due to the fact that less than half the energy stored in the NRL capacitor bank was expended in the plate explosion before the sheet left the gun, while virtually all the energy in the AFSWC bank was expended prior to plate exit.

*Pulse Power Laboratory, Air Force Special Weapons Center, Kirtland AFB, N. M.

NRL ACCELERATOR DEVELOPMENT

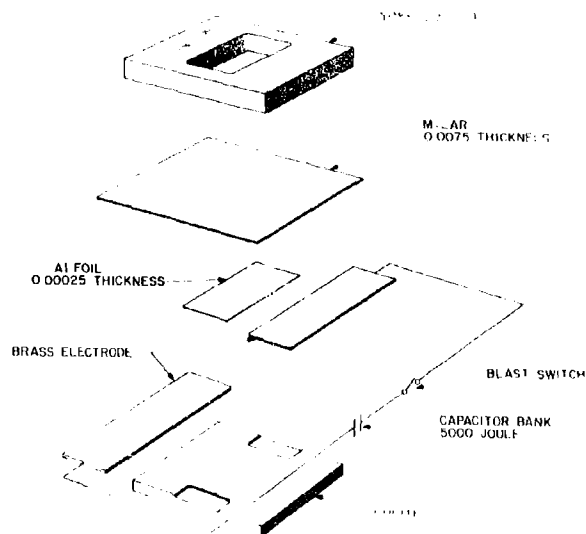


Figure 35 - Exploding foil launcher used to accelerate thin plates

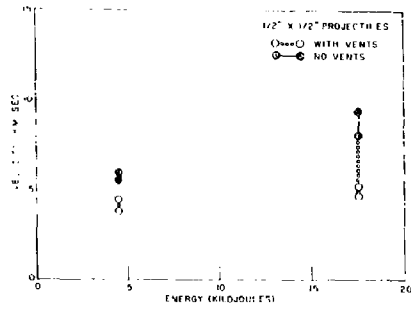
The effects of various parameters upon plate launching velocities are being studied. A second capacitor bank has been employed that can store 17,600 joules at 20 kv for conducting experiments at higher energy levels, and experiments were carried out using 1" x 2" x .0075" and 1/2" x 1/2" x .0075" launched sheets. Earlier experiments had demonstrated that considerable difficulty exists in measuring sheet velocity by observing the sheet motion with a high-speed framing camera since the sheet may be obscured by the rapidly expanding plasma moving around its edges. Two alternative velocity measurement techniques have been utilized to insure that quoted velocity values are accurate. A series of figures (x) were typed onto Mylar sheets before they were inserted into their launching holders and were viewed during launch through an optically clear target (Plexiglas) using a mirror system and the framing camera. The figures were clearly visible throughout the sheet motion but abruptly disappeared upon impact between the sheet and target. A second mirror system used the luminosity of the expanding plasma from the foil explosion to provide back-lighting of the Plexiglas target, which was also viewed edge on by the framing

NRL ACCELERATOR DEVELOPMENT

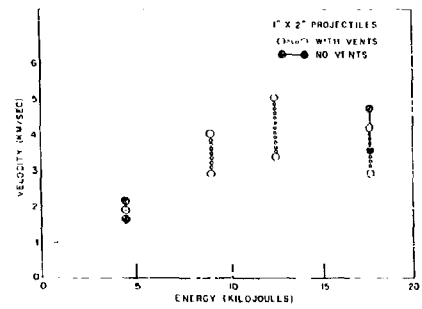
camera. This technique allowed the shock wave generated in the target by the impact to be photographed and its motion plotted. The time of sheet impact was determined by extrapolating the shock wave position to the front surface of the target. Sheet velocity was then computed from the gun-target spacing and the time-of-flight measurements. The velocity measurements from the three techniques are in agreement within experimental error, which indicates that the sheet remains at, or very near, the top of the plasma during its launch and flight to the target.

The firing results for the $1" \times 2" \times .0075"$ and $1/2" \times 1/2" \times .0075"$ Mylar sheets are presented in Figure 36. A maximum velocity of 5.0 km/sec was achieved with $1" \times 2" \times .0075"$ sheets and 9.2 km/sec with $1/2" \times 1/2" \times .0075"$ sheets. Note that two sets of data are presented for each set of firing parameters. One set represents the results of firing with gas vents in the holder, and the other without vents. Vents were placed in the holders near the front surface to allow the plasma to escape, which aids in taking clear photographs of the moving sheet. It has been noticed that these vents significantly reduce accelerator performance, indicating that significant sheet acceleration occurs after the sheet leaves the holder. The total launch efficiency decreases slowly as energy density is increased, which is probably attributable in part to early projectile exit from the holder as is discussed above. In any case, peak velocities in excess of 10 km/sec should be attainable with Mylar sheets. Attempts are being made to accelerate thicker plates made from plastics and low density metals to currently attainable velocities using larger capacitor banks.

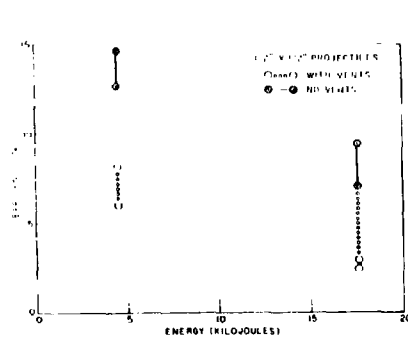
NRL ACCELERATOR DEVELOPMENT



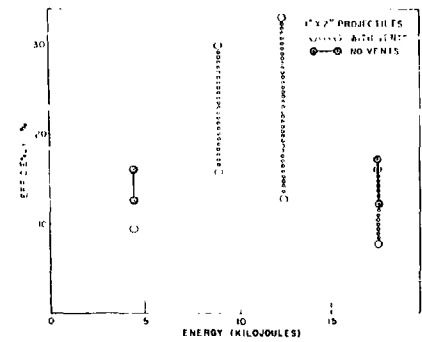
(a) Velocity of 0.0075 in. x 0.5 in. x 0.5 in. extended plates as a function of input energy



(b) Velocity of 0.0075 in. x 1 in. x 2 in. extended plates as a function of input energy



(c) Acceleration efficiency of 0.0075 in. x 0.5 in. x 0.5 in. extended plates as a function of input energy



(d) Acceleration efficiency of 0.0075 in. x 1 in. x 2 in. extended plates as a function of input energy

Figure 36 - Velocity and efficiency of electrically launched extended plates

NRL ACCELERATOR DEVELOPMENT

REFERENCES

1. Oakes, D., Carter, H., Shepherd, B., and Tiapiacese, R., "The Design and Testing of the NOL 2 Inch, 2 Stage Gun," Naval Ordnance Laboratory Report TR 62-12, 29 June 1962
2. Bailey, S.O., Clark, A.B.J., Hall, D.A., and Swift, H.F., "Facilities and instrumentation at the NRL Hypervelocity Laboratory," Proceedings of the Third Symposium on Hypervelocity Impact Effects, pp. 385-403, Chicago, Illinois
3. Hall, D.A., "Photographic Methods for Hypervelocity Measurements," Journal of the SMPTE 68:149
4. Porter, C.D., Swift, H.F., and Fuller, R.H., "Summary of NRL Hypervelocity Accelerator Development," Proceedings of the Fifth Symposium on Hypervelocity Impact, Volume 1, pp. 23-52, Denver, Colorado, Nov. 1961
5. Rast, J.J., "The Design of Flat-Scored High Pressure Diaphragms for Use in Shock Tunnels and Gas Guns," NAVORD Report 6865, 6 September 1962. Published January 1961
6. Gay, H.P., "The Evolution of Gauges for Measuring Pressure in Guns and Rockets at the Ballistic Research Laboratories," BRL Memorandum Report 1402, May 1962
7. Swift, H.F., and Porter C.D., "Hypervelocity Capabilities and Impact Research," NRL Memorandum Report 1135, Semi-Annual Progress Report No. 1, 1 July - 31 December 1961
8. Swift, H.F., Porter, C.D., "Hypervelocity Capabilities and Impact Research," NRL Memorandum Report 1249, 1 January - 30 June 1961, Published December 1961
9. Swift, H.F., and Porter, C.D., "Hypervelocity Capabilities and Impact Research," NRL Memorandum Report 1274, 1 July - 31 December 1961, published February 1962
10. Unpublished NRL Data
11. Keenan, J.H., Kaye, J., Gas Tables, John Wiley and Sons, Inc., N.Y., 1946.
12. Swift, H.F., "Electroballistic Techniques," Proceedings of the 4th Hypervelocity Impact Effects Symposium, Volume 1. Eglin Field, Florida, April 1960

NRL ACCELERATOR DEVELOPMENT

13. Swift, H.F., and Porter, C.D., "Hypervelocity Capability and Impact Research," Semi-Annual Progress Report to ARPA on No. 70 for period January - June 1962. NRL Memorandum Report No. 1348, July 1962
14. Baker, J.R., Maher, W.E., and Swift, H.F., "RLC Circuit Analysis," NRL Memorandum Report No. 1229, published October 1962
15. Chase, W.G., Moore, H.K., (editors) Exploding Wires, Plenum Press, New York, 1962 (Volume 2)

PERFORMANCE OF A THREE STAGE ARC HEATED LIGHT

GAS GUN

by

J. Eckerman
W. L. McKay

RESEARCH AND ADVANCED DEVELOPMENT DIVISION
AVCO CORPORATION
Wilmington, Massachusetts

This work supported by Ballistics Systems Division, United States Air Force
under contract #AFO4(694)-239

THREE STAGE GAS GUN

CONTENTS

	<u>Page</u>
ABSTRACT	249
INTRODUCTION	250
I. LAUNCHER OPERATION AND DESIGN	253
II. LAUNCHER PERFORMANCE	258
A. Experimental Results	258
B. Pressure Measurements	261
C. Theoretical Performance	264
Analysis	266
Conclusions	269
REFERENCES	271
APP. I - The Length of the Equivalent Adiabatic Compressor	272
APP. II - Calculation of Launcher Performance	274
1. General Adiabatic Compression	274
2. Modification of the General Case to Include Arc Discharge	276
NOMENCLATURE	280
TABLES AND FIGURES	283

THREE STAGE GAS GUN

ABSTRACT

The design, operation, performance and internal ballistics are described for a caliber 0.600 light gas gun with arc discharge heating of the driver gas.

The complete development of the launcher is detailed. This includes the 300,000 joule capacitor bank construction, the effect of discharge time on performance, the effect of discharging at different times during the compression stroke, discharge chamber design and switching technique.

In this paper, it is shown that improved launcher performance was obtained by arc discharge heating over the unheated configuration for the same mass projectile at the same maximum reservoir pressures.

The interior ballistics analysis presented for this type of modified adiabatic compressor follows the procedure of Chambers, Denardo and Rossow. The computation given is generalized to include variation of the discharge energy as well as the discharge-compression cycle.

THREE STAGE GAS GUN

Introduction

Improvement of gun performance has been a task which has occupied the attention of ballistic laboratories for many years. The problem can be summarized by considering the relation between velocity gradient $\frac{du}{dx}$ and pressure gradient $\frac{dp}{dx}$ along a gun barrel

$$\frac{1}{p} \frac{dp}{dx} = - \left(\frac{a}{RT} \right) \frac{du}{dx} = - \sqrt{\frac{\gamma M}{R_0 T}} \frac{du}{dx}$$

Thus the pressure drop between the reservoir and projectile base is proportional to the velocity of the projectile. The magnitude of the pressure drop varies as $\sqrt{\frac{\gamma m}{R_0 T}}$ where: γ is the ratio of specific heats, R_0 the universal gas constant, m the gas molecular weight, T the gas temperature.

Ultimate launcher performance is limited by the strength of either the model or the gun components. Thus at the maximum (limiting) pressure in the reservoir, or equivalently high pressure on the projectile, higher projectile velocity can be achieved by (a) decreasing the molecular weight of the gas, (b) increasing the reservoir temperature, or, (c) both. Historically, the New Mexico School of Mines (NMSM) developed the first light gas gun using hydrogen. That is, higher performance was obtained by decreasing the molecular weight.¹ A similar approach to the NMSM was adopted by the Naval Research Laboratories² group and the Ames Research Center NASA.³ In both these launchers, a heavy subsonic piston is employed to adiabatically compress hydrogen or helium. The high pressure, high temperature hydrogen is then employed as the gas which drives the projectile.

THREE STAGE GAS GUN

The Naval Ordnance Laboratory ballistics group was the proponent of two techniques to improve performance: (i) heating of driver gas by multiple reflection of a shock wave as in a reflected shock tube configuration, (ii) increase initial temperature of the driver by the addition of heat from the reaction of hydrogen and oxygen. The increase in the molecular weight of the driver gas by the addition of oxygen reduces somewhat the effectiveness of the heat addition.

At NASA, the NOL shock heating principle was further improved by addition of a light piston to drive the shock wave within the driver section. This configuration was also employed in the launchers developed at Avco RAD⁴ and more recently at Arnold Engineering and Development Center (AEDC).⁵

The use of electrical energy by electrical discharge to preheat the driver gas without increasing molecular weight was suggested by the Utah Research and Development Company.⁶ This design involved addition of the electrical energy at the end of the piston stroke. Partial preheating ($T \sim 500^{\circ}\text{K}$) of the driver has been successfully employed at AEDC.⁷

The launcher to be described in this paper employs arc discharge heating of the driver gas before compression. This design was selected to maximize the performance of fragile (acceleration limited) models, since the reservoir sound speed (temperature) will be higher than for a similar discharge at any other time during the pump cycle.

The light gas guns currently in use at Avco RAD⁴ operate consistently at hypervelocity speeds (20,000 to 25,000 feet per second). These two-stage

THREE STAGE GAS GUN

light gas guns utilize a supersonic piston in the pump tube. This generates a shock wave in the driver gas which undergoes multiple reflection from the base of the projectile. The steep pressure pulse applied to the model during shock reflection caused either tip or interface failure of double element models.

Using a new technique for ruggedizing model construction, titanium-base, steel-tipped slender cones (half angle 10°) have been launched to velocities in excess of 17,000 feet per second at RAD. However, these models failed at higher loading conditions.

In order to launch cone models at velocities greater than 20,000 feet per second, a shock-free compression stage was considered mandatory. This requires adiabatic compressor type pump stage. The launcher described in this paper is such an adiabatic compressor. However, by constant volume heat addition before-compression, a much shorter compression stroke is required to achieve the same temperature and pressure as an adiabatic compressor which operates with 300°K hydrogen prior to compression. In Appendix (I) of this paper, it is shown that a one mile long pump tube would be necessary to adiabatically achieve the same conditions as the discharge-then-pump cycle.

The three stage arc discharge gun was fabricated by modification of an existing caliber 0.60 piston compression gun to accept an arc heating stage. A capacitor bank capable of delivering 300,000 joules of energy in 40 microseconds was constructed and used to heat the gas.

In the following sections, actual launcher design, operation, and performance will be discussed as well as theoretical internal ballistics calculation of performance.

THREE STAGE GAS GUN

I. LAUNCHER OPERATION AND DESIGN

The launcher described in this paper is illustrated in figure I. The sequence of operation is listed below for two types of compression cycles.

(A) FAST DISCHARGE

1) An electric signal fires an electric primer which ignites the powder charge. Upon reaching a predetermined pressure, the piston shear disc releases and the piston begins acceleration.

2) After about four feet of travel, (midway in pump tube) the piston enters the electrode assembly. The conductive face of the piston shorts the gap and the electrical energy stored in the capacitor bank is discharged into the hydrogen. The discharge time is approximately 40 microseconds.

3) The piston then continues onward, further compressing the hydrogen. The gate valve opens or projectile hold-back device then releases. Further compression by the piston continues.

4) Projectile acceleration down gun barrel begins.

(B) LONG DURATION DISCHARGE

1) Same as for fast discharge.

2) Soon after the piston begins accelerating, the compression waves propagated by its motion arrive at the electrode assembly. A thin, metallic strip suspended from the upper electrode is pushed against the lower electrode. This is called a "wind" switch by our engineers, since as the strip flaps, it closes the interelectrode gap and initiates the discharge. When this trigger mode is used, a large inductance is used to slow down the discharge

THREE STAGE GAS GUN

to 500 microseconds. The switch components are vaporized.

3) The piston completes the compression stroke, acting against higher hydrogen pressure. Since the gas being compressed is heated, ($T_{H1} = 1500^{\circ}\text{K}$) the compression is nearly adiabatic.

4) Same as in mode (A).

A detailed description of the separate components design and operation follows.

1a. The following table gives the geometry of the gun and the materials used in the different sections.

TABLE

<u>Component</u>	<u>Material</u>	<u>Length</u>	<u>Diameter</u>
(1) Powder Chamber	4340 Steel (R-"C"-42)	16.75"	2.30" ID 5.50" OD
(2) Pump Tube	4340 Steel (R-"C"-42)	96"	1.50" ID
	(two 4-foot sections)		4.5" OD
(3) High Pressure Section	4340 Steel (R-"C"-42)	9.5"	1.5" ID 6.0" OD
(4) Launch Tub	4140 Steel (R-"C"-42)	72"	0.60" ID 2.0" OD
(5) Arc Chamber	Liner-Teflon	7.5"	1.5" ID x 3/8" thick
	Body 4340 Steel (R-"C"-42)	7.5"	7.25" OD

In the original arc chamber design an alumina liner was shrink-fitted into the body of the chamber after which it was finish machined. This liner was later replaced by teflon which was much more economical and just as efficient. Two electrodes are housed in this chamber; one is grounded to

THREE STAGE GAS GUN

the chamber, the other is attached to the chamber by means of a teflon sleeve and connected to a collector plate. Both electrodes are tipped with Avcomet (copper impregnated tungsten) to minimize erosion and thereby gas contaminants. The chamber is clamped to the pump tubes by means of a tie-bolt assembly as shown in Fig. 2. The mating ends of the pump tubes and arc chamber are designed to insure proper alignment of the bores.

The collector plate which feeds the arc chamber by collecting the energy from the individual capacitors is made up of two 1/8" thick copper sheets three feet square with several mylar sheets between them for electrical insulation. Bakelite clamps are used to hold this assembly together. Double shielded coaxial cables from the bank are connected to the edges of the copper plates.

The electrical energy for the discharge is stored in a 300-kilojoule capacitor bank. The bank consists of 100, 15-microfarad, 20-kilovolt Aerovox capacitors housed in 5 racks. The twenty capacitors in each rack are inter-connected by means of a parallel plate transmission line. Each rack is connected by 20 low-impedance cables to a flat collector plate fitted to the arc chamber, as shown in Fig. 3. The ringing frequency for a dead short at the collector plate is 25 kilocycles. The charging supply is capable of delivering full energy to the bank in 3 minutes. Approximately 50 microseconds are required to discharge the energy across a 1-1/2" gap of 500 psi of hydrogen, the actual firing conditions.

At present the collector plate is provided with a 0.5 microhenry inductor to reduce the ringing frequency to 5.8 kilocycles. The inductor consists of two parallel single loops of 5/8" diameter copper rod lying in

THREE STAGE GAS GUN

a common plane, Fig. 4. The magnetic force tending to open the loops are thus balanced, and the mutual inductance between the loops is at a minimum. For these parameters, the calculated critical damping resistance is $R_c = 36.5 \times 10^{-3} \Omega$. The actual average arc resistance under firing conditions is $5 \times 10^{-3} \Omega$. This indicates that the discharge circuit is underdamped causing a damped oscillation. The oscillation lasts for two or three cycles before the arc extinguishes, resulting in a discharge time of approximately 500 microseconds. The peak current is reached in 30 microseconds after the initiation of the discharge. In all cases approximately 90% of the stored energy has been dissipated in the discharge.

Two techniques have been used to switch the bank. The first utilizes two pieces of .040 diameter copper bus wire extending from the electrode approximately 4 inches toward the piston end of the chamber, Fig. 5. The bus wire is pegged into holes in the electrodes and suspended 1/2 inch away from the walls of the chamber. A one-half inch gap is maintained between the ends of the wires. The gap is closed by the piston which consists of a plastic cylinder with a metallic face. When contact is made, the wires explode resulting in a conductive path through which the discharge is completed. In the second technique the discharge is initiated by means of an exploding foil trigger placed between the electrodes, Fig. 6. A small strip of brass foil is attached to the high voltage electrode and bent away from the ground electrode extension toward the piston. The separation between the foil and the ground electrode is sufficient to hold off the maximum voltage to be used. When the piston begins to move, it compresses the driver gas causing a flow past the switch. The foil moves with the gas, due to aerodynamic drag, thereby reducing the gap. When the gap becomes sufficiently

THREE STAGE GAS GUN

small, an arc is struck to the ground electrode exploding the foil. The resulting metal plasma provides current carriers between the electrodes which maintain the arc within the chamber. Initiation of the discharge occurs almost simultaneously with the start of the piston as determined from direct measurements.

The switching mode determines the discharge duration which can be used. The piston-contact switch is used exclusively with the short discharge time, since the time of initiation to the arrival of the piston at the electrodes is very short. The wind switch, on the other hand, may be used with either the long or short discharge, although it was designed primarily to be used with the former.

The launcher has been designed so that the arc chamber may be placed at the beginning, the middle, or the end of the compression stroke. Firings to date have been made with the chamber in the intermediate position. The operating sequence begins with the ignition of the gun powder propellant which ruptures a diaphragm releasing the piston. The ignition of the arc may occur at this point or at the half-way position depending on the switch being used. The point at which the arc is struck determines the pressure and temperature history of the reservoir. When a predetermined pressure is reached, a diaphragm is ruptured releasing the projectile. The piston velocity must be adjusted to maintain the necessary reservoir conditions to sustain pressure on the projectile base. The piston generally extrudes into the expendable section at the end of its stroke.

In the following section, results of firings made with this launcher will be discussed.

THREE STAGE GAS GUN

II. LAUNCHER PERFORMANCE

A. Experimental Results

A program of experimental firings was carried out to determine the effect of various parameters on gun performance. The variable parameters are listed below:

1. Electrical discharge energy (300,000 joules-maximum)
2. Powder propellant energy (limited by existing powder chamber)
3. Projectile release pressure
4. Piston mass
5. Hydrogen loading pressure

Five groups of firings were made. In each group a single parameter was varied through a range of values sufficient to indicate a maximum. The resulting empirical performance curves are given in Fig. 7 (a-c). Since the parameters were treated independently, their interrelation is not fully accounted for; however, one could qualitatively predict the effect of multiple variations on the performance based on the above results. The performance curves therefore established the firing conditions necessary to obtain the maximum projectile velocity for the launcher geometry discussed in section I and the projectile mass used throughout this program, 8.2 grams. The resulting conditions are as follows:

1. 120,000 joules of electrical energy added at the beginning of the piston stroke.
2. 225 grams #4895, gun powder propellant.
3. 90,000 psi, projectile release pressure.
4. 2,000 gram piston.
5. 540 psi or 10 grams of hydrogen, initial loading pressure.

THREE STAGE GAS GUN

Using the above loading conditions, a projectile velocity of 21,000 feet per second was obtained at a peak reservoir pressure of 150,000 psi.

The results of the above study indicated two major limitations in the existing launcher.

1. The launch tube was too short.

2. The size and strength of the existing powder chamber was insufficient.

An indication that the launch tube was too short was obtained when, for a given reservoir pressure, the projectile velocity decreased as the discharge energy was raised above 120,000 joules. As a result, several pressure transducers were used in the bore of the launch tube near the muzzle end. Relatively high pressures, up to 50,000 psi, were measured at a point 10 inches from the muzzle. This pressure increased as the discharge energy increased. The qualitative result, therefore, was that for a given discharge energy there exists an optimal length of launch tube. The existing gun barrels are 120 calibers long, which appears to be optimum for 120,000 joules discharge energy. Appendix I discusses the effective pump tube length after the addition of electrical energy. It is the effective pump tube length to which the launch tube must be matched.

The powder chamber strength and size were determined to be inadequate when the maximum powder charge at maximum discharge energy was only capable of compressing the hydrogen to approximately 100,000 psi. As a result, for a given powder charge, the projectile velocity decreased with increasing discharge energy. The pressure records shown in Fig. 8 (a,b) illustrate this effect. The reason for the above lies in the fact that the higher hydrogen

THREE STAGE GAS GUN

pressure resulting from constant volume heat addition requires a greater piston energy in order to obtain the same pressure without heat addition. A larger powder chamber will be required if the maximum discharge energy is to be used. The above phenomenon is discussed more quantitatively in section IV and Appendix II.

The projectile release pressure was controlled by a shear disc in all cases. The addition of weight to the payload by increasing the release pressure was compensated by reducing the weight of the projectile. A release pressure of 90,000 psi was necessary to achieve maximum velocity when the electrical energy was added to the gas. Without the addition of energy, a 40,000 psi shear disc could be tolerated. In general, the release pressure increased with increasing electrical energy. The basis for this can be seen in Fig. 9. For a given piston velocity the pressure rise is slower at a given release pressure as the energy is increased. In order to compensate for this, the release pressure must be increased.

The piston mass determines the pressure-time history in the reservoir and therefore at the base of the projectile. If the piston is too light, it will come to the end of its stroke and reverse direction while the projectile is accelerating. On the other hand, if the piston is too heavy, the projectile will have left the barrel while the piston has a considerable amount of energy. Both extreme cases result in low efficiency of energy transfer between the gas and the projectile. An optimum piston mass of 1800 grams was obtained from these firings.

The hydrogen loading pressure determines the temperature rise of the

THREE STAGE GAS GUN

gas after constant volume heat addition. A reduction in loading pressure results in an increase in temperature, Appendix II. The effect of loading pressure on the gun performance was relatively small over the range of values covered in these firings. A value of 540 psi or 10 grams of hydrogen was selected as the optimum.

A list of the firings, results and conditions is given in Table I. It should be noted that all rounds from #28 on employed the inductance or long duration discharge mode. The instrumentation failure experience in many of the rounds was a result of the RF noise generated by the discharge and picked up by the downrange instrumentation. It is noteworthy here to comment that these rounds were not a total loss since the pressure history was still obtained.

In conclusion, it should be noted that the above-mentioned conditions are optimum for this launcher geometry only. An improved performance is expected with the longer launch tube and heavier powder chamber.

B. Pressure Measurements

In the majority of firings the reservoir pressure was monitored at a point one inch from the entrance to the launch tube. As a result, the time of projectile release can be seen on many of the pressure traces. In several firings the pressure in the bore of the launch tube was measured; however, because of the deleterious effect of the pressure port on the projectile, this was done only a few times. The pressure records on the whole enabled us to determine the effect of various parameters on the pressure history and projectile velocity. For the most part, the results were what one would intuitively predict.

Kistler piezo-electric pressure transducers were used to monitor the pressure. The basic Kistler 401 ballistics pressure transducer is capable

THREE STAGE GAS GUN

of measuring pressure pulses from 0 to 5,000 psi with a maximum frequency response of 200 kc. Adapters were used to extend the range up to 300,000 psi with a corresponding reduction in frequency response to 100 kc as the range increased to the maximum. The adapter selected for a given pressure measurement was determined by the position on the launch system where it was to be used. For instance, the 0-5,000 psi adapter was used at the arc chamber position to measure heating efficiencies, the 0-35,000 psi adapter at positions greater than 4 feet down the launch tube, the 0-100,000 psi adapter at the entrance to the expendable section, and the 0-300,000 psi adapter at the entrance to the launch tube.

Several pressure records are given in Fig. 9 (a-f). These records indicate more or less chronologically the steps taken to tailor the pressure pulse to a shock-free or weak shock condition. In all cases, except (c), the gage was located one inch from the projectile. In the latter case, the gage was located near the arc chamber to measure heating efficiency.

Figure 10a illustrates the pressure history resulting from compression of the hydrogen by a subsonic piston in which no electrical energy was added to the gas. The scope was adjusted to trigger when a 5,000 psi level was reached at the gage. The step-like increments in pressure are the result of a weak shock wave generated by the piston and reflected back and forth between it and the projectile. It can be shown from shock tube theory^{8,9} that a shock wave is generated as long as the piston is moving. e.g. the shock strength $\bar{\xi} = \frac{P_0}{P_1} \rightarrow 1$ when the piston velocity $M_p \rightarrow 0$. The piston velocity in this case is 1,000 feet per second and the projectile velocity is 8,700 feet per second. The purpose of this test was to obtain a comparison between the "heat" and "no heat" cases.

THREE STAGE GAS GUN

In Fig. 10b an attempt was made to determine the shock strength generated by the short duration discharge and to determine if it was sufficient to rupture the shear disc. In this case, the rear section of pump tube was plugged up to the arc chamber, thereby simulating the actual chamber volume when the arc is struck by the piston (piston contact switch). This volume was then charged with hydrogen to a pressure corresponding to actual conditions. The bank was charged to maximum voltage in an effort to break down the gap and discharge the bank. It was necessary to reduce the hydrogen pressure to 800 psi before the gap conducted. The resulting shock wave was traveling at 10,000 feet per second and had a peak of 40,000 psi. The reflected shock wave can be seen at the end of the trace, weakened as the contact surface decelerates and equilibrium is approached. The shear disc, designed to rupture at 40,000 psi, did not shear when subjected to this short duration impulse.

An attempt was made to determine the amount of electrical energy which goes into raising the temperature and, specifically, the pressure of the gas. From the measurement of the pressure rise, one can calculate the efficiency, η .

$$\eta = \frac{(P_f - P_1) V_1}{Q_{st} (\gamma - 1)} = \frac{P \text{ measured}}{P \text{ calculated}}$$

where

$P_f - P_1$ = the measured pressure rise

V_1 = volume at discharge

Q_{st} = stored energy

γ = 1.3 for heated hydrogen.

THREE STAGE GAS GUN

In Fig. 10c the sweep was initiated by the discharge of the bank. Approximately 1 millisecond from t_0 an equilibrium pressure of about 4,000 psi is reached. The shock waves moving past the gage are generated by the piston and somewhat confuse the equilibrium pressure measurement. In order to calculate the efficiency, one must correct for the pressure rise due to the movement of the piston, in this case 100 psi. The pressure rise after discharge (App. II) and compression is calculated to be 5,340 psi. The efficiency is

$$\frac{P_{\text{measured}}}{P_{\text{calculated}}} = \eta = \frac{4000}{5340} = 75\%.$$

It is interesting to observe from this trace the recompression of the powder gas by piston reversal. In Fig. 10 (d - f) steps were taken to eliminate the strong shocks generated by the discharge. Fig. 10d illustrates the most severe case of shock heating in which the short duration discharge is used with the piston contact switch. A variation of this Fig. 10e, utilized the short duration discharge with the wind switch theorizing that if the gas were allowed to expand axially in both directions, the shock strength would be reduced. Very little, if any, improvement resulted. Fig. 10f is the closest approach to a shock-free compression and heating obtained to date. This was achieved by increasing the discharge time by a factor of 10 and allowing it to expand axially in both directions by employing the wind switch trigger.

In summary, one can see that pressure records are invaluable pieces of data in analyzing the performance of a gun. A considerable reduction in the number of experimental firings have resulted from these pressure records. From the pressure records obtained from this parametric study, one can

THREE STAGE GAS GUN

essentially tailor the pressure pulse to suit a given required launch condition.

C. Theoretical Performance

A procedure for computing the performance of the arc heated three-stage launcher is discussed in detail in Appendix II of this report. Several calculations were made to determine optimum operating conditions as well as to assist in the evaluation of the gun performance. Figs. 11, 12 and 13 indicate the computational predictions for the launcher geometry discussed in this paper. Figure 12 illustrates a case in which no arc heating occurs. A projectile mass of 5 grams was used in all computations.

1. Comparison of theoretical performances of the adiabatic compressor with the three stage (heat-compress) launcher. Let us determine, using Fig. 11 through 13, the conditions necessary to achieve a projectile velocity of 10,000 feet per second for each case.

(a) Compression only (Fig. 13)

The mass of gas required is 18 grams as given by the upper curve. The pressure obtained from the lower curve at 18 grams of hydrogen is approximately 60,000 psi.

(b) Three stage (heat then compress) (Figs. 11 and 12)

In this case there are several loading conditions which can be used to achieve 10,000 feet per second. Using 3 grams of hydrogen and referring to Fig. 11, it can be seen that a pressure $P_2 = 25,000$ is required. From Fig. 12 the required discharge energy, $Q = 160,000$ joules is obtained. Using 18 grams of hydrogen, $Q = 40,000$ joules and $P_2 = 45,000$ psi.

THREE STAGE GAS GUN

The lower P_2 resulting in the case of the three-stage launcher is desirable from the standpoint of accelerating two-piece models.

2. Comparison of theoretical performance of the three-stage launcher with the observed performance.

The empirical performance curves for the two cases (with and without heating) are given in Fig. 14. In this graph the measured reservoir pressure is plotted against the measured projectile velocity. An initial hydrogen pressure of 540 psi or 10 grams was used in all cases. The discharge energy was 120,000 joules.

The actual conditions required to achieve 20,000 feet per second with the above loading values were

- (a) $P_2 = 130,000$ psi
- (b) $Q = 120,000$ joules

Referring to Figs. 11 and 12 one obtains the following conditions to obtain 20,000 feet per second at a loading pressure of 10 grams.

- (a) $P_2 = 160,000$ psi
- (b) $Q = 270,000$ joules

It is difficult to obtain a good comparison in this manner since the projectile weight and exact loading conditions are not duplicated. However, a reasonable agreement is obtained.

In order to determine more rigorously the accuracy of the predicted performance, the loading conditions for several actual firings were substituted into the equations of Appendix II. The results showed agreement within 1%.

Analysis

The primary concern in the design of the three stage arc heated launcher

THREE STAGE GAS GUN

was to provide a smooth shock-free acceleration of the projectile. In the early firings where a short discharge was used to heat the gas, large amplitude short duration pressure pulses were observed, Fig. 10d. It was later determined by means of a static firing of the bank that these pulses, Fig. 10b, were generated by the discharge. The explanation for this phenomena is given in the following discussion.

The occurrence of the pressure pulses may be attributed to the shock tube effect caused by the rapid discharge of energy in the volume between the piston and the electrodes. A discontinuity occurs from the local short duration heating thereby creating a slug of hot gas which acts as a piston (or contact surface in a shock tube) which expands into the unheated volume. The expansion velocity is sufficient to generate a strong shock wave in the unheated gas. The shock wave moves into the unheated gas at a greater velocity than the contact surface, raising the temperature and pressure as it passes.

The shock heating process proceeds through a series of reflections between the projectile and the contact surface until the contact surface is sufficiently slowed down. The pressure record in Fig. 10b shows two passes of a shock wave generated by a short duration discharge.

From this pressure history in the pump tube, shock velocity and strength were measured. The calculated values, using shock tube theory^{8,9} correlated well with the measured values. The high shock strengths caused pressure overshoots on the projectile base equal to or greater than those obtained in the supersonic (light piston) two stage launcher, without discharge. The addition of inductance into the circuit stretched the discharge

THREE STAGE GAS GUN

time and decreased the pressure overshoot effect, Fig. 10f. This long duration discharge required switching earlier in the cycle. A simple "wind" switch was installed which closed the gap when the first weak compression waves arrived at the electrode assembly from the accelerating piston. This type discharge was more effective since not only was the gas heated more slowly, but the plasma was free to expand both toward the piston and in the direction of the projectile.

Two further advantages were gained from the long duration discharge: The heat loss due to radiation was reduced as a result of the lower peak temperature and the amount of contaminant produced by the erosion of the electrodes was decreased. However, by heating early in the compression cycle, the gas is at an elevated temperature for a longer time thereby increasing the conductive heat losses.

The elevation of the initial gas pressure at the beginning of the compression cycle increases the work which must be done by the piston during the compression stroke. This effect is demonstrated in figure 8 (a,b) where the pressure records taken at several values of the discharge energy are shown. Increasing the discharge energy increases the hydrogen pressure. For a fixed mass of gun powder, the piston decelerates earlier along the stroke. The final hydrogen pressure which drives the projectile is then lower. Consequently, the powder mass and volume must be adjusted carefully or the launcher performance will degrade under that obtained without discharge. The following equation illustrates this principle and enables one to calculate the piston velocity at a given position in the pump tube as a function of the initial hydrogen pressure (or pressure after discharge) and powder

THREE STAGE GAS GUN

gas pressure.

$$u_p = \frac{2 A_p}{m_p (1 - \Gamma)} \left\{ P_1' X_c \left[\left(1 + \frac{X}{X_c}\right)^{1-\Gamma} - 1 \right] - P_1 X_p \left[1 - \left(1 - \frac{X}{X_p}\right)^{1-\Gamma} \right] \right\} \quad (2)$$

A typical example illustrating the piston velocity (calculated) with and without heating is given in Fig. 9. This correlates the observed and predicted results.

Conclusions

The arc augmented light gas gun has proven to be an ideal launcher for accelerating projectiles to velocities in excess of 20,000 feet per second as can be seen in Fig. 14. The high sound speed has enabled us to launch projectiles using a lower base pressure for a given velocity than with the shock heated type light piston launcher.

A longer launch tube is expected to increase the performance of this gun.

The versatility of this launcher lies in the fact that the chamber can be placed at virtually any position along the pump stroke and its energy dissipated over any duration from 50 microsecond to many milliseconds. It can therefore be used as an ultra-high velocity particle launcher as well as fragile projectile launcher. Many combinations of reservoir pressure and temperature can be obtained in small geometry launchers which formerly required long adiabatic compressors.

The ultimate application of this launcher to the fragile cone model has not yet been accomplished. However, many of the problems e.g. cycle

THREE STAGE GAS GUN

selection, electrode design, insulation erosion, electrode high pressure seals, projectile hold back, etc. are essentially solved. This method appears to us to hold great promise for the next generation of hypervelocity launchers.

Acknowledgments

The authors are the representatives of a ballistics research team. As such this paper represents the collective contributions from many individuals. Mr. George Theophanis deserves the major credit for his role in arc chamber, capacitor bank, switching techniques, bank charging and discharging circuitry, collector plate design, etc. Mr. Robert Gagnon painstakingly helped in making these elements an operation system.

William Galeazzi, Walter Johnson and Albert McNaney were invaluable in carrying out their range operations tasks.

George Skoda was responsible for the interior ballistics computations.

THREE STAGE GAS GUN

REFERENCES

1. Workman, E.J., Hydrogen Gun Development (Final Rep.), NMSM/RDD/T-720, New Mexico School of Mines, Research and Development Division, 30 June 1962.
2. Bailey, S.O., Clark, A.B.J., Hall, A.A., and Swift, H.F., "Facilities and Instrumentation at the NRL Hypervelocity Laboratory," Proceeding of Third Symposium on Hypervelocity Impact Effects, ARF, Chicago, Ill., pp. 385-403, October 7-9, 1958.
3. Charters, A.C., Denardo, B.P., Rossow, U.J., Development of a High Velocity Free-Flight, The Ames Light Gas Gun, NACARM A55G11, (1955).
4. Eckerman, J. and McKay, W., Internal Ballistics of a Two Stage Light Gas Gun, Avco RAD-9-TM-60-62, 30 September 1960, Confidential.
5. Stephenson, W.B., Performance of a Small Two-Stage, Light-Gas Gun Used for Impact Testing, AEDC-TN-61-166, January 1962.
6. Partridge, W.S., Harris, L.D., Boyd, W.A., Feasibility Study for a Hypervelocity Projector (Light-Gas Type), APGC-TR-58-142, December 1958.
7. Stephenson, W.B. and Knapp, R.E., Performance of a Two Stage Launcher Using Hydrogen, AEDC-TDR-62-32, March 1962.
8. Glass, I.I., Hall, G.J., Handbook of Supersonic Aerodynamics, Section 18, Shock Tubes, Navord Rep. 1480, 6.
9. Laporte, Otto, On the Interaction of a Shock with a Constriction, Los Alamos Scientific Laboratory, LA-1740, January 4, 1955.
10. Duff, R.E., The Use of Real Gases in a Shock Tube, Engineering Res. Inst., Rep. 51-3.

THREE STAGE GAS GUN

APPENDIX I

THE LENGTH OF THE EQUIVALENT ADIABATIC COMPRESSOR

The heat addition in the arc discharge configuration occurs at constant volume, while heat conduction to the walls and radiation are neglected. It is instructive to determine the length of adiabatic compression which would produce the same conditions. The compression by the piston in the heat addition case is also adiabatic, thus the complete arc discharge cycle can be interpreted in terms of a single adiabatic stroke from an initial length Y_1 at same intermediate point in the cycle, the piston is a distance X_1 from the end of the tube. Where X_1 is the length of the arc discharge pump tube. At this instant, the pressure and temperature as well as the mass of hydrogen is the same in both cycles.

$$\text{Pressure in Ad. Comp. } P_{X_1} = P_1 \left(\frac{Y_1}{X_1} \right)^\delta = \quad \text{I}$$

$$\text{Pressure in Arc. Discharge } \bar{\pi}_{X_1} = \bar{\pi}_1 + \frac{Q(\gamma - 1)}{V_1} \quad \text{II}$$

Mass of Gas Ad. Comp. = Mass of Gas Arc Discharge

$$P_1 Y_1 = \bar{\pi}_1 X_1 \quad \text{III}$$

Equating (I) and (II) and substitution from III yields

$$\frac{Y_1}{X_1} = \left[1 + \frac{Q(\gamma - 1)}{\bar{\pi}_1 V_1} \right]^{\frac{1}{\delta - 1}} \quad \text{IV}$$

The relation for the temperature at X_1 also satisfies equation IV which is the desired equation for the ratio of the two strokes. Application of (IV)

THREE STAGE GAS GUN

to the launcher considered in this paper:

$$Q(\max) = 3(10^5) \text{ Joules}$$

$$\gamma \approx \frac{4}{3}$$

$$V_1 \approx 3000 \text{ cc.}$$

$$P_1 \approx 600 \text{ psi } (4 \times 10^7 \text{ dyne/cm}^2)$$

$$\therefore \frac{Y_1}{X_1} \approx (9)^3 = 739$$

$$\text{or, } Y_1 = 5832 \text{ feet.}$$

So that a simple adiabatic stroke over one mile in length would be required to obtain the same gas conditions as in the discharge-then-compress eight foot stroke.

THREE STAGE GAS GUN

APPENDIX II CALCULATION OF LAUNCHER PERFORMANCE

1. General Adiabatic Compression

An excellent interior ballistics analysis of the adiabatic compressor type light gas launcher has been carried out by Charters, Denardo, and Rossow¹. A procedure will be developed here which builds upon their results. In reference Newton's second law is integrated to provide velocity-time and distance-time relationships for the projectile within the launch tube which are

$$\bar{u}_s = 1 - \left(1 - \frac{\gamma - 1}{\delta - 1} \bar{t} \right)^{\frac{\delta - 1}{\gamma + 1}} \quad (1)$$

$$\bar{z} = \frac{\gamma - 1}{2} \left[1 - \frac{2}{\delta - 1} \bar{t} - \left(1 - \frac{\gamma + 1}{\delta - 1} \bar{t} \right)^{\frac{2}{\delta + 1}} \right] \quad (2)$$

where $\bar{u}_s = \frac{u}{a_2}$ is the dimensionless velocity; $\bar{t} = \frac{t_L}{\frac{m_s \alpha_2}{P_2 S}}$ is

the dimensionless time; and $\bar{z} = \frac{z}{\frac{m_s \alpha_2^2}{P_2 S}}$ is the dimensionless distance. m_s

is the projectile mass; $\alpha_2 = \frac{2 a_2}{\gamma - 1}$; $\gamma = \frac{c_p}{c_v}$ the ratio of specific heats;

a_2 is the reservoir sound speed; P_2 is reservoir pressure; S is the cross-sectional area of the launch tube.

Then,

$$t_L = \frac{\bar{t} m_s \alpha_2}{P_2 S} \quad (3)$$

THREE STAGE GAS GUN

and

$$\alpha_2 = \frac{2 a_2}{\gamma - 1} \quad (4)$$

The subscript 2 denotes conditions at the start of launch.

In reference 1, the position X_2 of the piston in the pump tube at the start of launch is given as

$$X_2 = t_L a_2 \frac{g}{A_p} \left(\frac{2}{\gamma - 1} \right)^{\frac{\gamma + 1}{2(\gamma - 1)}} \quad (5)$$

It was assumed that as the projectile leaves the launch tube, the piston arrives at the end of the pump tube.

Combining Equations (3) and (5) yields

$$\bar{t} = \frac{M_g}{m_s} \left(\frac{\gamma - 1}{2\gamma} \right) \left(\frac{2}{\gamma + 1} \right)^{\frac{\gamma + 1}{2(\gamma - 1)}} \quad (6)$$

From the definition of \bar{z} is obtained

$$P_2 = \frac{\bar{z} \alpha_2^2 m_s}{SL} \quad (7)$$

The mass of driver gas $M_g = \rho_2 A_p X_2 = \frac{P_2}{RT_2} A_p X_2$. Utilizing this relation, equation (3) can be rewritten as

$$X_2 = \frac{(\gamma - 1)^2 SL M_g}{4 \gamma A_p \bar{z} m_s} \quad (8)$$

THREE STAGE GAS GUN

The adiabatic expansion equations will be useful in this derivation. They are

$$(a) \frac{P_2}{P_1} = \left(\frac{X_1}{X_2} \right)^\lambda \quad (b) \frac{T_2}{T_1} = \left(\frac{X_1}{X_2} \right)^{\lambda - 1} \quad (c) \frac{a_2}{a_1} = \left(\frac{X_1}{X_2} \right)^{\frac{\lambda - 1}{2}} \quad (9)$$

By definition

$$u_s = \alpha_2 \bar{u}_s \quad (10)$$

Then,

$$u_s = \alpha_2 \bar{u}_s = \left(\frac{X_1}{X_2} \right)^{\frac{\lambda - 1}{2}} \frac{2 a_1 \bar{u}_s}{\lambda - 1} \quad (11)$$

2. Modification of the General Case to Include Arc Discharge

The discussion of the arc-heated driver section requires another equation which is derived from the first law of thermodynamics for constant volume heat addition.

$$T_d = T_{bd} + \frac{Q}{M_g C_v} \quad (12)$$

Here Q is the energy added to M_g grams of gas. Subscripts "bd" denote before discharge, "d" at discharge. The equation of state can be written

$$P_d V_d = M_g R T_d \quad (13)$$

THREE STAGE GAS GUN

Combining Equations (12) and (13) an expression for p the pressure after discharge is obtained.

$$P_d = P_{bd} + \frac{QR}{C_v V_d} \quad (14)$$

For the case where the discharge occurs after the piston is accelerated by the burning powder, Equations (12) and (13) can be rewritten as

$$T_d = T_1 \left(\frac{X_1}{X_d} \right)^{\gamma-1} + \frac{Q}{M_g C_v} ; \quad (12')$$

$$P_d = P_1 \left(\frac{X_1}{X_d} \right)^{\gamma} + \frac{QR}{C_v V_d} \quad (14')$$

The adiabatic relations (9) are now used to determine the final state (2) after the piston compresses the arc heated driver gas from P_d to P_2

$$\frac{P_d}{P_2} = \left(\frac{X_2}{X_d} \right)^{\gamma} \quad (15)$$

Or, using (14') in (15) there is obtained

$$P_1 \left(\frac{X_1}{X_d} \right)^{\gamma} + \frac{QR}{C_v V_d} = P_2 \left(\frac{X_2}{X_d} \right)^{\gamma} \quad (16)$$

Using $V_d = V_1 \left(\frac{X_d}{X_1} \right)$ Equation (16) becomes

THREE STAGE GAS GUN

THREE STAGE GAS GUN

$$Q = \frac{\left[P_2 \left(\frac{x_2}{x_d} \right)^{\gamma} - P_1 \left(\frac{x_1}{x_d} \right)^{\gamma} \right] C_v v_1 \left(\frac{x_d}{x_1} \right)}{R}$$

and also

$$Q = \frac{\left[P_2 \left(\frac{x_2}{x_1} \right)^{\gamma} - P_1 \right] C_v v_1 \left(\frac{x_1}{x_d} \right)^{\gamma-1}}{R} \quad (17)$$

The mass of the piston is determined from Newton's law of motion

$$m_p = \frac{A_p (P_2 - P_2') t_L^2}{2 x_2} \quad (18)$$

and the piston velocity

$$u_p = \frac{2 x_2}{t_L} \quad (19)$$

The initial powder pressure P_1' required is given by

$$P_1' = \frac{\left\{ \frac{\gamma-1}{A_p \gamma_1} \frac{m_p u_p^2}{2} + \frac{M R T_1}{\gamma-1} \left[\left(\frac{x_1}{x_2} \right)^{\gamma-1} - 1 \right] + Q \left[\left(\frac{x_d}{x_2} \right)^{\gamma-1} - 1 \right] \right\}}{1 - \left(\frac{1}{1 + \frac{x_1 - x_2}{\gamma_1}} \right)^{\gamma-1}} \quad (20)$$

THREE STAGE GAS GUN

Here γ is the ratio of specific heats of the powder gas, $y_1 = \frac{U}{A_p}$ the length of the powder chamber if it were the same cross-sectional area as the pump tube. Final powder pressure

$$P_2 = P_1 \left[\frac{y_1}{y_1 + X_1 - X_2} \right]^{\gamma} \quad (21)$$

The mass of powder to be used m_c is determined from the following equation:

$$m_c = \frac{P_1 U}{K} \quad (\text{kg}) \quad (22)$$

where

$K = 11.8 (10^6)$ cm, and U is the chamber volume.

THREE STAGE GAS GUN

F. NOMENCLATURE

- A_p = area of pump tube
- S = area of launch tube
- L = length of launch tube
- X = distance along pump tube from the projectile to piston face
- X_p = initial length of pump tube
- X_1 = adjusted length of pump tube
- X_c = initial length of powder chamber
- m_s = projectile mass
- M_g = light gas mass
- h = mass of hydrogen
- p = mass of powder
- n = number of moles of hydrogen
- M_h = molecular weight of hydrogen
- v_h = specific heat of hydrogen
- u_s = muzzle velocity
- \bar{u}_s = dimensionless velocity
- x_2 = efflux velocity
- t_L = launch time
- \bar{t} = dimensionless time
- z = length
- \bar{z} = dimensionless length
- a_1 = initial sound speed

THREE STAGE GAS GUN

- a_d = sound speed after electrical discharge
 a_2 = sound speed at the beginning of the launch
 P_1 = original charging pressure of light gas
 P_d = pressure just after electrical discharge in light gas
 P_2 = pressure at the beginning of launch
 X_2 = distance from the front face of piston to the projectile at
 the instant of launch
 Y = distances along pump tube of equivalent adiabatic compression
 V_1 = volume of pump tube ahead of piston
 R = hydrogen gas constant 42.1×10^3 cm
 R_0 = universal gas constant
 Q = electrical energy across electrodes
 T = room temperature $^{\circ}K$
 T_d = temperature of light gas after discharge $^{\circ}K$
 T_2 = temperature at beginning of launch angle $^{\circ}K$
 C_v = specific heat of hydrogen taken at 2.6 cal/gr
 η = efficiency of discharge
 $\gamma = \frac{C_p}{C_v}$ for hydrogen = 1.4 at room temperature at $1000^{\circ}C$
 $C_v = 2.75$ and $C_p = 1.358$
 Γ = ratio of specific heats for powder propellant gas
 U = powder chamber volume
 m_p = piston mass
 u_p = piston velocity

THREE STAGE GAS GUN

P_1 = powder gas pressure at burn-out

P_2 = powder gas pressure at beginning of launch

m_c = powder charge

1. Subscripts

1 = conditions at the instant of piston release

2 = conditions at the instant of projectile release

d = conditions at the time of electrical discharge

THREE STAGE GAS GUN

TABLE I
TABLE A. 1200-2

Round	Powder Charge (grains)	Chamber Volume (cm ³)	Case Mass (gms)	Case Pressure (psi)	Electrical Energy (Joules)	Stroke Pressure (psi)	Stroke Mass (gms)	Stroke Velocity (ft/sec)	Stroke Time (msec)	Stroke Distance (in)	Stroke Angle (deg)	Stroke Remarks
3	120	149	2.1	140	22	22	2.1	22	22	22	22	Stroke 1/2 Stroke Tube Discharged Through Liner
4	120	149	2.1	140	22	22	2.1	22	22	22	22	Stroke 1/2 Stroke Tube Discharged Through Liner
5	120	149	2.1	140	22	22	2.1	22	22	22	22	Stroke 1/2 Stroke Tube Discharged Through Liner
6	120	149	2.1	140	22	22	2.1	22	22	22	22	Stroke 1/2 Stroke Tube Discharged Through Liner
7	120	149	2.1	140	22	22	2.1	22	22	22	22	Stroke 1/2 Stroke Tube Discharged Through Liner
8	120	149	2.1	140	22	22	2.1	22	22	22	22	Stroke 1/2 Stroke Tube Discharged Through Liner
9	120	149	2.1	140	22	22	2.1	22	22	22	22	Stroke 1/2 Stroke Tube Discharged Through Liner
10	120	149	2.1	140	22	22	2.1	22	22	22	22	Stroke 1/2 Stroke Tube Discharged Through Liner
11	120	149	2.1	140	22	22	2.1	22	22	22	22	Stroke 1/2 Stroke Tube Discharged Through Liner
12	120	149	2.1	140	22	22	2.1	22	22	22	22	Stroke 1/2 Stroke Tube Discharged Through Liner
13	120	149	2.1	140	22	22	2.1	22	22	22	22	Stroke 1/2 Stroke Tube Discharged Through Liner
14	120	149	2.1	140	22	22	2.1	22	22	22	22	Stroke 1/2 Stroke Tube Discharged Through Liner
15	120	149	2.1	140	22	22	2.1	22	22	22	22	Stroke 1/2 Stroke Tube Discharged Through Liner
16	120	149	2.1	140	22	22	2.1	22	22	22	22	Stroke 1/2 Stroke Tube Discharged Through Liner
17	120	149	2.1	140	22	22	2.1	22	22	22	22	Stroke 1/2 Stroke Tube Discharged Through Liner
18	120	149	2.1	140	22	22	2.1	22	22	22	22	Stroke 1/2 Stroke Tube Discharged Through Liner
19	120	149	2.1	140	22	22	2.1	22	22	22	22	Stroke 1/2 Stroke Tube Discharged Through Liner
20	120	149	2.1	140	22	22	2.1	22	22	22	22	Stroke 1/2 Stroke Tube Discharged Through Liner
21	120	149	2.1	140	22	22	2.1	22	22	22	22	Stroke 1/2 Stroke Tube Discharged Through Liner
22	120	149	2.1	140	22	22	2.1	22	22	22	22	Stroke 1/2 Stroke Tube Discharged Through Liner
23	120	149	2.1	140	22	22	2.1	22	22	22	22	Stroke 1/2 Stroke Tube Discharged Through Liner
24	120	149	2.1	140	22	22	2.1	22	22	22	22	Stroke 1/2 Stroke Tube Discharged Through Liner
25	120	149	2.1	140	22	22	2.1	22	22	22	22	Stroke 1/2 Stroke Tube Discharged Through Liner
26	120	149	2.1	140	22	22	2.1	22	22	22	22	Stroke 1/2 Stroke Tube Discharged Through Liner
27	120	149	2.1	140	22	22	2.1	22	22	22	22	Stroke 1/2 Stroke Tube Discharged Through Liner
28	120	149	2.1	140	22	22	2.1	22	22	22	22	Stroke 1/2 Stroke Tube Discharged Through Liner
29	120	149	2.1	140	22	22	2.1	22	22	22	22	Stroke 1/2 Stroke Tube Discharged Through Liner
30	120	149	2.1	140	22	22	2.1	22	22	22	22	Stroke 1/2 Stroke Tube Discharged Through Liner
31	120	149	2.1	140	22	22	2.1	22	22	22	22	Stroke 1/2 Stroke Tube Discharged Through Liner
32	120	149	2.1	140	22	22	2.1	22	22	22	22	Stroke 1/2 Stroke Tube Discharged Through Liner
33	120	149	2.1	140	22	22	2.1	22	22	22	22	Stroke 1/2 Stroke Tube Discharged Through Liner
34	120	149	2.1	140	22	22	2.1	22	22	22	22	Stroke 1/2 Stroke Tube Discharged Through Liner
35	120	149	2.1	140	22	22	2.1	22	22	22	22	Stroke 1/2 Stroke Tube Discharged Through Liner

THREE STAGE GAS GUN

Round	Powder Charge (grams)	Charge Weight (gms)	Initial Pressure (psi)	Velocity (ft/sec)	Notes
36	225	225	27	1120	Launch 1000
37	275	275	27	1120	Launch 1000
38	275	275	27	1120	Launch 1000
39	225	225	27	1120	Launch 1000
40	225	225	27	1120	Launch 1000
41	225	225	27	1120	Launch 1000
42	225	225	27	1120	Launch 1000
43	225	225	27	1120	Launch 1000
44	225	225	27	1120	Launch 1000
45	225	225	27	1120	Launch 1000
46	225	225	27	1120	Launch 1000
47	225	225	27	1120	Launch 1000
48	225	225	27	1120	Launch 1000
49	225	225	27	1120	Launch 1000
50	225	225	27	1120	Launch 1000
51	225	225	27	1120	Launch 1000
52	225	225	27	1120	Launch 1000
53	225	225	27	1120	Launch 1000
54	225	225	27	1120	Launch 1000
55	225	225	27	1120	Launch 1000
56	225	225	27	1120	Launch 1000
57	225	225	27	1120	Launch 1000
58	225	225	27	1120	Launch 1000
59	225	225	27	1120	Launch 1000
60	225	225	27	1120	Launch 1000
61	225	225	27	1120	Launch 1000
62	225	225	27	1120	Launch 1000
63	225	225	27	1120	Launch 1000
64	225	225	27	1120	Launch 1000
65	225	225	27	1120	Launch 1000
66	225	225	27	1120	Launch 1000
67	225	225	27	1120	Launch 1000
68	225	225	27	1120	Launch 1000
69	225	225	27	1120	Launch 1000
70	225	225	27	1120	Launch 1000
71	225	225	27	1120	Launch 1000
72	225	225	27	1120	Launch 1000
73	225	225	27	1120	Launch 1000
74	225	225	27	1120	Launch 1000
75	225	225	27	1120	Launch 1000
76	225	225	27	1120	Launch 1000
77	225	225	27	1120	Launch 1000
78	225	225	27	1120	Launch 1000
79	225	225	27	1120	Launch 1000
80	225	225	27	1120	Launch 1000
81	225	225	27	1120	Launch 1000
82	225	225	27	1120	Launch 1000
83	225	225	27	1120	Launch 1000
84	225	225	27	1120	Launch 1000
85	225	225	27	1120	Launch 1000
86	225	225	27	1120	Launch 1000
87	225	225	27	1120	Launch 1000
88	225	225	27	1120	Launch 1000
89	225	225	27	1120	Launch 1000
90	225	225	27	1120	Launch 1000
91	225	225	27	1120	Launch 1000
92	225	225	27	1120	Launch 1000
93	225	225	27	1120	Launch 1000
94	225	225	27	1120	Launch 1000
95	225	225	27	1120	Launch 1000
96	225	225	27	1120	Launch 1000
97	225	225	27	1120	Launch 1000
98	225	225	27	1120	Launch 1000
99	225	225	27	1120	Launch 1000
100	225	225	27	1120	Launch 1000

THREE STAGE GAS GUN

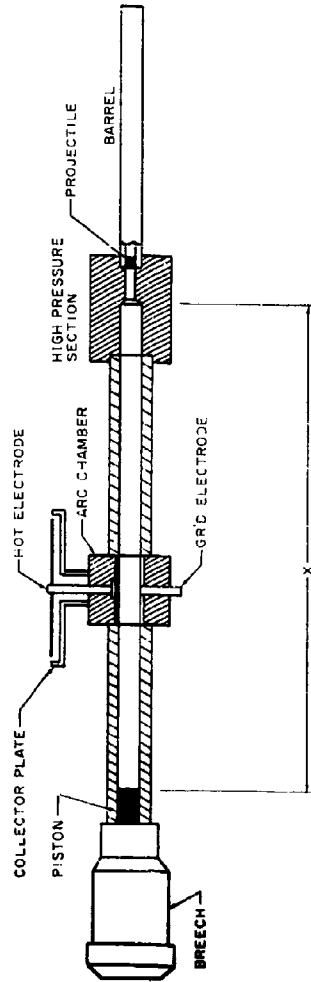


Figure 1 CALIBER .500 LIGHT GAS GUN WITH ARC CHAMBER
62-2016

THREE STAGE GAS GUN

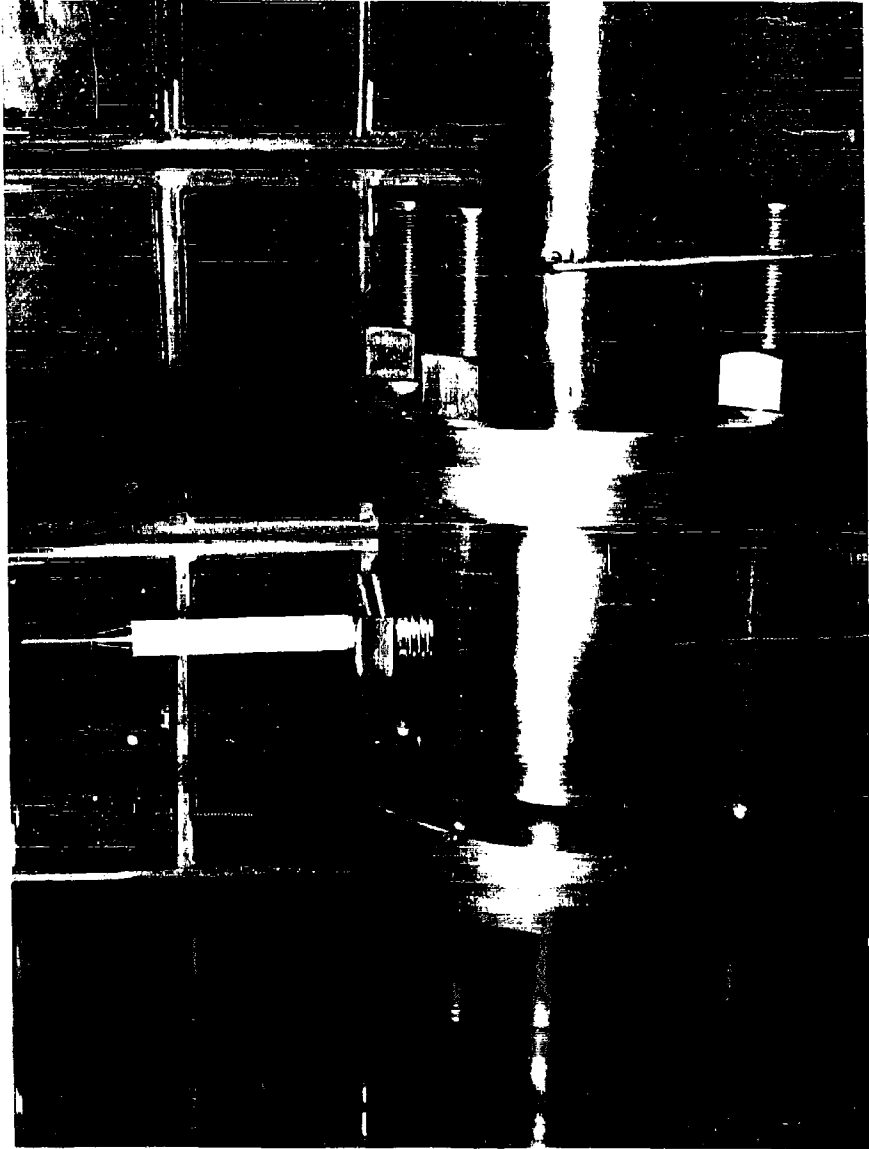


Figure 2 1cc Chamber Assembly

4 11/11/11 1/11

THREE STAGE GAS GUN



FIGURE 3 Three stage launcher

THREE STAGE GAS GUN

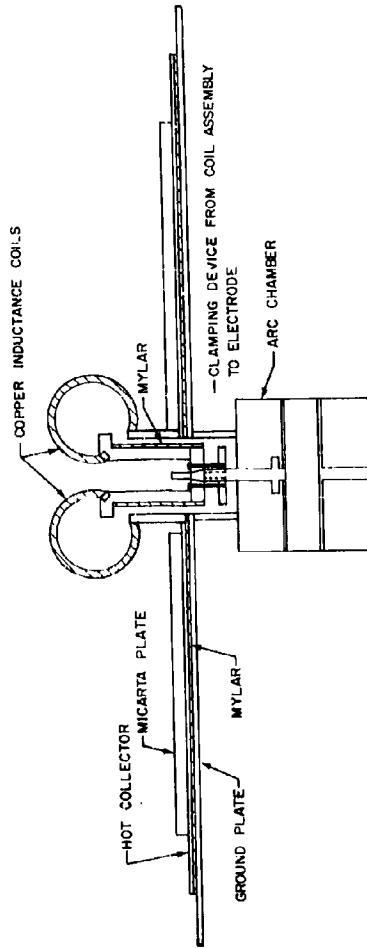


Figure 4 INDUCTION COIL ASSEMBLY SCHEMATIC
p2-557

THREE STAGE GAS GUN

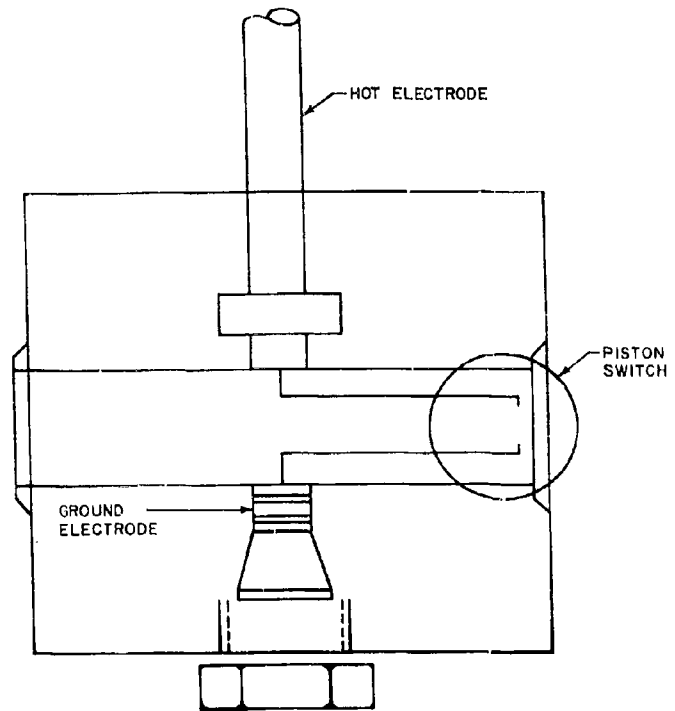


Figure 5 PISTON CONTACT SWITCH
62-5579

THREE STAGE GAS GUN

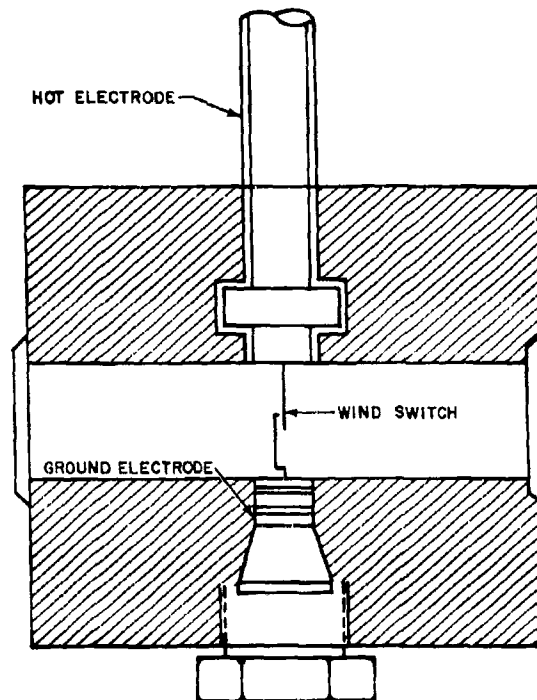


Figure 6 WIND SWITCH
62-5580

THREE STAGE GAS GUN

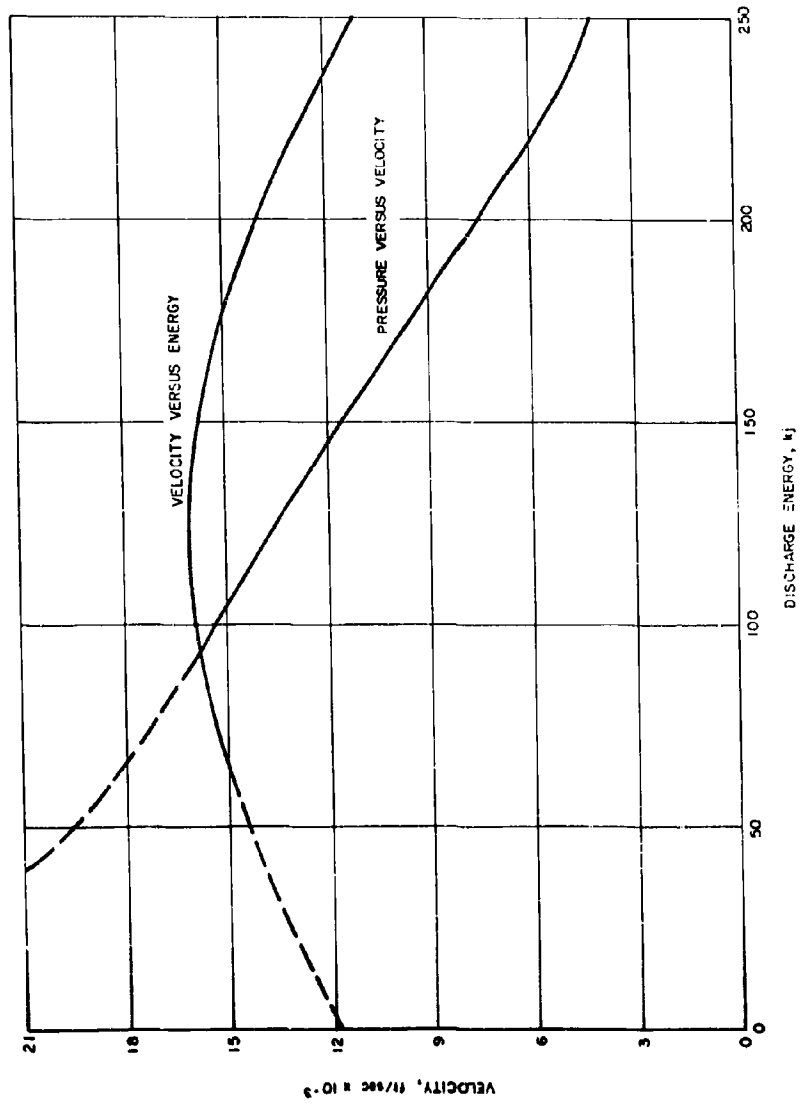


Figure 7a DISCHARGE ENERGY VERSUS VELOCITY
62-10414

THREE STAGE GAS GUN

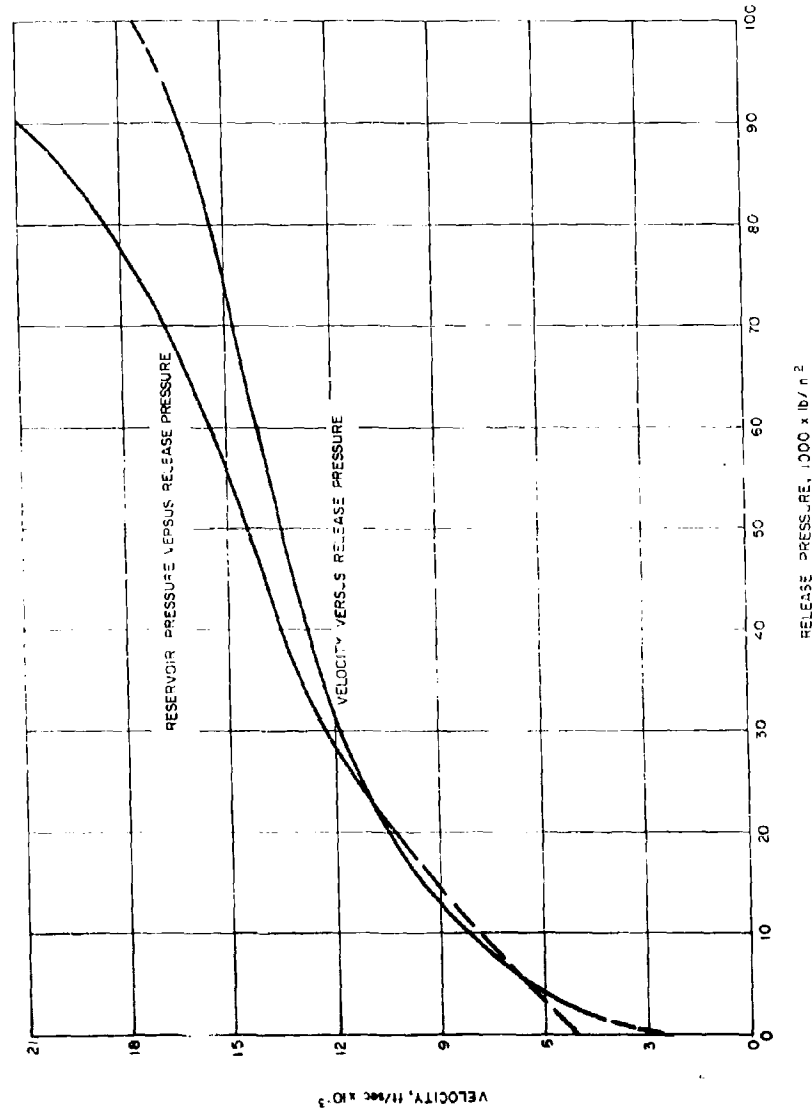


Figure 7b RELEASE PRESSURE VERSUS RESERVOIR PRESSURE AND VELOCITY
62-10415

THREE STAGE GAS GUN

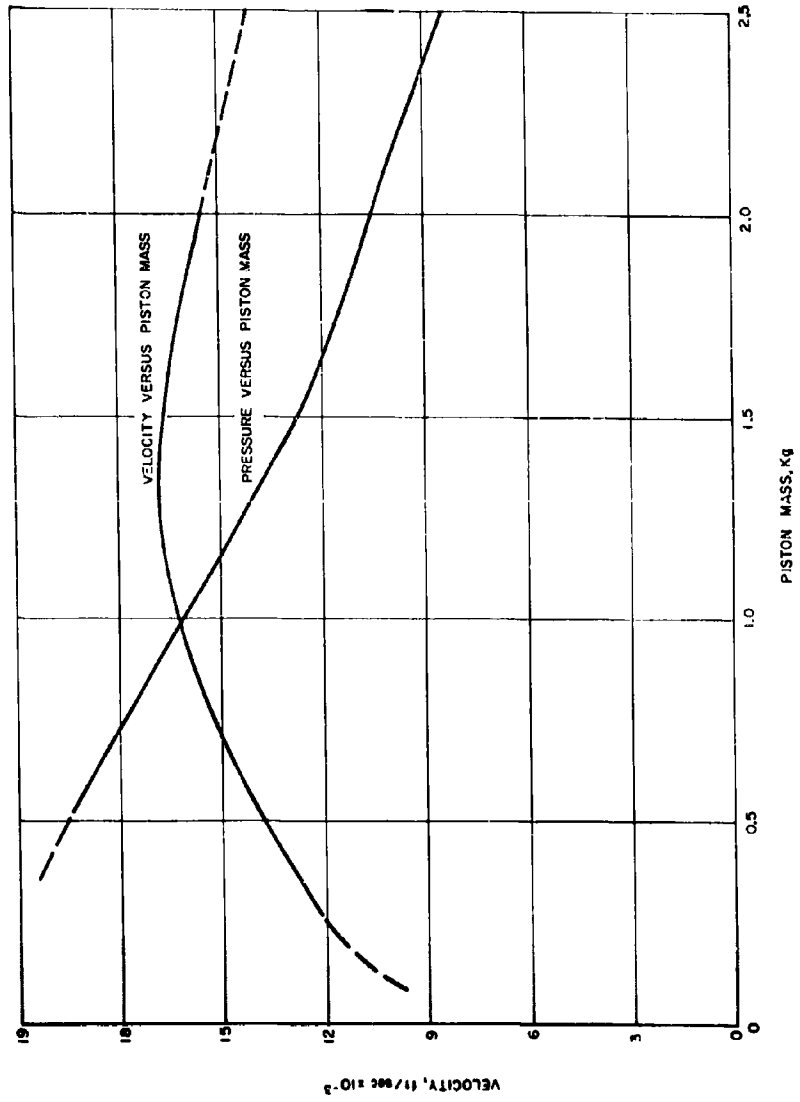


Figure 7c PISTON MASS VERSUS PRESSURE AND VELOCITY
62-10416

THREE STAGE GAS GUN

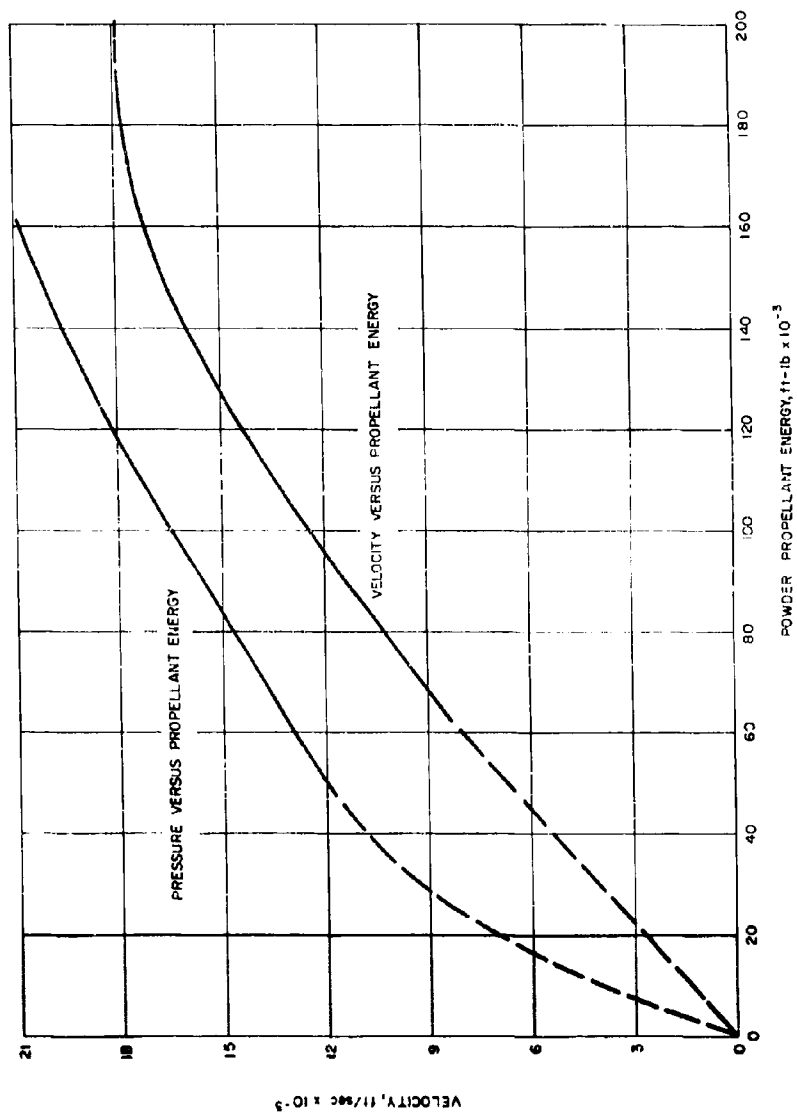


Figure 7d POWER PROPELLANT ENERGY VERSUS PRESSURE AND VELOCITY
62-10417

THREE STAGE GAS CUN

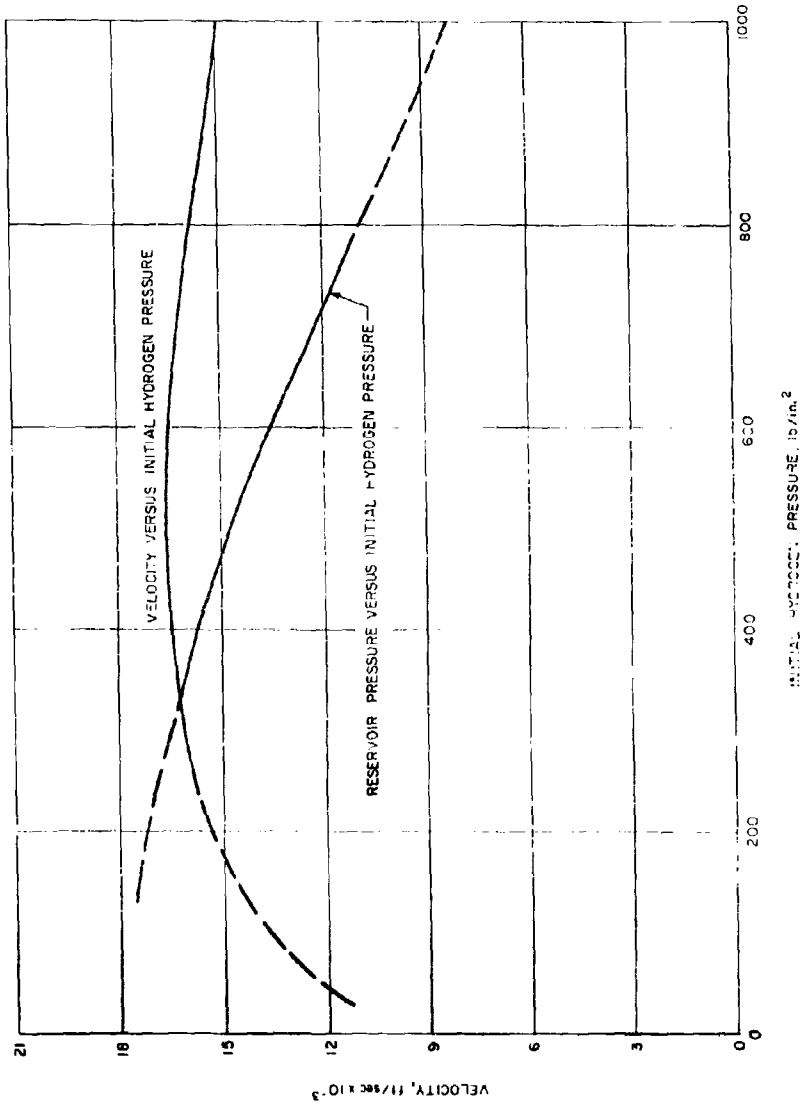
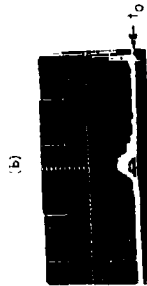


Figure 7c INITIAL HYDROGEN PRESSURE VERSUS PRESSURE AND VELOCITY
G2-1-415

THREE STAGE GAS GUN



DISCHARGE THEN COMPRESS ON WIND SWITCH
 TRIGGER
 1 MSEC CM
 75,000 PSI CM
 DISCHARGE ENERGY = 120,000 JOULES
 DISCHARGE TIME = 500 μSEC
 200 GRAMS NO. 4895 POWDER PROPELLANT
 PROJECTILE VELOCITY = 16,320 FT/SEC



DISCHARGE THEN COMPRESS ON WIND SWITCH
 TRIGGER
 1 MSEC CM
 75,000 PSI CM
 DISCHARGE ENERGY = 200,000 JOULES
 DISCHARGE TIME = 500 μSEC
 200 GRAMS NO. 4895 POWDER PROPELLANT
 PROJECTILE VELOCITY = 17,000 FT/SEC

FIGURE 1
 Pressure (P) vs. Time (t)

THREE STAGE GAS GUN

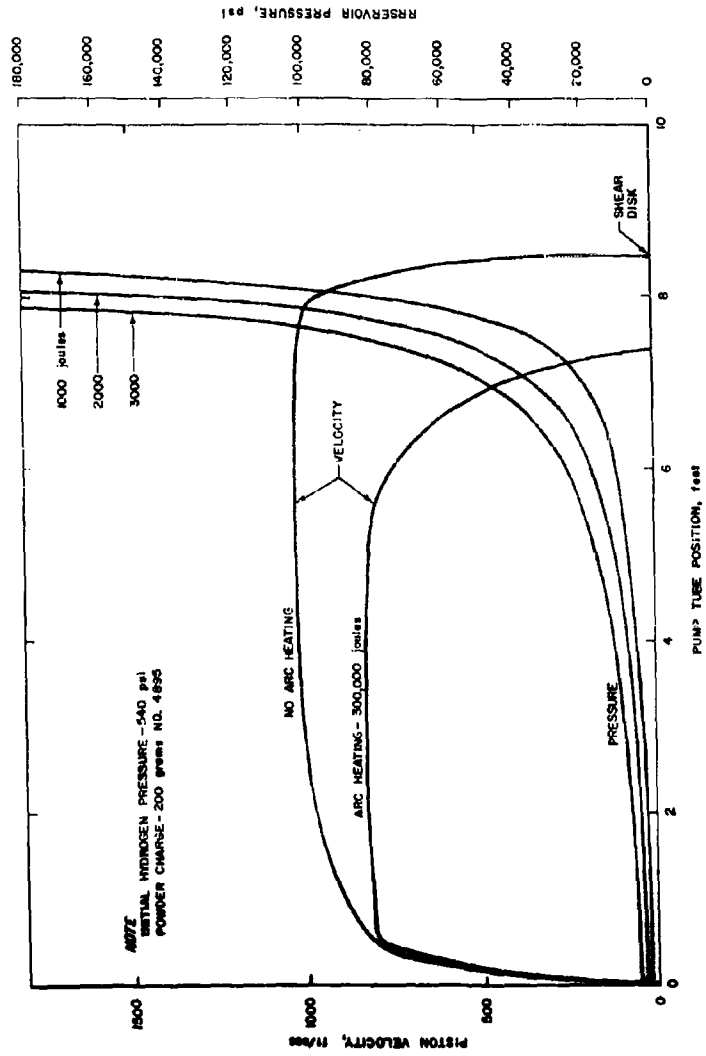
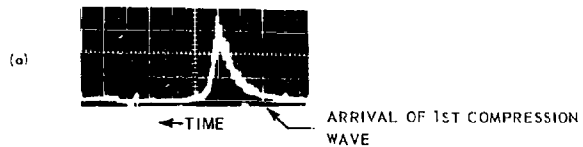
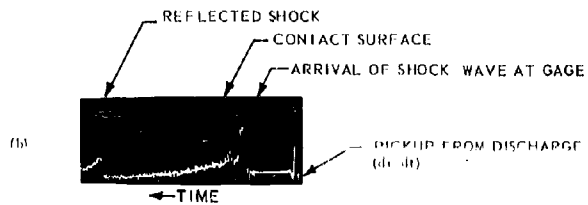


Figure 9 PISTON VELOCITY AND RESERVOIR PRESSURE
62-5583

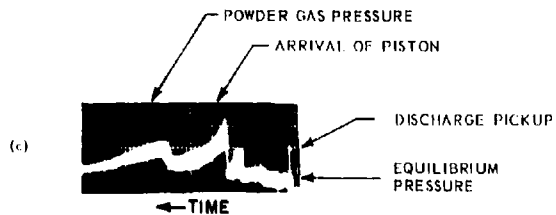
THREE STAGE GAS GUN



NO ARC HEATING
1 MSEC/CM
25,000 PSI/CM



ARC HEATING, NO COMPRESSION
200 μ SEC/CM
10,000 PSI/CM
DISCHARGE TIME 50 μ SEC
HANGFIRE CONDITIONS
120,000 JOULES DISCHARGE ENERGY

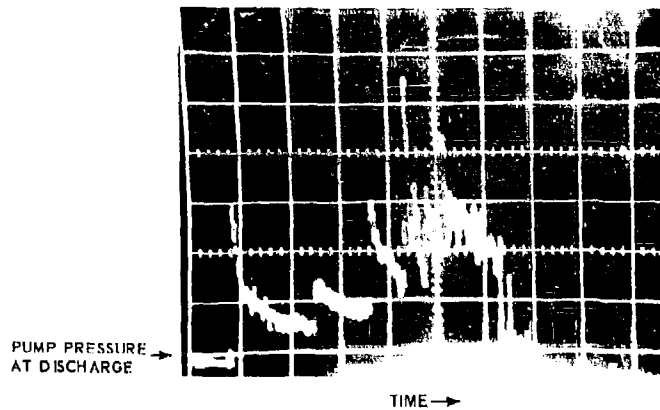


ARC HEATING PLUS COMPRESSION
1 MSEC/CM
15,000 PSI/CM
DISCHARGE ENERGY - 500 μ SEC
PRESSURE GAGE IN ARC CHAMBER
WIND SWITCH TRIGGER

Figure 10 Pressure Records

THREE STAGE GAS GUN

(d)



ARC HEATING PLUS COMPRESSION
500 μ SEC/CM
14,200 PSI/CM
DISCHARGE ENERGY = 120,000 JOULES
DISCHARGE TIME = 50 μ SEC
PISTON CONTACT SWITCH TRIGGER

(e)



ARC HEATING PLUS COMPRESSION
500 μ SEC/CM
25,000 PSI/CM
DISCHARGE ENERGY = 180,000 JOULES
DISCHARGE TIME = 50 μ SEC
WIND SWITCH TRIGGER

(f) PROJECTILE
RELEASE



ARC HEATING PLUS COMPRESSION
1 μ SEC/CM
25,000 PSI/CM
DISCHARGE ENERGY = 300,000 JOULES
DISCHARGE TIME = 500 μ SEC
WIND SWITCH TRIGGER

Figure 10 (continued) Pressure Records

THREE STAGE GAS GUN

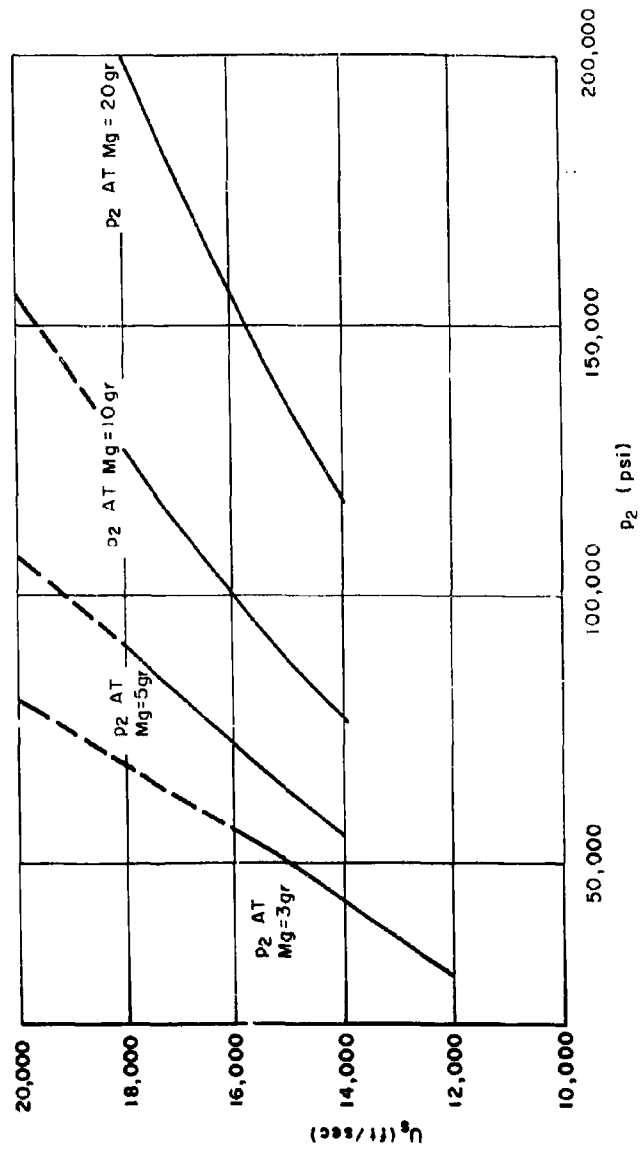


Figure II - Theoretical Performance Curves

THREE STAGE GAS GUN

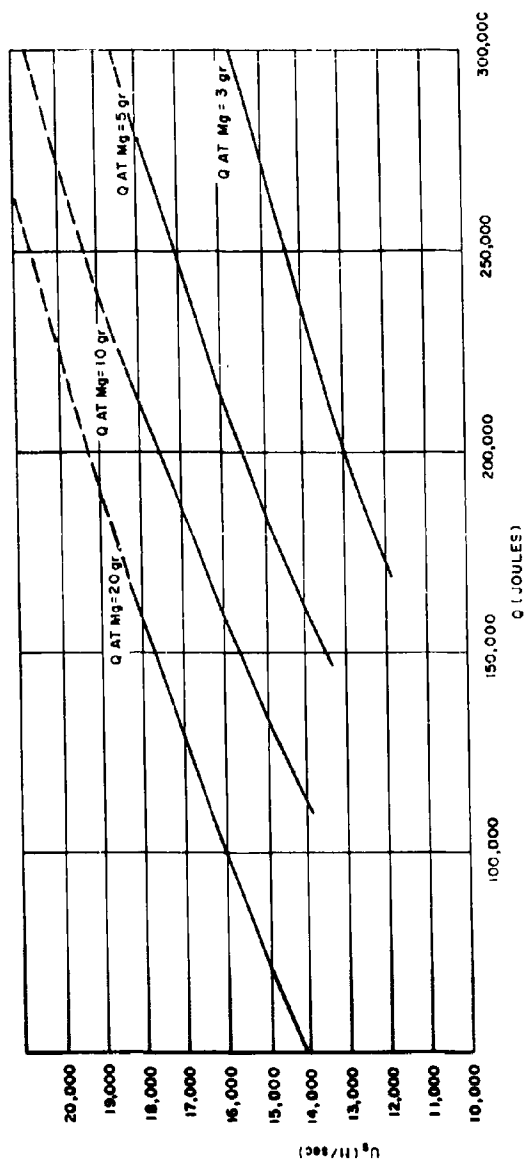


Figure 12 - Theoretical Performance Curves

THREE STAGE GAS GUN

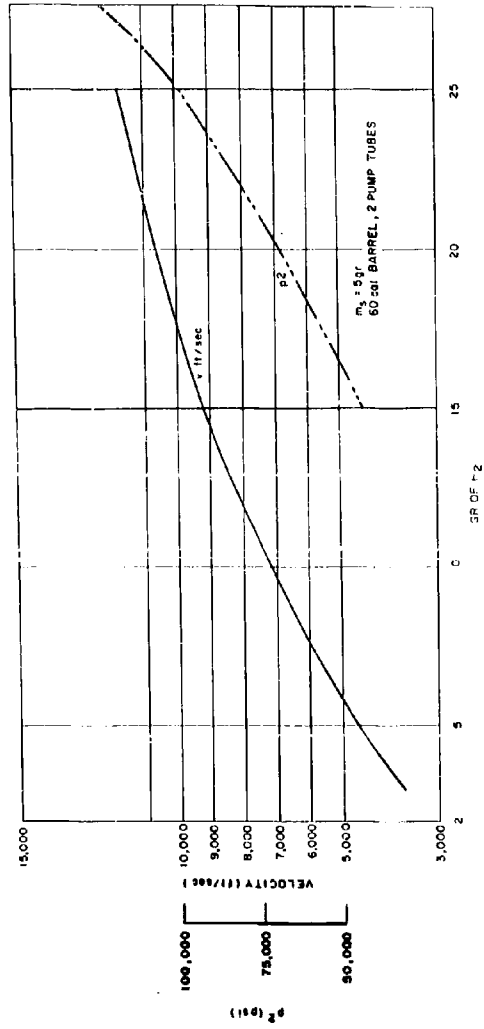


Figure 13 - Performance Curves

THREE STAGE GAS GUN

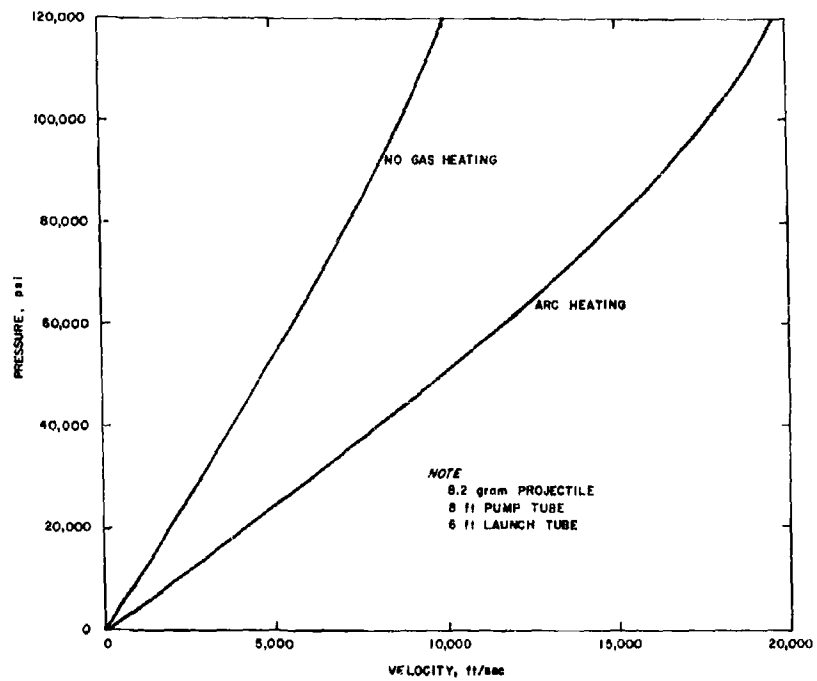


Figure 14 PERFORMANCE CURVE
62-558-1

HYPERVELOCITY AUGMENTATION TECHNIQUES

by

William G. Howell, Research Engineer; Rodney F. Recht,
Research Engineer; and Thomas W. Ipson, Materials Specialist

University of Denver
Denver Research Institute

HYPERVELOCITY AUGMENTATION TECHNIQUES

by

William G. Howell, Research Engineer; Rodney F. Recht, Research Engineer; and Thomas W. Ipson, Materials Specialist; Denver Research Institute, University of Denver, Denver 10, Colorado

ABSTRACT

This paper presents analytical and experimental results from an initial investigation of a light gas gun projection system which shows promise of providing a break-through into the 35,000 to 50,000 f.p.s. velocity range. In this projection system a third stage is added to the end of the launch tube of a conventional two-stage light gas projector. This third stage is designed to make use of the kinetic energy which is available in the sabot at the time that a sabot-projectile combination is normally fired from the launch tube. It has a convergent section which acts as an acceleration chamber leading into a final launch tube having a smaller bore. The projectile is carried centrally on the face of the sabot and fits the bore of the final launch tube. It is obvious that this method of acceleration has many problems, but the analyses and experimental results presented lend support to the conclusion that these problems may be satisfactorily solved by optimization of this launch technique.

HYPERVELOCITY AUGMENTATION TECHNIQUES

by

William G. Howell, Research Engineer; Rodney F. Recht, Research Engineer; Thomas W. Ipson, Materials Specialist; Denver Research Institute, University of Denver, Denver 10, Colorado.

Introduction

The Denver Research Institute has, for several years, been engaged in a research effort aimed toward the development of an electrically augmented hypervelocity projector capable of launching discreet particles at velocities in the 30,000 to 50,000 fps range. This program, sponsored by the Air Force and monitored by personnel of the Arnold Engineering Development Center, is in the final stages of development and evaluation; the work to date is adequately covered in a previous paper.¹ * We have also been involved in hypervelocity impact research and it was in our studies of impact work that we evolved the idea leading to the investigation reported here. In impact studies, a sabot supports the projectile and provides a gas seal during the launch cycle. Once out of the launch tube, the sabot becomes an unwanted missile which often impacts the target and clouds the data for which the test was run. Yet the kinetic energy of this sabot may be many times that of the projectile because of the mass difference. In stripping the sabot from the projectile, it should be possible to devise a means for imparting some of this excess kinetic energy to the projectile. Having observed the fluid-like effect exhibited by polyethylene in the Ames accelerated reservoir, it was concluded that a similar effect might be expected at the end of a launch tube. This is the approach used in the program discussed here.

A third stage was added to the end of a conventional two stage light gas gun. This third stage had a conical convergent section, or accelerator, leading into a smaller final bore as illustrated in Figure 1. The final launch tube was only three inches long in all tests except round 13. A short test program was planned in which there would be two geometric variables in the accelerator; the convergent angle, (θ), and the final bore, (d). For most of these tests a solid polyethylene sabot, as shown in Figure 2B, was used. A spherical projectile sized to fit the final bore was

* Superscripts refer to Bibliography.

HYPERVELOCITY AUGMENTATION TECHNIQUES

HYPERVELOCITY AUGMENTATION TECHNIQUES

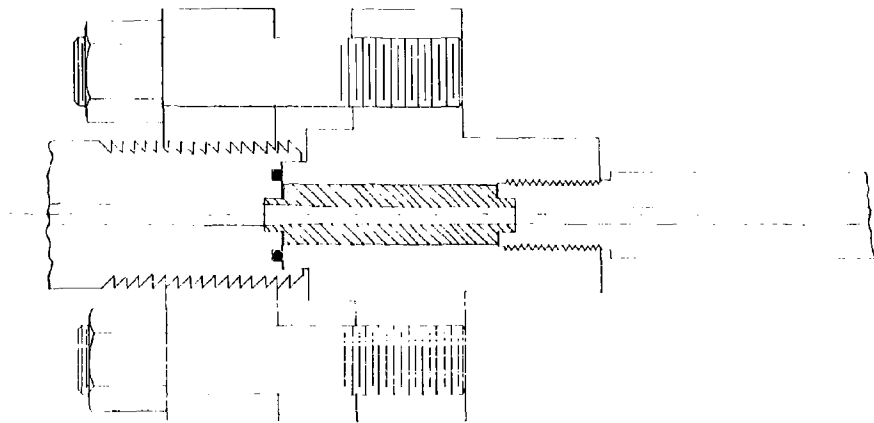


Figure 1
Cross-Sectional View of Third Stage Accelerator

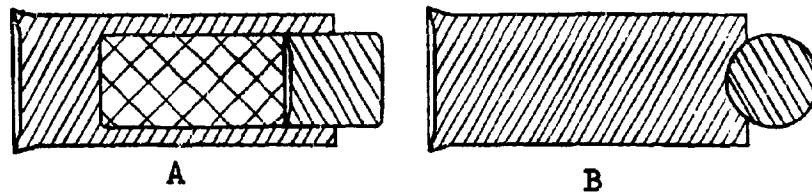


Figure 2
Sabot Configurations

HYPERVELOCITY AUGMENTATION TECHNIQUES

carried centrally on the face of the sabot. It was correctly assumed that the front face of the sabot would be accelerated as the sabot passed thru the convergent section, imparting kinetic energy to the projectile. All tests were run with a five foot long pump tube having a bore of .75 in., a caliber .30 second stage launch tube, and with loading conditions which should have produced approximately 15,000 fps without the third stage accelerator. Experimental results obtained are shown in Table I.

Theoretical Analysis

The transient form of the Euler differential equation of flow would probably represent the process being considered here in a rigorous fashion.² Pressure, density, and time are extremely important variables; viscous and friction forces would not be expected to be highly influential. Thus, a rigorous mathematical model would consider transient compressible flow relative to a short cylinder of frictionless fluid passing through a convergent section. The lack of pertinent equations of state and other information required to evaluate the Euler equation and the associated boundary conditions preclude such an analysis at the present time. A non-rigorous mathematical model was developed to partially explain the process by which the energy exchange takes place. The following derivation serves to identify some parameters which influence the increase in velocity due to the convergent section.

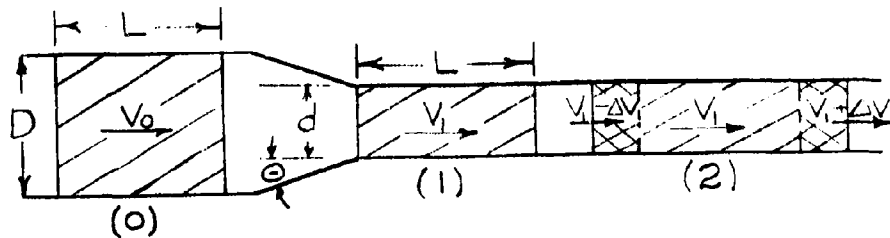


Figure 3

In Figure 3, a plastic cylinder (at position 0) moving at hyper-velocity, V_0 , in a bore of diameter, D , passes through a convergent

HYPERVELOCITY AUGMENTATION TECHNIQUES

section into a smaller bore of diameter, d . The time required to pass through the convergent section is very short. It is assumed that the change in length, L , is negligible during this time. Shear, viscous, and friction energy losses are assumed to be very small compared to the initial kinetic energy and are ignored. The plastic is thereby considered to be a compressible non-viscous fluid. Momentum transferred to the tube in the convergent section reduces the velocity of the center of the mass to V_1 . The plastic cylinder of diameter, d , and length, L , is highly compressed at position (1). Release waves progress inward from each free end of the compressed cylinder, increasing the velocity of the front surface, and decreasing the velocity of the rear surface by a value ΔV ; as illustrated at position (2).

A projectile, whose mass is small when compared to that of the cylinder, placed upon the front surface, will achieve a velocity approaching $V_1 + \Delta V$. If ΔV is greater than $(V_0 - V_1)$ the projectile will be accelerated to a higher velocity than V_0 . A plastic sabot moving at hypervelocity could, in this manner, transfer kinetic energy to a hypervelocity projectile.

Momentum Loss. The maximum impulse transferred to the gun barrel in the convergent section can be approximated. Since no energy is added to the initial kinetic energy of the plastic cylinder, the average velocity in the convergent section cannot exceed V_0 . The maximum average velocity normal to the wall is, therefore, $V_0 \sin \Theta$. Compression waves will move into the plastic from the walls. Pressure at the wall can be approximated from,

$$p = \rho_0 C V \quad (1)$$

where p is pressure - psi

ρ_0 is initial mass density - $\frac{\text{lb sec}^2}{\text{in}^4}$

C is wavefront velocity - in/sec

V is particle velocity - in/sec

Since the compression process is taken to be frictionless, only a normal force is transmitted to the wall. Substituting $\sqrt{\frac{K_s}{\rho_0}}$ for C and $V_0 (\sin \Theta)$ for V , equation (1) becomes,

$$p = V_0 \sqrt{K_s \rho_0} \sin \Theta \quad (2)$$

HYPERVELOCITY AUGMENTATION TECHNIQUES

where K_0 is the bulk modulus - psi

Θ is the convergent half angle

The surface area of the convergent section is:

$$A = \frac{\pi(R^2 - r^2)}{\sin \Theta} \quad (3)$$

where R is $D/2$

r is $d/2$

The average time for a given particle to get through the convergent section at a maximum velocity of V_0 is,

$$\Delta t = \frac{R - r}{V_0 \tan \Theta} \quad (4)$$

The impulse transferred to the wall will be equal to the product of equations (2), (3), and (4); however, only the impulse transfer in the direction of motion will effect the momentum of the center of mass. Thus, this product is multiplied by $\sin \Theta$ to obtain the impulse which changes V_0 to V_1 ,

$$\begin{aligned} \Delta(MV) &= pA(\Delta t) \sin \Theta \\ &= \pi \sqrt{K_0} (R^2 - r^2)(R - r) \cos \Theta \end{aligned} \quad (5)$$

Initial momentum is,

$$MV_0 = \pi R^2 L \rho_0 V_0 \quad (6)$$

The ratio of momentum loss to initial momentum is obtained by dividing equation (5) by equation (6); hence,

$$\frac{V_0 - V_1}{V_0} = \frac{\sqrt{K_0} \left[1 - \frac{r^2}{R^2}\right] \left(\frac{R-r}{L}\right) \cos \Theta}{V_0} \quad (7)$$

When V_0 is a hypervelocity, the right side of equation (7) has a very low value; hence an assumption that there is no loss in momentum, and that $V_1 = V_0$, is reasonable for determining the feasibility of using a convergent section to deform and thus pressurize a sabot and accelerate a projectile to higher hypervelocities.

HYPERVELOCITY AUGMENTATION TECHNIQUES

Increase in Velocity. Bulk compression is related to pressure by,

$$dp = K \frac{d\rho}{\rho} \quad (8)$$

K is a function of density. The relationship is not known for plastics which are subjected to such high changes in pressure and density as those associated with this process. Assume that the relationship is of the form,

$$K = K_0 \left(\frac{\rho}{\rho_0} \right)^n \quad (9)$$

This assumed function permits evaluation assuming a constant value of K, a value of K which is proportional to density, a value of K proportional to the square of the density, and values of K which are proportional to any other power, n, of the density.

Using this function for K in equation (8), and integrating between the limits of $p = 0$ to $p = P_1$, and ρ_0 to ρ_1 , the pressures within the compressed cylinder becomes,

$$P_1 = \frac{K_0}{\rho_0^n} \left[\frac{\rho_1^n}{n} - \frac{\rho_0^n}{n} \right] \quad (10)$$

From equation (1), the wavefront velocity resulting from the release of this pressure is,

$$\Delta V = \frac{P_1}{\rho_1 c_1} = \frac{K_0 [\rho_1^n - \rho_0^n]}{n \rho_0^n \rho_1 c_1} \quad (11)$$

but

$$\frac{\rho_1}{\rho} = \frac{D^2}{d^2} \quad (12)$$

and since $c_1 = \sqrt{\frac{K_1}{\rho_1}}$, the velocity may be expressed as
(for $n > 0$),

$$\Delta V = \frac{1}{n} \sqrt{\frac{K_0}{\rho_0}} \left[\left(\frac{D}{d} \right)^{n+1} - \left(\frac{d}{D} \right)^{n+1} \right] \quad (13)$$

For a value of $n = 0$, equation (13) is indeterminant. If $n = 0$, the bulk modulus, K, is constant. Integration of equation (8) and substitution for P_1 as before yields,

HYPERVERLOCITY AUGMENTATION TECHNIQUES

$$\Delta V = \frac{d}{D} \sqrt{\frac{K_0}{\rho_0}} \ln \frac{D^2}{d^2} \quad (14)$$

(for $n = 0$).

Equations (13) and (14) are plotted as a function of $\frac{d}{D}$ on

Figure 4 using values of n equal to 0, 1, and 2. The physical constants used are those approximated for polyethylene. The experimental test results are also shown on this figure. The use of $n = 2$ in equation (13) results in the best correlation with the experimental data.

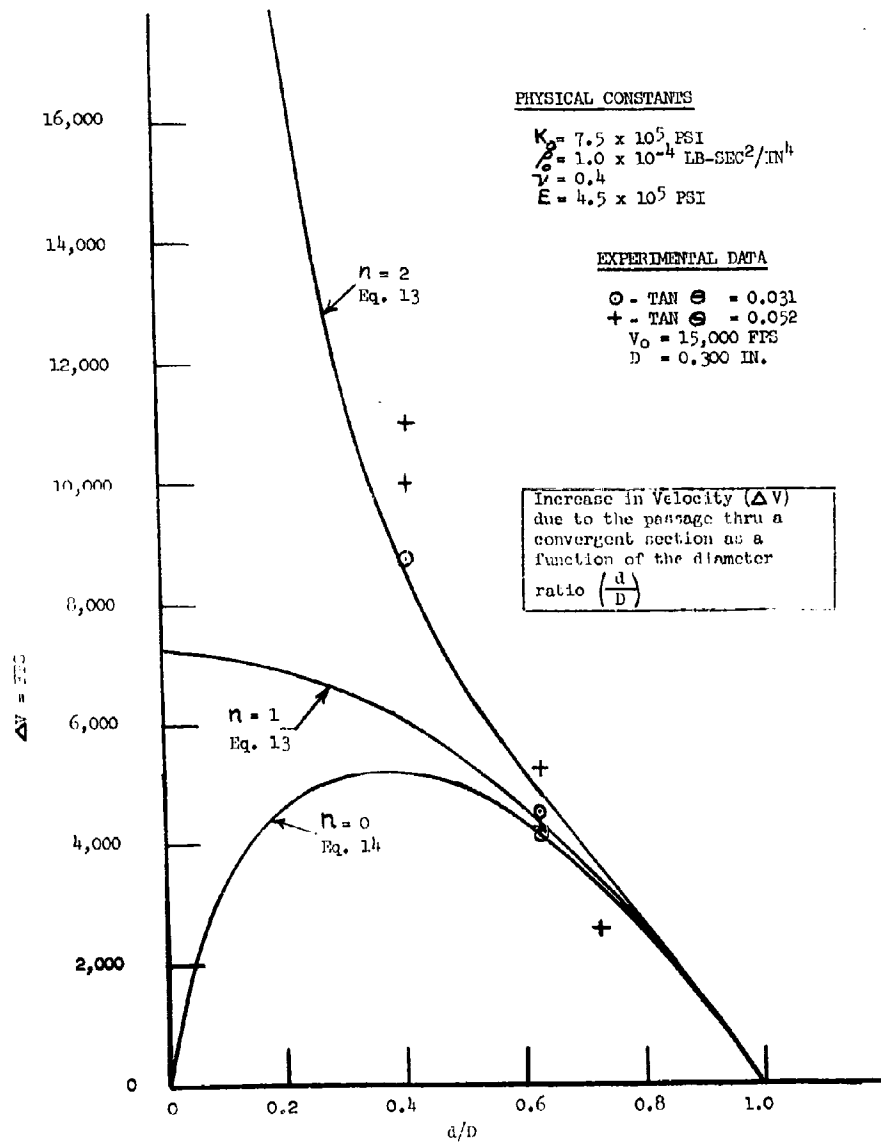
Test Results

Up to this point in the discussion we have ignored some of the more obvious problems such as the acceleration which the projectile must undergo in this process. As might have been expected, the projectile was broken up in all tests and many pieces of the sabot usually came downrange behind the fastest particles launched. However, it is the belief of the authors that this technique which has been proven to have great potential for velocity increase, may be optimized to produce useful results. To bear this out, a sabot as shown in Figure 2A was used in rounds 5, 6 and 13. The central portion of the main sabot was loaded with a plastic explosive which was intended to provide a gas cushion behind the smaller sabot, designed to fit the final launch tube. Tests 5 and 6 were run with a very short final launch tube with the purpose of determining that the C-4 explosive could withstand initial acceleration without detonation. Detonation at the third stage acceleration was definitely accomplished in these tests. Further, in these tests the smaller sabot was broken up, but not severely. Also, the main sabot appeared to be completely eliminated and only the smaller sabot impacted the target. In round 13, a twenty-four inch long final launch tube was used to extract some of the additional energy from the C-4 gas. As can be seen from comparison with round 12, an additional increase of approximately 2400 fps was obtained, apparently due to work done by this expanding gas. In this test the small sabot was observed to be in two pieces which impacted the target almost simultaneously.

Conclusions

Tests have conclusively demonstrated the usefulness of a convergent section in the launch tube of a light gas gun to deform a plastic sabot so as to further accelerate a hypervelocity projectile carried by the sabot. This technique is especially attractive since it tends to increase velocity by an amount independent of the initial value of the hypervelocity.

HYPERVELOCITY AUGMENTATION TECHNIQUES



HYPERVELOCITY AUGMENTATION TECHNIQUES

TABLE I

RESULTS OF TESTS WITH THIRD STAGE ACCELERATOR:

<u>Round</u>	<u>Tan θ</u>	<u>d (in.)</u>	<u>Final Velocity (f.p.s.)</u>	<u>ΔV (f.p.s.)</u>	<u>Remarks</u>
1	0.031	.125	23,800	8,800	
2	"	.125	21,400	6,400	Accelerator Damaged by Previous Test
3	"	.187	19,500	4,500	
4	"	.187	19,250	4,250	
5	"	.187	19,700	4,700	Sabot Loaded with C-4 Explosive
6	"	.187	19,800	4,800	Sabot Loaded with C-4 Explosive
7	"	.300	15,000	--	Control Test ($V_0 = 15000$ f.p.s.)
8	0.052	.125	25,000	10,000	
9	"	.125	26,000	11,000	
10	"	.187	20,250	5,250	
11	"	.187	19,300	4,300	
12	"	.217	17,600	2,600	
13	"	.217	20,000	5,000	Sabot Loaded with C-4 Explosive. Final Launch Tube 24" Long

HYPERVELOCITY AUGMENTATION TECHNIQUES

During feasibility analyses, momentum loss in the convergent section has been neglected; the projectile mass has been ignored and an assumption has been made that the length of the projectile does not change while passing through the convergent section. Internal dynamic effects within the deforming sabot are not considered.

Momentum loss was shown to be relatively insignificant; however, other assumptions and neglected effects are not so readily defended. Even so, it appears that an equation of the form of equation (13) will be useful in the design of sabots and tapers and for the correlation of data.

Bibliography

1. Howell, W.C., W. R. Orr and A. M. Krill, "Electrical Augmentation of a Light Gas Hypervelocity Projector", Proceedings, Second Symposium on Hypervelocity Techniques, University of Denver, Denver Research Institute, March 1962.
2. Knudsen, J.G. and D. L. Katz, Fluid Dynamics and Heat Transfer, McGraw Hill, 1958, pp. 36-37.

THE
MAGNETOHYDRODYNAMIC HYPERVELOCITY GUN

R. L. Chapman
D. E. Harms
G. P. Sorenson

MB ASSOCIATES
1279 Boulevard Way
Walnut Creek, California

MAGNETOHYDRODYNAMIC GUN

ABSTRACT

A magnetohydrodynamic hypervelocity projector system is described which is potentially capable of accelerating a 0.1 gm mass to a velocity of 27 kilometers/second. The energy for compressing the accelerating magnetic field to megagauss values is derived from high explosives. A containment tank is included in the system so that the explosive can be detonated in a regular laboratory building. Theoretical and experimental work has been done, and 9.5 kilometers/second has been achieved to date.

The Magnetohydrodynamic Hypervelocity Gun

R. L. Chapman, D. E. Harms, and G. P. Sorenson

MB Associates
Walnut Creek, California

Introduction

In order to properly simulate the effects of micrometeorite bombardment in the laboratory, different acceleration techniques than those currently operational are required. This paper describes a magnetohydrodynamic hypervelocity gun system capable of accelerating projectile masses up to 0.1 gm to velocities up to 27 kilometers per second. The accelerating force is provided by the $B^2/8\pi$ pressure of a magnetic field which is compressed to megagauss values by an explosively driven conductor. The system includes a containment tank so that high explosives may be fired in the laboratory and a condenser bank for providing the energizing magnetic field. Experimental work to date has been encouraging, and a total mass of 0.21 gm has been accelerated to 9.5 kilometers per second.

Description of Operation

A diagram of the velocity amplifier system utilizing electrochemical propulsion is shown in Figure 1. In the diagram are shown the magnetohydrodynamic compression loop called the "transducer loop"; the launch tube with sabot and projectile in place; the coils which provide the initial magnetic field; the explosive charge with a line wave generator for uniform initiation of the explosive; and the piston which compresses the magnetic field by convergence towards the launch tube corner of the loop. The operation of the system is as follows:

The condenser bank is discharged into the coils. The detonator which starts the line wave generator is fired at such a time that when the explosive has sheared off the piston, thus closing the loop, the current from the condenser bank has reached its peak discharge. Thus the maximum possible magnetic field is trapped. This time is typically 50 μ s. The average peak fields in the center of the loop are between 35 and 70 kilogauss, depending on the experiment. The sabot region is shaped to increase the current density, so that the field strength there can be as high as 200 kilogauss. As the piston continues to move inward at the velocity of approximately 4 mm/microsecond, the magnetic field is compressed to high density and the resulting mechanical pressure on the back of the sabot accelerates it down the launch tube. Acceleration times are generally several tens of microseconds, and magnetic fields of a few megagauss are

MAGNETOHYDRODYNAMIC GUN

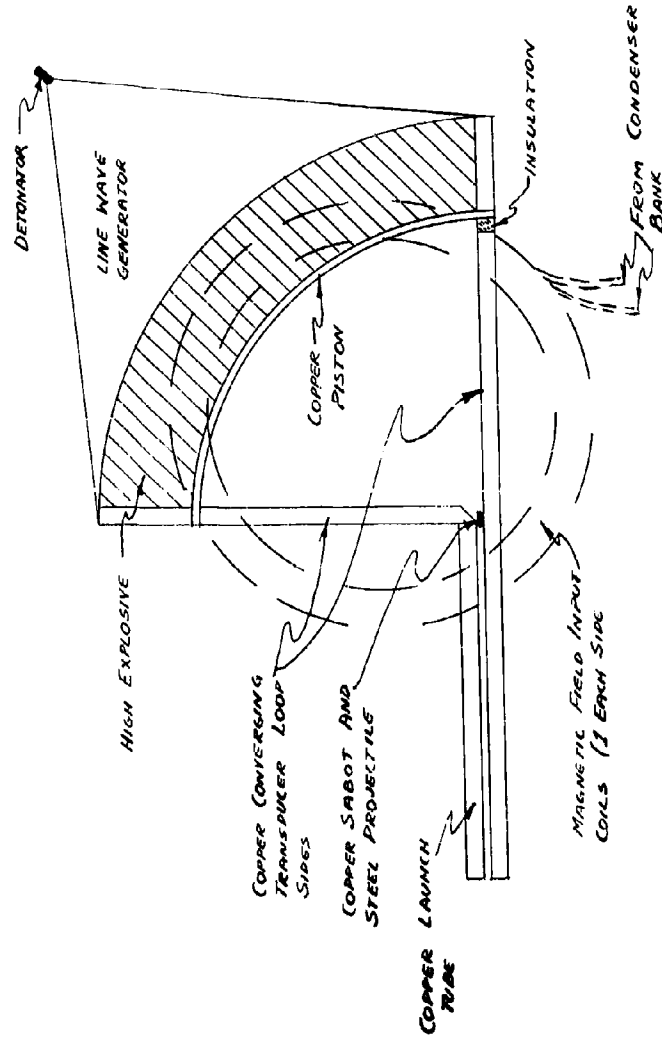


Figure 1

DIAGRAM OF MAGNETOHYDRODYNAMIC HYPERVELOCITY GUN

MAGNETOHYDRODYNAMIC GUN

reached. The peak pressure is of the order of 5 million psi. Up to 500 grams of composition C-3 explosive are used. Five hundred grams of composition C-3 has a stored chemical energy of about 2.5 megajoules. This energy is extracted from the explosive by the performance of PdV work on the magnetic field.

Analysis

The magnetic energy of the system is given by W_m where

$$W_m = \int_V PdV = \frac{1}{2} LI^2 \quad (1)$$

L = inductance of circuit

i = current

V = volume of magnetic field

P = pressure of magnetic field ($H^2/8\pi$ dynes/cm²)

Due to volume compression, work is done on the field, and for adiabatic compression

$$\frac{d}{dt} W_m = - \int_A P \vec{v} \cdot d\vec{S} \quad (2)$$

where

\vec{v} = velocity of compressing conductor

A = cross sectional area

Equations (1) and (2) combine to yield

$$\frac{d}{dt} (LI) = 0$$

or

$$LI = \text{constant}$$

which is merely the conservation of flux in a lossless magnetic system,

$$LI = \phi \quad (3)$$

where

ϕ = magnetic flux

Since the circuit has resistance, there are losses and Kirchoff's law applies. Thus, the sum of the voltages around the circuit must be zero, or, from Faraday's Law and Ohm's law,

$$\frac{\partial \phi}{\partial t} + RI = 0 \quad (4)$$

MAGNETOHYDRODYNAMIC GUN

which, in an elementary form, is the idealized circuit equation for a closed flux containing loop with moving boundaries.

Substituting Equation (3) into Equation (4), we have

$$\frac{\partial \phi}{\partial t} + \frac{R \phi}{L} = 0 \quad (5)$$

The solution of Equation (5) is $\phi = \phi_0 e^{-\int \frac{R}{L} dt}$

$$\text{or } LI = L_0 I_0 e^{-\int \frac{R}{L} dt} \quad (6)$$

Thus, I increases essentially linearly with decreasing L if the collapse time of the system $t \ll \tau = L/R$. The magnetic energy of the system $W_m = 1/2 LI^2$ will then increase exponentially.

From this expression, the current can be calculated for any loop motion once the inductance and resistance are known. The exponential term in Equation (6) is the loss term due to resistance heating of the conductor. This heating causes a corresponding increase of resistance, thereby loss of magnetic field. In equation form the heating is given by

$$\eta J^2 dt = \rho c dT \quad (7)$$

where

- η = resistivity
- J = current density
- ρ = mass density
- c = specific heat
- dT = temperature change

Using the approximation that $\eta = \eta_0 \frac{T}{T_0}$ (good for most metals up to the melting point), the terms in Equation (7) can be rearranged to give

$$\frac{dT}{T} = \frac{\eta_0}{\rho c T_0} J^2 dt$$

which has the solution

$$\ln T/T_0 = k \int J^2 dt \quad (8)$$

MAGNETOHYDRODYNAMIC GUN

where $k = \frac{\eta_0}{\rho c T_0}$ (k is nearly constant for most metals up to the melting point)

Equations (6) and (8) can be used in an iterative process to calculate the performance of the magnetohydrodynamic hypervelocity gun.

Once the sabot begins to move, a correction must be applied to the inductance profile, which includes the inductance added by the sabot motion. Also, deceleration of the piston due to magnetic field pressure must be accounted for. Because the loop is a converging system, and the sectional density of the piston increases as it travels, this effect is not serious. Although the temperature of the sabot rises to large values, it can be shown from the equation of thermal conduction that in the times involved, the temperature increase of the projectile is only a few degrees.

Numerous combinations of parameters were calculated to determine theoretical feasibility of the magnetohydrodynamic hypervelocity gun. These were done not only for the converging system just described, but also for loops of rectangular shape. Although a satisfactory combination of parameters was found for the rectangular loop system, it is generally conceded that the converging system offers the greatest potential of reaching high velocity. This is primarily because piston deceleration in the converging loop is much less than in the rectangular loop, thus higher peak field strengths are attainable. The converging loops which have been used have an arc radius of 12 cm and a piston thickness of 2 mm, and contain 500 gm of explosive. The calculated profile of Magnetic Field Strength vs. Time is shown in Figure 2a. Figure 2b is the calculated Projectile Velocity vs. Time for an accelerated mass area density of 0.5 gm/cm².

Design

Engineering design of the hypervelocity gun system is based primarily on hydrodynamic considerations. A photograph of the assembly is shown in Figure 3. The material used in loop and launch rail construction is copper. The design must provide for proper shearing of the copper piston, and good initial contact when the piston shears off and closes the circuit. Because of the thickening action of the piston, it is necessary to enclose the loop with side pieces of a relatively high density material which is also non-conductive. Epoxy loaded with lead powder has been used for this and for tamping of the explosive charge. An explosive efficiency of 20% is desired, so that 400 to 500 kilojoules of energy will be available to the sabot and projectile. This has been achieved in the laboratory.

Description of Experimental Facility

A steel containment tank was designed so that the explosive could be fired in a building which is located in a populated area. This tank is shown in Figure 4. It is a cylinder three feet in diameter and has a wall thickness of 3/4 inch. One end of the tank is a one inch thick dome from which the evacuated barrel and target chamber projects.

MAGNETOHYDRODYNAMIC GUN

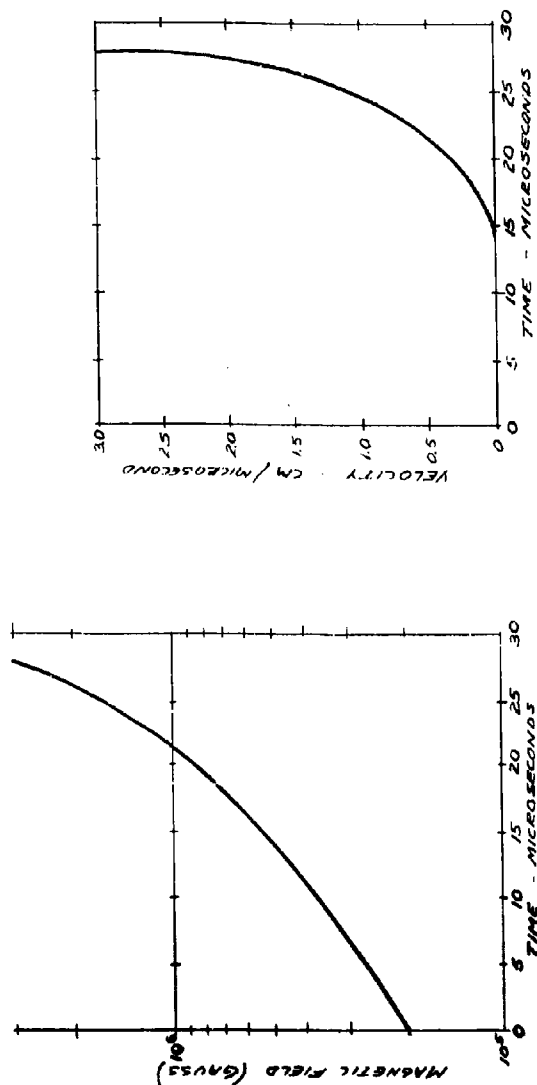


Figure 2-b

PROJECTILE VELOCITY vs. TIME

Figure 2-a

MAGNETIC FIELD STRENGTH
AT SABOT vs. TIME

MAGNETOHYDRODYNAMIC GUN



Figure 3

MAGNETOHYDRODYNAMIC HYPERVELOCITY GUN ASSEMBLY

MAGNETOHYDRODYNAMIC GUN



Figure 4

EXPLOSION CONTAINMENT TANK

MAGNETOHYDRODYNAMIC GUN

The other end is a two inch thick steel door which is attached to the tank by a ring of close spaced one inch diameter bolts. The overall length of the tank is five feet. Inside the tank are a 1/4 inch thick shrapnel liner and wood staves for slowing the high velocity fragments which result from the explosion. Instrumentation cables are lead out through a port in the side of the tank and the energizing current for the initial magnetic field is lead in through another port. A 30 kilojoule condenser bank provides the current for the initial magnetic field. Figure 5 is a plan view drawing of the experimental facility. The tank and the condenser bank are enclosed in a concrete block room. Outside the room is a barrier wall with the control station on the other side. A single rack cabinet houses the condenser bank charging and control equipment, vacuum control, and timing and firing systems. Instrumentation and other items of electronic equipment are housed in the additional racks. Mechanical and electronic sequence timers automatically operate all functions of an experiment from the closure of a single remotely located switch.

Results of Experiments

Fifteen experiments have been conducted so far in the program. Several of these were designed to check the theory. Others were designed to achieve a particle impact on a target. Some have suffered from malfunctions of instrumentation or other equipment, or failure to trap the initial magnetic field.

An important measurement was the velocity of the piston. This was necessary to confirm the predicted explosive energy to piston kinetic energy efficiency. Figure 6 is a plot of Piston Position vs. Time as measured in a typical experiment. This shows a velocity of 4.2 mm/ μ sec on a 62.3 gram piston, using 500 grams of explosive. The measured efficiency was 22.3%, which compares well with the predicted value of 20%.

Measurements of magnetic field strength and projectile velocity have also been made. The maximum peak field which has been achieved is 2 megagauss (2.4×10^6 psi pressure). The highest velocity which has been reached is 9.5 kilometers/second. This is shown in Figure 7, which is a plot of Projectile Position vs. Time as measured in that experiment. The peak acceleration measured from this curve was 132 mega g.

The experiments at high velocities have suffered from fragmentation of the projectile, possibly because of acceleration forces, but most probably because of the method of velocity instrumentation then used. A number of lower energy shots were fired to show that single particle impact could be attained by this acceleration method. These experiments were successful and craters have been produced in aluminum targets from three shots. Diagnostics have been minimal and additional equipment is now being acquired. Future experimental work will be detailed rather than exploratory in nature.

MAGNETOHYDRODYNAMIC GUN

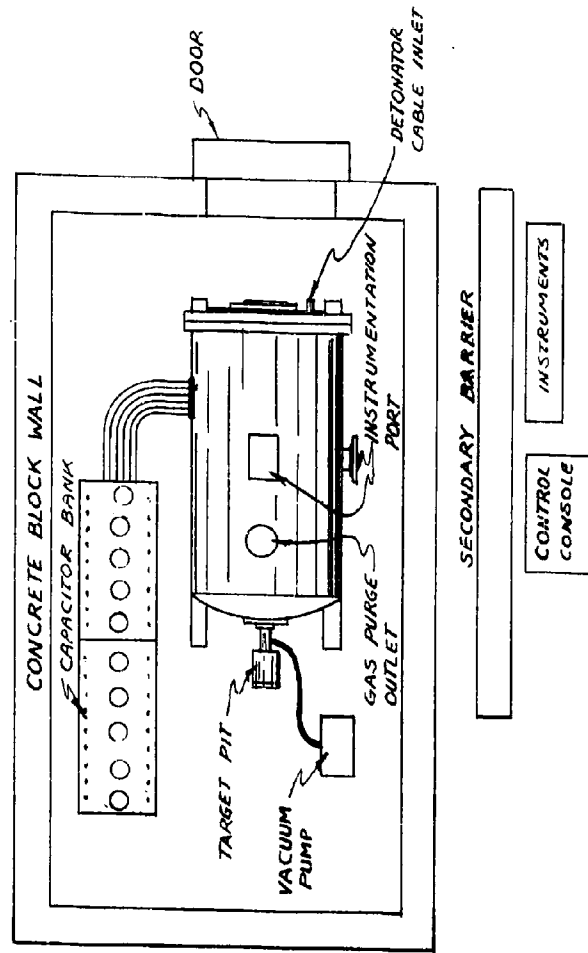


Figure 5

MAGNETOHYDRODYNAMIC HYPERVELOCITY GUN - EXPERIMENTAL FACILITY

MAGNETOHYDRODYNAMIC GUN

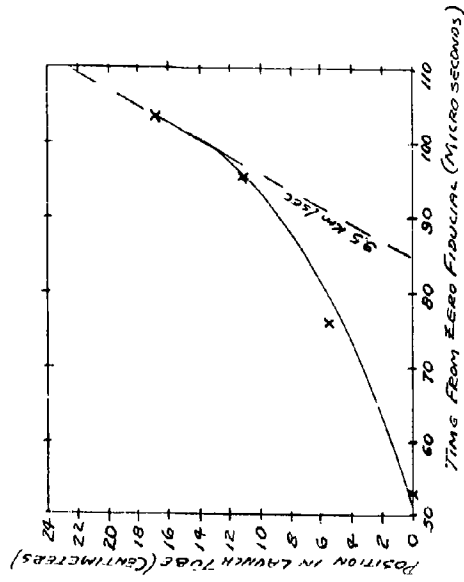


Figure 7
Projectile Position vs. Time
(best experiment)

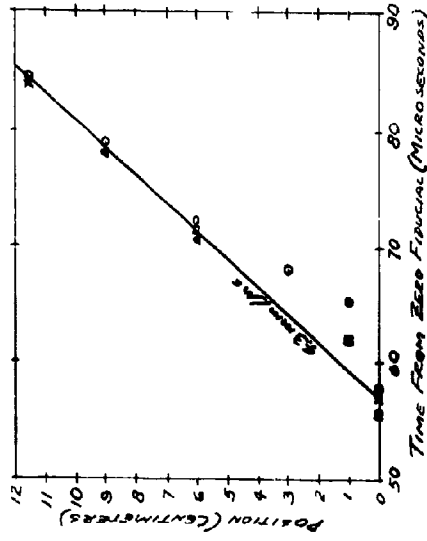


Figure 6
Piston Position vs. Time
(typical experiment)

MAGNETOHYDRODYNAMIC GUN

Conclusions

The results of the experiments fired to date are encouraging. It is reasonable to believe that the desired objectives will be obtained. Sabot heating and acceleration forces are serious, but not insoluble, problems. The current experimental program concerns the acceleration of small single particle projectiles (of the order of 10 mg) with average accelerations of about 20 mega g's.

BALLISTIC RESEARCH LABORATORIES

IMBEDDED JET CHARGE

G. Kronman
A. Merendino

INHIBITED JET CHARGE

ABSTRACT

In order to predict damage effects from impacts on space vehicles, a projection device capable of producing realistic mass and velocity levels is required. To achieve the more realistic impact conditions, an explosive projection device was developed at the BRL that utilizes the jet-forming properties of shaped charges. This device has been named the Inhibited Jet Charge and is basically a shaped charge in which the conventional non-steady state jet is inhibited such that only the leading particle is permitted to strike the target.

By application of known principles of shaped charge cone angle geometry and of scaling laws, inhibited jet charges have been developed that project aluminum pellets of masses ranging from 0.5 gram to 50 grams at velocities ranging from 7.6 km/sec to 11.7 km/sec. Pellet masses of several hundred grams are considered feasible with this device. Also preliminary tests have indicated that copper and steel pellets can also be provided.

INHIBITED JET CHARGE

I. INTRODUCTION

The development of explosive projection techniques is continuing at the Ballistic Research Laboratories to provide more realistic impact conditions for hypervelocity studies. In earlier studies^{1,2} such designs as the straight-ended and air-cavity charges were found inadequate for providing the mass and velocity necessary for certain aspects of hypervelocity research. To achieve more realistic impact conditions, the explosive projection techniques under current development exploit the high velocity jet-forming properties of shaped charges.

One shaped charge technique with the potential for high mass-velocity projection is the inhibited collapse charge. This principle was first studied by a group at CTF in 1952³. In the early studies, attempts were made to isolate a single jet particle by use of an inert plug placed within the conical liner. The plug was intended to allow the upper portion of the liner to form a conventional jet while inhibiting collapse of the remainder of the liner.

A single particle however was never achieved, however. In subsequent work at BRL, Zernow⁴ recognized the value of an inhibited jet pellet for hypervelocity application. Although several promising approaches were tried, a fully successful charge design was not evolved.

The success of the present inhibited-jet design was made possible

INHIBITED JET CHARGE

in part by additional knowledge of the jet-formation process obtained from shaped charge research based on radioactive tracer studies¹. From these studies, it has been possible to identify various portions of the liner as the sources of corresponding jet elements. The studies indicated that, for an unconfined charge, almost ninety percent of the effective armor penetration is provided by the lower half of the liner. The area of the cone for which the collapse must be inhibited was thus more clearly defined and a workable inhibited jet charge was designed^{*}. The charge design was used in studies to determine the mass velocity combinations that can be effectively produced. Application of known principles of shaped-charge cone angle geometry and of linear scaling laws has yielded results consistent with predictions. Preliminary results have been obtained indicating the feasibility of using various liner materials as the source of pellets.

II. BASIC CHARGE DESIGN

The basic inhibited charge design is shown in Figure 1. The special spit-back tube aluminum liner has the advantage of producing a jet with a massive symmetrical leading particle. The jet is shown in Figure 2. The radiograph shows the jet tip after approximately 42 inches of travel indicating that symmetry is maintained

^{*} BRL report being prepared

INHIBITED JET CHARGE

over on appreciable distance of travel. The entire leading particle of the jet or a portion of the leading particle can be isolated from the jet by an appropriately designed lucite ring or inhibitor. The ring is inserted at the base of liner as shown in Figure 1. The inhibitor controls the collapse of the liner such that only the front portion of the jet is formed. Also by use of a suitable size hole in the lucite ring, a preselected portion of the jet can be obtained. The length of the leading particle, however, is more easily controlled by varying the height of the inhibitor and maintaining a constant hole diameter. The semi-circular increment of explosive located at the base of the main charge (Figure 1) is used to deflect slag material formed by the upper liner wall. The slugs shown in Figure 3 have an estimated velocity of 1.5 and 1.0 km/sec. In target impact studies, the jet is allowed to pass through a hole in a baffle plate designed to absorb the impacts of the deflected slugs. As indicated earlier, the length of the leading jet particle can be controlled by varying inhibitor height. The degree of control is illustrated in Figure 4 which shows the leading jet particles obtained with inhibitor heights ranging from 1.0 to 1.375 inches. **The 1.25 inch inhibitor height has been incorporated in the standard design.**

Other factors that influence the length of the leading particle are ablation and an apparent reverse velocity gradient (decrease in

INHIBITED JET CHARGE

velocity from tip to back). The gradient is suggested by the change in pellet geometry during flight as shown in Figure 5. The two successive radiographs cover a pellet travel distance of 17 inches. The increase in pellet diameter coinciding with a reduction in length suggests the presence of a reverse velocity gradient. Ablation, of course, is a primary cause of pellet shortening. As a consequence of velocity gradients and ablation the pellet aspect ratio will vary with target distance. With the standard design, a target distance of 42 inches results in a pellet with an aspect ratio of approximately 2.5. The mass of the pellet is 3.7 grams and the average velocity is 9.6 km/sec.

III. PELLET VELOCITY

The velocity of the inhibited-jet pellets can be controlled over an appreciable range by varying the liner cone angle. When the angle is varied, the pellet geometry remains fairly uniform, provided the inhibitor height is adjusted accordingly. The pellet velocities measured for different cone angles are plotted in Figure 6. The liner was aluminum of 0.125 inch wall thickness with the spit-back tube configuration shown in Figure 1. A constant explosive head of 1.25 inches was maintained for all charges.

The pellet velocity of 7.6 km/sec obtained with the 60° liner is not considered a lower limit, since it appears feasible to obtain lower velocities with larger cone angles. At the upper velocity extreme, present evidence indicates that the 25° liner may be a practical limit for the present charge design. Tests conducted with a 20° liner produced the expected higher velocity; (11.7 km/sec) however, a useable pellet was not formed as indicated in

INHIBITED JET CHARGE

Figure 7. It may be possible by a suitable apex design, to exploit the narrow angle cones in order to extend the velocity range.

IV. PELLETT MASS

For the velocity range shown in Figure 6, the pellet mass can be varied by scaling the basic charge dimensions. The jets produced by half-scale and double-scale models are shown in Figure 8. The standard scale jet is included for comparison and the radiographs were taken at distances scaled for each size. The expected velocity of 9.6 km/sec was obtained in all cases. It is seen that the leading jet particles scale linearly and inhibiting these jets will provide pellet masses ranging from 0.5 gram for the half-scale model to 50 grams for the double-scale model. Pellet masses of several hundred grams can be provided by larger charges.

V. PELLETT MATERIAL

The charge designs considered up to the present time have been those providing aluminum pellets. Designs for projecting pellets of other materials are being investigated. Preliminary tests with copper and steel liners have indicated that pellets of these materials can be produced provided the inhibitor design is modified. Figure 9 shows the copper and steel pellets obtained with standard scale liners. (37° apex angle, 0.12 in. wall thickness). For the pellets shown in Figure 9, the deflector charge was not used. A sketch of the

INHIBITED JET CHARGE

modified inhibitor design used to obtain these pellets is included in the figure. The copper pellet has a velocity of 7.5 km/sec and an estimated mass of 2.4 grams; the steel pellet a velocity of 7.8 km/sec and the estimated mass is 1.2 grams. It is expected that cleaner pellets will be obtained when the deflector charge is used.

V. CONCLUSIONS

It has been shown that the inhibited jet charge is a useful projection device for hypervelocity studies. Its potential for projecting several pellet materials at a wide range of mass and velocity levels has been demonstrated.

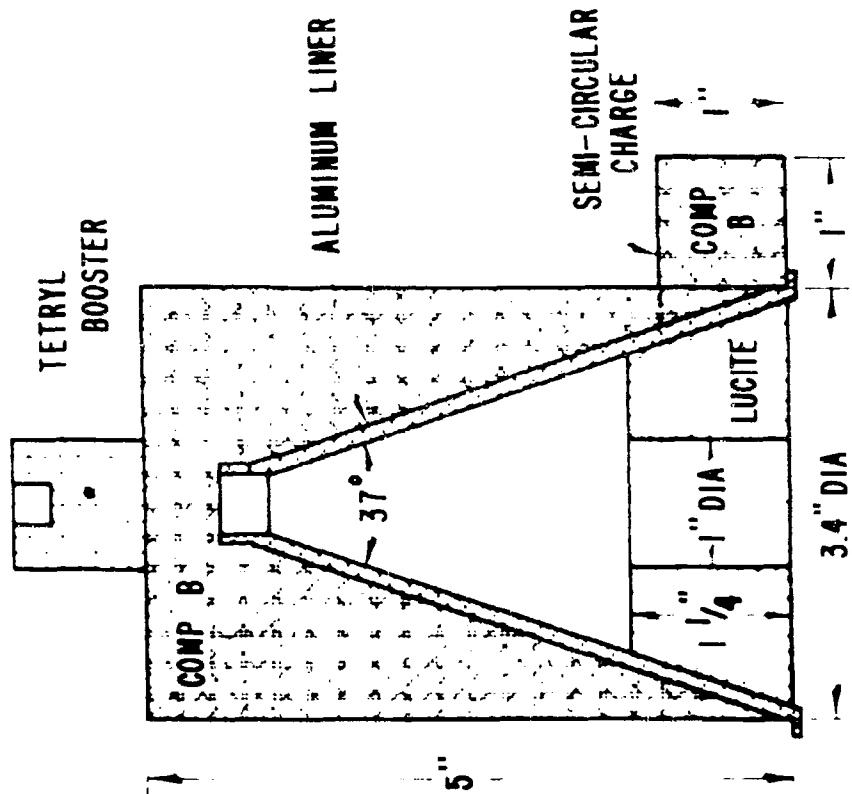
Studies are continuing in order to increase pellet velocities by liner geometry variation. Also under investigation are methods of obtaining the large pellet masses from relatively smaller charges.

INHIBITED JET CHARGE

REFERENCES

1. Kineke, J. H., Jr., "Proceedings of Fourth Symposium on Hypervelocity Impact".
2. Kronman, S., and Kineke, J. H., Jr., "Proceedings of Fifth Symposium on Hypervelocity Impact".
3. Eichelberger, R. J., Linder, C. T., and Allison, F. E., "Fifth Bi-monthly Report (CIT-ORD-40) Fundamentals of Shaped Charges" August 31, 1952, Contract No. DA-36-061-ORD-122.
4. Zernow, L., "Proceedings of the Rand Symposium on High-Speed Impact" May 1, 1955.
5. Gainer, M. K., "The Application of Radioactive Tracers to Shaped Charge Levers", BRL Memorandum Report No. 1242, January 1960.

INHIBITED JET CHARGE



INHIBITED JET CHARGE
FIGURE I

INHIBITED JET CHARGE



ALUMINUM JET

INHIBITED JET CHARGE



FIGURE 3

INHIBITED JET CHARGE

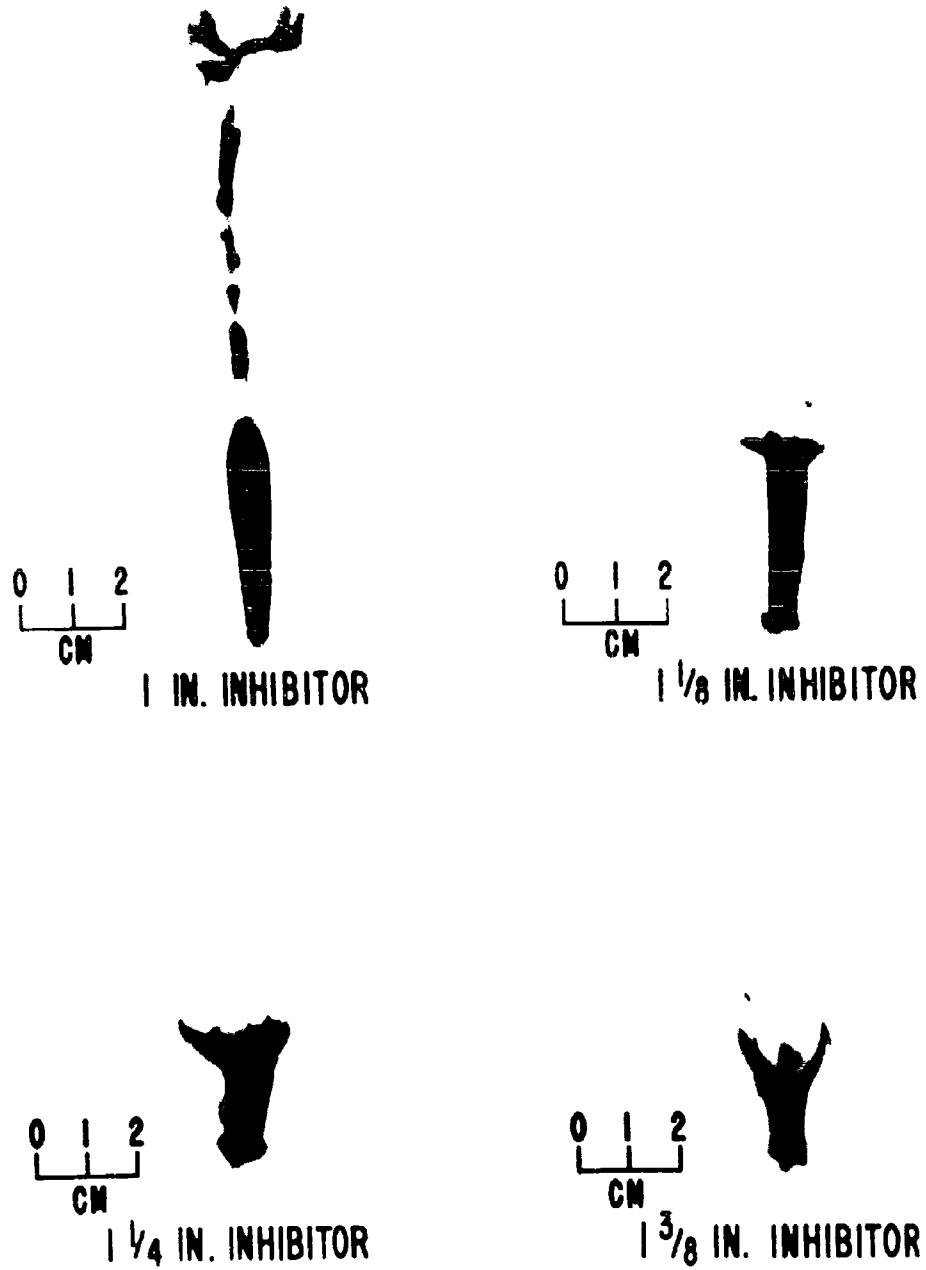
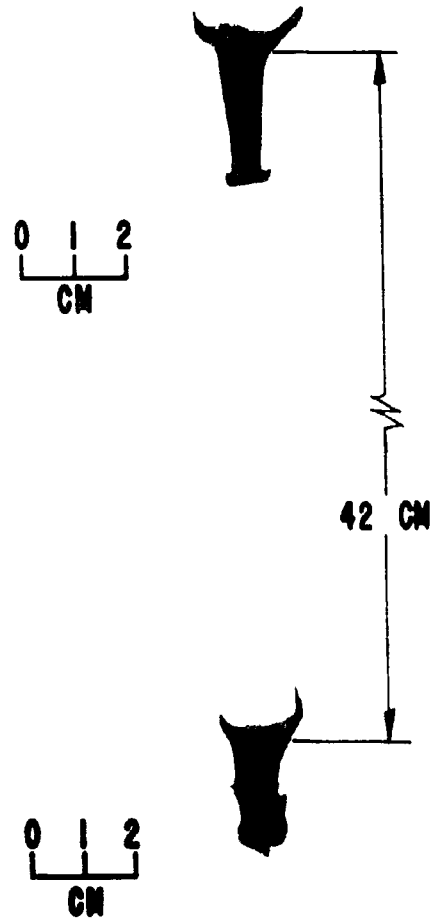


FIGURE 4

INHIBITED JET CHARGE



ALUMINUM

FIGURE 5

INHIBITED JET CHARGE

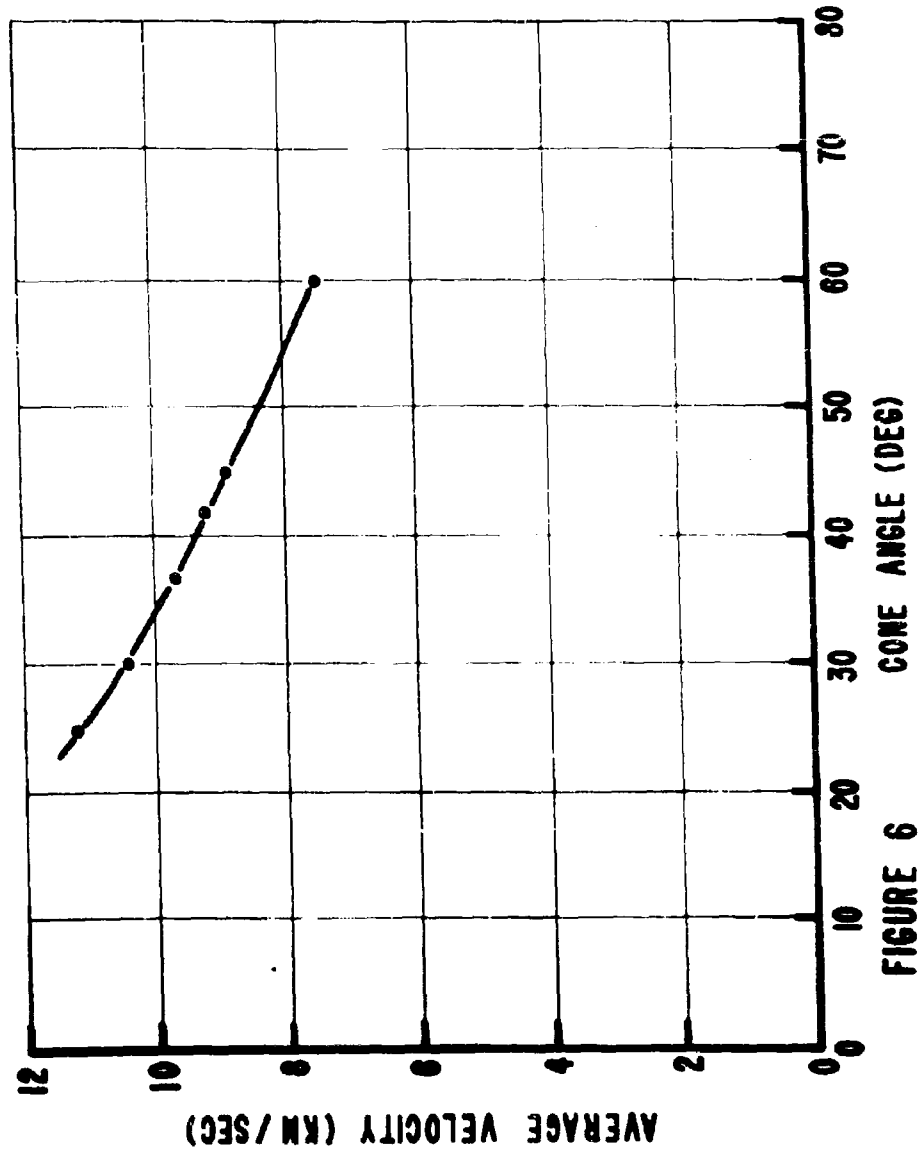


FIGURE 6

INHIBITED JET CHARGE

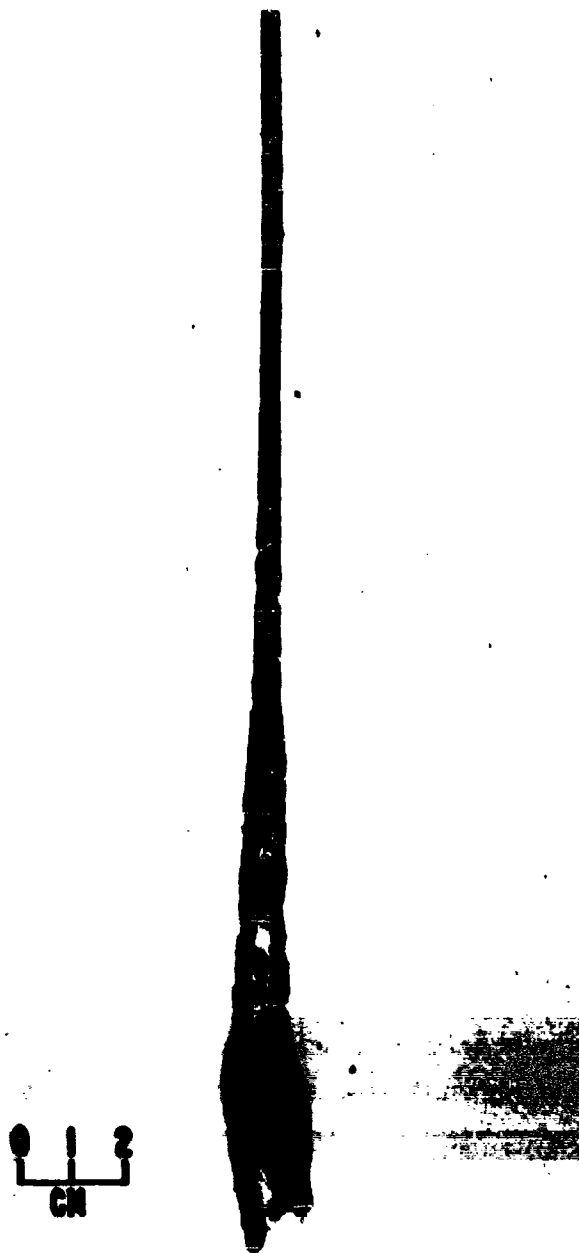


FIGURE 7

INHIBITED JET CHARGE

INHIBITED JET CHARGE



FIGURE 8



INHIBITED JET CHARGE

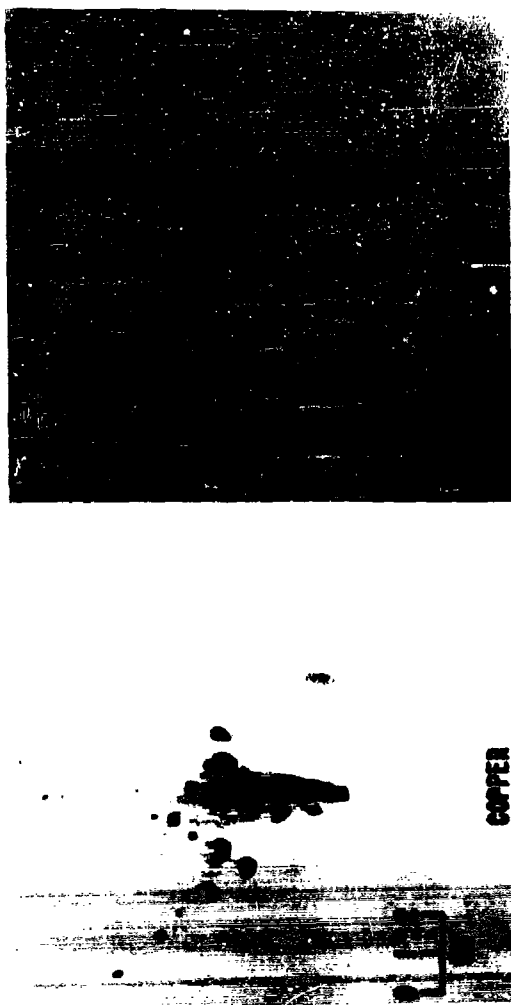
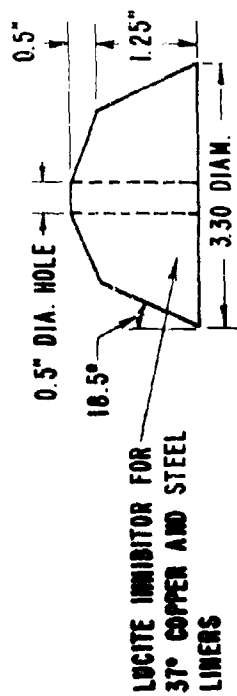


FIGURE 9

SPECIAL EXPLOSIVE PROJECTORS

I. SHAPED CHARGE ACCELERATOR

II. TARGET PLATE ACCELERATOR

K. N. Kreyenhagen
J. E. Ferguson
R. R. Randall
J. P. Joyce

AEROJET-GENERAL CORPORATION
Ordnance Division
11711 Woodruff Avenue
Downey, California

SPECIAL EXPLOSIVE PROJECTORS

I. SHAPED CHARGE ACCELERATOR

II. TARGET PLATE ACCELERATOR

K. N. Kreyenhagen
J. E. Ferguson
R. R. Randall
J. P. Joyce

Aerojet-General Corporation
Downey, California

SUMMARY

Two explosive accelerator techniques have been developed for gathering hypervelocity terminal ballistic data. Both of these techniques are based upon existing explosive phenomenology, adapted or modified as necessary for ballistic studies. The Shaped Charge Accelerator is currently being used to investigate impact phenomena for compact projectile shapes impacting individually at velocities in the range from 30,000 to 39,000 fps. Individual impacts are obtained by jet dispersion achieved through asymmetrical initiation. Individual projectile characteristics (velocity, shape, mass, orientation) are determined with multiple flash radiographs of the projectiles just prior to impact. It appears possible to launch Shaped Charge Accelerators with a large light gas gun, such as the 8-in./2.5-in. Atkins gun at NRL, and thereby to achieve impact velocities in the 20 km/sec range. The Target Plate Accelerator projects a flat plate which is allowed to impact a stationary "projectile" in its path. Damage to the plate is assessed by observing the plate in flight with flash radiographs subsequent to impact. This technique provides a unique means for studying impact effects of fragile or sensitive projectiles. Current accelerator designs provide impact velocities up to 3.5 km/sec.

SPECIAL EXPLOSIVE PROJECTORS

I. SHAPED CHARGE ACCELERATOR

At the Rand Symposium in 1955, Zernow⁽¹⁾ described some methods by which the inherent high velocity features of the explosive shaped charge might be adapted to the gathering of discrete impact terminal ballistic data, thereby providing a technique for conducting investigations in a velocity regime 2-3 times higher than was possible by other techniques available at that time. Over the past two-three years, under Contracts AF08(635)-975 and AF08(635)-2809 with the Air Proving Ground Center, Eglin AFB, we have successfully developed the technique, using one of the methods suggested, and have been utilizing it for terminal ballistic studies in the 30,000-39,000 fps range.

The basic shaped charge is normally a conical metal liner around which a cylindrical explosive charge is cast or pressed. Detonation is initiated at the end opposite to the conical cavity. As the detonation wave progresses down the charge, it exerts pressure on the liner, collapsing it to form a high speed jet and a slower slug of the liner material. With the normal charge design, this jet flies out as a plastically-deforming stem of metal. Upon impact, the jet causes the well-known deep penetration of targets.

To adapt the shaped charge to the gathering of single impact terminal ballistic data, the following must be accomplished:

- a. the continuous jet must be separated into individual identifiable fragments or projectiles (or, alternatively, the rear of the jet must be cut off, or inhibited)
- b. The individual fragments must be laterally dispersed so as to produce separate impacts on the target, and
- c. The velocity, mass, shape, and orientation of the fragments prior to impact must be determined.

1. Axial Separation

The jet which is formed by a conical shaped charge contains a velocity gradient due to the non-steady-state process by which it is formed. The jet therefore stretches until it breaks into fragments. These fragments, or projectiles, continue to separate as they fly. Dispersion in an axial direction is thereby achieved. This process is illustrated quite well in Figure 1, which shows a sequence of three radiographs, taken of an iron jet from a normal shaped charge as it elongates, breaks up, and separates.

SPECIAL EXPLOSIVE PROJECTORS



Figure 1. Radiograph Series
Showing Breakup of Iron Jet
from Normal Shaped Charge
(taken from ref. 1)

SPECIAL EXPLOSIVE PROJECTORS

2. Lateral Separation

For targets at short standoff, the fragments such as are shown in Figure 1 will all impact at nearly the same point. At long standoffs, the fragments will gradually disperse laterally, due to small deviation in velocity vectors caused by the breakup process. The desired individual impacts can therefore be expected on targets at long standoffs. However, this is not generally satisfactory, first because the evacuated firing chamber size becomes too great, and second, because instrumentation synchronization problems increase at longer standoffs.

As an alternative, we found that asymmetrical initiation was very effective in causing lateral dispersion of the jet fragments. Figures 2 and 3 show series of radiographs of asymmetrically-initiated aluminum and copper cones. Note that the emerging jets are distinctly deflected from the axis of the charge. Figure 4 shows a group of laterally dispersed fragments in flight several feet down-range from a shaped charge accelerator. Figure 5 shows a pattern of impacts from such a charge on a target plate at a range of 17 feet from the accelerator. Several of the holes are sufficiently separated so that they can be considered as individual impacts.

3. Projectile Characteristics

The initial breakup of the jet occurs in a more or less random fashion, with the gross characteristics being determined by the properties of the liner material. Jets of ductile, face-centered-cubic metals such as aluminum and copper fail by necking down at frequent intervals along the stretching jet. The projectiles which result therefore tend to be ellipsoids, or short cylinders with rounded ends. For a given material, the average mass of the projectiles will be determined by the cone angle and thickness of the liner. The range of masses and shapes, however, is relatively large, even for the fragments in one test. Hence it is mandatory that the characteristics of each projectile which is to be used in obtaining an impact data point must be accurately determined prior to impact.

The projectile characteristics of interest are the velocity, mass, shape, and orientation. High speed photography or radiography are suitable for measuring these characteristics.

SPECIAL EXPLOSIVE PROJECTORS

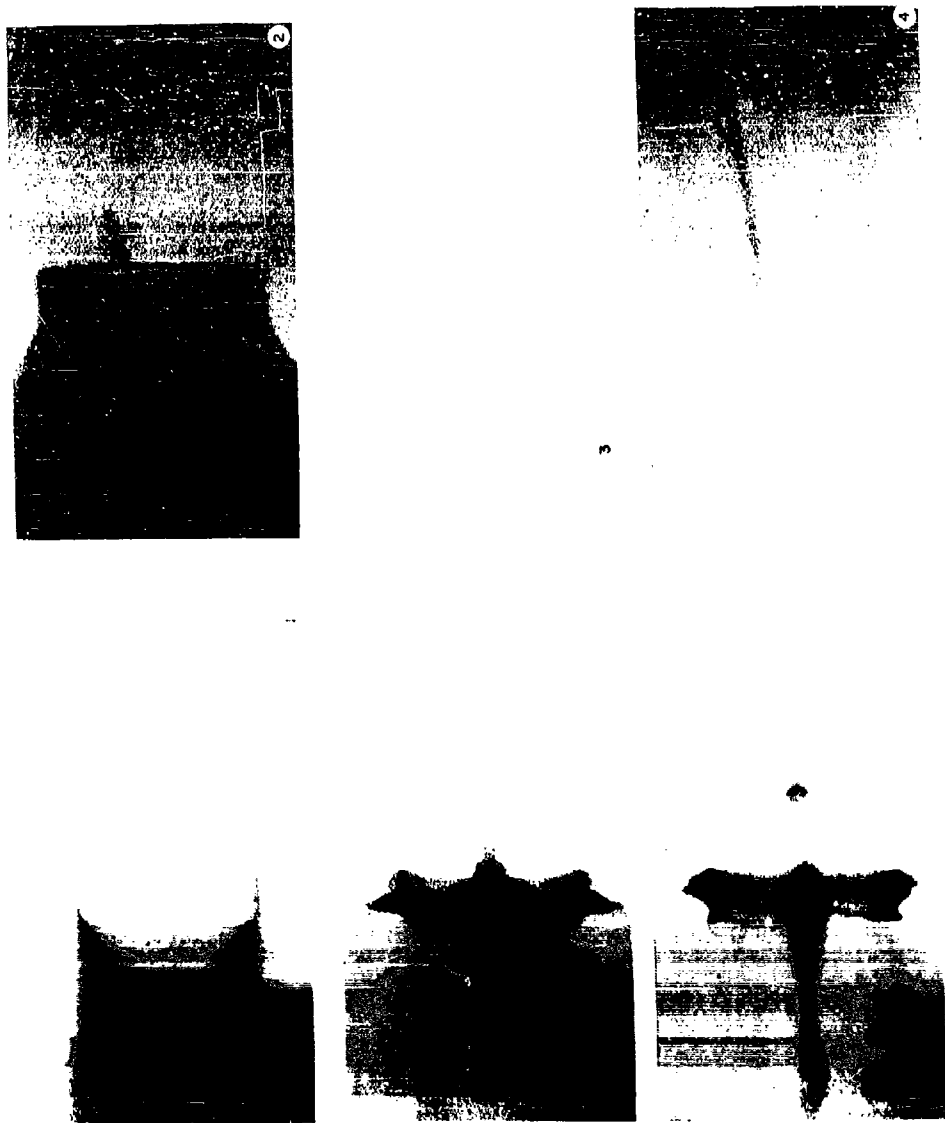


Figure 2. Radiographs Showing Development of Aluminum Jet from Asymmetrically-Initiated Shaped Charge.

SPECIAL EXPLOSIVE PROJECTORS

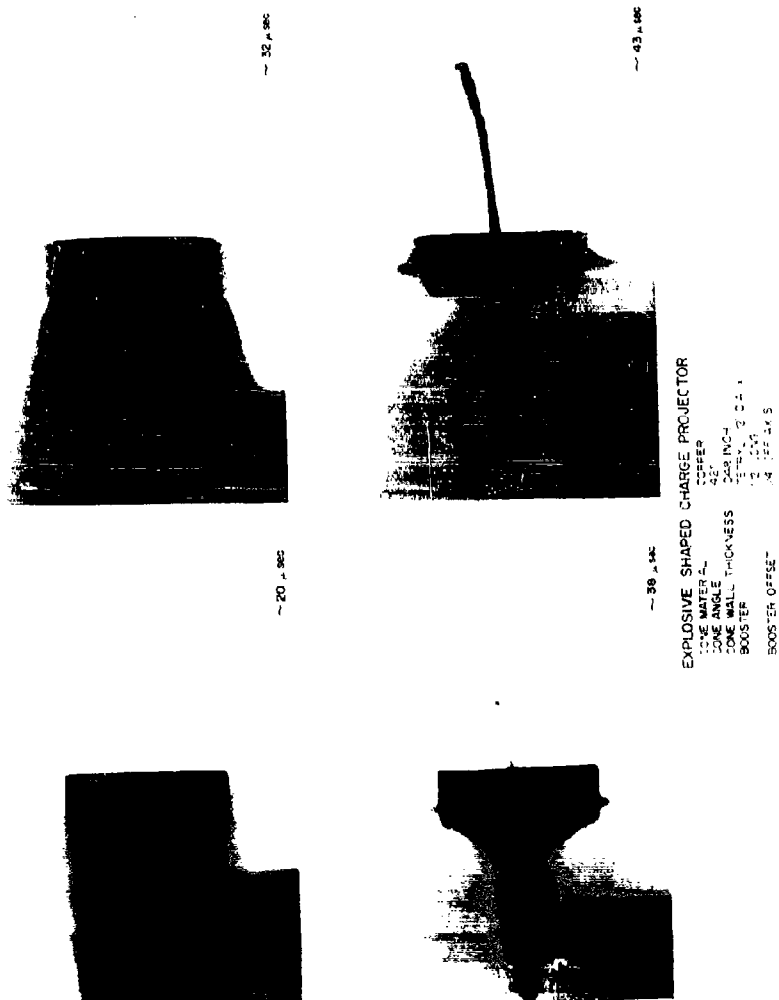


Figure 3. Radiographs Showing Development of Copper Jet from Asymmetrically-Initiated Shaped Charge.

SPECIAL EXPLOSIVE PROJECTORS

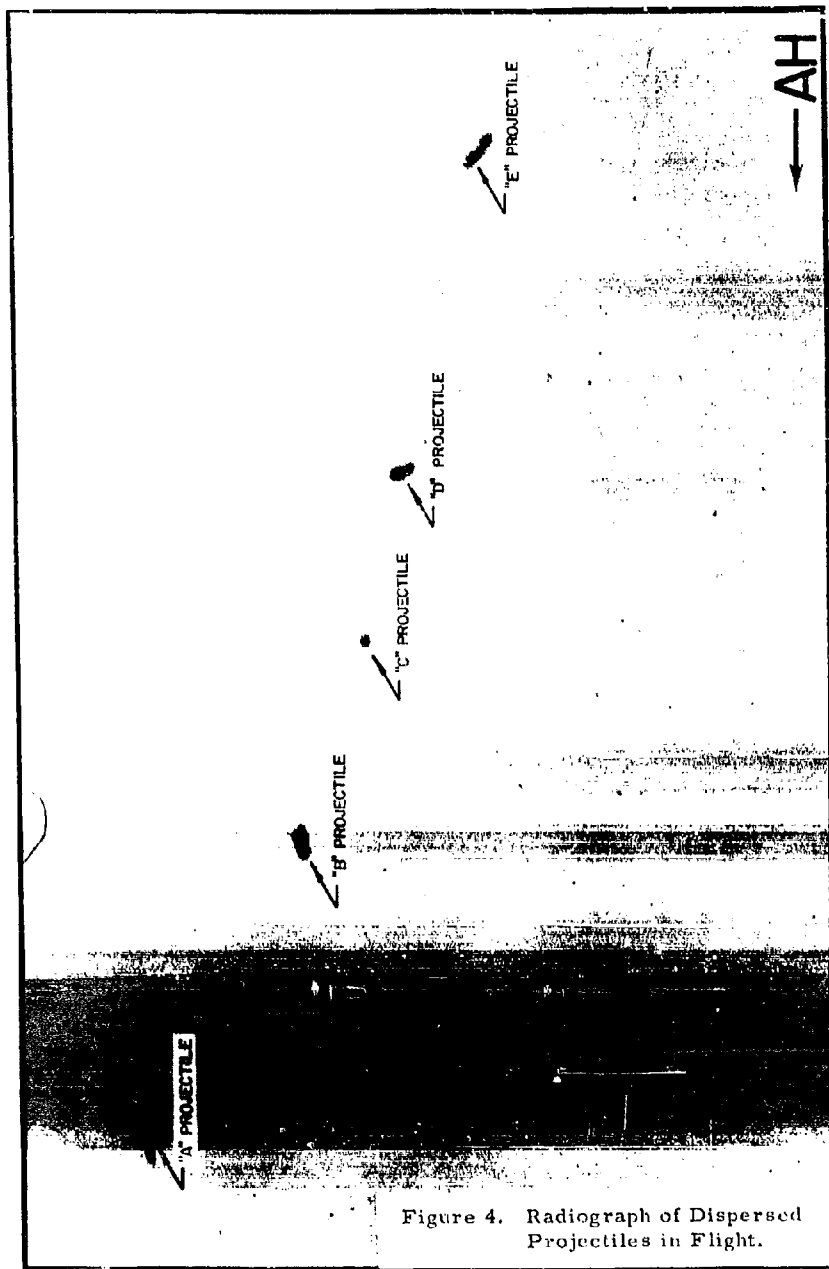


Figure 4. Radiograph of Dispersed Projectiles in Flight.

SPECIAL EXPLOSIVE PROJECTORS

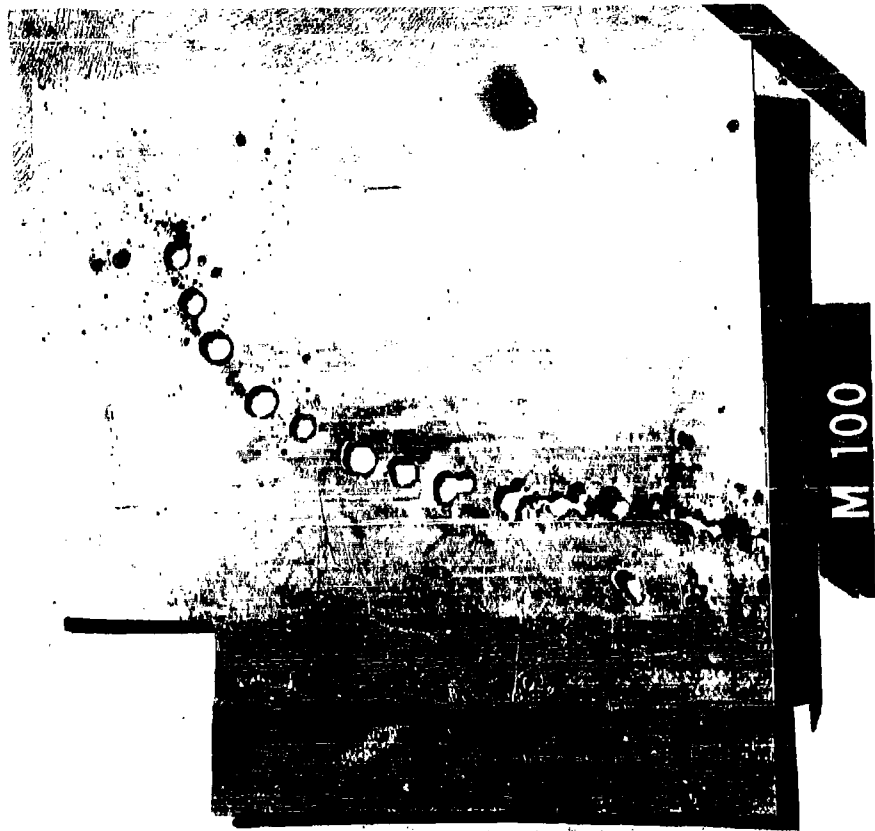


Figure 5. Dispersion of Impacts on Target Plate.

SPECIAL EXPLOSIVE PROJECTORS

The framing camera has the advantage of providing a large number of exposures so that the projectile can be recorded at several points and the impact itself can be observed. The following factors, however, must be considered if a framing camera is used:

- a. The projectiles must be intensely backlighted
- b. To avoid self-luminescence (from ionization due to ablation) the jets must be fired in a very low pressure environment.
- c. A continuous writing camera (such as the Beckman and Whitley Model 192) must be used in order to avoid serious synchronization problems.
- d. A sufficiently short exposure time must be available to assure a clear image of projectiles moving at 10-15 km/sec. To illustrate the magnitude of this problem, at 12 km/sec, a 0.5-cm long projectile moves a distance approximately equal to 1/4 of its length in 0.1 microsecond. The resultant poor definition of projectile boundaries would introduce large errors in the determination of projectile mass.

The alternative instrumentation technique, multiple flash radiography, avoids some, but not all, of the framing camera problems. In our experiments, 100 kv Field Emission Model 730-4-C-231 Flash X-Ray Units are used to obtain shadow-radiographs of the projectile in flight. These units emit x-rays over a duration of approximately 0.03 microseconds. At each of two stations uprange of the target, a pair of x-ray tubes are so arranged as to obtain simultaneous orthogonal views of the projectiles. Correlation of target holes or craters with corresponding x-ray shadow-graph images is performed on the apparatus sketched in Figure 6.

The shape and mass of the individual projectiles are measured from the four profile views which are obtained. Velocity is measured from the displacement of each projectile which occurs during the time between stations. Orientation is observed on the radiographs taken closest to the target just prior to impact.

On the basis of an error analysis, we believe that this technique permits determination of the mass of solid, simple-shaped projectiles to within approximately $\pm 10\%$. Projectiles which are hollow, which have reentrant sections, or which are otherwise irregular in shape are very difficult to assess by this technique. We therefore examine the x-ray shadowgraphs carefully for suspicious density gradients or other evidences of irregularity, and discard such projectiles.

SPECIAL EXPLOSIVE PROJECTORS

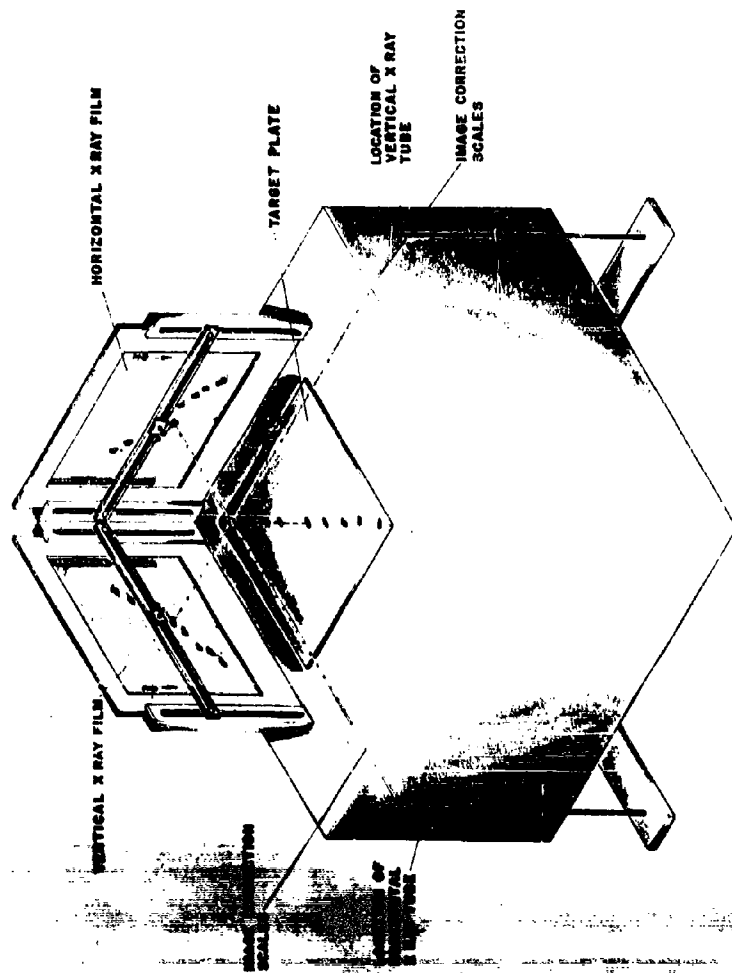


Figure 9.
TARGET - X RAY CORRELATION
APPARATUS

SPECIAL EXPLOSIVE PROJECTORS

4. Over-All System

Figure 7 shows the over-all arrangement of our firing and instrumentation system. The asymmetrically-initiated charges are fired through a thin mylar diaphragm into an evacuated chamber. Preset timing triggers the two x-ray tubes at the first instrumentation station to obtain the first orthogonal pair of radiographs. The tubes at the second station (at the target) are triggered either by preset timing or by impact of the fastest projectile on the target surface.

A typical shaped charge for these experiments is shown in Figure 8. This is a 42° cone, which accelerates projectiles to a maximum velocity of about 33,000 fps. For velocities up to 39,000 fps, we use a 25° cone angle design. Cone angles less than 25° should produce higher velocities, but we have generally found that the projectiles which are formed are not useful from a terminal ballistic standpoint. Designs employing detonation wave shapers show the greatest promise for achieving higher velocities in the future.

Figure 9 illustrates the over-all results which are obtained from a successful test with this technique. Shown are a pair of orthogonal views of the projectiles in flight, together with the corresponding impacts on the target.

Approximately 75% of the tests performed will yield at least one impact data point. This means that the mass of at least one of the projectiles could be confidently established, and that this projectile could be correlated with a crater or hole on the target which is sufficiently separated from its neighbors to prevent significant interactions.

5. Typical Data

To date, this technique has been primarily utilized to study impact effects on thin plate targets. This work is reported in references 2 and 3, and also in another paper at this symposium⁽⁴⁾. Some experiments have also been performed against 4-inch thick aluminum targets at velocities from 29,000-33,000 fps. Data from these experiments are presented in one form in Figure 10, where they are compared with other experimental data and with Bjork's theoretical predictions. The observed scatter is primarily due to the fact that the data includes impacts of various shaped projectiles at various orientations.

SPECIAL EXPLOSIVE PROJECTORS

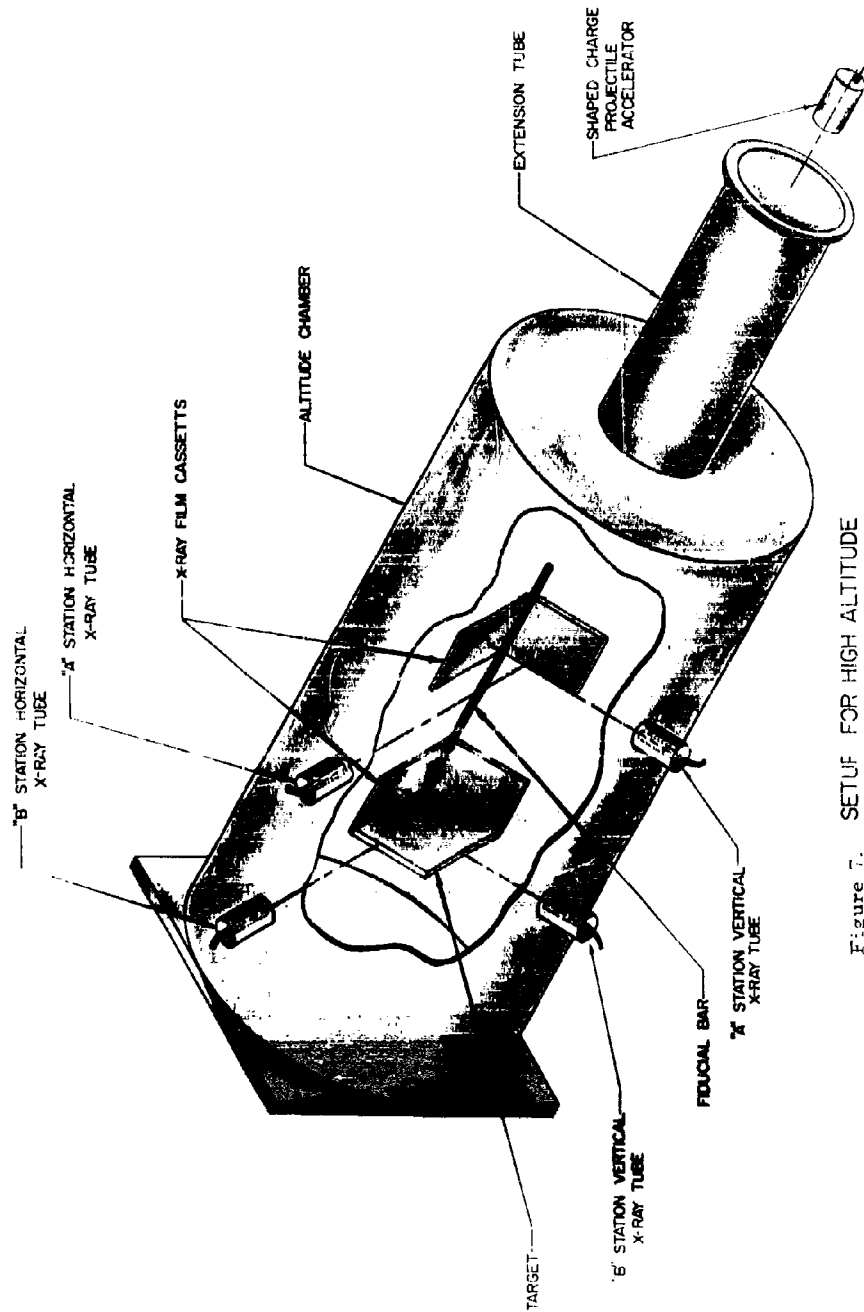


Figure 7. SETUP FOR HIGH ALTITUDE HYPERVELOCITY EXPERIMENTS

SPECIAL EXPLOSIVE PROJECTORS

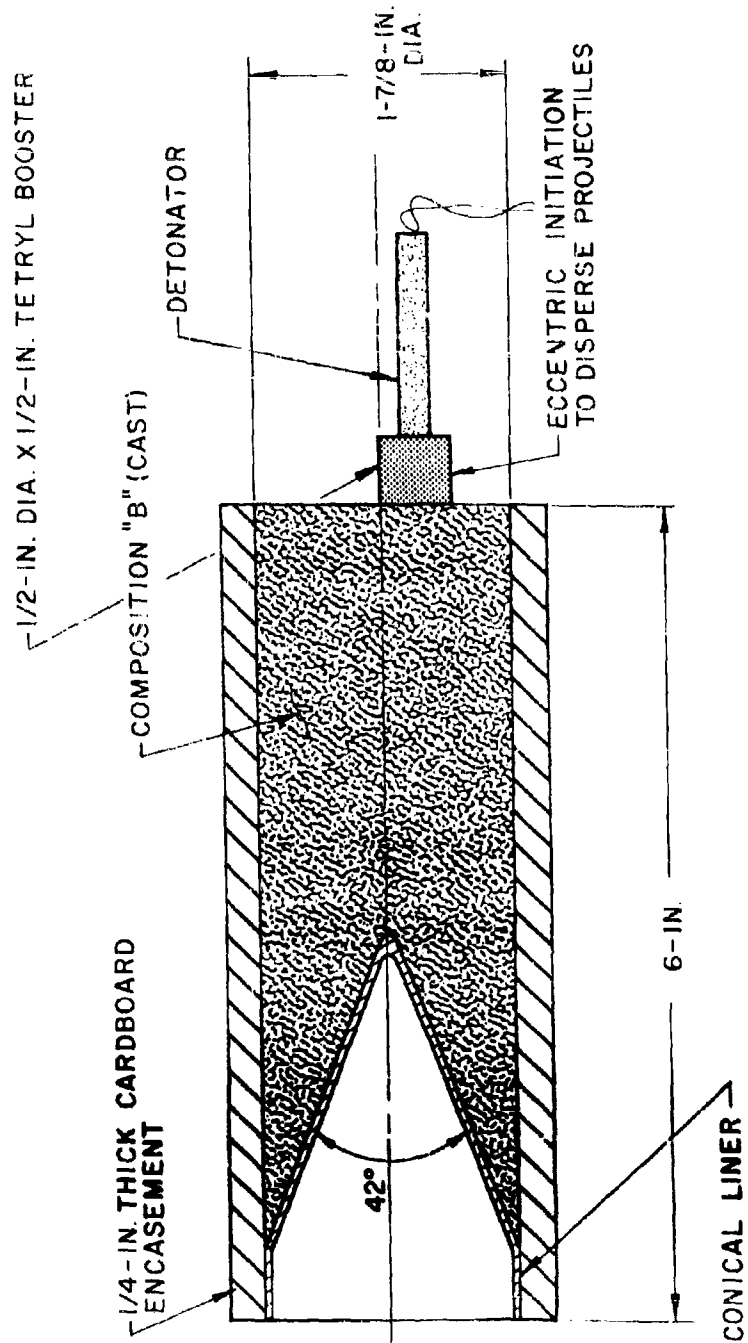
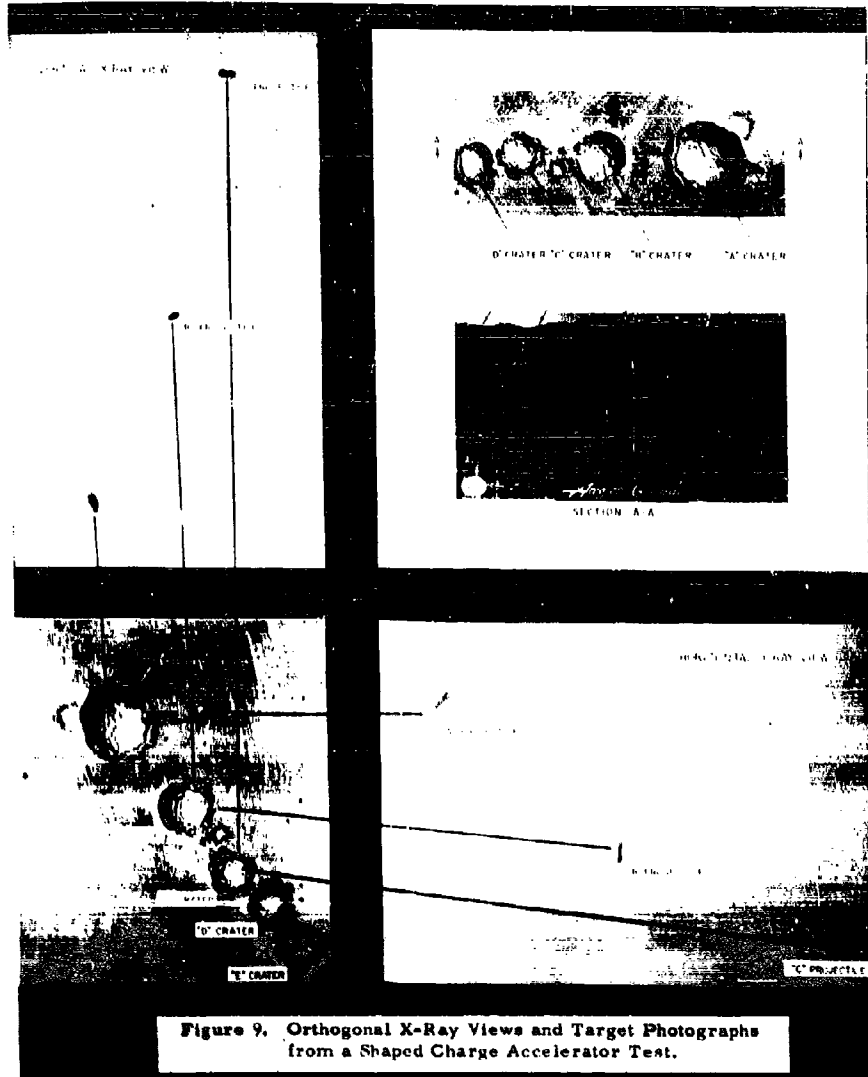


Fig. 8 - SHAPED CHARGE EXPLOSIVE PROJECTOR
EMPLOYING 42° LINER

SPECIAL EXPLOSIVE PROJECTORS



SPECIAL EXPLOSIVE PROJECTORS

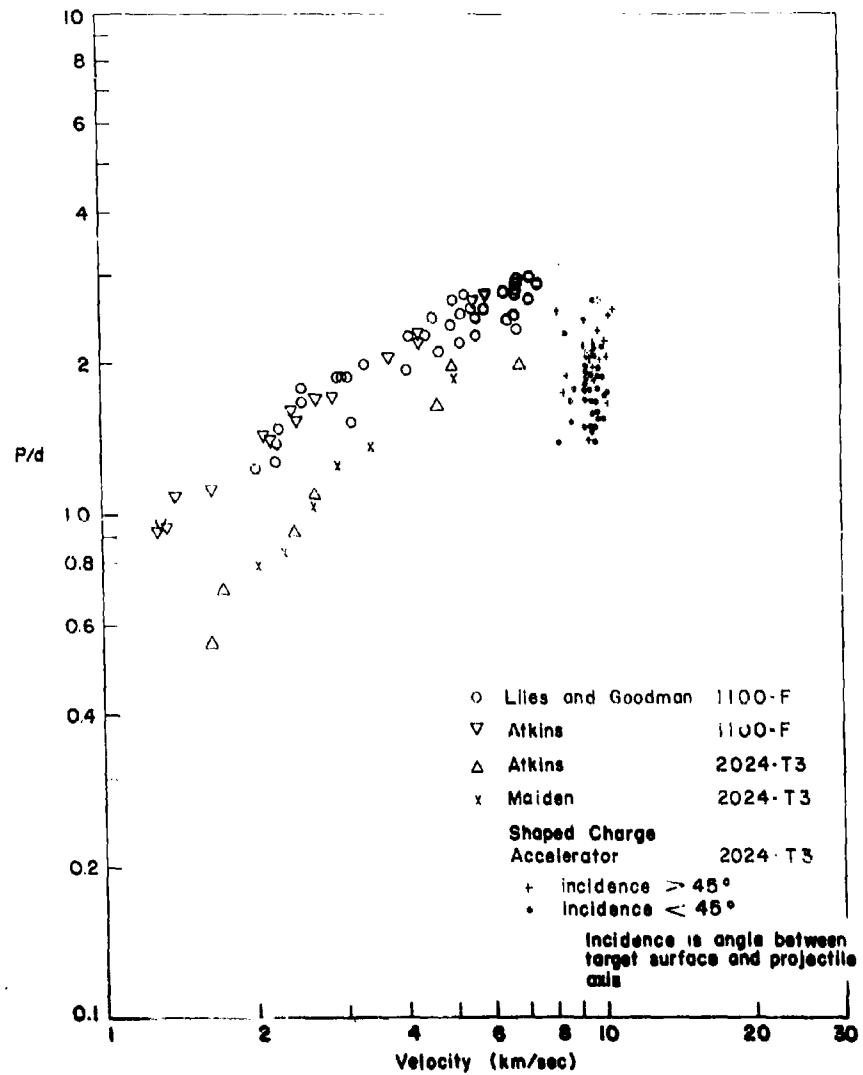


Fig.10 Normalized penetration versus velocity for aluminum into 1100-F and 2024-T3 aluminum targets

SPECIAL EXPLOSIVE PROJECTORS

5. A Proposed Method for Obtaining Data at 20 km/sec

Despite the optimistic assurances by many at the Fifth Symposium that accelerators were available or would be available for obtaining useful impact data at 20 km/sec, it now appears that this velocity is far from being achieved. Indeed, no significant amount of data is known to be available beyond that obtained with the Shaped Charge Accelerator at 12 km/sec, as reported in reference 3. It therefore seems appropriate to propose a promising means by which large velocity increases can be obtained through a combination of two existing, proven accelerators.

Specifically, by a combination of the shaped charge accelerator and the light gas gun, it is believed that 20 km/sec velocities can be achieved. The large Atkins light gas gun at the Naval Research Laboratory⁽⁵⁾, which has an 8-inch pump tube and a 2.5 or 3-inch launch tube, could possibly be used to accelerate shaped charges to velocities of 20,000-25,000 fps. Subsequent to leaving the launch tube muzzle, the charge would be electrically initiated, functioning during free flight in the same manner as described previously.

Atkins⁽⁶⁾ estimates that the gun will accelerate 200 grams to 23,000 fps, or 400 grams to 23,000 fps, or 600 grams to 20,000 fps. Our current shaped charge accelerator designs, such as is shown in Figure 8, have an over-all weight of approximately 500 grams. We have never sought to decrease this weight, but we believe that both the cone and explosive dimensions can be reduced substantially. For gun launching the explosive would be contained in a metal cup with a heavy base. The initiating system would be contained in the base. An external energy source would fire the initiator after the charge left the launch tube muzzle.

The mass per unit area for a 2.5-inch launch tube is 6.3 gms/cm² for a 200 gram projectile, and 12.6 and 18.9 gm/cm² respectively for 400 and 600 gram projectiles. Certainly 18.9 gm/cm² appears high enough for the liner, explosive, and base of a well-designed shaped charge. Also of importance will be the maximum pressure in the column of explosive. Assuming a maximum acceleration of 10⁶g, the base pressure in a 10-cm long column of explosive pushing ahead of it a 0.5-cm thick layer of aluminum liner will be 16 kilobars. A pressed, laterally-contained explosive with no voids should be able to withstand such an acceleration pressure.

SPECIAL EXPLOSIVE PROJECTORS

To assess the feasibility of this combination, a design study should be made of the techniques required for initiation, baffling, fragmentation shielding, and instrumentation. In addition, the ability of explosives to withstand extreme acceleration should be assessed with relatively small quantities of explosives launched in smaller guns.

II. PLATE ACCELERATION TECHNIQUE

The acceleration of flat plates has been developed by investigators for the purpose of introducing strong, planar shock waves in various materials to permit determination of dynamic compressibilities (i. e. Hugoniot equations-of-state). Under ARPA Order 149 and Contract AF08(635)-1382 with the Weapons Laboratory, Eglin AFB, we have adapted this technique to terminal ballistic studies by suspending stationary projectiles in the path of the flying plate.

The general technique is illustrated by the schematic shown in Figure 11. The plate to be accelerated is placed in contact with a slab of explosive. This explosive is then initiated along one edge with a line wave generator. As the detonation front progresses in a straight line down the slab of explosive, the target plate is folded off, eventually reaching a flat configuration when the entire slab has detonated. Due to edge effects, the plate will not be perfectly flat, but a large central area of the plate is sufficiently flat to permit the gathering of useful terminal ballistic data. We achieve velocities up to about 3.5 km/sec using this technique.

At these velocities, recovery of the intact plates becomes impractical, since the decelerating forces destroy the plates. The area of the hole which a projectile will make in the plate, however, can be determined by high speed photographic or radiographic observation of the plate in flight immediately after impact. We have found either the 300 kv or 600 kv Field Emission units (Model PS-300-1000-0.15 or Model PS-600-2000-0.2-1200) to be suitable for this purpose. The experimental setup is shown in Figure 12.

Figure 13 shows a 6-in. x 6-in. target plate in flight shortly after acceleration. The flat center area is apparent from this radiograph. Figure 14 shows a plate after impact with a 3/8-in. dia x 1/8-in. titanium disc. The hole dimensions are distinctly shown. Residual fragments from the titanium disc are also evident.

SPECIAL EXPLOSIVE PROJECTORS

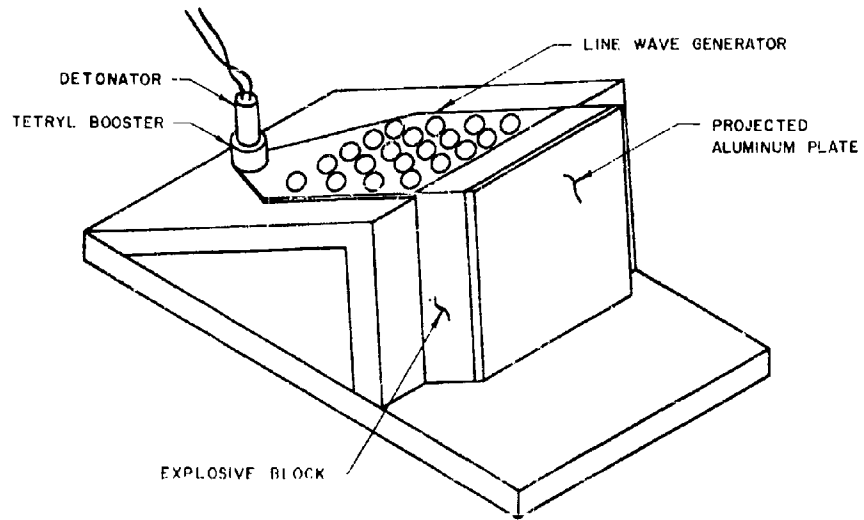
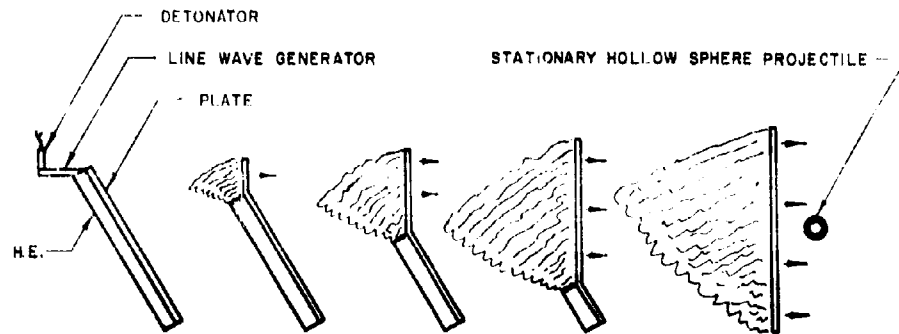


PLATE ACCELERATION TECHNIQUE



FOLDING OFF OF ACCELERATING PLATE

Fig. 11 - TARGET PLATE ACCELERATOR

SPECIAL EXPLOSIVE PROJECTORS

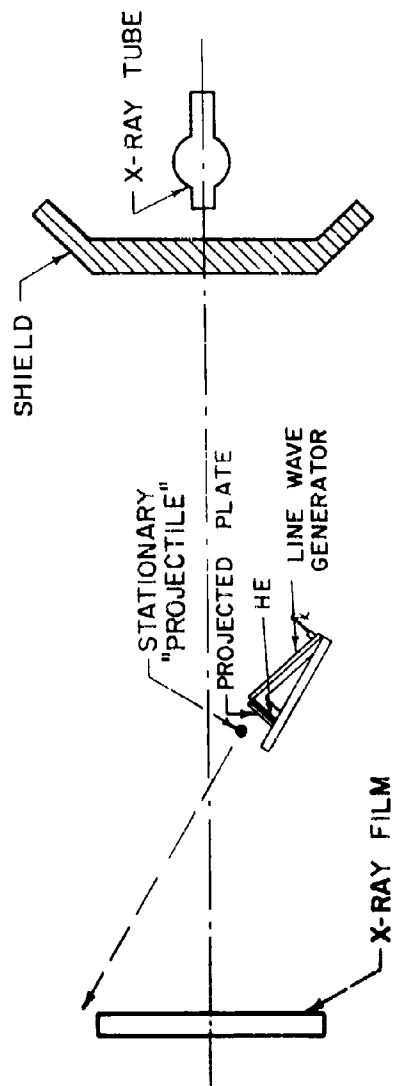


Fig.12- INSTRUMENTATION ARRANGEMENT FOR TARGET
PLATE ACCELERATOR EXPERIMENTS

SPECIAL EXPLOSIVE PROJECTORS

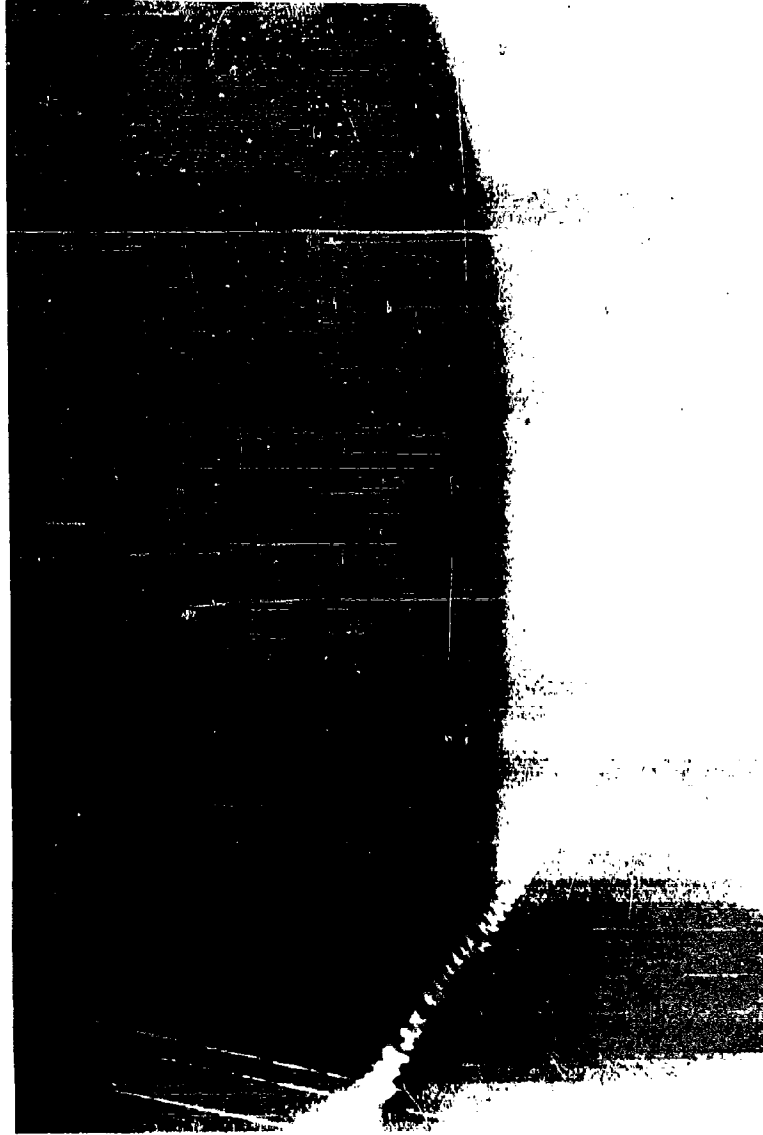


Figure 13. Radiograph Showing Side View of Plate in Flight.

SPECIAL EXPLOSIVE PROJECTORS

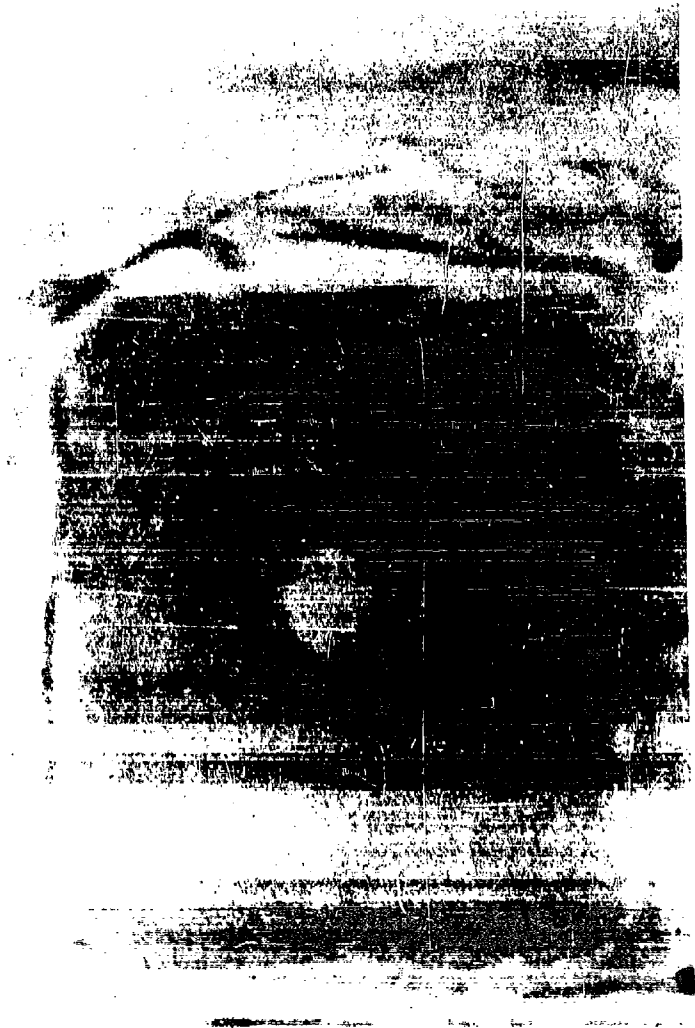


Figure 14. Radiograph Showing Oblique Front View of Target Plate in Flight After Impacting 1-gm. Titanium Pellet at 3.5 km/sec.

SPECIAL EXPLOSIVE PROJECTORS

Acceleration of a target plate against a stationary projectile represents, of course, a reversal of the normal coordinates for laboratory impact studies. This reversal in no way affects the basic impact physics. There are some side effects, however, which must be considered in evaluating the validity of the technique. The effects involve the alteration of the plate properties during acceleration, and the build up of an air cushion in front of the plate as it travels through the air.

The fold-off of the plate during acceleration involves high strain rate plastic deformation. Subsequent flash radiographs show whether the plate is fractured as a result of this deformation. To minimize work hardening, we use plates of maximum hardness, i. e. aluminum in a T-6 condition.

The air layer which builds up on the face of target plate may slightly cushion the impact with the stationary projectile. This effect is not believed to be too important; however, it can be avoided altogether by performing experiments in an evacuated chamber.

To test the validity of the technique, experiments have been performed in which results obtained by firing projectiles from a light gas gun into a stationary target plate are compared with identical projectiles impacted at the same velocity by the flying plate. These experiments showed that the same hole areas are produced in both situations. In addition to these comparative experiments flying plates which had been projected and impacted at lower velocities have been recovered intact; it was found that the hole sizes in the recovered plates matched the sizes as determined by flash radiography.

Primary applications of the flying plate technique have been for evaluating effects of unusual projectiles impacting on thin target plates in the range around 3.5 km/sec. Papers describing some of these results are being presented at this symposium for long-rods, thin sheets, and washers⁽⁴⁾ and for hollow spheres⁽⁷⁾. These are all shapes which are difficult or impractical to launch using guns or other explosive techniques. It has been possible, for example, to examine the impact effects of very thin metal sheets or foils, and projectiles consisting of bare high explosives. In addition to such applications to fragile or sensitive explosives, the technique is also applicable to large projectiles of any type.

SPECIAL EXPLOSIVE PROJECTORS

A modification of the technique permits extension of the attainable velocity regime. This modification consists of a counterfiring arrangement, in which the target plate is projected towards another type of accelerator, such as a gas gun or explosive cavity charge. In this manner, the impact velocity is the combined velocity of both accelerators. We have utilized this technique with the explosive cavity charge to attain impact velocities up to 8 km/sec.

SPECIAL EXPLOSIVE PROJECTORS

REFERENCES

1. L. Zernow, "The Effects of High Speed Impact by Shaped Charge Jets and Jet Fragments," Proceedings of the Rand Symposium on High Speed Impact (Held January 31-February 2, 1955) Rept. No. S-34, Rand Corporation, Santa Monica, California, May 1, 1955.
2. K. N. Kreyenhagen, J. E. Ferguson, R. R. Randall, Impact and Penetration of 0.109-inch Aluminum Plates by Aluminum Projectiles at 29,000-33,000 feet per second, Report APGC-TDR-62-10, Air Proving Ground Center, Eglin AFB, Florida, September 1961.
3. J. E. Ferguson, An Impact and Penetration Effects Study, APGC-TDR-63-2, Air Proving Ground Center, Eglin AFB, Florida, January 1963.
4. R. B. Mortensen, J. E. Ferguson, J. P. Joyce, K. N. Kreyenhagen, "Effects of 3 to 12 Km/Sec Impacts On Finite Targets," Proceedings Sixth Symposium On Hypervelocity Impact, Vol. III, p. 197.
5. C. D. Porter, H. P. Swift, and R. H. Fuller, Summary of Naval Research Laboratory Accelerator Development, Proceedings of the Fifth Symposium on Hypervelocity Impact (Held Denver, Colorado, October 30-November 1, 1964).
6. W. W. Atkins, Private Communication.
7. W. H. Dittrich, D. R. Christman, J. W. Gehring, K. N. Kreyenhagen, R. B. Mortensen, "Lethality of Hollow Shapes," Proceedings Sixth Symposium On Hypervelocity Impact, Vol. IV (Secret).

SUMMARY REMARKS

By

H.F. Swift

Imposing arrays of hypervelocity accelerator techniques are presently at the disposal of terminal ballistic research workers. Three basic groupings of hypervelocity accelerators (light-gas guns, explosive accelerators and special accelerators) have been significantly developed during the past 18 months and are now largely complementary. Gas guns have proven useful where precise control of ballistic parameters such as model shape, mass, velocity, and possibly orientation are required. Explosive accelerators are most applicable to studies where large numbers of firings must be made at velocities below 10 km/sec and are the only accelerators currently available for launching macroparticles at velocities above 10 km/sec. The special accelerators have found use in launching projectiles of extreme shapes and sizes such as thin plates and microparticles, and some may become important for more general applications in the future.

The performance requirements placed upon light-gas guns can only be met by launching sabot models. The increase in sabot-launching capability during the past 18 months has been greater than any other similar period in the past. This increase is particularly striking in view of the fact that no significant increase in maximum gun velocity has been reported during the same period. At present, small glass and plastic spheres may be launched at 9.5 km/sec, small steel and copper spheres (1/8" dia) can be fired at 8.25 km/sec and larger steel spheres (1/4" dia) can be accelerated to 7.75 km/sec. These performance capabilities have been brought about largely by developing techniques for launching sabot packages at the peak velocity-mass capabilities of various gas guns. Careful sabot design, empirical optimization of firing parameters and the application of realistic gun operation theories have been responsible for these developments.

SUMMARY REMARKS

Present computational techniques appear to be capable of determining the optimum firing parameters of most current light-gas guns and are also useful for the design of new guns that use relatively familiar modes of operation. They are not sufficiently reliable in their present form to use as the sole justification for acceptance or rejection of new gun design concepts. Studies have demonstrated the possibility that at least part of the present difficulties with gun computational techniques arise from inaccuracies in some of the commonly made assumptions, i.e., zero leakage of the driver gas and constant projectile bore friction.

Future increases in gas-gun capabilities will probably be brought about by the use of new methods for increasing gun performance. The most promising new techniques presented at this meeting involve preheating the driver gas either before or during the compression stroke. Both theoretical and experimental results show that heated gas will produce significant increases in model velocities provided that initial temperatures above 600°K can be achieved. Preheated gas has been shown also to reduce peak acceleration levels required to reach particular velocities and this effect should speed the trend toward launching sabot models at the maximum velocity-mass capabilities of gas guns.

The theoretical treatments of explosive accelerators have been developed to the point where the potential capability of many configurations can be predicted. This fact has led to very rapid development of explosive accelerator capability. The primary emphasis in explosive accelerator development during the past 18 months has been placed upon the development of techniques for launching useful pellets for terminal ballistic research. The most striking advances reported during this session are the development of conical-liner charges that generate discrete particles. Conical liner charges have the advantage that pellet mass and velocity may be adjusted without drastic changes of the charge geometry.

Studies were conducted during the past 18 months to develop traveling-charge guns and electromagnetic accelerators into effective hypervelocity accelerators.

SUMMARY REMARKS

Results of these efforts are promising but further work is needed to make either device operational. The electrical acceleration of thin plastic sheets at velocities up to 9.5 km/sec has been demonstrated. A constricted-bore velocity augmentor capable of substantially increasing the velocity of malleable pellets launched from light-gas guns also has been developed. Both of these techniques are highly specialized but useful for particular applications.

Although no significant increases have been reported in the velocity capability of accelerators, the maximum velocities at which useful terminal ballistic data are gathered have been substantially increased by advances in projection techniques. Further large increases in the velocity at which terminal ballistic data may be gathered must await advances in overall accelerator capability. These advances should be achieved in the next 18 months.

ATTENDANCE ROSTER

ANTHONY L. ALESI, Quartermaster R&E Command, Natick
 F. E. ALLISON, Ballistic Research Laboratories, APG
 ELTON L. ANDERSON, GM Defense Research Laboratories, Warren
 HOMER T. ARMSTRONG, Chance Vought Corporation
 EDWARD H. ASHER, Firestone T. & R. Co.
 W. W. ATKINS, U.S. Naval Research Laboratory
 HARKER T. AUGUST, Jr., McDonnell Aircraft Corp.
 JOHN A. BACHMAN, Jr., Minneapolis Honeywell Regulator Co., Washington
 PAUL G. BAER, Ballistic Research Laboratories, APG
 RICHARD N. BAILEY, Sundstrand Aviation/Denver
 J. R. BAKER, U. S. Naval Research Laboratory
 LOUIS A. C. BARBAREK, Armour Research Foundation, Illinois Institute of
 Technology
 SAMUEL B. BAIDORE, Aerospace Corporation
 K. R. BECKER, U. S. Department of Interior, Bureau of Mines, Brighton
 EDGAR BENDOR, Republic Aviation
 MYRON H. BENGSON, G.E. Co., Space Technology Center
 EDWARD R. BERUS, Firestone T. & R. Co.
 ANDREW C. BILEK, USAF Ballistic Directorate, Eglin AFB
 ROBERT L. BLOK, The Rand Corporation
 JAMES E. BLOWER, OSD/ARPA/BMDE, Pentagon
 FREDERICK K. BUCKWOLD, GM Defense Research Laboratories
 RAY G. BOYD, Martin Co., Orlando
 ALONZA D. BRINSON, Det. 3, ASD (ASQWR), Eglin AFB
 CARL A. BROWN, G.E. Co., Space Technology Center
 JOHN C. BROWN, A.F. D. Co., Arnold Air Force Station
 DANIEL T. BROWNING, Jr., Field Lamination Corp.
 EDGAR P. BRUCE, G.E. Co., Re-entry System Division
 EARL F. BRYANT, Malaker Laboratories, Inc.
 PAIGE B. BURBANK, NASA, Houston
 H. H. CALVIT, Pennsylvania State University
 EMERSON L. CANNON, Utah Research & Development Co.
 CHARLES R. CARSON, Research & Technology Division, Bolling AFB
 ROBERT L. CHANDLER, Armour Research Foundation, Illinois Institute
 of Technology
 MARC CHAPDELAINE, Computing Devices of Canada
 ROBERT L. CHAPMAN, MB Associates
 A. C. CHARLERS, GM Defense Research Laboratories
 MASON L. CHARAK, NASA, Washington
 PEI CHI CHOU, Drexel Institute of Technology
 D. R. CHRISTMAN, GM Defense Research Laboratories
 ERIC N. CLARK, Picatinny Arsenal
 WALLACE G. CLAY, MIT Lincoln Lab.
 NESTOR CLOUGH, NASA Lewis Research Center

MARIO CLOUTIER, CARDE
 J. J. CONDON, U. S. Naval Research Laboratory
 M. A. COOK, University of Utah
 WILLIAM C. COOLEY, Esotech, Inc.
 BURTON G. COUR-PALAIS, NASA, Houston
 C. M. COX, Firestone I. & R. Co.
 GEORGE C. CREWS, Ballistic Research Laboratories, APG
 J. J. DALLEY, Ballistic Research Laboratories, APG
 PHILLIP J. D'ANNA, Northrop Space Laboratories
 CHARLES T. D'AIUTOLO, NASA, Washington
 NORMAN DAVIDS, Pennsylvania State University
 DALE M. DAVIS, Det. 4, ASD (ASQWR), Eglin AFB
 JOHN A. DAVIS, U. S. Naval Research Laboratory
 LOUIS J. DEL DO, FC, DASA, Sandia Base
 RICHARD T. DELLON, Sandia Corp., Sandia Base
 WALTER H. DETTRICH, Det. 4, ASD (ASQWR), Eglin AFB
 HANS K. DOETSCH, A. E. D. C., Arnold Air Force Station
 STEPHEN J. DOHERTY, US Army Materials Research Agency
 COLEMAN DUP DONALDSON, AERC, Research Associates
 DONALD M. DONOHUE, NASA, Houston
 DONALD R. DUDAS, Det. 4, ASD (ASQWR), Eglin AFB
 RUSSELL E. DUFF, University of California, Lawrence Radiation Laboratories
 BRIAN E. DUNNE, Jr., General Atomic
 KENNETH B. EACOTT, Computing Devices of Canada
 STEPHEN E. EBLESON, Chance Vought Corporation
 JOHN E. EHRENFIELD, Geophysics Corp. of America
 R. J. EICHELBERGER, Ballistic Research Laboratories, APG
 NORMAN S. EISS, Jr., Cornell Aeronautical Laboratory
 RAY M. ELAM, Boeing Company
 OLIVE G. ENGEL, National Bureau of Standards
 CHARLES W. FERGUSON, Douglas Aircraft Co.
 WILFRED J. FERGUSON, U. S. Naval Research Laboratory
 RICHARD H. FISH, NASA, Ames Research Center
 EDWARD M. FISHER, U. S. Bureau of Naval Weapons
 CARL W. FLEISCHER, Jr., Frankford Arsenal
 JOHN T. FRASIER, Ballistic Research Laboratories, APG
 JOSEPH F. FRICHTENICHI, Space Technology Laboratories
 VERNE C. FROST, Aerospace Corporation
 OTTO P. FUCHS, Temple University
 ALBERT E. GAEDE, Astropower, Incorporated
 MICHAEL F. GARMAN, Nortronics
 DONALD E. GAULT, NASA, Ames Research Center
 GEORGE M. GAYDOS, Picatinny Arsenal
 J. WILLIAM GEHRING, GM Defense Research Laboratories
 DONALD N. GIDEON, Battelle Memorial Institute
 DAVID I. GILBERT, Aerojet-General Nucleonics
 ROBERT L. GLASSER, Aerospace Corporation
 CHARLES S. GODFREY, Physics International

JACK GOLDSTEIN, Aerospace Corporation
HOWIN H. GOODMAN, ARO, Incorporated, Arnold Air Force Station
CHARLES C. GORDON, General Dynamics/Convair
J. J. GREEN, DND-DRB/CARDE
EUGENE S. GRUBIN, Falcon Research & Development Co.
FRANK J. GRUNDHAUSER, Field Emission Corp.
ALBERT C. HAKE, Martin Company, Baltimore
DONALD A. HALL, U. S. Naval Research Laboratory
STANLEY M. HALPERSON, U. S. Naval Research Laboratory
CARROLL R. HARDER, Atomics International
JERE G. HARLAN, Physics International
RAYMOND W. HARR, North American Aviation
ROBERT J. HARRIS, Grumman Aircraft Corp.
JAMES FORMAN HAWK, Hayes International Corp.
ROBERT L. HAYFORD, Space Systems Division, USAF
EZRA D. HEITOWIT, NASA, Ames Research Center
IRVIN G. HENRY, Hughes Aircraft
WALTER HERRMANN, MIT Lincoln Laboratory
JOSEPH HERSHKOWITZ, Picatinny Arsenal
JAMES F. HEYDA, G. E. Co., Missile & Space Division
JOSEPH E. HIMES, Analytic Services, Inc.
ALVIN A. HOLTON, Jr., Martin Co., Denver
ALFRED HOLZER, Univ. of California, Lawrence Radiation Laboratories
ALAN K. HOPKINS, ASD B&M, Wright-Patterson AFB
HARRY G. HOPKINS, Royal Armament Research & Development Establishment
EDWIN F. HORNUNG, Cleveland Procurement District
WILLIAM G. HOWELL, Univ. of Denver, Denver Research Institute
ORLOK, HUDSON, NASA, Huntsville
NORRIS J. HUFFINGTON, Martin Co., Baltimore
WILLIAM C. HULL, Hayes International Corp.
DONALD H. HUMES, NASA, Langley Research Center
RONALD C. HUPE, General Dynamics, Pomona
WALLACE A. HURD, Raytheon Company
ROBERT H. IMES, Mallory Metallurgical Co.
SIGMUND J. JACOBS, U. S. Naval Ordnance Laboratory
DAVID M. JEFFREYS, General Electric Co., Burlington
ROBERT J. JOHNSON, Northrop Space Laboratories
WALLACE E. JOHNSON, General Atomics
A. H. JONES, MIT Lincoln Laboratory
ENNIS E. JONES, Minneapolis-Honeywell, Hopkins
AHMED D. KAFADAR, Ordnance Engineering Associates
HENRY C. KASHAN, Sylvania Electronic Systems
MAHMOUD I. KAZIMI, Hexcel Products, Incorporated
RICHARD C. KELLAGHER, Central Intelligence Agency
JAMES W. KELLER, NASA, Washington
JAMES C. KELTON, Development & Proof Services, APC
FRED J. KENDELL, Utah Research & Development

WALTER J. KERTHULA, Army Materiel Command, AMCRD-RS-PL-15
JOHN H. KINEKE, Jr., Ballistic Research Laboratories, APG
RAY KINSELOW, Aero, Inc., Arnold Air Force Station
EARL C. KLAUBERT, Thiokol Chemical Corp., Denville
WILLIAM F. KONIG, Columbia University
JAMES T. KRAMER, NASA Lewis Research Center
HARRY KRAUS, Pratt-Whitney Aircraft, East Hartford
K. N. KREYENHAGEN, Aerojet-General Corporation
SEYMOUR KRONMAN, Ballistic Research Laboratories, APG
EDWIN T. KRUSZEWSKI, NASA, Langley Research Center
DAVID D. KURTOVICH, Boeing Company
JOHN L. LACKLER, Applied Physics Lab/Johns Hopkins University
D. C. LANE, U.S. Naval Ordnance Laboratory
GEORGE H. LEE, Minneapolis-Honeywell Regulator Co., Washington
THOMAS W. LEE, Utah Research & Development Company
BASIL P. LEFTHERIS, Republic Aviation
BO LEMCKE, MIT Lincoln Laboratory
WALTER F. LENDSEY, NASA, Langley Research Center
MARVIN E. LEVY, Frankford Arsenal
SEYMOUR LIEBLIN, NASA Lewis Research Center
RICHARD E. LORENS, Drexel Institute of Technology
IRVIN J. LOEFFLER, NASA Lewis Research Center
V. E. LUCAS, Firestone T. & R. Co.
CHILDE G. LUKHARDT, Esotech, Inc.
DAVID B. LULL, Geophysical Corporation of America
JOHN F. LUNDEBERG, Boeing Company
ELMER R. LURKER, U.S. Naval Research Laboratory
JOHN L. LUTTRELL, U.S. Naval Ordnance Laboratory
ROBERT W. MAC CORMACK, NASA Ames Research Center
RICHARD MADDEN, NASA, Langley Research Center
C. J. MAIDEN, GM Defense Research Laboratories
PAUL K. MARGOLIS, Aerospace Corporation
PAUL MARNELLI, Technik Inc.
EARL B. MASSENGILL, Jr., Naval Weapons Evaluation Facility, Kirtland AFB
KENNETH A. MAURER, Raytheon Manufacturing Company
NORMAN J. MAYER, NASA, Washington
STEPHEN A. D. MELEK, Field Emission Corp.
JOHN M. MESHEJIAN, Hayes International Corp.
DOUGLAS A. J. MILLAR, Computing Devices of Canada
J. L. MILLER, Firestone T. & R. Co.
HENRY J. MOORE, US Geological Survey, Menlo Park
ROBERT H. MORRISON, NASA Ames Research Center
RENE B. MORTENSEN, Aerojet-General Corporation
PENN E. MULLOWNEY, Army Missile Command, Redstone Arsenal
WILLIAM D. MURPHREE, NASA, Marshall Space Flight Center
PHILIP F. MURRAY, Firestone T. & R. Co.
EDWIN N. MYERS, Headquarters, USAF, Washington

JOE C. MC CASLIN, Douglas Aircraft Co., Inc., Charlotte
WILLIAM L. MC KAY, Avco Corp.
ROBERT R. MC MATH, Avco Corp.
ALLAN R. MC MILLAN, GM Defense Research Laboratories
ROBERT L. MC NALL, Ballistic Research Laboratories, APG
WILLIAM NACHBAR, Stanford University, Dept. Aeronautics & Astronautics
ROBERT J. NAUMANN, NASA, Huntsville
AMINA NORDIO, Picatinny Arsenal
C. ROBERT NYSMITH, NASA Ames Research Center
ROBERT V. O'CONNELL, Unitelectron, Inc.
FLOYD A. ODELL, Field Emission Corp.
ARNOLD E. OLSHAKER, Rand Corp.
ALBERT S. ORR, Firestone T. & R. Co.
G. T. ORROK, Bellcomm, Incorporated
EDWARD P. PALMER, University of Utah
RALPH P. PAPIRNO, Aracon Laboratories
JAMES A. PARK, Computing Devices of Canada
JAMES C. PEARSON, Picatinny Arsenal
MARIO A. PERSECHINO, U.S. Naval Research Laboratory
DANTE PIACESI, U.S. Naval Ordnance Laboratory
ROBERT PIACESI, U.S. Naval Ordnance Laboratory
ROBERT B. POND, Johns Hopkins University
C. D. PORTER, U.S. Naval Research Laboratory
FELIX C. POSEVER, North American Aviation, Downey
EDWARD C. POSLON, Det. 1, ASD (ASOWR), Edin Air Force Base
WILLIAM E. PRESTON, U.S. Naval Ordnance Laboratory
EMERSON M. PUGH, Carnegie Institute of Technology
WILLIAM J. RAE, Cornell Aeronautical Laboratories
ROY E. RAYLE, Avco Corp., Richmond
RODNEY F. RECHT, Univ. of Denver, Denver Research Institute
JOHN A. REGALBUTTE, General Dynamics, Fort Worth
B. W. REYNOLDS, Goodyear Aerospace Corporation
THOMAS D. RINEY, G. E. Co., Missile & Space Div.
MURRAY ROCKOWITZ, Avco Corporation
JAMES W. ROGERS, U.S. Naval Ordnance Test Station
MATTHEW ROTHMAN, North American Aviation, Columbus
FRANK A. RUMSEY, Jr., USA Air Defense School, Fort Bliss
FRED J. SACKLEH, ASD, Wright-Patterson AFB
WILLIAM B. SANDE, Boeing Company
PAUL E. SANDORFF, Lockheed Missile & Space Company, Palo Alto
LUIGI A. SANTALESIA, Columbia University
SOLOMON SAUL, Republic Aviation Corp.
HERALD EUGENE SAWDY, Firestone T. & R. Co.
MORRIS F. SCHARFF, General Atomic
JACK SCHIFF, G. E. Co., Re-Entry Systems Div.
ELLIS H. SCOTT, U.S. Naval Ordnance Laboratory
CHARLES N. SCURRY, North American Aviation, Downey

ARNOLD E. SEIGEL, U. S. Naval Ordnance Laboratory
 HOWARD W. SEMON, General Electric Co., Philadelphia
 MARTIN S. SILVERSTEIN, Frankford Arsenal
 RALPH G. H. SIU, U.S. Army Materiel Command, Washington
 JACK C. SLATTERY, Space Technology Laboratories
 RICHARD E. SLATTERY, MIT Lincoln Laboratory
 GORDON T. SMITH, NASA Lewis Research Center
 LOUIS F. SMITH, University of Denver
 MARTIN SOLOMON, Lear Siegler, Inc., Grand Rapids
 RICHARD E. SOLOSKI, Avco Corp.
 NEIL R. SORESENEN, Utah Research & Development Co.
 JOSEPH SPERRAZZA, Ballistic Research Laboratories, APG
 GEORGE STALK, USAF, Office of Aerospace Research
 ROBERT A. STEIN, Battelle Memorial Institute
 SAMUEL D. STEIN, Picatinny Arsenal
 STEWART B. STEINER, Firestone T. & R. Co.
 WILLIAM B. STEPHENSON, Avco, Incorporated
 FRANCIS S. STEPKA, NASA Lewis Research Center
 WILLIAM STERBENTZ, Lockheed Missiles & Space Company
 HYMAN M. STERNBERG, U.S. Naval Ordnance Laboratory
 CLIFTON STEVENS, Goodyear Aerospace Corporation
 RENE R. STUDLER, Firestone T. & R. Co.
 HALLOCK F. SWIFT, U.S. Naval Research Laboratory
 PAUL SYMONDS, Brown University
 VICTOR G. SZEBEHELY, General Electric Co., Philadelphia
 EDWARD R. THULO, USA Munitions Command, Frankford Arsenal
 ROBERT W. THORBURN, Firestone T. & R. Co.
 E. SEFTON THORN, Firestone T. & R. Co.
 JAMES H. TILLOTSON, General Atomic
 JAMES E. TRAINER, Firestone T. & R. Co.
 HOWARD J. VANDERSLUIS, Jr., USA Engineering Res. & Dev. Laboratories,
 Fort Belvoir
 BERNARD VAN ZYL, Martin Co., Orlando
 RICHARD VITALI, Ballistic Research Laboratories, APG
 VINCENT F. VOLPE, Armour Research Foundation, Illinois Institute of
 Technology
 JOHN M. WALSH, General Atomic
 RAYMOND D. WALTRAM, Det. 4, ASD (ASQWR), Eglin Air Force Base
 DONALD R. WARD, NASA Lewis Research Center
 ROBERT H. WASER, U.S. Naval Ordnance Laboratory
 THOMAS WATMOUGH, Armour Research Foundation, Illinois Institute of
 Technology
 RICHARD W. WATSON, Department of Interior, Bureau of Mines, Pittsburgh
 MILTON G. WEISMAN, Atomics International
 A. PHILLIP WELCH, General Dynamics
 JERRY N. WELLNITZ, General Dynamics/Astronautics
 FREDERICK W. WENDT, General Electric Co., Philadelphia

ALBERT K. WEYMOUTH, Office of the Chief of Naval Operations
GEORGE P. I. WILLNIUS, Computing Devices of Canada
MARK L. WILKINS, Univ. of California, Lawrence Radiation Laboratories
RICHARD J. WISNIEWSKI, NASA, Washington
WILLIAM H. WORKENBERG, General Electric Co., Philadelphia
WILLIAM E. WOLSTENHOLME, United States Rubber Co., Wayne
WALTER W. WRINKLE, North American Aviation, Downey
ROBERT M. YATES, Dept. of Defense, 3D 118, Pentagon
SHAO WEN YUAN, University of Texas
MELVIN ZAID, Technik Inc.
THOMAS A. ZAKER, Armour Research Foundation, Illinois Institute of
Technology
LOUIS ZERNOW, Aerojet-General Corp.
FRANK J. ZIMMERMAN, Armour Research Foundation, Illinois Institute of
Technology
HARRIET J. ZIMNEY, Aerojet-General Corp.

AUTHORS

Atkins, W. W.	Vol. 3, p. 101
Baer, Paul G.	Vol. 4, p. 111
Baker, J. R.	Vol. 4, p. 11
Barbacek, Louis A.	Vol. 4, p. 207
Becker, K. R.	Vol. 3, p. 207
Bjork, R. L.	Vol. 3, p. 111
Brown, J. M.	Vol. 4, p. 111
Calvat, H. H.	Vol. 3, p. 111
Carey, Charles A.	Vol. 4, p. 201
Chandler, R. L.	Vol. 4, p. 111
Chapman, R. B.	Vol. 4, p. 111
Charters, A. C.	Vol. 4, p. 111
Christman, D. R.	Vol. 4, p. 111
Coley, R. B.	Vol. 4, p. 111
Condon, J. J.	Vol. 4, p. 111
Cox, C. M.	Vol. 4, p. 111
D'Anna, Philip J.	Vol. 4, p. 111
Deley, James J.	Vol. 4, p. 111
Davies, N.	Vol. 4, p. 111
Deves, Dale K.	Vol. 4, p. 111
Demardo, B. Pat.	Vol. 4, p. 111
Dutton, W. H.	Vol. 4, p. 111
Donaldson, Coleman D.	Vol. 4, p. 111
Eckerman, J.	Vol. 4, p. 111
Karchelberger, R. J.	Vol. 4, p. 111
Emmons, R. H.	Vol. 4, p. 111
Engel, Olive G.	Vol. 4, p. 111
Ferguson, J. F.	Vol. 4, p. 111
Friichtenicht, J. F.	Vol. 4, p. 111
Gates, D. F.	Vol. 4, p. 111
Gault, D. F.	Vol. 4, p. 111
Gaydos, George M.	Vol. 4, p. 111
Gehring, J. W.	Vol. 4, p. 111
Gibson, F. C.	Vol. 4, p. 111
Giroux, Richard	Vol. 4, p. 111
Glass, C. M.	Vol. 4, p. 111
Goodman, E. H.	Vol. 4, p. 543
Halperson, S. M.	Vol. 4, p. 525
Harms, D. E.	Vol. 1, p. 317
Harrity, Edmund M.	Vol. 4, p. 167